The Dissertation Committee for Harpreet Singh Dhillon
certifies that this is the approved version of the following dissertation:

Fundamentals of Heterogeneous Cellular Networks

Committee:

Jeffrey G. Andrews, Supervisor

Constantine Caramanis

Gustavo de Veciana

Robert W. Heath, Jr.

Howard C. Huang

Fundamentals of Heterogeneous Cellular Networks

by

Harpreet Singh Dhillon, B.Tech., M.S.

DISSERTATION

Presented to the Faculty of the Graduate School of

The University of Texas at Austin

in Partial Fulfillment

of the Requirements

for the Degree of

DOCTOR OF PHILOSOPHY

THE UNIVERSITY OF TEXAS AT AUSTIN

December 2013

Dedicated to my family.

Acknowledgments

I would first like to express my gratitude to my dissertation advisor Prof. Jeffrey G. Andrews for his guidance, support and encouragement. Working with Jeff for the past three years has been a wonderful experience for many reasons. First, his belief in my judgement and abilities has helped me mature as a researcher. Second, his encouragement to come up with my own original ideas has helped me appreciate the value of formulating meaningful research problems and has had a profound effect in shaping my vision for future research. Third, he sets high standards for his group, and most importantly leads by example. For instance, his seminal paper on cellular models with Prof. Baccelli and Prof. Ganti has not only motivated this dissertation but has opened up an altogether new area of research.

I would also like to thank my committee members Prof. Constantine Caramanis, Prof. Gustavo de Veciana, Prof. Robert W. Heath Jr. and Dr. Howard C. Huang for their invaluable comments and suggestions. During my stay at UT, I have been fortunate to foster collaboration with some wonderful researchers. My special thanks to Prof. Radha Krishna Ganti for being a mentor and a friend. His guidance was invaluable in getting me started with my graduate research. I would also like to express my appreciation for Prof. François Baccelli for always being welcoming to discuss my research, and also

for hosting me in Paris. A special thanks also to Prof. Marios Kountouris for hosting me at Supelec, which led to our joint work on MIMO HetNets. Thanks also to Prof. Mischa Dohler for inviting me to speak at the Femto Winter School in Barcelona. Amongst my colleagues, I would like to thank Sarabjot Singh and Tom Novlan for the countless discussions we have had on various topics.

I thank Cockrell school of engineering at UT Austin for supporting my research, in part, with Microelectronics and Computer Development (MCD) fellowship. The support from National Science Foundation (NSF) grant CIF-1016649 is also greatly appreciated. During my graduate studies, I was also fortunate to gain some useful industry experience. Thanks to Dr. Howard C. Huang, Dr. Harish Viswanathan and Dr. Reinaldo A. Valenzuela for hosting me at Alcatel-Lucent Bell Labs, Holmdel, NJ, during summer 2011. It has indeed been a great pleasure to continue our collaboration on M2M communications for the past two years. Thanks also to Dr. Ying Li, Dr. Pavan Nuggehalli and Zhouyue (Jerry) Pi for hosting me at Samsung Research America, Richardson, TX, during summer 2012, and letting me work on understanding the fundamentals of self-powered HetNets, which ended up being a chapter in this dissertation.

My stay at UT would not have been so memorable without the friends that I have made along the way, most of them also being my colleagues in the Wireless Networking and Communications Group (WNCG). Thanks to Ankit, Deepjyoti, Guneet, Omar, Sarabjot, Srinadh and Virag for some wonderful

discussions. I would especially like to thank Sarabjot for being a special friend and a very inspiring colleague. I take this opportunity to thank Melanie Gulick from ECE office, and Janet Preuss, Jennifer Graham and Karen Little from WNCG office, for taking care of all the paperwork and other logistics.

I thank my parents for their unconditional love and support. Their high values and emphasis on quality education have made me the person I am today. I will never be able to thank them enough for that. I also thank my brother Harsimran for taking a good care of our parents while I was away for the graduate school. I thank my parents-in-law for their constant encouragement to achieve perfection, and my brother-in-law Teglovy for being a perfect stress buster. Finally, a sincere thanks to my best friend and wife Donia, for standing by me through thick and thin of graduate school. Her constant encouragement and emphasis on hard work has brought a positive change in my life.

Fundamentals of Heterogeneous Cellular Networks

Publication No. _____

Harpreet Singh Dhillon, Ph.D.
The University of Texas at Austin, 2013

Supervisor: Jeffrey G. Andrews

The increasing complexity of heterogeneous cellular networks (HetNets) due to the irregular deployment of small cells demands significant rethinking in the way cellular networks are perceived, modeled and analyzed. In addition to threatening the relevance of classical models, this new network paradigm also raises questions regarding the feasibility of state-of-the-art simulation-based approach for system design. This dissertation proposes a fundamentally new approach based on random spatial models that is not only tractable but also captures current deployment trends fairly accurately.

First, this dissertation presents a general baseline model for HetNets consisting of K different types of base stations (BSs) that may differ in terms of transmit power, deployment density and target rate. Modeling the locations of each class of BSs as an independent Poisson Point Process (PPP) allows the derivation of surprisingly simple expressions for coverage probability and average rate. One interpretation of these results is that adding more BSs or

tiers does not necessarily change the coverage probability, which indicates that fears of "interference overload" in HetNets are probably overblown.

Second, a flexible notion of BS load is incorporated by introducing a new idea of *conditionally thinning* the interference field. For this generalized model, the coverage probability is shown to increase when lightly loaded small cells are added to the existing macrocellular networks. This is due to the fact that owing to the smaller loads, small cells typically transmit less often than macrocells, thus contributing less to the interference power. The same idea of conditional thinning is also shown to be useful in modeling the non-uniform user distributions, especially when the users lie closer to the BSs.

Third, the baseline model is extended to study multi-antenna HetNets, where BSs across tiers may additionally differ in terms of the number of transmit antennas, number of users served and the multi-antenna transmission strategy. Using novel tools from stochastic orders, a tractable framework is developed to compare the performance of various multi-antenna transmission strategies for a fairly general spatial model, where the BSs may follow any general stationary distribution. The analysis shows that for a given total number of transmit antennas in the network, it is preferable to spread them across many single-antenna BSs vs. fewer multi-antenna BSs.

Fourth, accounting for the load on the serving BS, downlink rate distribution is derived for a generalized cell selection model, where shadowing, following any general distribution, impacts cell selection while fading does not. This generalizes the baseline model and all its extensions, which either ignore

the impact of channel randomness on cell selection or lumps all the sources of randomness into a single random variable. As an application of these results, it is shown that in certain regimes, shadowing naturally balances load across various tiers and hence reduces the need for artificial cell selection bias.

Fifth and last, a slightly futuristic scenario of self-powered HetNets is considered, where each BS is powered solely by a self-contained energy harvesting module that may differ across tiers in terms of the energy harvesting rate and energy storage capacity. Since a BS may not always have sufficient energy, it may not always be *available* to serve users. This leads to a notion of *availability region*, which characterizes the fraction of time each type of BS can be made available under variety of strategies. One interpretation of this result is that the self-powered BSs do not suffer performance degradation due to the unreliability associated with energy harvesting if the availability vector corresponding to the optimal system performance lies in the availability region.

Table of Contents

List of Tables

List of Figures

Chapter 1

Introduction

The mathematical analysis of cellular networks, even in their most primitive form consisting of a single type of base stations (BSs), is known to be hard. This prompted the use of highly simplified system models for analysis and system level simulations for design. To make matters worse, the complexity of cellular networks is rapidly increasing because of the irregular deployment of various types of low-power BSs, such as microcells, picocells, femtocells, and distributed antennas. This not only threatens the conventional cellular models with obsolescence, but also questions the feasibility of state-of-the-art simulation-based approach for system design. In particular, the addition of several types of low-power BSs increases the number of simulation scenarios significantly, resulting in a prohibitive complexity of detailed system level simulations. As a result, the current paradigm shift demands significant rethinking in the way cellular networks are perceived, modeled and analyzed. Recognizing this urgent need for better modeling tools, this dissertation develops a fundamentally new analytical approach that not only captures the current deployment trends accurately, but also facilitates analysis leading to simple and easy to use expressions for key performance metrics under sufficiently general settings. The main idea is to use random spatial models,

where the BS locations of each tier are endowed with a probability distribution instead of being considered fixed as is typically the case in the popular grid-based models [1–4]. Contrary to the conventional wisdom, the added randomness lends tractability by allowing the use of powerful mathematical tools from stochastic geometry for performance analysis [1, 5].

This introductory chapter is divided into three main parts. The first part, spanning Sections 1.1-1.2, provides a background on cellular networks and discusses main challenges involved in the downlink analysis using popular grid-based models. For the same setup, the proposed idea of modeling the BS locations with a stochastic process, in particular the Poisson Point Process (PPP), is shown to simplify the analysis significantly. The second part, spanning Sections 1.3-1.4, provides a broad overview of why heterogeneity in cellular networks is inevitable in order to cope up with the current usage trends. It then argues why the conventional models are insufficient to study this new network paradigm. Section 1.5 forms the third part, where the key contributions of this dissertation are summarized.

1.1 Background

A fundamental property of wireless signals is that they get attenuated as the separation between the transmitter and receiver is increased [6]. This attenuation is termed as *distance-based path loss*. As a result, the strength of the wireless signal beyond a certain distance from the transmitter is so weak that it is impossible for the receiver to differentiate it from thermal noise,

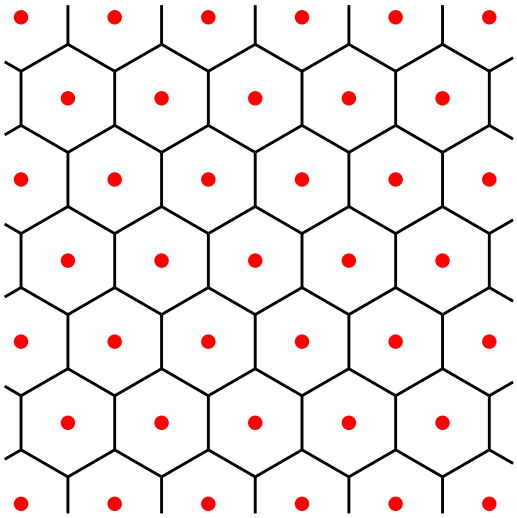

Figure 1.1: Hexagonal grid model for BS locations.

i.e., the signal gets buried in noise. Due to this property, two transmitters sufficiently far apart in space do not pose significant interference to each other even if they use the same time-frequency resources. This forms the basis of frequency reuse, which is at the heart of the cellular concept. Frequency reuse enables the division of space into "cells" each served by one BS, utilizing time-frequency resources that may be reused by other cells [7]. The resulting network, termed the *cellular network*, is the main focus of this dissertation.

An equivalent interpretation of the distance-based path loss is that the network area that can be served by a BS, often termed the *coverage area*, is limited. In the absence of obstructions and interferers, this area can be modeled as a circular disc centered at the BS. In the presence of interferers, however, the coverage area depends upon other factors such as the locations of the interferers, their transmit powers and the propagation environment. The

most popular and widely accepted model for this purpose is the hexagonal grid model, where the BSs are assumed to be located on a grid, with their coverage areas modeled as hexagons, as shown in Figure 1.1. Although a simple abstraction of reality, this model captures several key aspects of cellular networks and has been an industry standard since cellular networks were first conceptualized [6, 7]. However, despite its simplicity, it is surprisingly intractable, especially for downlink analysis, and is useful mainly for the system level simulations. The key challenges involved in the analysis are discussed in the next section in the context of the downlink coverage probability in a conventional single-tier setup where only single type of BSs, e.g., macrocells, are present. For the same setup, we show that the proposed model simplifies the analysis significantly.

1.2 Coverage Probability

A key metric of interest in the downlink of cellular networks is the probability of coverage, where *coverage* simply means that the strength of downlink connection to a randomly chosen user is such that it allows the user to receive both the control signaling and the actual data at a certain minimum rate. Mathematically, it can be expressed as the probability of the downlink signal-to-interference-plus-noise ratio (SINR) for an arbitrary user being greater than a predefined target β. In this section, we formulate the downlink coverage probability problem in a general single-tier setup. It is then specialized to two cases of interest: i) hexagonal grid model to highlight

the key analytical challenges, and ii) the proposed model to highlight how the new modeling approach is useful in addressing these challenges. Please note that the sole purpose of this *toy example* is to introduce key ideas using the simplest possible setup. More elaborate scenarios and other key performance metrics are left for the following chapters.

1.2.1 General Problem Setup

Consider a cellular network with N_b BSs transmitting on the same time-frequency resources, with the possibility that N_b can be infinite. Further details about the exact partitioning of time-frequency resources are not required for this discussion. Let a randomly selected user is served by a BS located at a distance R_0. Note that the selection of the serving BS is based on a predefined selection law, e.g., based on the maximum received power. Further details on cell selection will be provided when required. All the other $N_b - 1$ BSs, except the serving BS, act as interferers. Denote the distance of the randomly selected user to these interferers by $\{R_i\}$, where the subscript $1 \leq i < N_b$ denotes the index of the interferer. All the transmitters are assumed to transmit at a fixed power P. Each wireless link suffers from a distance based path-loss with exponent α and Rayleigh fading. Therefore, the received power at a distance r from the transmitter is $P_r = Phr^{-\alpha}$, where $h \sim \exp(1)$ models Rayleigh fading. For the ease of exposition, the thermal noise is assumed to be negligible compared to inter-cell interference so that the received `SINR` can be approximated by signal-to-interference ratio (`SIR`). The downlink `SIR` for

the randomly chosen user in this setup is

$$\mathtt{SIR} = \frac{h_0 R_0^{-\alpha}}{\sum_{i=1}^{N_b-1} h_i R_i^{-\alpha}}. \tag{1.1}$$

Note that SIR is a random variable due both to the random channel gains and the random distances to the serving BS and the interferers. The coverage probability ($\mathtt{P_c}$) for this general setup can be derived as follows:

$$\begin{aligned}
\mathtt{P_c} &= \mathbb{P}(\mathtt{SIR} > \beta) && (1.2)\\
&= \mathbb{P}\left(\frac{h_0 R_0^{-\alpha}}{\sum_{i=1}^{N_b-1} h_i R_i^{-\alpha}} > \beta\right) && (1.3)\\
&= \mathbb{P}\left(h_0 > \beta R_0^{\alpha} \sum_{i=1}^{N_b-1} h_i R_i^{-\alpha}\right) && (1.4)\\
&\overset{(a)}{=} \mathbb{E}\left[\exp\left(-\beta R_0^{\alpha} \sum_{i=1}^{N_b-1} h_i R_i^{-\alpha}\right)\right] && (1.5)\\
&\overset{(b)}{=} \mathbb{E}\left[\prod_{i=1}^{N_b-1} \mathbb{E}_{h_i} \exp\left(-\beta R_0^{\alpha} h_i R_i^{-\alpha}\right)\right] && (1.6)\\
&\overset{(c)}{=} \mathbb{E}\left[\prod_{i=1}^{N_b-1} \frac{1}{1+\beta R_0^{\alpha} R_i^{-\alpha}}\right], && (1.7)
\end{aligned}$$

where (a) follows from $h_0 \sim \exp(1)$, (b) from the fact that the fading gains across interfering links are independent, and (c) from $h_i \sim \exp(1)$. For further simplification, we need the distribution of the distances $\{R_i\}$ of the serving BS and the interferers to the randomly chosen mobile user. These in turn depend upon the spatial model of the BS locations and the cell selection rule. We first specialize the analysis to the hexagonal grid model in the following subsection.

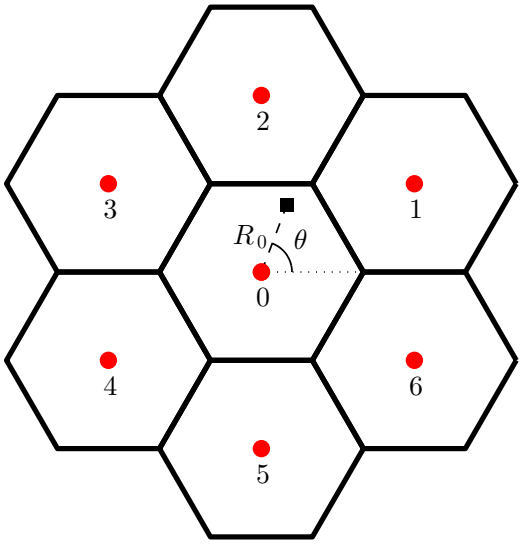

Figure 1.2: Seven-cell hexagonal grid model with BSs denoted by red dots. A randomly selected user in the center cell is depicted by a square. It lies at a distance R_0 from the center BS and forms angle θ with the horizontal axis.

1.2.2 Coverage Probability using Hexagonal Grid Model

For simplicity, consider a seven-cell version of the grid model shown in Figure 1.2, where the interference field is limited to the first ring of interferers. Note that limiting the interference field to first or at most second ring of interferers is a common practice in literature [8]. The inter-site distance is assumed to be D. We assume maximum average power based cell selection, where each user lying in a particular hexagon is served by the BS lying at the center of that hexagon. For downlink analysis, a user uniformly distributed in the center cell is selected, as shown in Figure 1.2. In addition to its distance to the serving BS, its location is characterized by the angle θ it makes with the horizontal axis, with the origin being the BS corresponding to the center

cell. For this setup, the distance of the chosen user to the i^{th} interferer can be expressed as

$$R_i = \sqrt{(D\cos\theta_i - R_0\cos\theta)^2 + (D\sin\theta_i - R_0\sin\theta)^2}, \tag{1.8}$$

with θ_i being the angle formed by the location of the i^{th} interferer with horizontal axis. The values of θ_i for all the six interferers are as follows: $\theta_1 = \frac{\pi}{6}, \theta_2 = \frac{\pi}{2}, \theta_3 = \frac{5\pi}{6}, \theta_4 = \frac{7\pi}{6}, \theta_5 = \frac{3\pi}{2}$ and $\theta_6 = \frac{11\pi}{6}$. Clearly R_i is random because of its dependence on R_0 and θ. The general coverage probability expression given by (1.7) can be specialized for this case to

$$\mathtt{P_c} = \mathbb{E}_{R_0,\theta}\left[\prod_{i=1}^{6} \frac{1}{1+\beta R_0^{\alpha}\left((D\cos\theta_i - R_0\cos\theta)^2 + (D\sin\theta_i - R_0\sin\theta)^2\right)^{-\frac{\alpha}{2}}}\right], \tag{1.9}$$

where the expectation is with respect to the joint distribution of R_0 and θ. Due to the complexity of this expression, it is not possible to reduce it any further, even under further simplifications, e.g., approximating the hexagonal cell as a circle [9]. The only way forward is to numerically solve this expression, which in this case is the same as simulating the network deployment. This is primarily the reason why the hexagonal grid model is typical termed *intractable* for downlink analysis [1]. Also note that, with the increasing complexity of cellular networks due to the addition of several types of low-power BSs, the number of simulation scenarios and hence the complexity of system level simulations is also becoming increasingly prohibitive, thereby motivating the need for tractable models, which is the main focus of this dissertation. A preview of the new approach is provided in the next subsection.

1.2.3 Coverage Probability using Random Spatial Model

We now discuss a relatively less accepted approach of modeling BS locations, where instead of putting a rigid stricture as in the hexagonal grid model, the BS locations are endowed with a probability distribution [1–4]. In particular, the BS locations are sampled from a PPP. This enables the use of powerful tools from stochastic geometry to derive simple expressions for key performance metrics such as coverage probability. Although this idea will be applied to much general setups in the following chapters, in this section we continue with the same simple setup as above. The goal is to specialize (1.7) for this new modeling approach. Please refer to [1] for a detailed exposition of coverage probability for this single-tier setup.

Assume that the BS locations are modeled by a homogeneous PPP Φ with density λ, as shown in Figure 1.3. The users are also modeled by an independent PPP. Without loss of generality, the downlink analysis is conducted at the typical mobile user located at the origin. To be consistent with the assumptions made for the hexagonal case above, assume that the typical user connects to the BS that provides the maximum average received power, i.e., the one that is closest to the origin. Using null probability of a PPP, the distribution of the distance of the typical user to the serving BS is

$$f_{R_0}(r_0) = 2\pi\lambda r_0 \exp(-\lambda\pi r_0^2). \tag{1.10}$$

Using the same approach as [1], the coverage probability expression

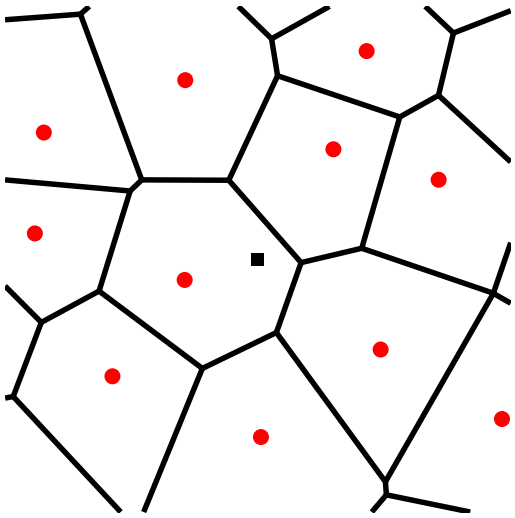

Figure 1.3: The red dots represent BS locations sampled from a PPP. The typical user is represented by a square.

(1.7) can be simplified using simple tools from stochastic geometry as follows:

$$\mathtt{P_c} = \int_0^\infty \mathbb{E}_\Phi \left[\prod_{\substack{x_i \in \Phi \\ \|x_i\| > r}} \frac{1}{1+\beta r^\alpha \|x_i\|^{-\alpha}} \right] f_{R_0}(r)\mathrm{d}r \tag{1.11}$$

$$\overset{(a)}{=} \int_0^\infty \exp\left(-2\pi\lambda \int_r^\infty 1 - \frac{1}{1+\beta r^\alpha u^{-\alpha}} u \mathrm{d}u \right) f_{R_0}(r)\mathrm{d}r \tag{1.12}$$

$$\overset{(b)}{=} \int_0^\infty \exp\left(-\pi\lambda r^2 \beta^{\frac{2}{\alpha}} \int_{\beta^{-\frac{2}{\alpha}}}^\infty \frac{1}{1+v^{\frac{\alpha}{2}}} \mathrm{d}v \right) f_{R_0}(r)\mathrm{d}r \tag{1.13}$$

$$\overset{(c)}{=} \int_0^\infty \exp\left(-\pi\lambda r^2 \rho(\alpha,\beta) \right) f_{R_0}(r)\mathrm{d}r \tag{1.14}$$

$$\overset{(d)}{=} \frac{1}{1+\rho(\alpha,\beta)}, \tag{1.15}$$

where (a) follows from the probability generating functional (PGFL) of a PPP, (b) follows by the substitution $\beta^{-\frac{2}{\alpha}} r^{-2} u^2 \to v$, (c) by defining a constant $\rho(\alpha,\beta) = \beta^{\frac{2}{\alpha}} \int_{\beta^{-\frac{2}{\alpha}}}^\infty \frac{1}{1+v^{\frac{\alpha}{2}}} \mathrm{d}v$, and (d) follows by substituting the distribution

of R_0. Interestingly, the coverage probability in this case reduces to a closed form expression, hence circumventing the need for simulation. Such simple expressions are useful to gain key system design insights. For instance, the above expression clearly shows that the coverage probability is independent of the density of the BSs when the cellular network is interference limited. We leave more such insights, in significantly more general setups, for the following chapters.

From the above discussion, it is evident that the new approach is significantly more tractable than the state-of-the-art deterministic grid model. However, the idea of modeling the BS locations with a stochastic process may seem questionable to certain readers, especially because the grid-based models have been deeply ingrained in the cellular industry for over three decades. In the following sections, we address these doubts by explaining why heterogeneity and uncertainty in cellular networks is inevitable while handling the changing usage trends, especially the rising mobile data traffic, and why random spatial models are especially attractive to study these new and more complex cellular networks.

1.3 Changing Usage Trends and 1000x Capacity Goal

Although cellular networks have been designed and optimized primarily for voice-centric applications over the past three decades, the popularity of advanced communication devices, such as smartphones, laptops and most recently tablets, has shifted the focus rather quickly towards data-hungry ap-

plications, such as, live streaming of high definition videos, mobile television, and symmetric video calls [10]. A direct implication of this social change is a much sharper increase in mobile data traffic compared to the past. For instance, the global mobile data traffic has more than doubled in 2012 for the fifth consecutive year, and this trend is expected to continue for at least a few years more [10]. A straightforward calculation reveals around 1000x increase in capacity of cellular networks required over a decade. This has in fact been acknowledged as the main goal by the cellular industry, e.g., by 3GPP [11], and Qualcomm's "1000x data challenge". However, increasing the capacity at such a rapid rate is challenging and requires a fundamental change in the way cellular networks are designed and deployed. Several possible approaches to cope up with this data deluge are discussed below.

Improving spectral efficiency. First and somewhat obvious direction towards improving the capacity of cellular networks is by increasing the spectral efficiency (bps/Hz) of the wireless links by using advanced physical layer techniques, such as multiple input multiple output (MIMO), or by using smart scheduling. However, these techniques are already relatively mature, being part of multiple wireless standards such as IEEE 802.11e WiMAX and 3GPP LTE-A [12], apart from plethora of theoretical research activities in academia [13]. For instance, in case of MIMO, current LTE-A standard already supports as much as 8 antennas in the downlink and 4 in the uplink [14], leaving a little room for improvement at the current transmission frequencies, especially since the goal is a whopping 1000x gain. Furthermore, due to adap-

tive modulation and coding, the wireless links are already operating close to their theoretical limits, which further limits the gains [15].

A promising exception is that of massive MIMO, where the idea is to have hundreds or even thousands of antennas to serve tens of users simultaneously in each resource block [16, 17]. With the possibility of using the extra degrees of freedom to form very narrow beams, the theoretical gains in the throughput are undoubtedly large. Since the antenna size decreases with the increase in transmission frequency, massive MIMO systems are more meaningful at higher transmission frequencies because otherwise the size of antennas makes it impossible to pack a massive number of antennas on a reasonably sized base station (BS). This has led to an increasing interest in "millimeter-wave massive MIMO" systems with transmission frequencies proposed to be in 3-300GHz range, which are currently under active research [18, 19].

Adding more spectrum. The second main direction is to provide more spectrum to cellular systems, which relies on the fact that the capacity of a wireless link scales linearly with the signal bandwidth. As of 2013, the cellular system has around 600 MHz of licensed spectrum in the US [20], which along with 440 MHz of usable WiFi spectrum [21], makes a total spectrum of over 1 GHz. Therefore, for any meaningful capacity gains, the additional spectrum needs to be significantly higher than 1 GHz. Since the current cellular spectrum is mostly in the sub-3 GHz range, with the exception of the new WiFi spectrum added in the 5 GHz range, to avoid significant changes in the system design or hardware it is preferable that the new spectrum added to

the system is also in this range. However, additional spectrum in this range is scarce and expensive, and is hence not an attractive and cost-effective option for the service providers. If the recent auctions of 700 MHz band are any indication, service providers may have to pay around $2 per user for each additional MHz of bandwidth [22]. Although, Federal Communications Commission (FCC) is considering releasing additional 500 MHz of spectrum in this range by 2020 [23, 24], it will perhaps come at an already prohibitive cost of $1000 per subscriber, and is not even enough to provide a 2x gain in capacity.

Another possible option is to utilize the abundant non-congested spectrum in 3-300 GHz range, as discussed above for millimeter-wave massive MIMO systems. While the spectrum is inexpensive in this range, these higher transmission frequencies exhibit very different propagation characteristics, such as signal attenuation, multipath and reflection, compared to the current cellular frequencies, which necessitates fundamental changes in the system design, e.g., in the air interface [18, 25]. Additionally, these higher transmission frequencies require significant changes in the hardware, including amplifiers and transceiver architectures [25–27]. Despite these challenges, there have been some early indications of the promising future of this technology [28]. However, as is the case with any new technology, it requires time to mature and is not expected to make it to the cellular systems anytime soon.

Network densification. Third and perhaps the most realistic approach is to harness the cell splitting gain by densifying the network, i.e., reduce the frequency reuse distance by adding more infrastructure. Historically,

most of the capacity gains in cellular networks are in fact driven by shrinking cell sizes. For instance, out of the million-fold capacity increase over the past 45 years, only about 25x is attributed to more spectrum, 5x to the division of spectrum into narrower slices, further 5x to better modulation schemes, and the remaining 1600x to the smaller cell sizes [29]. However, to cope up with the current capacity demand, we need a much more aggressive spectrum reuse than the pre-smartphone era. This is not possible exclusively with the macrocells, due to their prohibitive capital expenditure (CapEx) and high operational expenditure (OpEx). Other restrictions such as cell site availability and need for fast dedicated backhaul further limit their deployment especially in the dense urban markets where most of the data demand originates.

The inability of macrocellular networks to keep up with the rising data demands has led to the popularity of low-power BSs, collectively termed as *small cells* [30]. The small cells typically have orders of magnitude lower deployment costs, smaller transmit power and hence lower energy costs, and can be deployed organically based on the capacity demand with comparatively less cell site restrictions. With high speed wireless backhaul rapidly becoming a reality [31], there is no apparent limitation on the number of small cells that can be deployed in a given area. This means that there is no restriction on the rate at which the area spectral efficiency (bps/Hz/Km^2) can be increased, thus presenting a feasible solution to handle the current data deluge.

A cellular network consisting of different classes of BSs, such as macrocells and various types of small cells, is termed as a heterogeneous cellular

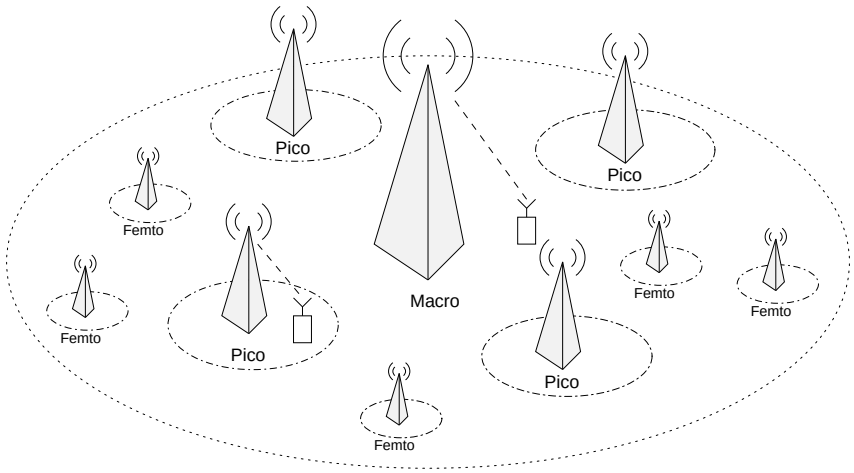

Figure 1.4: Illustration of a three-tier heterogenous network utilizing a mix of macro, pico and femtocell BSs. Only a single macro-cell is shown for the sake of simplicity.

network, or in short a *HetNet*. Due to the above mentioned advantages, HetNets have been embraced enthusiastically by the cellular industry, with their standardization activities already started in 3GPP release 10 [14]. The network operators have also started deploying small cells at "hot-spots", i.e., places of high user density, such as airports, to augment the capacity of macrocellular networks, and at "not-spots" to fill the coverage holes. Various features of HetNets are under active investigation in both academia and industry, with early deployments and industry predictions indicating fairly promising gains [32–34]. In the next section, we take a closer look at this new network paradigm and motivate the need for rethinking the way cellular networks are perceived and modeled. The focus will be on highlighting the increasing relevance of random spatial models, especially to capture the irregular deployments of small cells.

1.4 Increasing Relevance of Random Spatial Models

Cellular networks are becoming increasingly complex due to the deployment of multiple classes of BSs that have distinctly different traits [35,36]. For example, a typical 3G or 4G cellular network already has traditional macrocellular BSs that are long-range and guarantee near-universal coverage; operator-managed picocells [37, 38] and distributed antennas [39–42] that have a more compact form factor, a smaller coverage area, and are used to increase capacity while eliminating coverage deadzones; and femtocells, which have emerged more recently and are distinguished by their end-user installation in arbitrary locations, very short range, and possibility of having a closed-subscriber group [29, 43, 44]. A typical HetNet utilizing a mix of macro, pico and femtocells is illustrated in Figure 1.4. This evolution toward heterogeneity will continue to accelerate due to crushing demands for mobile data traffic caused by the proliferation of data-hungry devices and applications.

An immediate effect of the increasing heterogeneity and uncertainty of current deployments on the study of cellular networks is that it has limited the applicability of classical cellular models based mainly on the regularity assumption of BS locations, such as deterministic grid-based models [7] and Wyner model [45], to HetNets. For instance, consider Figure 1.5, where we compare the hexagonal grid model with the actual 4G deployment in a sprawling land-locked city, and a typical 2-tier deployment. While the actual single tier deployment already deviates significantly from the deterministic grid model, the addition of small cells changes the coverage footprints dramatically.

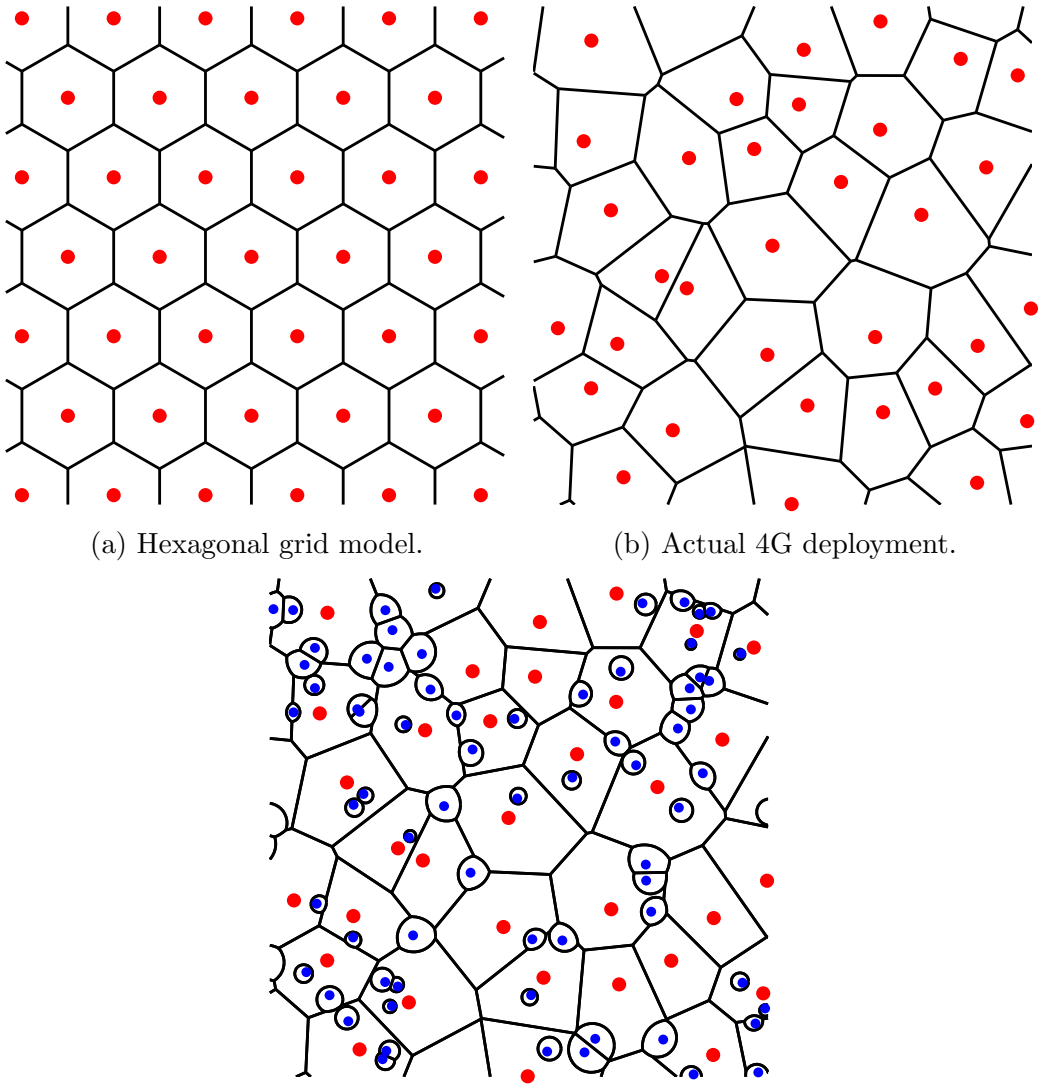

(a) Hexagonal grid model.

(b) Actual 4G deployment.

(c) Two tier HetNet.

Figure 1.5: (a) Hexagonal grid model with the locations of macrocells indicated by red circles. (b) Coverage regions with macrocell locations drawn from an actual 4G deployment [1]. (c) Coverage regions in a two tier HetNet with macrocell following the same locations as in (b), and small cells (denoted by smaller circles) overlaid randomly.

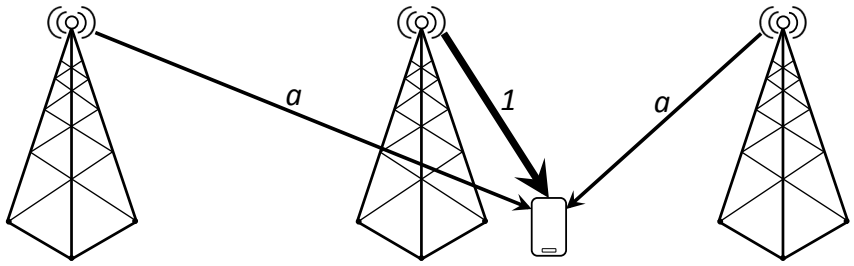

Figure 1.6: Illustration of Wyner model, where the channel gain from the desired BS is normalized to one, and channel gain from each interfering BS is modeled as a constant $a < 1$.

Mathematically, as discussed in detail in Chapter 2, the coverage plots in case of HetNets can no longer be characterized by a standard Voronoi tessellation due to the differences in the transmit powers across different classes of BSs [5]. Instead, they closely resemble a *circular Dirichlet tessellation*, also called a multiplicatively weighted Voronoi diagram [46]. Comparing Figures 1.5a and 1.6, we note that the Wyner model is even more simplistic. We will revisit this comparison in Chapter 2.

As evident from Figure 1.5, the experience of mobile users in terms of coverage, rate, and reliability would be quite different in the HetNets as compared to the familiar macrocellular networks. To capture key characteristics of HetNets and facilitate a realistic performance evaluation, we propose a new and more appealing way of modeling HetNets by using random spatial models, where the locations of the BSs are assumed to form a realization of a spatial point process [1–4, 47]. In comparison to the conventional models, these are especially attractive in the context of HetNets due to their: (i) realism: to capture the inherent uncertainty in deployments involving both operator and user

deployed BSs, (ii) scalability: to model ever-increasing heterogeneity in the infrastructure elements and, (iii) tractability: to gain system design insights using tools from stochastic geometry, as demonstrated for a simple single-tier setup earlier in this chapter in Section 1.2.

1.5 Contributions

There are two main challenges in understanding HetNets: (i) to develop system models that capture the heterogeneity in infrastructure, irregularity in the BS locations, and other key characteristics of these networks with enough accuracy to be realistic but enough simplicity to be useful, and (ii) to develop corresponding analytical frameworks to study metrics like outage probability as a function of an arbitrary `SINR`, loading across different tiers, and average rate, with the end goal of better understanding the fundamental system design principles for HetNets. This dissertation develops a comprehensive framework to tackle these challenges. The main contributions are summarized below.

New tractable model for K-tier HetNets. In Chapter 2, we develop a tractable, flexible, and accurate model for a downlink HetNet consisting of K tiers of randomly located BSs, where each tier may differ in terms of average transmit power, supported data rate and BS density. Assuming a mobile user connects to the strongest candidate BS in terms of received power and a fairly general channel model, we derive an expression for the probability of coverage (equivalently outage) over the entire network under both open and closed access. It assumes a strikingly simple closed-form when the resulting

SINR is greater than 1 and the background noise is neglected. For external validation, we compare against an actual LTE network (for tier 1) with the other $K-1$ tiers being modeled as independent PPPs and show that the closed form expression is accurate down to about -4 dB. We further derive the average rate achieved by a typical mobile and the average load on each tier of BSs. One interesting observation for interference-limited open access networks is that at a given SINR, adding more tiers and/or BSs neither increases nor decreases the coverage probability when all the tiers have the same target-SINR.

Incorporating load in random spatial models for HetNets. A major limitation of the K-tier model proposed in Chapter 2 and all its extensions [48–56] so far is the neglect of network traffic and load: all BSs are assumed to always be transmitting. Small cells in particular will have a lighter load than macrocells, and so their contribution to the network interference is probably significantly overstated in a fully loaded model. Chapter 3 incorporates a flexible notion of BS load by introducing a new idea of *conditionally thinning* the interference field. For a K-tier HetNet model developed in Chapter 2 where BSs across tiers differ in terms of transmit power, supported data rate, deployment density, and now load, we derive the coverage probability for a typical mobile, which connects to the strongest BS signal. Conditioned on this connection, the interfering BSs of the i^{th} tier are assumed to transmit independently with probability p_i, which models the load. Our analysis concretely demonstrates that the coverage probability always increases when lightly loaded small cells are added to the existing macrocellular networks.

This is a useful rebuttal to the viewpoint that unplanned infrastructure might bring down a cellular network due to increased interference.

Modeling non-uniform user distributions. In Chapters 2 and 3, the analysis is performed at a typical user located at the origin assuming user distribution to be uniform. At least one shortcoming of this approach is its inability to model non-uniform user distributions, especially when there is dependence in the user and the BS locations. To facilitate analysis in such cases, we develop a new method of sampling users by using the same idea of *conditionally thinning* the BS point process as in Chapter 3 and show that the resulting framework can be used as a tractable generative model to study current capacity-centric deployments, where the users are more likely to lie closer to the BSs. Since this analysis is a direct application of the ideas developed in Chapter 3, we present it in Appendix B.

Modeling and performance analysis of MIMO HetNets. Due to the relative maturity of both multiple antenna technique and HetNets, both in academic research and cellular standards, it is clear that the two will coexist and complement each other in the future wireless standard. Therefore, we extend the baseline model developed in Chapter 2 to study multi-antenna HetNets in Chapter 4. In addition to the transmit power, target `SIR` and deployment density, the BSs across tiers may differ in terms of the number of transmit antennas and the type of multi-antenna transmission. In particular, we consider and compare space division multiple access (SDMA), single user beamforming (SU-BF), and baseline single-input single-output (SISO) trans-

mission. For this general model, the main contributions are (i) ordering results for both coverage probability and per user rate in closed form for any BS distribution for the three considered techniques, using novel tools from stochastic orders, (ii) upper bounds on the coverage probability assuming a Poisson BS distribution, and (iii) a comparison of the area spectral efficiency (ASE). The analysis concretely demonstrates, for example, that for a given total number of transmit antennas in the network, it is preferable to spread them across many single-antenna BSs vs. fewer multi-antenna BSs. Another observation is that SU-BF provides higher coverage and per user data rate than SDMA, but SDMA is in some cases better in terms of ASE.

Generalized cell selection model and effect of shadowing on downlink SIR and rate distributions. All the prior work on random spatial models for HetNets, including Chapters 2 and 3, either ignores the impact of channel randomness on cell selection or lumps all the sources of randomness into a single variable, with cell selection based on the instantaneous signal strength, which is unrealistic. In Chapter 5, we consider both small-scale fading and long-term shadowing, and characterize the downlink SIR and rate distributions at a typical user, where shadowing, following any general distribution, impacts cell selection while fading does not. As an application of the results, we study the impact of shadowing on load balancing in terms of the optimal per-tier selection bias needed for rate maximization. We show that in certain regimes shadowing naturally balances load across various tiers and hence reduces the need for artificial cell selection bias.

Fundamentals of HetNets with energy harvesting. The possibility of having a self-powered BS is becoming realistic due to several parallel trends, such as the increasing relevance of low-power BSs, and the cost effectiveness of energy harvesting techniques, such as solar power, due both to technological improvements as well as market forces, e.g., increasing costs and taxes on conventional power sources, and subsidies and regulatory pressure for greener techniques. In Chapter 6, we develop a new tractable model for K-tier HetNets, where each BS is powered solely by a self-contained energy harvesting module. The BSs across tiers differ in terms of the energy harvesting rate, energy storage capacity, transmit power and deployment density. Since a BS may not always have enough energy, it may need to be kept OFF and allowed to recharge while nearby users are served by neighboring BSs that are ON. We show that the fraction of time a k^{th} tier BS can be kept ON, termed *availability* ρ_k, is a fundamental metric of interest. Using tools from random walk theory, fixed point analysis and stochastic geometry, we characterize the set of K-tuples $(\rho_1, \rho_2, \dots \rho_K)$, termed the *availability region*, that is achievable by general uncoordinated operational strategies, where the decision to toggle the current ON/OFF state of a BS is taken independently of the other BSs. If the availability vector corresponding to the optimal system performance, e.g., in terms of rate, lies in this availability region, there is no performance loss due to the presence of unreliable energy sources. As a part of our analysis, we model the temporal dynamics of the energy level at each BS as a birth-death process, derive the energy utilization rate, and use hitting/stopping time analysis to

prove that there exists a fundamental limit on ρ_k that cannot be surpassed by any uncoordinated strategy.

1.6 Organization

The technical contributions of this dissertation are covered in Chapters 2 through 6. Chapter 2 describes a novel baseline downlink model for the analysis of K-tier HetNets. Simple expressions for the downlink coverage and rate experienced by a typical user are derived using tools from stochastic geometry. Chapter 3 extends the baseline model and proposes a flexible load model for HetNets by introducing a new idea of conditional thinning. In Appendix B, the same idea of conditional thinning is used to develop a tractable generative model for current capacity-centric deployments, where the users are more likely to lie closer to the BSs. Chapter 4 studies multi-antenna HetNets, where the number of transmit antennas and the transmission strategy may differ across tiers. New tools with foundations in stochastic orders are developed to compare the performance of various multi antenna transmission strategies. Chapter 5 presents a generalized cell selection model that differentiates between small-scale fading and long-term shadowing. Downlink rate distribution at a typical user is characterized assuming shadowing, following any general distribution, impacts cell selection while fading does not. The final contribution of this dissertation is presented in Chapter 6, where we study HetNets with self-power BSs that may additionally differ across tiers in terms of energy harvesting rate and energy storage capacity. A new notion of avail-

ability region is introduced to study the "optimality" of such networks. The dissertation concludes with Chapter 7, which summarizes the key contributions and discusses promising future directions of research in HetNets.

Chapter 2

Modeling and Analysis of K-Tier Downlink HetNets

A straightforward unifying model for HetNets would consist of K spatially and spectrally coexisting tiers, where each tier is distinguished by its transmit power, base station (BS) density, and data rate. For example, traditional BSs (first tier) would typically have a much higher transmit power and lower density and offered rate than the lower tiers (e.g. pico and femtocells). To visualize what the coverage areas in such a network might look like, consider Figures 2.1-2.4, which show average power-based (equivalently average `SINR`-based) coverage regions for some plausible two and three tier networks. Clearly, the coverage, rate, and reliability that mobile users experience in such networks can be expected to be quite different than in traditional cellular networks that use familiar models like the hexagonal grid.

The objective of this chapter is to provide a flexible baseline model for HetNets, and to show how it can be used to provide tractable and reasonably accurate analysis of important metrics like the `SINR` statistics, outage probability and average rate. Those familiar with cellular network analysis will recognize that this goal is fairly ambitious since such results have been hard

to come by even for traditional single tier cellular networks.

2.1 Related Work and Motivation

The study and design of conventional one-tier cellular networks has often tended towards two extremes. For analysis and academic research, very simplistic models are typically employed in order to maintain tractability, while for design and development (e.g. in industry) complex system-level simulations with a very large number of parameters are generally used. This has made it difficult to estimate the actual gain that new techniques developed by researchers might provide in real systems. Well-known examples include multiuser detection [57], multiuser MIMO [58], and BS cooperation [59,60]; all of which promised much larger gains in theory than have been achieved thus far in practice [61, 62].

A popular analytical model for multicell systems is the Wyner model [45], which assumes channel gains from all (usually only 1 or 2) interfering BSs are equal and thus constant over the entire cell. Such a model does not distinguish between cell edge and interior users and in most cases does not even have a notion of outage since `SINR` is fixed and deterministic. It can be tuned to reasonably model average metrics in a system with lots of averaging, such as the CDMA uplink, but is not accurate in general and particularly for systems with 1 or 2 strong interferers, like a typical OFDMA-based 4G network [63]. Another common approach is to consider only a small number of interfering cells (as few as one) and abstract the desired and interfering

BSs to an interference channel [64, 65]. Finally, perhaps the most popular and accepted model is the two-dimensional hexagonal grid model. The grid model is frequently used as the basis of system-level simulations but analysis is not generally possible [66–68]. This was also demonstrated in Chapter 1. Additionally, both the scalability and the accuracy of grid model are questionable in the context of network heterogeneity (see Figures 2.1-2.4).

A less accepted model is to allow the locations of the BSs to be drawn from a stochastic point process [2–4]. Such a model seems sensible for femtocells – which will take up unknown and unplanned positions – but perhaps dubious for the higher tiers which are centrally planned. Nevertheless, as Figures 2.1-2.4 show, the difference between randomly placed and actual planned locations may not be as large as expected, even for tier 1 macro BSs. Indeed, the recent work [1] showed that for a one-tier network, even with the BS locations drawn from a Poisson Point Process (PPP), the resulting network model is about as accurate as the standard grid model, when compared to an actual 4G network. Importantly, such a model allows useful mathematical tools from stochastic geometry to be brought to bear on the problem [69–72], allowing a tractable analytical model that is also accurate.

2.2 Contributions and Outcomes

General K-tier downlink model. In Section 2.3, we define a tractable model for downlink multi-tier networks that captures many (but not all) of the most important network parameters. The model consists of K indepen-

dent tiers of PPP distributed BSs, where each tier may differ in terms of the average transmit power, the supported data rate, and the BS density (the average number of BSs per unit area). The plausibility of the model versus planned tiers is verified through comparisons in Section 2.6 with an actual 4G macro-cell (1 tier) network with randomly placed lower tiers.

SINR distribution, coverage probability ($\mathtt{P_c}$), outage probability ($1-\mathtt{P_c}$). Assuming (i) a mobile user connects to the strongest candidate BS, (ii) that the resulting Signal-to-Interference-plus-Noise-Ratio (SINR) is greater than 1 when in coverage, and (iii) Rayleigh fading, we derive an expression for the probability of coverage (equivalently outage) over the entire network under both open and closed access, which allows a remarkably simple closed-form in the high SINR regime (where interference power dominates noise power) and is shown to be accurate down to -4dB even under weaker assumptions. When all tiers have the same target SINR threshold, the coverage probability is the complementary cumulative distribution function (CCDF) of effective received SINR for an arbitrary randomly located mobile user. For completeness, in Appendix A we derive general expression for the probability of coverage that is applicable to any given target SINR, i.e., the assumption $\mathtt{SINR} > 1$ is relaxed. This generalization, however, comes at a significant loss of tractability.

Average data rate in coverage, ergodic rate and load per tier. We derive the average data rate experienced by a randomly chosen mobile when it is in coverage, assuming interference is treated as noise but otherwise that the Shannon bound is achieved, i.e. the average rate in coverage is $\mathbb{E}[\log(1+$

SINR)|coverage]. This expression is readily computable but involves an integral so is not closed-form. Using the general coverage probability result derived in Appendix A, an exact expression for ergodic rate, i.e., $\mathbb{E}[\log(1+\mathtt{SINR})]$, is also derived.

We also provide the average load per tier, which is the average fraction of users served by the BSs belonging to a particular tier or equivalently the probability that a mobile user is served by that tier. In line with intuition, the per-tier load is directly proportional to the density of its BSs and their average transmit power, and inversely proportional to its SINR target.

Key design insights. Some interesting observations can be made from these results. For example, we show that when the SINR targets are the same for all tiers in a dense network (thermal noise power negligible compared to interference power), the coverage (and hence outage) probability does not depend upon the number of tiers or the density of BSs in open access, but that $\mathtt{P_c}$ generally decreases with both in closed-access. This means that the trend towards increased density and heterogeneity and the resulting increase in interference need not reduce the typical SINR, as is commonly feared. On the contrary, aggregate network throughput will increase linearly with the number of BSs since the SINR statistics will stay the same per cell.

2.3 System Model

We model a HetNet as a K-tier cellular network where each tier models the BSs of a particular class, such as those of femtocells or pico-cells. The BSs

across tiers may differ in terms of the transmit power, the supported data rate and their spatial density. We assume that the BSs in the i-th tier are spatially distributed as a PPP Φ_i of density λ_i, transmit at power P_i, and have a SINR target of β_i. More precisely a mobile can reliably communicate with an i^{th} tier BS located at $x_i \in \Phi_i$ only if its downlink SINR with respect to that BS is greater than β_i. Thus, each tier can be uniquely defined by the tuple $\{P_i, \beta_i, \lambda_i\}$.

The mobiles are also modeled by an independent PPP Φ_m of density λ_m. Without loss of generality, we conduct analysis on a typical mobile user located at the origin. The fading (power) between a BS located at point x and the typical mobile is denoted by h_x and is assumed to be i.i.d exponential (Rayleigh fading). More complex channel distributions can be considered in this framework, e.g. in [1] a general interference fading model capable of handling any statistical distribution was used, and using the Fourier integral techniques in [73] general fading to the selected BS can also considered. The standard path loss function is given by $l(x) = \|x\|^{-\alpha}$, where $\alpha > 2$ is the path loss exponent. Hence, the received power at a typical mobile user from a BS located at point $x_i \in \Phi_i$ is $P_i h_{x_i} \|x_i\|^{-\alpha}$, where $h_{x_i} \sim \exp(1)$. The resulting SINR expression assuming the user connects to this BS is

$$\texttt{SINR}(x_i) = \frac{P_i h_{x_i} \|x_i\|^{-\alpha}}{\sum_{j=1}^{K} \sum_{x \in \Phi_j \setminus x_i} P_j h_x \|x\|^{-\alpha} + \sigma^2}, \tag{2.1}$$

where σ^2 is the constant additive noise power. One of the ways to set the value of σ^2 is according to the desired received SNR at the cell-edge. We will

comment more on this in Section 2.6, where we show that self-interference dominates noise in the typical HetNets. We assume each mobile user connects to its strongest BS instantaneously, i.e., the BS that offers the highest received SINR. Mathematically the typical node at the origin is in coverage if

$$\max_{x \in \Phi_i} \texttt{SINR}(x) > \beta_i,$$

for some $1 \leq i \leq K$. An assumption that greatly simplifies the analysis is that $\beta_i > 1$ (0 dB). Lemma 1 shows that under this assumption, at most one BS in the entire network can provide SINR greater than the required threshold. Although some users in commercial cellular networks indeed have operating SINR below 0 dB, they are in a distinct minority (cell edge users) and in Section 2.6 we show numerically that this model holds very accurately at least to -4 dB, which covers cell edge users as well. As demonstrated in Appendix A, the relaxation of this assumption entails significant loss in tractability. Therefore, for the simplicity of exposition, we will assume $\beta_i > 0$ dB for all the tiers in the rest of the chapter, with the corresponding general results given in Appendix A. The following Lemma characterizes the number of potential BSs that a mobile can connect to and will be used in the later sections.

Lemma 1. *Given positive real numbers* $\{a_1, a_2 \dots a_n\}$*, which correspond to the received power from each BS at the typical mobile user and defining* $c_i = \frac{a_i}{\sum_{j \neq i} a_j + \sigma^2}$*, which corresponds to the* SINR *of the* i^{th} *BS, at most* m c_i*'s can be greater than* $1/m$ *for any positive integer* m*.*

Proof. Since $\texttt{SINR} < \texttt{SIR}$ for all the BSs, defining $b_i = \frac{a_i}{\sum_{j \neq i} a_j}$ as the $\texttt{SIR}$ corresponding to the i^{th} BS, it suffices to show that at most m b_i's can be greater than $1/m$ for any positive integer m. This is shown below.

$$\begin{aligned} b_i = \frac{a_i}{\sum_{j \neq i} a_j} &= \frac{a_i}{\sum_j a_j - a_i} \\ \Rightarrow \frac{b_i}{1 + b_i} &= \frac{a_i}{\sum_j a_j} \\ \Rightarrow \sum_{i=1}^{n} \frac{1}{1/b_i + 1} &= 1. \end{aligned} \tag{2.2}$$

We first prove the result for $m = 1$ (by contradiction) and then show that it can be trivially extended to the case of general m. We first observe that (2.2) is satisfied if only one of the b_i's is greater than 1. Now assume that two b_i's are greater than one and without loss of generality, assume that they are b_1 and b_2. This implies $1/b_1$ and $1/b_2 \in (0, 1)$. Therefore, $\frac{1}{1/b_i+1}$ and $\frac{1}{1/b_i+1} \in (1/2, 1)$. Thus,

$$\begin{aligned} \sum_{i=1}^{n} \frac{1}{1/b_i + 1} &= \sum_{i=1}^{2} \frac{1}{1/b_i + 1} + \sum_{i=3}^{n} \frac{1}{1/b_i + 1}, \\ &> 1 + \sum_{i=3}^{n} \frac{1}{1/b_i + 1}, \end{aligned} \tag{2.3}$$

which is in contradiction with (2.2). Since (2.2) does not even hold for two b_i's greater than one, it proves that the only one of the b_i's can be greater than one. Similarly for the case of general m, it is easy to observe that (2.2) is trivially satisfied if at most m of the b_i's are greater than $1/m$. Now assume that $m + 1$ b_i's are greater than $1/m$ and without loss of generality, assume

that they are $b_1, b_2, \ldots, b_{m+1}$. Proceeding as in (2.3),

$$\sum_{i=1}^{n} \frac{1}{1/b_i + 1} > 1 + \sum_{i=m+2}^{n} \frac{1}{1/b_i + 1}, \tag{2.4}$$

which is in contradiction to (2.2). Therefore, at most m b_i's can be greater than $1/m$. □

2.3.1 Coverage Regions

Before going into the analysis and main results, it may be helpful to first build some intuition about the proposed model, and its resulting coverage regions. The illustrative HetNet coverage regions can be visually plotted in two steps, resulting in Figures 2.1-2.4. First, we randomly place K different types of BSs on a 2-D plane according to the aforementioned independent PPPs. Ignoring fading, the space is then fully tessellated following the maximum `SINR` connectivity model, which is equivalent to maximum `SIR` and maximum power connectivity models in the absence of fading. Please note that in reality the cell boundaries are not as well defined as shown in these coverage regions due to fading. Therefore, these plots can be perceived as the average coverage footprints over a period of time so that the effect of fading is averaged out. Due to the differences in the transmit powers over the tiers, these average coverage plots do *not* correspond to a standard Voronoi tessellation (also called a Dirichlet tessellation) [74]. Instead, they closely resemble a *circular Dirichlet tessellation*, also called a multiplicatively weighted Voronoi diagram [46]. The coverage regions for a two-tier network – for example comprising macro and

femtocells – are depicted in Figures 2.1 and 2.2 for two cases: 1) the macro-cell BSs are distributed according to PPP (our model), and 2) the macro-cell BSs correspond to an actual 4G deployment over a relatively flat urban region. The femtocells are distributed according to an independent PPP in both cases. Qualitatively, the coverage regions are quite similar in the two cases.

In Figures 2.3 and 2.4, the coverage regions are now shown with an additional pico-cell tier. As is the case in the actual networks, we assume that the macro-cells have the highest and the femtocells have the lowest transmit power, with pico-cells somewhere in between. For example, in LTE [75], typical values are on the order of 50W, .2W, and 2W, respectively. Therefore, femtocell coverage regions are usually much smaller than the other two tiers, particularly when they are nearby a higher power BS. Similarly, we observe that the coverage footprint of pico-cells increases when they are farther from the macro BSs. These observations highlight the particularly important role of smaller cells where macrocell coverage is poor.

2.3.2 Applicability of the Model

The model is applicable both to non-orthogonal (CDMA) and orthogonal (TDMA, OFDMA) cellular networks. For CDMA networks, although the *received* `SINR` is generally much smaller than 1, the post-despreading `SINR`, which is what determines coverage/outage, is often greater than or at least close to 1, so the assumption $\beta_i > 1$ and Lemma 1 are still reasonable if the interference term is divided by the spreading factor. The analysis is for

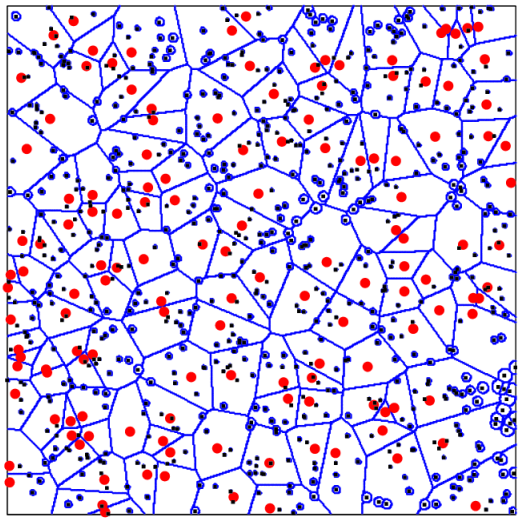

Figure 2.1: Coverage regions in a two-tier network as per the model used in this chapter. Both macro (large circles) and femto (small dark squares) BSs are distributed as independent PPPs with $P_1 = 1000P_2$ and $\lambda_2 = 5\lambda_1$.

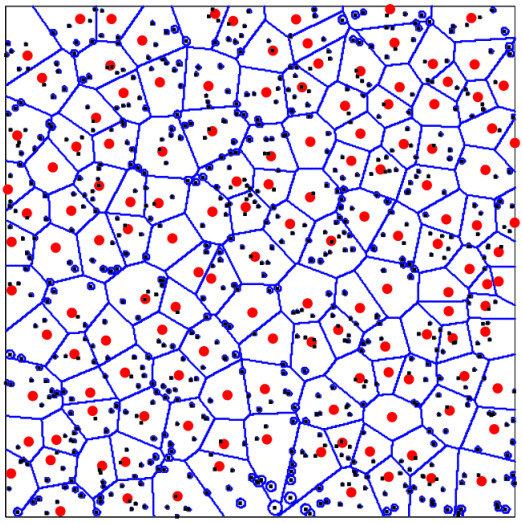

Figure 2.2: Coverage regions in a two-tier network where Macro (tier-1) BS locations (large circles) correspond to actual 4G deployment. Femto BSs (small dark squares) are distributed as a PPP ($P_1 = 1000P_2$ and $\lambda_2 = 5\lambda_1$).

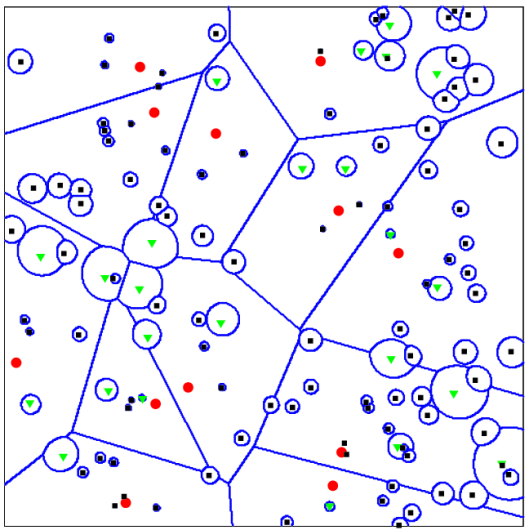

Figure 2.3: Close-up view of coverage regions in a three-tier network. All the tiers, i.e., tier-1 macro (large circles), tier-2 pico (light triangles) and tier-3 femto (small dark squares), are modeled as independent PPPs. $P_1 = 100P_2 = 1000P_3$, $\lambda_3 = 4\lambda_2 = 8\lambda_1$.

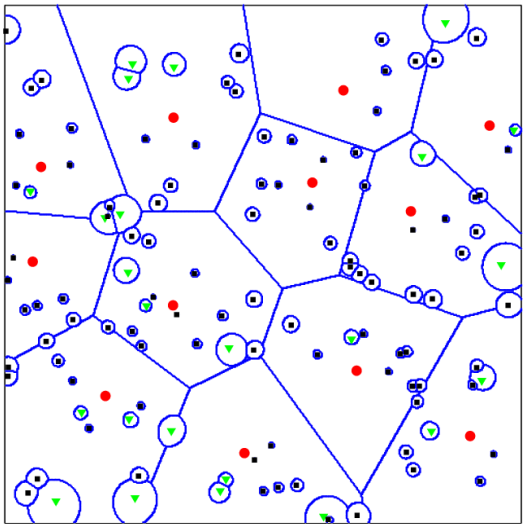

Figure 2.4: Coverage regions in a three-tier network where macro BS locations (large circles) now correspond to actual 4G deployment. Other parameters are same as Figure 2.3.

a single frequency band and assumes that all BSs are transmitting continuously in all time slots at constant power, although if some fraction f of time slots were not used (at random), then the resulting density of interfering BSs would simply be $(1-f)\lambda$ and the analysis could be extended. In OFDMA-based networks, it is desirable to move strongly interfering neighbors or tiers to orthogonal resources in time and/or frequency and so the coverage can be improved. Similarly, additional enhancements like opportunistic scheduling or multiple antenna communication should increase coverage and/or rate and this framework could be extended to indicate the gains of different approaches. Although we do not explicitly consider antenna sectoring, it can be easily incorporated in the current model if sectoring is done randomly. If the beam is partitioned into n equal sectors, the density of interfering BSs reduces by a factor of n because the probability that the beam of any BS would point towards a randomly chosen BS is $1/n$. Cellular engineers will note that further details are missing from this model. In addition to shadowing, we do not consider frequency reuse, power control, or any other form of interference management, leaving these to future extensions. In short, this is a baseline tractable model for HetNets.

2.4 Coverage Probability and Average Load per Tier

A typical mobile user is said to be in coverage if it is able to connect to at least one BS with `SINR` above its threshold. In the case when all the tiers have same `SINR` threshold β, coverage probability is precisely the complementary

cumulative distribution function (CCDF) of the effective received SINR, outage being the CDF, i.e., $1 - \text{CCDF}$. With this understanding, we now derive the probability of coverage for a randomly located mobile user both for *open* and *closed access* networks (defined below). Using these results, we also derive a measure of average load per tier in terms of the fraction of users served by each tier.

2.4.1 Open Access

We first assume the open access strategy where a typical mobile user is allowed to connect to any tier without any restriction. Under the current system model, this strategy reduces to choosing the strongest BS, i.e., the one that delivers the maximum received SINR.

2.4.1.1 Coverage Probability

The main result for the probability of coverage in open access networks is given by Theorem 1.

Theorem 1 (General case)**.** *When $\beta_i > 1$, the coverage probability for a typical randomly located mobile user in open access is* $\mathtt{P_c}(\{\lambda_i\},\{\beta_i\},\{P_i\}) =$

$$\sum_{i=1}^{K} \lambda_i \int_{\mathbb{R}^2} \exp\Big(- C(\alpha) \left(\frac{\beta_i}{P_i}\right)^{2/\alpha} \|x_i\|^2 \sum_{m=1}^{K} \lambda_m P_m^{2/\alpha}\Big) \exp\Big(- \frac{\beta_i \sigma^2}{P_i} \|x_i\|^{\alpha}\Big) \mathrm{d}x_i, \tag{2.5}$$

where $C(\alpha) = 2\pi^2 \csc(\frac{2\pi}{\alpha})\alpha^{-1}$.

Proof. For notational simplicity, denote the set $\{1, 2, \ldots K\}$ by $\mathcal{K}$. The cover-

age probability in a K-tier network under *maximum* SINR *connectivity model* can be derived as follows:

$$\begin{aligned}
&\mathtt{P_c}(\{\lambda_i\},\{\beta_i\},\{P_i\}) \\
&= \mathbb{P}\left(\bigcup_{i\in\mathcal{K},x_i\in\Phi_i} \mathtt{SINR}(x_i) > \beta_i\right) \\
&= \mathbb{E}\left[\mathbf{1}\left(\bigcup_{i\in\mathcal{K},x_i\in\Phi_i} \mathtt{SINR}(x_i) > \beta_i\right)\right] \\
&\overset{(a)}{=} \sum_{i=1}^{K} \mathbb{E}\sum_{x_i\in\Phi_i} \left[\mathbf{1}\left(\mathtt{SINR}(x_i) > \beta_i\right)\right] \\
&\overset{(b)}{=} \sum_{i=1}^{K} \lambda_i \int_{\mathbb{R}^2} \mathbb{P}\left(\frac{P_i h_{x_i} l(x_i) x_i)}{I_{x_i}+\sigma^2} > \beta_i\right) \mathrm{d}x_i \\
&\overset{(c)}{=} \sum_{i=1}^{K} \lambda_i \int_{\mathbb{R}^2} \mathcal{L}_{I_{x_i}}\left(\frac{\beta_i}{P_i l(x_i)}\right) e^{\frac{-\beta_i\sigma^2}{P_i l(x_i) x_i)}} \mathrm{d}x_i, \qquad (2.6)
\end{aligned}$$

where (a) follows from Lemma 1 under the assumption that $\beta_i > 1\ \forall\ i$, (b) follows from Campbell Mecke Theorem [69], and (c) follows from the fact that the channel gains are assumed to be Rayleigh distributed. Here $\mathcal{L}_{I_{x_i}}(.)$ is the Laplace transform of the cumulative interference from all the tiers when the randomly chosen mobile user is being served by the i^{th} tier. Since the point processes are stationary, the interference does not depend on the location x_i. Therefore, we denote $\mathcal{L}_{I_{x_i}}$ by $\mathcal{L}_{I_i}$, which is given by

$$\mathcal{L}_{I_i}(s) = \prod_{j=1}^{K} \mathbb{E}_{I_i}\left[\prod_{x_j\in\Phi_j/x_i} \exp\left(-sP_j h_{x_j} l(x_j)\right)\right].$$

Using the independence of the fading random variables $\mathcal{L}_{I_i}(s)$ equals

$$\begin{aligned}
&\prod_{j=1}^{K} \mathbb{E}_{\Phi_j}\left[\prod_{x_j\in\Phi_j/x_i} \mathbb{E}_h\left[\exp\left(-sP_j h_{x_j} l(x_j)\right)\right]\right] \\
&\overset{(a)}{=} \prod_{j=1}^{K} \mathbb{E}_{\Phi_j}\left[\prod_{x_j\in\Phi_j/x_i} \frac{1}{1+sP_j l(x_j)}\right] \\
&\overset{(b)}{=} \prod_{j=1}^{K} \exp\left(-\lambda_i \int_{\mathbb{R}^2}\left(1-\frac{1}{1+sP_j||x_j||^{-\alpha}}\right)\mathrm{d}x_j\right) \\
&\overset{(c)}{=} \prod_{j=1}^{K} \exp\left(-2\pi\lambda_i (sP_j)^{2/\alpha}\int_0^\infty r\int_0^\infty e^{(-t(1+r^\alpha))}\mathrm{d}t\ \mathrm{d}r\right), \qquad (2.7)
\end{aligned}$$

where (a) follows from the Rayleigh fading assumption (i.e., $h\sim\exp(1)$), (b) follows from probability generating functional (PGFL) of PPP [69] and, (c) results from algebraic manipulation after converting from Cartesian to polar coordinates Using some properties of Gamma function, (2.7) can be further simplified to

$$\mathcal{L}_I(s) = \exp\left(-s^{2/\alpha}C(\alpha)\sum_{i=1}^{K}\lambda_i P_i^{2/\alpha}\right), \qquad (2.8)$$

where $C(\alpha) = \frac{2\pi^2\csc(\frac{2\pi}{\alpha})}{\alpha}$. Using (2.6) and (2.8) the coverage probability $\mathtt{P_c}(\{\lambda_i\},\{\beta_i\},\{P_i\})$ is

$$\sum_{i=1}^{K}\lambda_i\int_{\mathbb{R}^2} e^{-\left(\frac{\beta_i}{P_i}\right)^{2/\alpha}C(\alpha)||x_i||^2\sum_{m=1}^{K}\lambda_m P_m^{2/\alpha}} e^{\frac{-\beta_i\sigma^2}{P_i}||x_i||^\alpha}\mathrm{d}x_i,$$

which completes the proof. □

Theorem 1 gives a simple and fairly general expression for coverage probability. For better understanding of the proof, we now provide a brief

description of the main steps. First recall that a mobile user is in coverage if it is able to connect to at least one BS with SINR above its threshold. Now assuming, $\beta_i > 1, \forall\, i$, we know from Lemma 1 that a mobile can connect to at most one BS. Therefore, $\mathtt{P_c}$ can now be defined as the sum of the probabilities that each BS connects to the mobile (with the understanding that all the events are mutually exclusive and at most one of them happens at any time). This leads to a sum of probabilities over PPP, which can be converted to a simple integral of Laplace transform of cumulative interference using Campbell-Mecke Theorem [69]. A closed form expression for the Laplace transform can be evaluated in two main steps. Firstly, the nature of interference function (sum over PPP) leads to a product form for its Laplace transform. Using probability generating functional (PGFL) of PPP [69] and the fact that fading power is exponentially distributed, we arrive at the closed form expression for Laplace transform which directly leads to the final result of the Theorem. This result can be simplified further for the interference-limited case, where it reduces to a remarkably simple closed-form expression given by Corollary 1. When the system is interference-limited, SINR and signal-to-interference-ratio (SIR) can be used interchangeably since thermal noise is negligible compared to the interference power. However, for concreteness we will henceforth use SIR when assuming interference-limited network.

Corollary 1 (No-noise)**.** *In an interference limited network,* i.e.*, when self-interference dominates thermal noise, the coverage probability of a typical mo-*

bile user simplifies to

$$\mathtt{P_c}(\{\lambda_i\},\{\beta_i\},\{P_i\}) = \frac{\pi}{C(\alpha)} \frac{\sum_{i=1}^{K} \lambda_i P_i^{2/\alpha} \beta_i^{-2/\alpha}}{\sum_{i=1}^{K} \lambda_i P_i^{2/\alpha}}, \quad \beta_i > 1.$$

Proof. Follows from Theorem 1 with $\sigma^2 = 0$. □

The simplicity of this result leads to some important observations. Firstly, setting $K = 1$ leads to the single-tier case, where the coverage probability is given by:

$$\mathtt{P_c}(\lambda, \beta, P) = \frac{\pi}{C(\alpha)\beta^{2/\alpha}}. \tag{2.9}$$

From (2.9), we note that the $\mathtt{P_c}$ in an interference-limited single-tier network is independent of the density of the BSs, and is solely dependent upon the target SIR. This is consistent with [1], where a similar observation was made for a single-tier network using *nearest neighbor connectivity model*. The intuition behind this observation is that the change in the density of BSs leads to the change in the received and interference powers with the same factor and hence the effects cancel.

From Corollary 1, it also follows that, if $\beta_i = \beta$, $\forall\ i$, in an interference-limited network then $\mathtt{P_c}(\{\lambda_i\}, \beta, \{P_i\}) = \frac{\pi}{C(\alpha)\beta^{2/\alpha}}$. This is perhaps an unexpected result since it states that the coverage probability is not affected by the number of tiers or their relative densities and transmit powers in an interference-limited network. In fact, it is exactly the same as that of the single-tier case. Therefore, more BSs can be added in any tier without affecting the coverage and hence the net *network capacity* can be increased linearly

with the number of BSs. The intuition behind this result is that the decision of a mobile user to connect to a BS depends solely on the received SIR from that BS and a common target SIR, unlike the general case where it also depends upon the tier to which the BS belongs. Thus, the mobile user does not differentiate between the tiers when the SIR thresholds are the same. Surprisingly, this leads to a situation similar to the one discussed for the single-tier case above, where the change in the received power due to the change in the density or the transmit power of BSs of some tier is equalized by the change in the interference power. Significantly, this implies that the interference from smaller cells, such as femtos and picos, need not decrease network performance in open access networks.

2.4.1.2 Average Load per Tier

The average load on each tier is defined as the average fraction of users in coverage served by that tier. This can also be interpreted as the average fraction of time for which each mobile is connected to the BSs belonging to a particular tier. The main result for the average load per tier in *open access* is given by Proposition 1.

Proposition 1. *The average fraction of users served by j^{th} tier (also the average load on j^{th} tier) in open access is*

$$\bar{N}_j = \frac{\lambda_j}{\mathtt{P_c}(\{\lambda_i\},\{\beta_i\},\{P_j\})} \int_{\mathbb{R}^2} \exp\Big(- C(\alpha) \left(\frac{\beta_i}{P_i}\right)^{2/\alpha} ||x_i||^2 \sum_{m=1}^{K} \lambda_m P_m^{2/\alpha} \Big) \exp\Big(- \frac{\beta_i \sigma^2}{P_i} ||x_i||^{\alpha} \Big) \mathrm{d}x_i. \tag{2.10}$$

Proof. Let $B_n \in \mathbb{R}^2$ denote an increasing sequence of convex sets with $B_n \subset B_{n+1}$ and $\lim_{n\to\infty} |B_n| = \infty$. For this proof, we denote $\mathtt{SIR}_{x_m}(x_b)$ as the received $\mathtt{SIR}$ when the mobile is located at $x_m \neq 0$ connects to BS located at x_b. Please recall that the subscript is dropped and $\mathtt{SIR}$ is denoted as $\mathtt{SIR}(x_b)$ when the mobile user is located at the origin. The average fraction of users served by the j^{th} tier can now be expressed as:

$$\begin{aligned}
\bar{N}_j &= \lim_{n\to\infty} \frac{1}{|B_n|} \sum_{x_m \in B_n \bigcap \Phi_m} \mathbf{1}\left(\bigcup_{x_j\in\Phi_j} \mathtt{SINR}_{x_m}(x_j) > \beta_j \Big| \bigcup_{i\in\mathcal{K}, x_i\in\Phi_i} (\mathtt{SINR}_{x_m}(x_i) > \beta_i) \right) \\
&\overset{(a)}{=} \mathbb{P}^{!o}\left(\bigcup_{x_j\in\Phi_j} \mathtt{SINR}(x_j) > \beta_j \Big| \bigcup_{i\in\mathcal{K}, x_i\in\Phi_i} (\mathtt{SINR}(x_i) > \beta_i) \right) \\
&\overset{(b)}{=} \frac{\mathbb{P}\left(\bigcup_{x_j\in\Phi_j} \mathtt{SINR}(x_j) > \beta_j, \bigcup_{i\in\mathcal{K}, x_i\in\Phi_i} (\mathtt{SINR}(x_i) > \beta_i) \right)}{\mathbb{P}\left(\bigcup_{i\in\mathcal{K}, x_i\in\Phi_i} (\mathtt{SINR}(x_i) > \beta_i) \right)} \\
&= \frac{\mathbb{P}\left(\bigcup_{x_j\in\Phi_j} \mathtt{SINR}(x_j) > \beta_j \right)}{\mathbb{P}\left(\bigcup_{i\in\mathcal{K}, x_i\in\Phi_i} (\mathtt{SINR}(x_i) > \beta_i) \right)}
\end{aligned} \tag{2.11}$$

where (a) follows from the stationarity and the ergodicity of PPP [69]. $\mathbb{P}^{!o}$ denotes the reduced Palm distribution of a PPP and (b) follows from the Slivinak's theorem [69, 76] and Bayes rule. Noting that $\mathbb{P}\left(\bigcup_{x_j\in\Phi_j} \mathtt{SINR}(x_j) > \beta_j \right)$ is the probability of coverage with a single tier j, the result follows from Theorem 1. □

In an interference-limited scenario, this result reduces to a simple closed form expression, which is given by the following Corollary.

Corollary 2. *When noise is neglected,* i.e., $\sigma^2 = 0$,

$$\bar{N}_j = \frac{\lambda_j P_j^{2/\alpha} \beta_j^{-2/\alpha}}{\sum_{i=1}^{K} \lambda_i P_i^{2/\alpha} \beta_i^{-2/\alpha}}.$$

From Corollary 2, we observe that the load on each tier is directly proportional to the quantity $\lambda_j P_j^{2/\alpha} \beta_j^{-2/\alpha}$. In line with intuition, a tier will serve more users if it has a higher BS density or higher transmit power or a lower `SIR` threshold. When the thresholds of all tiers are equal to β and the transmit powers of all BSs equal to P, the average load on each tier is $\bar{N}_j = \frac{\lambda_j}{\sum_{i=1}^{K} \lambda_i}$. Hence, as expected the average load on each tier is directly proportional to the density of its BSs.

2.4.2 Closed Access

Under closed access, also known as a closed subscriber group, a mobile user is allowed to connect to only a subset of tiers and the rest of the tiers act purely as interferers. The motivation for closed access particularly applies to privately owned infrastructure, such as femtocells or perhaps custom picocells mounted on a company's roof to improve service to their staff. The desirable aspects of closed access can include protection of finite backhaul capacity, security, and the reduction in the frequency of handoffs experienced by mobile users and the associated overhead required. In the context of our model, closed access means that if the strongest BS lies in the restricted tier, it by definition leads to an outage event irrespective of the received `SINR` associated with that BS. Furthermore, since closed access is a constraint on connectivity, it would

naturally lead to reduced coverage probability. This intuition is verified in the following discussion.

2.4.2.1 Coverage Probability

The main result of coverage probability in closed access networks is given by Lemma 2.

Lemma 2. *When a typical mobile user is allowed to connect to only a subset* $\mathcal{B} \subset \{1, 2, , \ldots, K\}$*, the coverage probability for closed access is*

$$\mathtt{P_c}(\{\lambda_i\}, \{\beta_i\}, \{P_i\}) = \sum_{i \in \mathcal{B}} \lambda_i \int_{\mathbb{R}^2} \exp\Big(- C(\alpha) \left(\frac{\beta_i}{P_i}\right)^{2/\alpha} \|x_i\|^2 \sum_{m=1}^{K} \lambda_m P_m^{2/\alpha} \Big) \exp\Big(- \frac{\beta_i \sigma^2}{P_i} \|x_i\|^{\alpha} \Big) \mathrm{d}x_i. \tag{2.12}$$

Proof. The coverage probability is

$$\begin{aligned} \mathtt{P_c}(\{\lambda_i\}, \{\beta_i\}, \{P_i\}) &= \mathbb{P}\left(\bigcup_{i \in \mathcal{B}, x_i \in \Phi_i} \mathtt{SINR}(x_i) > \beta_i \right) \\ &\overset{(a)}{=} \sum_{i \in \mathcal{B}} \mathbb{E} \sum_{x_i \in \Phi_i} \left[\mathbf{1}\left(\mathtt{SINR}(x_i) > \beta_i \right) \right], \end{aligned}$$

where (a) again follows from Lemma 1 under the assumption that $\beta_i > 1$. Following the same steps as the proof of Theorem 1, we arrive at the final result. □

The following corollary specializes from Lemma 2 to interference-limited HetNets.

Corollary 3. *When* $\sigma^2 = 0$,

$$\mathtt{P_c}(\{\lambda_i\},\{\beta_i\},\{P_i\}) = \frac{\pi}{C(\alpha)} \frac{\sum_{i\in\mathcal{B}} \lambda_i P_i^{2/\alpha} \beta_i^{-2/\alpha}}{\sum_{i=1}^{K} \lambda_i P_i^{2/\alpha}}.$$

If the threshold of each tier to be same (and equal to β) and the transmit power of each tier to be same (and equal to P), the coverage probability is $\frac{\pi}{C(\alpha)\beta^{2/\alpha}} \frac{\sum_{i\in\mathcal{B}} \lambda_i}{\sum_{i=1}^{K} \lambda_i}$. So, if the thresholds and transmit powers of all the tiers are same, closed access has a lower coverage than open access by a factor of $\frac{\sum_{i\in\mathcal{B}} \lambda_i}{\sum_{i=1}^{K} \lambda_i}$.

2.4.2.2 Average Load per Tier

The main result for the average load per tier under closed access is given by Proposition 2. The proof directly follows from the proof of Proposition 1 with the understanding that the coverage event would now be defined by only the "allowed" tiers.

Proposition 2. *The average fraction of users in coverage served by* j^{th} *tier (also the average load on* j^{th} *tier) in closed access is*

$$\bar{N}_j = \begin{cases} \frac{\lambda_j \delta_j}{\mathtt{P_c}(\{\lambda_i\},\{\beta_i\},\{P_j\})} & j \in \mathcal{B}, \\ 0 & \textit{otherwise.} \end{cases} \tag{2.13}$$

where $\mathtt{P_c}(\{\lambda_i\},\{\beta_i\},\{P_j\})$ *is the coverage probability under closed access given by Lemma 2 and*

$$\delta_j = \int_{\mathbb{R}^2} e^{-\left(\frac{\beta_j}{P_j}\right)^{2/\alpha} C(\alpha)||x||^2 \sum_{m=1}^{K} \lambda_m P_m^{2/\alpha}} e^{-\frac{\beta_j \sigma^2}{P_j}||x||^\alpha} \mathrm{d}x.$$

The corresponding result for the interference-limited networks is

$$\bar{N}_j = \begin{cases} \frac{\lambda_j P_j^{2/\alpha} \beta_j^{-2/\alpha}}{\sum_{i\in\mathcal{B}} \lambda_i P_i^{2/\alpha} \beta_i^{-2/\alpha}} & j \in \mathcal{B}, \\ 0 & \textit{otherwise.} \end{cases} \tag{2.14}$$

2.5 Average Rate

In this section, we derive the average rate $\bar{R}$ achievable by a random mobile user when it is in coverage both for the open and closed access strategies. It is worth noting that since the rate is computed conditioned on the mobile being in coverage, it is not the same as the classic ergodic rate $\mathbb{E}[R]$. The motivation behind considering this metric is that given the coverage/outage information, the service providers are interested in knowing the average rate they can provide to the users that are in coverage. Please refer to Appendix A for the ergodic rate expression.

2.5.1 Open Access

The main result for the average rate in open access is given in Theorem 2. In this section, for notational simplicity, we restrict our attention to the case of $\sigma^2 = 0$. However, the results can be extended to the general case with noise in a straightforward manner.

Theorem 2. *The average rate achievable by a randomly chosen mobile in open access when it is in coverage is*

$$\bar{R} = \log\left(1 + \beta_{min}\right) + \frac{\sum_{i=1}^{K} \lambda_i P_i^{2/\alpha} \mathcal{A}(\alpha, \beta_i, \beta_{min})}{\sum_{i=1}^{K} \lambda_i P_i^{2/\alpha} \beta_i^{-2/\alpha}}, \tag{2.15}$$

where

$$\mathcal{A}(\alpha, \beta_i, \beta_{min}) = \int_{\beta_{min}}^{\infty} \frac{\max(\beta_i, x)^{-2/\alpha}}{1+x} \mathrm{d}x,$$

and $\beta_{min} = \min\{\beta_1, \beta_2, \ldots, \beta_K\}$.

Proof. Denoting the coverage event $\bigcup_{i=1}^{K}\bigcup_{x\in\Phi_i}(\texttt{SIR}(x)>\beta_i)$ by $\mathbf{C}(\{\beta_i\})$, the average rate achievable by a randomly chosen mobile user when it is under coverage can be expressed as:

$$\bar{R}=\mathbb{E}\left[\log\left(1+\max_{x\in\bigcup\Phi_i}(\texttt{SIR}(x))\right)\Big|\mathbf{C}(\{\beta_i\})\right]. \tag{2.16}$$

We first derive the conditional complementary cumulative density function (CCDF) of $\max_{x\in\bigcup\Phi_i}(\texttt{SIR}(x))$ as follows:

$$\begin{aligned}
&\mathbb{P}\left(\max_{x\in\bigcup\Phi_i}(\texttt{SIR}(x))>T\;\Big|\;\mathbf{C}(\{\beta_i\})\right)\\
&\overset{(a)}{=}\frac{\mathbb{P}\left(\max_{x\in\bigcup\Phi_i}(\texttt{SIR}(x))>T,\mathbf{C}(\{\beta_i\})\right)}{\mathbb{P}(\mathbf{C}(\{\beta_i\}))}\\
&\overset{(b)}{=}\frac{\mathbb{P}\left(\mathbf{C}(\{T\}),\mathbf{C}(\{\beta_i\})\right)}{\mathbb{P}(\mathbf{C}(\{\beta_i\}))},\\
&=\frac{\mathbb{P}\left(\mathbf{C}(\{\max(T,\beta_i)\})\right)}{\mathbb{P}(\mathbf{C}(\{\beta_i\}))},\\
&\overset{(c)}{=}\begin{cases}\frac{\sum_{i=1}^{K}\lambda_i P_i^{2/\alpha}\max(\beta_i,T)^{-2/\alpha}}{\sum_{i=1}^{K}\lambda_i P_i^{2/\alpha}\beta_i^{-2/\alpha}} & ;\quad T>\beta_{min}\\ 1 & ;\quad \text{otherwise}\end{cases},
\end{aligned} \tag{2.17}$$

where (a) follows from Bayes' theorem, (b) follows from Lemma 1 under the assumption $\beta_i>1\;\forall\;i$, (c) follows from Theorem 1, and β_{min} denotes $\min\{\beta_1,\beta_2,\ldots,\beta_K\}$.

Denoting random variable $\max_{x\in\bigcup\Phi_i}(\texttt{SIR}(x))$ by X, $\bar{R}$ can be evaluated as follows:

$$\begin{aligned}
\bar{R} &= \int_0^\infty \log(1+x)f_X(x\mid\mathbf{C}(\{\beta_i\}))\mathrm{d}x,\\
&= \int_{x=0}^{\infty}\int_{y=0}^{x}\frac{1}{1+y}f_X(x\mid\mathbf{C}(\{\beta_i\}))\;\mathrm{d}y\;\mathrm{d}x,
\end{aligned}$$

$$\begin{aligned} &\overset{(a)}{=} \int_{y=0}^{\infty} \left(\int_{x=y}^{\infty} f_X(x \mid \mathbf{C}(\{\beta_i\}))\, \mathrm{d}x \right) \frac{1}{1+y}\, \mathrm{d}y, \\ &= \int_0^{\infty} \frac{\mathbb{P}\left(X > y \mid \mathbf{C}(\{\beta_i\})\right)}{1+y} \mathrm{d}y, \end{aligned} \tag{2.18}$$

where (a) follows from changing the order of integration. Now we substitute (2.17) in (2.18) to get the average rate as:

$$\begin{aligned} \bar{R} &= \int_0^{\beta_{min}} \frac{1}{1+y} dy \; + \frac{1}{\sum_{i=1}^{K} \lambda_i P_i^{2/\alpha} \beta_i^{-2/\alpha}} \sum_{i=1}^{K} \lambda_i P_i^{2/\alpha} \int_{\beta_{min}}^{\infty} \frac{\max(\beta_i, x)^{-2/\alpha}}{1+x} \mathrm{d}x \\ &= \log(1+\beta_{min}) + \frac{1}{\sum_{i=1}^{K} \lambda_i P_i^{2/\alpha} \beta_i^{-2/\alpha}} \sum_{i=1}^{K} \lambda_i P_i^{2/\alpha} \int_{\beta_{min}}^{\infty} \frac{\max(\beta_i, x)^{-2/\alpha}}{1+x} \mathrm{d}x. \end{aligned} \tag{2.19}$$

This completes the proof. □

Thus we observe that the average rate expression involves only a single integral which can be easily evaluated numerically.

Corollary 4. *Using the same threshold β for all tiers, the average rate achievable by a randomly chosen mobile that is in coverage in open access is:*

$$\bar{R} = \log(1+\beta) + \beta^{2/\alpha} \mathcal{A}(\alpha, \beta, \beta). \tag{2.20}$$

The above result shows that the average rate is independent of the density of BSs of each tier when the `SIR` thresholds are same for all the tiers. This is expected because the distribution of max `SIR` does not depend upon the density of BSs in this case (follows from Theorem 1).

2.5.2 Closed Access

The average rate $\bar{R}_c$ achievable by a randomly chosen mobile under closed access (assuming it is under coverage) can be expressed as:

$$\mathbb{E}\left[\log\left(1+\max_{x\in\bigcup_{i\in\mathcal{B}}\Phi_i}(\texttt{SIR}(x))\right)\Big|\bigcup_{i\in\mathcal{B}}\bigcup_{x\in\Phi_i}(\texttt{SIR}(x)>\beta_i)\right]. \tag{2.21}$$

Following the same steps as in proof of Theorem 2, we arrive at the following Proposition.

Proposition 3. *Assuming a mobile user is allowed to connect to only a subset $\mathcal{B}$ of the K tiers, the average rate (assuming mobile is under coverage) can be expressed as:*

$$\bar{R}_c = \log\left(1+\beta_{min}\right) + \frac{\sum_{i\in\mathcal{B}}\lambda_i P_i^{2/\alpha}\mathcal{A}(\alpha,\beta_i,\beta_{min})}{\sum_{i\in\mathcal{B}}\lambda_i P_i^{2/\alpha}\beta_i^{-2/\alpha}}, \tag{2.22}$$

where $\beta_{min} = \min_{i\in\mathcal{B}}\{\beta_i\}$.

Corollary 5. *Assuming the threshold of each tier is the same and equal to β, the average rate achievable by a randomly chosen mobile in coverage under closed access is*

$$\bar{R}_c = \log(1+\beta) + \beta^{2/\alpha}\mathcal{A}(\alpha,\beta,\beta). \tag{2.23}$$

From Corollaries 4 and 5, we observe that the average rate ($\bar{R}$) of the mobile while it is in coverage is not affected by access control when the thresholds are the same for all tiers. However, since the coverage probability is lower in case of closed access, it would naturally lead to a lower ergodic rate as compared to the open access networks. Interested readers can refer to [48] for the derivation of ergodic rate in this framework.

2.6 Numerical Results

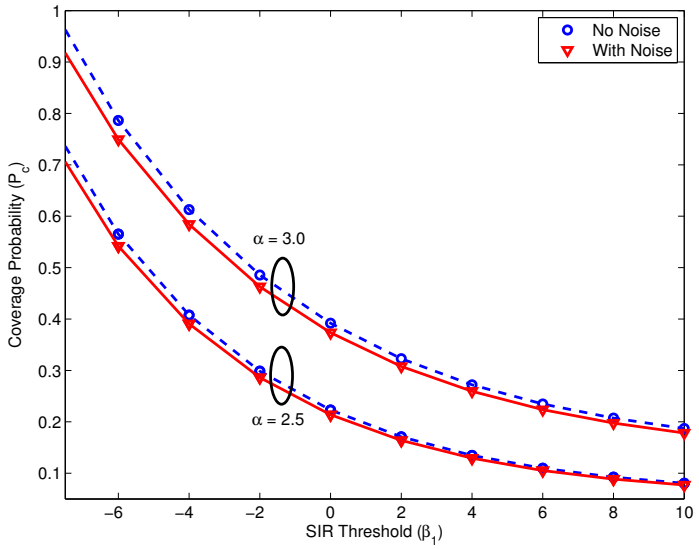

Figure 2.5: Coverage probability in a two-tier HetNet with and without thermal noise ($K = 2$, $P_1 = 25P_2$, $\lambda_2 = 5\lambda_1$, $\beta_2 = 1$ dB, $\mathtt{SNR}_{\text{edge}} = 0$ dB).

Most of the analytical results presented in this chapter are fairly self-explanatory and do not require a separate numerical interpretation. Therefore, to avoid repetition, we will present only non-obvious trends and validation of the model in this section.

2.6.1 Effect of Thermal Noise

We first study the effect of thermal noise on the coverage probability by considering a typical two-tier network consisting of macro-cells overlaid with pico-cells. To set the noise power, we use the following notion of cell-edge users in this example. Defining the distance of the the nearest macro BS to

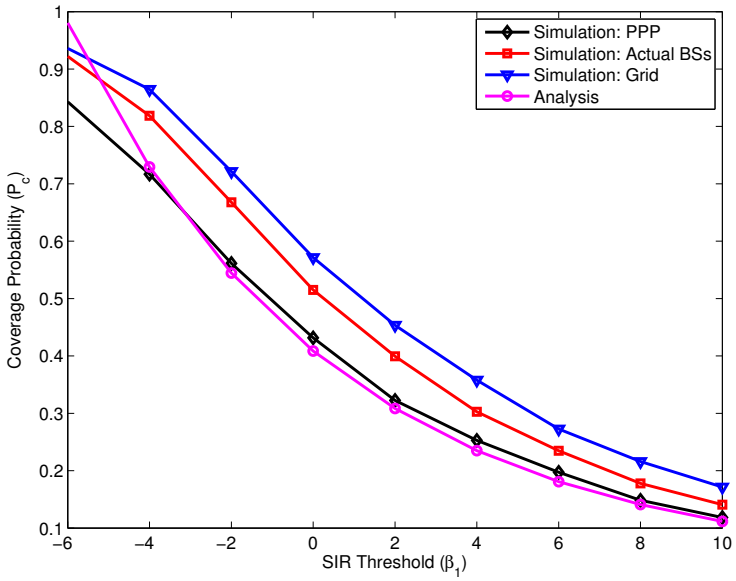

Figure 2.6: Coverage probability in a two-tier HetNet ($K = 2$, $\alpha = 3$, $P_1 = 100P_2$, $\lambda_2 = 2\lambda_1$, $\beta_2 = 1$ dB, No noise).

the typical mobile user to be r and the underlying random variable to be R, the mobile user is said to be on the cell edge if $\mathbb{P}(R \leq r) \geq \mathcal{P}_{\text{edge}}$, where $\mathcal{P}_{\text{edge}}$ is set to 0.9 for this illustration. For PPP(λ), $\mathbb{P}(R \leq r) = 1 - \exp(\lambda \pi r^2)$, giving $r \geq \sqrt{\frac{-\ln(1-\mathcal{P}_{\text{edge}})}{\pi\lambda}}$. For a desired edge-user $\texttt{SNR}$, say $\texttt{SNR}_{\text{edge}}$, σ^2 can be approximated as $\sigma^2 \approx \frac{P_t r_{\text{edge}}^{-\alpha}}{\texttt{SNR}_{\text{edge}}}$, where r_{edge} is the limiting value of r evaluated above. Under this setup, we present the coverage probability for various values of α in Figure 2.5. By comparing these results with the no-noise case, we note that the typical HetNets are interference limited and hence thermal noise has a very limited effect on coverage probability. Therefore, we will ignore noise in the rest of this section.

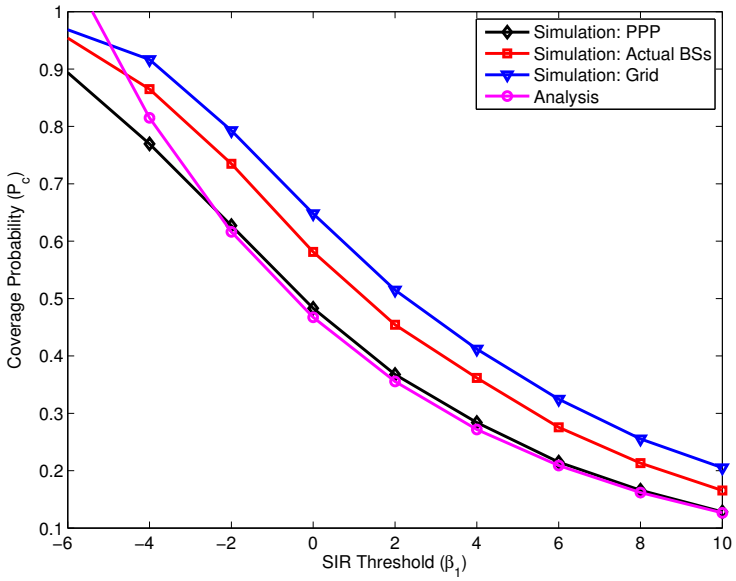

Figure 2.7: Coverage probability in a two-tier HetNet ($K = 2$, $\alpha = 3.2$, $P_1 = 1000P_2$, $\lambda_2 = 4\lambda_1$, $\beta_2 = 1$ dB, No noise).

2.6.2 Validity of PPP Model and $\beta > 1$ Assumption

While a random PPP model is probably the best that can be hoped for in modeling "unplanned" tiers, such as femtocells, its accuracy in modeling "planned" BS locations, such as those of macro-cells, is open to question. Therefore we verify the PPP assumption for macro-cells from a coverage probability perspective by considering a two-tier network in three different scenarios: 1) the macro-cell BSs are distributed according to PPP (our model), 2) the macro-cell BSs correspond to an actual 4G deployment, and 3) macro-cell BSs are distributed according to hexagonal grid model. The second tier is modeled as an independent PPP in all three cases. As shown in Figures 2.6 and 2.7, the actual coverage probability lies between the coverage probabilities of the

PPP and grid model. This is because the likelihood of a dominant interferer is highest for the PPP and lowest for the grid model. This comparison shows that the PPP assumption is nearly as accurate as the grid model in the case of macro-cells, with the PPP providing a lower bound and grid model providing an upper bound to the actual coverage probability.

We now focus on the $\beta > 1$ assumption by comparing the theoretical and simulated results for coverage probability in Figures 2.6 and 2.7. As expected, the simulated and analytical results match reasonably well for $\beta_i > 1$ but interestingly, the theoretical results also provide a tight upper bound to the exact solution even until about $\beta_1 = -4$ dB ($\approx .4$). Therefore, the analytical results also cover typical cell edge users. The same trend is observed in the case of average rate results presented in Figure 2.8, which are also accurate down to about -4 dB target `SIR`. Recall that the assumption $\beta_i > 1$ is relaxed in Appendix A, where general expressions for coverage probability and ergodic rate are derived.

2.7 Summary

In this chapter, we developed a tractable model for a downlink HetNet consisting of K tiers of randomly located BSs, where each tier may differ in terms of average transmit power, supported data rate and BS density. Assuming a mobile user connects to the strongest candidate BS in terms of received power and a fairly general channel model, we derived an expression for the probability of coverage (equivalently outage) over the entire network under

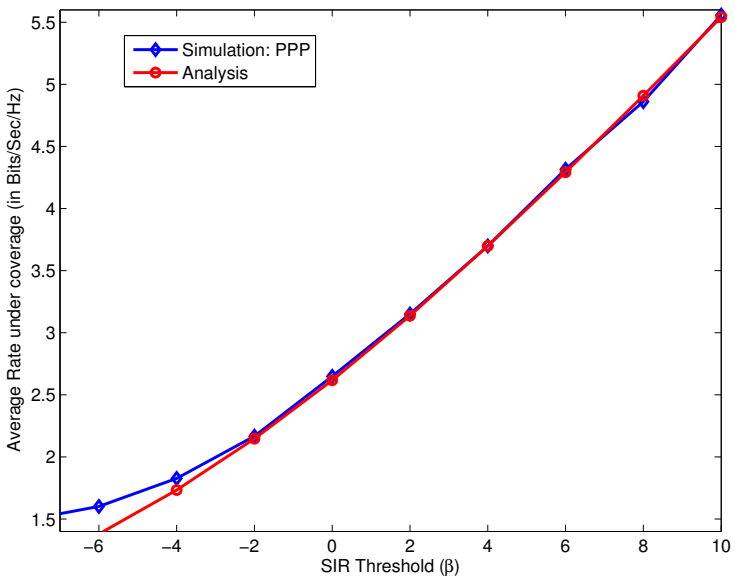

Figure 2.8: Average rate while mobile is in coverage ($K = 2$, $\alpha = 3$, $P_1 = 1000P_2$, $\lambda_2 = 2\lambda_1$, $\beta_1 = \beta_2 = \beta$, no noise, open access).

both open and closed access, which assumes a strikingly simple closed-form when the resulting SINR is greater than 1 and the network is interference limited. We also derived simple expressions for the average rate achieved by a typical mobile and the average load on each tier of BSs. One interesting observation for interference-limited open access networks is that at a given SINR, adding more tiers and/or BSs neither increases nor decreases the coverage probability when all the tiers have the same target SINR. The baseline model developed in this chapter will be generalized to various scenarios of interest for current and future HetNets in the following chapters.

Chapter 3

Load-Aware Modeling and Analysis of HetNets

As discussed in the previous chapter, HetNets are characterized by cells whose coverage areas may vary by orders of magnitude. It is natural therefore that their user populations (and hence traffic loads) will vary similarly. Yet, to date, random spatial models developed for HetNets generally assume that all base stations (BSs) are always transmitting and hence implicitly have the same load. This chapter incorporates a flexible notion of BS load by *conditionally thinning* the interference field, conditional on the connection of a typical mobile to its serving BS. We derive the coverage probability – i.e. the `SIR` distribution – for a typical mobile in a K-tier HetNet where each tier has an arbitrary load, characterized by an activity factor $p_k \in [0, 1]$, where $p_k = 1$ is fully loaded.

3.1 Related Work and Motivation

The idea of using random spatial models for K-tier HetNets discussed in the Chapter 2 was introduced by us in [5, 77] and extended in [48–56], and is surprisingly tractable: under fairly benign assumptions, the coverage probability could be derived in closed-form, which is not possible even for 1-

tier networks in the hexagonal grid model. The model further was shown to generally agree in several important ways with more sophisticated industry (e.g. 3GPP) simulations [33] and even early field deployments of HetNets [32].

Despite this encouraging progress, the baseline model and all its extensions lack in at least one important aspect, which is their neglect of network traffic and load. Rather, the work to date in this direction has assumed that all the BSs transmit concurrently all the time, which translates to a fully loaded (or full buffer) scenario resulting in pessimistic estimates of coverage and average rate. Although this might be justified for macrocells in peak traffic hours, this is not applicable for smaller cells whose smaller coverage areas will naturally accommodate fewer users, even if considerable biasing towards the small cells is introduced. Therefore, the main goal of this chapter is to incorporate a notion of BS load. Those familiar with random spatial models will recognize that a simple independent thinning of the point processes will not capture the load since it may also turn off the serving BS, which is not allowed if the analysis is performed for a typical active user. On the other hand, incorporating more sophisticated queueing models in the present multi cell scenario will render the analysis intractable due to the interference induced coupling in the service rates of various BSs [78, 79]. Moreover, this line of thought is not in the scope of the current chapter since we do not focus on the flow level performance evaluation. The readers interested in flow level models can refer to [80, 81]. With our main focus on the downlink coverage evaluation, we propose a middle way whereby we conditionally thin the inter-

ference field predicated on a connection to a typical active user, and we are able to maintain acceptable tractability with a realistic model of BS loading.

3.2 Contributions and Outcomes

Tractable load model for K-tier HetNets. In Section 3.3, we incorporate a notion of BS load in the baseline K-tier HetNet model proposed in Chapter 2. For a HetNet where BSs across tiers differ in terms of their transmit power, supported data rate and deployment density, we assume that a typical mobile connects to the strongest BS in terms of received power and conditioned on this connection, the i^{th} tier interfering BSs transmit independently with a probability p_i, which models the load. These BS activity factors $\{p_i\}$ may vary significantly across the tiers due to orders of magnitude differences in the coverage areas of each tier.

Coverage probability for both open and closed access networks. We derive exact expressions for the coverage probability of a typical mobile user in both open and closed access HetNets. Since these expressions involve an infinite summation, we also derive a set of upper and lower bounds that can be made arbitrarily tight with a finite number of terms. These bounds also give insights into the number of terms of the infinite summation required to approximate the coverage probability such that the approximation error is within some predefined limit.

Key system design insights. This chapter provides some potentially useful design insights for HetNets. First, we study the effect of proposed

"conditional thinning" on the coverage footprints of various tiers and show that this effect can be understood in two equivalent ways: i) thinning of interference, and ii) biasing of the typical mobile towards its serving BS. While the former is a direct result of thinning, the latter is an indirect consequence of the expansion of the coverage regions in the thinned interference field.

Second, our analysis sheds light into the effect of adding new tiers to already existing HetNets. In particular, we derive an exact condition under which the addition of a new tier to a general K-tier HetNet will increase the overall coverage probability. A relevant special case is the addition of small cells to existing macrocell networks, where we show that in the interference limited regime the overall open access coverage probability increases if the load on small cells is smaller than that of macrocells, which is a typical operating scenario because of the smaller loads handled by small cells. This is a strong rebuttal to the viewpoint that unplanned infrastructure might bring down a cellular network due to increased interference.

Third, we show that the coverage probability for a general K-tier interference-limited open-access network is invariant to changes in the power and deployment density when all the classes of BSs have same loads and target SINRs. Furthermore, this coverage probability is also the same as that of a single tier network with the same target SINR and the same BS activity factor.

3.3 System Model

As in Chapter 2, we model a downlink heterogeneous cellular network with K classes (or tiers) of BSs. For notational simplicity, we denote the set $\{1, 2, \ldots K\}$ by $\mathcal{K}$. BSs of the i^{th} class transmit with power P_i, have a target SINR of β_i and are assumed to form a realization of an independent homogeneous Poisson Point Process (PPP) Φ_i with density λ_i. As discussed in Chapter 2, such a model seems sensible for user deployed BSs such as femtocells but is dubious for the centrally planned tiers such as macrocells. Nevertheless, the difference is not as large as expected and PPP assumption for macrocells is shown to be about as accurate as the grid model when compared to an actual 4G network in [1]. More recently, [82] has validated the PPP assumption for certain cities using tools from spatial statistics. We will comment more on the accuracy of this assumption in the context of the proposed load model in the Numerical Results Section.

Without loss of generality, we perform analysis on a typical mobile user located at origin, which is made possible by Slivnyak's Theorem [69]. For cell association, we consider the max-SINR connectivity model, where a mobile user connects to the BS that provides highest downlink SINR. It should be noted that this model is the same as the max-power connectivity model where a mobile connects to the BS that provides highest downlink power. Since HetNets are typically interference-limited [83], we ignore thermal noise for notational simplicity. However, as would be evident from the analysis, this assumption can be relaxed without much extra work. To model the wireless

channel, we consider a standard distance based path loss with exponent $\alpha > 2$ along with Rayleigh fading. Hence the received power at a typical mobile from a BS located at point $x \in \Phi_i$ can be expressed as $P_i h_x \|x\|^{-\alpha}$, where $h_x \sim \exp(1)$ and $\|x\|^{-\alpha}$ is the distance based path loss. General fading distributions, e.g., log-normal shadowing, can be incorporated using techniques developed in Chapter 5. Assuming $\mathcal{Z}_k$ to be the set of k^{th} tier interfering BSs (possibly thinned version of Φ_k), the downlink SIR at the typical mobile user when it connects to the BS located at point $y \in \Phi_i$ is

$$\mathtt{SIR}(y) = \frac{P_i h_y \|y\|^{-\alpha}}{\sum_{k=1}^{K} \sum_{x \in \mathcal{Z}_k} P_k h_x \|x\|^{-\alpha}}. \tag{3.1}$$

3.3.1 Modeling Base-Station Load

In this K-tier random spatial model, we now incorporate network "load" perceived by each BS as the likelihood of its transmission at a randomly chosen time instant. This can also be visualized as the *BS activity factor*, formally defined as the fraction of time for which a BS transmits.

Relationship of BS activity factor with number of active users. A BS is inactive in a particular resource block, e.g., time-frequency resource block in LTE [75], if there is no active user scheduled. This can be due to an over provisioned system or a momentary lull in traffic due to the bursty nature of data access. Clearly, this model characterizes the load on each BS in terms of the total number of active users served by that BS at a random time instant. In the context of Orthogonal Frequency Division Multiple Access (OFDMA)

if a particular BS experiences high load, it will utilize more frequency time resources and hence the probability that a user is scheduled in a particular frequency time block increases. Therefore, the load perceived by a BS is directly related to the likelihood that an arbitrary resource block is utilized and hence is related to the BS activity in that particular block.

Temporal and spatial correlation in BS activity factors. In general, there is both temporal and spatial correlation in the activity factors of different BSs. Temporal correlation is induced across neighboring BSs by the mobility of users, i.e., if a user is associated to a particular BS, the likelihood of neighboring BSs transmitting at a future time instant is slightly higher. Spatial correlation is induced by interference and traffic/load patterns [78, 79]. To understand this, consider two neighboring BSs. When the first BS transmits, it increases net interference experienced by the second BS and hence reduces its data rate. As a result, the second BS now takes longer to transmit same amount of data than it would have taken if the first BS was not transmitting. Therefore, the activity factors of these two BSs are positively correlated. However, modeling the exact nature of these correlations is beyond the scope of the current chapter and we assume the BS activity factors to be independent. Although the spatio-temporal correlations haven't yet been modeled for this exact problem, it is worth noting that they have been handled in some related setups, e.g., the effect of spatio-temporal correlations of interference on coverage is discussed in [84, 85].

3.3.2 Proposed Load Model and Mathematical Preliminaries

We assume that a typical mobile connects to the strongest BS in terms of received power and conditioned on this connection, the interferer belonging to the i^{th} tier transmits independently with a probability p_i and is idle with a probability $1 - p_i$. This conditioning makes it harder to analyze this system model since we do not have *a priori* knowledge about the serving BS and hence it is not possible to isolate the interference field. To overcome this, we partition each tier Φ_m independently into two sets of BSs Ψ_m and Δ_m, where Ψ_m and Δ_m are both independent PPPs with densities $p_m\lambda_m$ and $(1 - p_m)\lambda_m$. The set Ψ_m represents the set of active BSs of tier m with the possibility of one of them being a serving BS, and Δ_m represents the set of idle BSs of tier m with an exception that it could also contain the serving BS since partitioning was done independently. The advantage of this partitioning is that the interferers are confined to the set $\Psi = \bigcup_{m\in\mathcal{K}} \Psi_m$. For ease of notation, we define the maximum signal strength from a set of nodes $\mathcal{A}$ as

$$M(\mathcal{A}) = \sup_{x\in\mathcal{A}} P_{\mathcal{A}} h_x \|x\|^{-\alpha}, \tag{3.2}$$

and the total received power at the origin from the set of active BSs as

$$I = \sum_{i=1}^{K} \sum_{x\in\Psi_i} P_i h_x \|x\|^{-\alpha}, \tag{3.3}$$

which denotes the net interference power if Ψ does not include the serving BS and the interference plus signal power if it includes the serving BS. From the definition of $M(\Psi_i)$ and I, it is easy to see that $\mathbf{1}\left(\frac{M(\Psi_i)}{I-M(\Psi)} < \beta_i\right) = 1$ only if no

active BS in the set Ψ_i can connect to the mobile. Similarly, $\mathbf{1}\left(\frac{M(\Delta_i)}{I} < \beta_i\right) = 1$ only if no BS in the set Δ_i is able to connect to the mobile. The second event is defined to cover the possibility that a serving BS may lie in the set Δ_i. Using these two events, we will now define the coverage probability of a typical mobile at the origin. We note that a mobile will be in outage (not in coverage) if none of the BSs in the whole network provides SIR that is greater than the corresponding target for that tier.

Definition 1 (Coverage Probability)**.** *Coverage probability,* $\mathtt{P_c}$*, can be formally defined as*

$$\mathtt{P_c} = 1 - \mathbb{E}\left[\prod_{i\in\mathcal{K}} \mathbf{1}\left(\frac{M(\Psi_i)}{I - M(\Psi)} < \beta_i\right)\mathbf{1}\left(\frac{M(\Delta_i)}{I} < \beta_i\right)\right]. \tag{3.4}$$

For this definition, we implicitly assumed an open access network where a mobile user is allowed to connect to any BS in the network without any restrictions. Another possible access strategy is closed access or closed subscriber group strategy in which a mobile is allowed to connect to only a subset $\mathcal{B} \subseteq \mathcal{K}$ of all the tiers. Coverage probability for closed access is also given by (3.4) with the only difference that the product is over the set $\mathcal{B}$ instead of $\mathcal{K}$.

For tractability, we assume that the target SIR thresholds β_i are greater than 0 dB, i.e., $\beta_i > 1, \forall\, i$. This is in fact the case for a large fraction of mobile users and only a few edge users might violate this assumption. Moreover, in the Numerical Results Section we show that the results derived under this weaker assumption hold down until around -2dB which covers a large fraction of cell edge users as well. This assumption has also been validated earlier for the

fully loaded K-tier HetNet in [5]. The reason why this assumption is helpful is because it ensures that at most one BS in the active set Ψ meets the target SIR requirements for a typical mobile user. Refer to [5] for a detailed discussion on this assumption and its application in coverage analysis of a fully loaded K-tier HetNet.

3.3.3 Coverage Regions

Before going into the detailed analysis of coverage probability, it will be useful to understand the effect of the proposed load model on the coverage footprints of various BSs. Consider a realization of a three tier HetNet in Figure 3.1. We first plot the coverage regions assuming a fully loaded network by tessellating the space according to max-SIR connectivity model in the left figure. As discussed in Chapter 2, this plot does not resemble a classical Voronoi tessellation due to the differences in the transmit powers of BSs across tiers. Moreover, it should be noted that the "cell edges" are not as sharp in reality due to fading and shadowing, which are averaged out for these illustrative plots. The effect of incorporating the proposed load model on coverage footprints can now be understood in two equivalent ways: i) thinning of the interference field conditional on the connection of a typical mobile to its serving BS, where the original coverage regions corresponding to the inactive BSs are removed to highlight conditional thinning (second figure), ii) biasing of a typical mobile towards its serving BS relative to the new cell edge defined by the set of active BSs (third figure). While the former is a direct result of

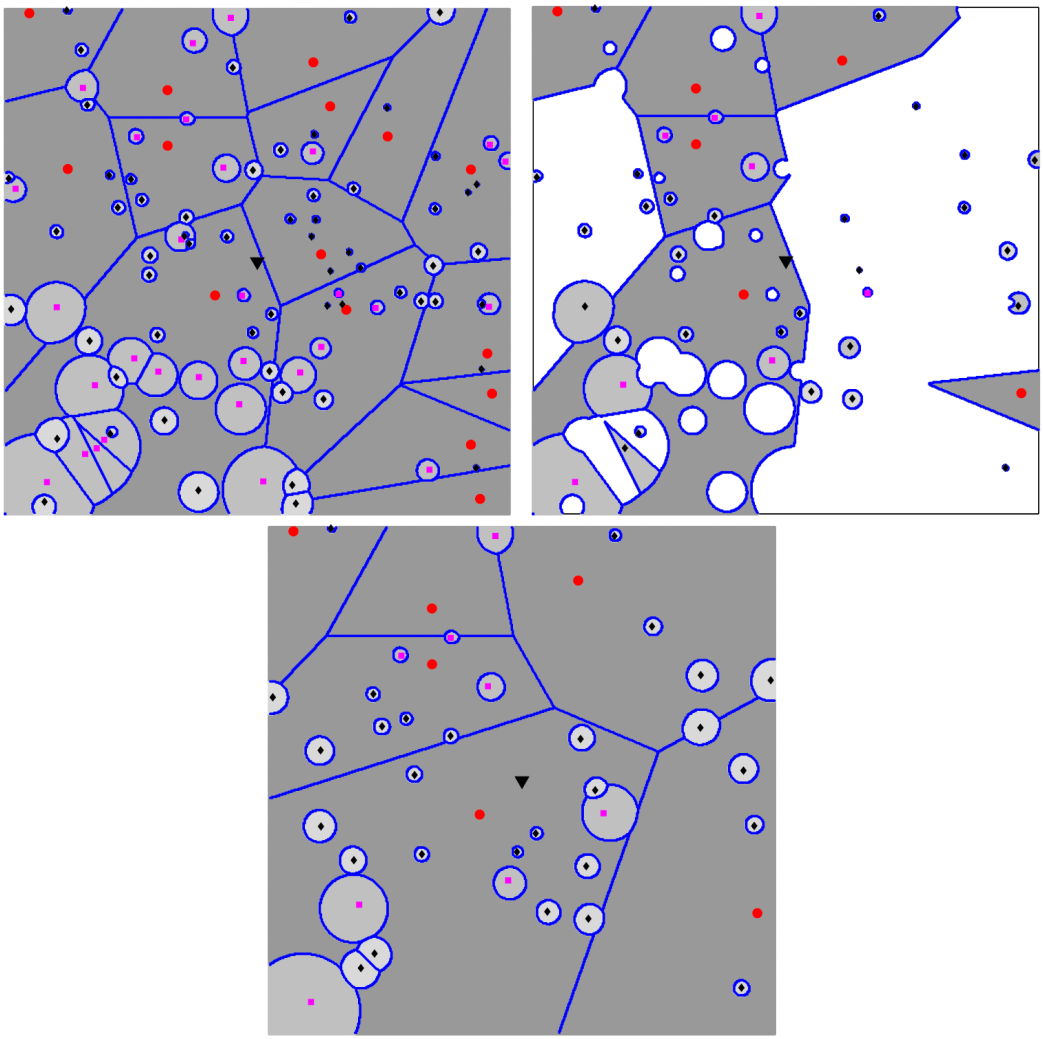

Figure 3.1: Illustration of the proposed load model in a realization of a three-tier network with $\lambda_2 = 2\lambda_1$, $\lambda_3 = 4\lambda_1$, $P_1 = 100P_2$, $P_1 = 1000P_3$, $p_1 = .6$ and $p_2 = p_3 = .4$. The big circles, squares, small diamonds and big triangle, respectively represent macrocells, picocells, femtocells and a typical mobile.

conditional thinning, the latter is an indirect consequence of the expansion of coverage regions in the thinned interference field. In Apendix B, we show that the same idea of conditional thinning can also be used to study non-uniform user distributions, especially the ones corresponding to the current capacity centric deployments, where the users are more likely to lie closer to the BSs.

3.4 Coverage Probability

This is the main technical section of this chapter where we derive the probability that a typical mobile is in coverage under the system model introduced in the last section. We first derive coverage probability for an open access network, from which the results for closed-access immediately follow.

3.4.1 Exact Expression for Coverage Probability

We start by stating the Laplace transform of I, i.e., $\mathcal{L}_I(s) = \mathbb{E}\left[\exp(-sI)\right]$, in Lemma 3, which will be useful in the derivation of coverage probability. The proof follows from the proof of Theorem 1 in Chapter 2 with some minor modifications and is hence skipped.

Lemma 3. *The Laplace transform of I can be expressed as*

$$\mathcal{L}_I(s) = \exp\left(-s^{\frac{2}{\alpha}} C(\alpha) \sum_{l=1}^{K} p_l \lambda_l P_l^{\frac{2}{\alpha}}\right), \tag{3.5}$$

where $C(\alpha)$ is given by

$$C(\alpha) = \frac{2\pi^2 \csc\left(\frac{2\pi}{\alpha}\right)}{\alpha}. \tag{3.6}$$

The following Lemma deals with fractional moments of interference and is the main technical result required to evaluate the coverage probability for this model.

Lemma 4. *Let Ψ_i denote the set of active transmitters of tier i and $\delta_i = \beta_i/(1+\beta_i)$. Let I denote the total received power from the BSs in the set Ψ and for notational simplicity define $\mathcal{T} = \mathbf{1}\left(\max_{i\in\mathcal{K}} \frac{M(\Psi_i)}{\delta_i} < I\right) I^{-2/\alpha}$. Then*

$$\mathbb{E}\left[\mathcal{T}^m\right] = \frac{m! g(m)}{(-A)^m},$$

where

$$g(m) = \left(-\frac{A}{\eta}\right)^m \left\{ \frac{1}{\Gamma(1+\frac{2m}{\alpha})} - \frac{B}{\eta} \frac{\pi\Gamma(1+\frac{2}{\alpha})}{\Gamma(1+\frac{(m+1)2}{\alpha})} \right\}, \tag{3.7}$$

and

$$A = \pi\Gamma\left(1+\frac{2}{\alpha}\right) \sum_{l\in\mathcal{K}} (1-p_l)\lambda_l P_l^{\frac{2}{\alpha}} \beta_l^{-\frac{2}{\alpha}}, \tag{3.8}$$

$$B = \sum_{i\in\mathcal{K}} \frac{\lambda_i p_i P_i^{\frac{2}{\alpha}} \beta_i^{-\frac{2}{\alpha}} {}_2F_1(1, \frac{2m}{\alpha}, 1+\frac{(m+1)2}{\alpha}, \frac{1}{1+\beta_i})}{(1+\beta_i)^{\frac{2m}{\alpha}}}, \tag{3.9}$$

$$\eta = C(\alpha) \sum_{l=1}^{K} p_l \lambda_l P_l^{\frac{2}{\alpha}}. \tag{3.10}$$

The hypergeometric function is denoted by

$${}_2F_1(a,b,c,z) = \frac{\Gamma(c)}{\Gamma(b)\Gamma(c-b)} \int_0^1 \frac{t^{b-1}(1-t)^{c-b-1}}{(1-tz)^a} \mathrm{d}t. \tag{3.11}$$

Proof. Being consistent with the definition of $\mathcal{T}$, we note that

$$\mathcal{T}^m = \mathbf{1}\left(\max_{i\in\mathcal{K}} \frac{M(\Psi_i)}{\delta_i} < I\right) I^{-2m/\alpha}. \tag{3.12}$$

To proceed with the proof, we represent $I^{-2m/\alpha}$ in terms of $\Gamma(x)$ as

$$I^{-2m/\alpha} = \frac{1}{\Gamma(2m/\alpha)} \int_0^\infty e^{-sI} s^{-1+\frac{2m}{\alpha}} \mathrm{d}s, \ m \geq 1, \tag{3.13}$$

where $\Gamma(x)$ is the standard gamma function. Using this representation of $I^{-2m/\alpha}$ we can express $\mathbb{E}[\mathcal{I}^m]$ as

$$\mathbb{E}\left[\mathbf{1}\left(\max_{i\in\mathcal{K}} \frac{M(\Psi_i)}{\delta_i} < I\right) \frac{1}{\Gamma\left(\frac{2m}{\alpha}\right)} \int_0^\infty e^{-sI} s^{-1+\frac{2m}{\alpha}} \mathrm{d}s\right]. \tag{3.14}$$

Using Fubini's theorem, we can exchange the expectation and the inner integral to obtain

$$\frac{1}{\Gamma\left(\frac{2m}{\alpha}\right)} \int_0^\infty s^{-1+\frac{2m}{\alpha}} \mathbb{E}\left[e^{-sI}\mathbf{1}\left(\max_{i\in\mathcal{K}} \frac{M(\Psi_i)}{\delta_i} < I\right)\right] \mathrm{d}s. \tag{3.15}$$

Under the assumption $\beta_i > 1, \ \forall \ i$, we know that only one BS in the whole network can establish a downlink connection with a typical mobile. Hence,

$$\mathbf{1}\left(\max_{i\in\mathcal{K}} \frac{M(\Psi_i)}{\delta_i} > I\right) = \sum_{i=1}^{K} \sum_{x\in\Psi_i} \mathbf{1}\left(\mathtt{SIR}(x) > \beta_i\right), \tag{3.16}$$

where $\mathtt{SIR}(x)$ is the received $\mathtt{SIR}$ when a typical mobile is camped to the BS located at $x \in \Psi_i$. Using this expression, the expectation term of (3.15) can be written as

$$\begin{aligned} &\mathbb{E}\left[e^{-sI}\mathbf{1}\left(\max_{i} \frac{M(\Psi_i)}{\delta_i} < I\right)\right] \\ &= \mathbb{E}\left[e^{-sI}\right] - \sum_{i=1}^{K} \mathbb{E}\left[e^{-sI} \sum_{x\in\Psi_i} \mathbf{1}(\mathtt{SIR}(x) > \beta_i)\right]. \end{aligned} \tag{3.17}$$

From Lemma 3, we know the Laplace transform of total interference and hence the first term in the above expression can be directly written as:

$$\mathbb{E}\left[e^{-sI}\right] = \exp\left(-s^{2/\alpha} C(\alpha) \sum_{l=1}^{K} p_l \lambda_l P_l^{2/\alpha}\right). \tag{3.18}$$

To evaluate the expectation in the second term of (3.17), we first denote the effective interference as $I' = I - P_i h_x \|x\|^{-\alpha}$ and note that the Laplace transforms of I and I' are the same. The expectation can now be simplified as

$$\mathbb{E}\left[e^{-sI}\sum_{x\in\Psi_i}\mathbf{1}(\mathtt{SIR}(x)>\beta_i)\right]$$

$$=\mathbb{E}\left[\sum_{x\in\Psi_i}\exp(-sI'+P_i h_x\|x\|^{-\alpha})\mathbf{1}\left(\frac{P_i h_x\|x\|^{-\alpha}}{I'}>\beta_i\right)\right] \tag{3.19}$$

$$\overset{(a)}{=}\mathbb{E}\left[\sum_{x\in\Psi_i}e^{-sI'}\mathbb{E}_{h_x}\left[e^{-P_i h_x\|x\|^{-\alpha}}\mathbf{1}\left(h_x>\beta_i I' P_i^{-1}\|x\|^{\alpha}\right)\right]\right] \tag{3.20}$$

$$\overset{(b)}{=}\mathbb{E}\left[\sum_{x\in\Psi_i}\frac{\mathbb{E}_{I'}\left[\exp(-I'(s(1+\beta_i)+\beta_i P_i^{-1}\|x\|^{\alpha}))\right]}{1+sP_i\|x\|^{-\alpha}}\right], \tag{3.21}$$

where (a) follows from the fact that fading is independent of all the other random variables and (b) follows from the fact that $h_x \sim \exp(1)$. Now, using the Laplace transform of I' and recalling $\eta = C(\alpha)\sum_{l=1}^{K}\lambda_l p_l P_l^{2/\alpha}$, it can be further simplified to

$$\mathbb{E}\left[\sum_{x\in\Psi_i}\frac{\exp(-\eta(s(1+\beta_i)+\beta_i P_i^{-1}\|x\|^{\alpha})^{\frac{2}{\alpha}})}{1+sP_i\|x\|^{-\alpha}}\right], \tag{3.22}$$

and using Campbell Mecke theorem [69] to

$$\lambda_i p_i\int_{\mathbb{R}^2}\frac{\exp(-\eta(s(1+\beta_i)+\beta_i P_i^{-1}\|x\|^{\alpha})^{\frac{2}{\alpha}})}{1+sP_i\|x\|^{-\alpha}}\mathrm{d}x. \tag{3.23}$$

With this we have now simplified both the terms of (3.17) given respectively by (3.18) and (3.23). We now substitute the first term in (3.15) and evaluate the integral with respect to s as

$$\int_0^{\infty}s^{-1+2m/\alpha}\exp\left(-\eta s^{2/\alpha}\right)\mathrm{d}s=\frac{\eta^{-m}\alpha(m-1)!}{2}, \tag{3.24}$$

where the solution follows from the substitution $s^{2/\alpha} \to y$ followed by integration by parts. Now substituting the second term (given by (3.23)) in (3.15), we get the following integral

$$\lambda_i p_i \int_0^\infty \int_{\mathbb{R}^2} \frac{s^{-1+2m/\alpha} e^{-\eta(s(1+\beta_i)+\beta_i P_i^{-1}\|x\|^\alpha)^{\frac{2}{\alpha}}}}{1+sP_i\|x\|^{-\alpha}} \mathrm{d}x\mathrm{d}s. \tag{3.25}$$

Now use the substitution $(sP_i)^{-1/\alpha}x \to x$, which leads to

$$\lambda_i p_i \int_0^\infty \int_{\mathbb{R}^2} \frac{s^{-1+2m/\alpha} e^{-\eta s^{\frac{2}{\alpha}}((1+\beta_i)+\beta_i\|x\|^\alpha)^{\frac{2}{\alpha}}}}{1+\|x\|^{-\alpha}} (sP_i)^{\frac{2}{\alpha}} \mathrm{d}x\mathrm{d}s. \tag{3.26}$$

Now exchange the integrals to obtain

$$\lambda_i p_i P_i^{\frac{2}{\alpha}} \int_{\mathbb{R}^2} \int_0^\infty \frac{s^{-1+\frac{2(m+1)}{\alpha}} e^{-\eta s^{\frac{2}{\alpha}}((1+\beta_i)+\beta_i\|x\|^\alpha)^{\frac{2}{\alpha}}}}{1+\|x\|^{-\alpha}} \mathrm{d}s\mathrm{d}x. \tag{3.27}$$

Now the inner integral (with respect to s) can be evaluated directly using the definition of $\Gamma(x)$ function or using the substitution $s^{2/\alpha} \to s$ to obtain the below integral.

$$\frac{\lambda_i p_i P_i^{\frac{2}{\alpha}} \alpha m!}{2\eta^{m-1}} \int_{\mathbb{R}^2} \frac{\mathrm{d}x}{(1+\|x\|^{-\alpha})(1+\beta_i+\beta_i\|x\|^\alpha)^{\frac{2}{\alpha}(m+1)}}. \tag{3.28}$$

Now the above integral can be expressed as

$$\frac{1}{(1+\beta_i)^{\frac{2}{\alpha}(m+1)}} \int_{\mathbb{R}^2} \frac{\mathrm{d}x}{(1+\|x\|^{-\alpha})(1+\frac{\beta_i}{1+\beta_i}\|x\|^\alpha)^{\frac{2}{\alpha}(m+1)}} \tag{3.29}$$

Now using the substitution $1+\frac{\beta_i}{1+\beta_i}\|x\|^\alpha \to t^{-1}$, the above expression can be simplified to

$$\frac{2\pi\beta_i^{-2/\alpha}}{\alpha(1+\beta_i)^{2m/\alpha}} \frac{\Gamma(2m/\alpha)\Gamma(1+2/\alpha)}{\Gamma(1+(m+1)2/\alpha)}$$

$$ {}_2F_1(1, 2m/\alpha, 1 + (m+1)2/\alpha, (1+\beta_i)^{-1}), \tag{3.30} $$

where ${}_2F_1$ is the generalized hypergeometric function. Combining all the above we obtain the result. □

Using these Lemmas, we now derive the main coverage probability result.

Theorem 3 (Open Access)**.** *The downlink coverage probability for a typical mobile user in a K-tier open access network assuming $\beta_i > 1,\ \forall\ i$, is*

$$ \mathtt{P_c} = \frac{\pi}{C(\alpha)} \frac{\sum\limits_{i \in \mathcal{K}} p_i \lambda_i P_i^{2/\alpha} \beta_i^{-2/\alpha}}{\sum_{i=1}^{K} p_i \lambda_i P_i^{2/\alpha}} - \sum_{m=1}^{\infty} g(m), \tag{3.31} $$

Proof. The coverage probability is given by (3.4). Since the point processes Δ_i and the corresponding fading random variables are independent, conditioning on the common interference, we can move the expectation inside the product. Hence

$$ 1 - \mathtt{P_c} = \mathbb{E}\left[\prod_{i=1}^{K} \mathbf{1}\left(\frac{M(\Psi_i)}{I - M(\Psi)} < \beta_i \right) \mathbb{E}\left[\mathbf{1}\left(M(\Delta_i) < \beta_i I \right) \right] \right], \tag{3.32} $$

where the inner expectation is with respect to the inactive transmitter sets. We first simplify this inner expectation as follows:

$$ \begin{aligned} &\mathbb{E}\left[\mathbf{1}\left(M(\Delta_i) < \beta_i I \right) \right] \\ &= \mathbb{E}\left[\prod_{x \in \Delta_i} \mathbf{1}\left(P_i h \|x\|^{-\alpha} < \beta_i I \right) \right] &(3.33) \\ &\overset{(a)}{=} \mathbb{E}\left[\prod_{x \in \Delta_i} \left(1 - \exp\left(-\beta_i P_i^{-1} I \|x\|^{\alpha} \right) \right) \right] &(3.34) \end{aligned} $$

$$\overset{(b)}{=} \exp\left(-(1-p_i)\lambda_i \int_{x\in\mathbb{R}^2} \exp\left(-\beta_i P_i^{-1} I\|x\|^\alpha\right) \mathrm{d}x\right) \tag{3.35}$$

$$\overset{(c)}{=} \exp\left(-(1-p_i)\lambda_i \beta_i^{-\frac{2}{\alpha}} I^{-\frac{2}{\alpha}} P_i^{\frac{2}{\alpha}} \pi\Gamma\left(1+\frac{2}{\alpha}\right)\right), \tag{3.36}$$

where (a) follows form the fact that fading is Rayleigh distributed, i.e., $h \sim \exp(1)$, (b) follows from the probability generating functional (PGFL) of PPP [69] and (c) follows from some algebraic manipulations to reduce the integral to a Gamma function. Now recalling the expression of A given by (3.8), we can write

$$1-\mathtt{P_c} = \mathbb{E}\left[\mathbf{1}\left(\max_{i\in\mathcal{K}} \frac{M(\Psi_i)}{\delta_i} < I\right) \exp(-AI^{-2/\alpha})\right]. \tag{3.37}$$

Using the Taylor series expansion of $\exp(-x)$, exchanging the infinite summation and expectation[1],

$$1-\mathtt{P_c} = \sum_{m=0}^{\infty} \frac{(-A)^m}{m!} \mathbb{E}\left[\mathbf{1}\left(\max_{i\in\mathcal{K}} \frac{M(\Psi_i)}{\delta_i} < I\right) I^{-2m/\alpha}\right].$$

The summation can be split as

$$1-\mathtt{P_c} = \mathbb{P}\left(\max_{i\in\mathcal{K}} \frac{M(\Psi_i)}{\delta_i} < I\right) + \sum_{m=1}^{\infty} \frac{(-A)^m}{m!} \mathbb{E}\left[\mathfrak{I}^m\right]. \tag{3.38}$$

The term $1-\mathbb{P}\left(\max_i \frac{M(\Psi_i)}{\delta_i} < I\right)$ is the coverage probability in a fully loaded heterogeneous network where the m-th tier density is $p_m\lambda_m$. This is derived in [5] and is given by

$$1-\mathbb{P}\left(\max_i \frac{M(\Psi_i)}{\delta_i} < I\right) = \frac{\pi}{C(\alpha)} \frac{\sum_{i=1}^{K} p_i\lambda_i P_i^{2/\alpha} \beta_i^{-2/\alpha}}{\sum_{i=1}^{K} p_i\lambda_i P_i^{2/\alpha}}. \tag{3.39}$$

Using Lemma 4 to evaluate $\mathbb{E}\left[\mathfrak{I}^m\right]$, we obtain the result. □

[1]The average of the series is absolutely convergent.

We note that the expression of coverage probability involves infinite summation over the sequence $g(m)$. Therefore, we first show that the infinite summation converges by showing that $|g(m)| \to 0$ as $m \to \infty$. Observe that

$$|g(m)| \leq \left(\frac{A}{\eta}\right)^m \frac{1}{\Gamma(1+\frac{2m}{\alpha})} \leq \frac{(A/\eta)^m}{\lfloor 1+\frac{2m}{\alpha} \rfloor !}$$
$$= \frac{(A/\eta)^m}{\lceil \frac{2m}{\alpha} \rceil !} = \frac{\left[(A/\eta)^{\frac{m}{\lceil \frac{2m}{\alpha} \rceil}}\right]^{\lceil \frac{2m}{\alpha} \rceil}}{\lceil \frac{2m}{\alpha} \rceil !} \to 0, \tag{3.40}$$

where the limiting argument follows from the fact that the sequence of the form $x^n/n! \to 0$. In addition to proving that the series converges, this upper bound on $|g(m)|$ also sheds light on the behavior of the sequence $g(m)$. If $A/\eta < 1$, the bound decreases monotonically with m and hence it is enough to consider only a few significant terms to closely approximate the infinite sum. However, if $A/\eta > 1$, especially if $A/\eta \gg 1$, the upper bound first increases until $\lceil \frac{2m}{\alpha} \rceil \leq (A/\eta)^{\frac{m}{\lceil \frac{2m}{\alpha} \rceil}}$ and decreases thereafter. Therefore, the number of significant terms of $g(m)$ required to approximate the infinite sum would be higher. It can be easily shown that $A/\eta < 1$ for all choices of system parameters when the activity factor of each tier satisfies the following condition

$$p_l > \frac{1}{1 + C(\alpha)\beta_l^{2/\alpha} \left[\pi\Gamma(1+2/\alpha)\right]^{-1}}. \tag{3.41}$$

For $\beta_l = 1$ and $\alpha = 4$, this value of p_l comes out to be ≈ 0.36. Therefore, the infinite sum can be tightly approximated by the first few significant terms of $g(m)$ in most operating scenarios. We will comment more on the convergence of $g(m)$ and the number of terms required to tightly approximate the coverage probability later in this section and in the Numerical Results Section. We now

provide the exact expression for the coverage probability in a closed access network in the following Theorem. We recall that that coverage probability in closed-access is given by (3.4) with the only change that the product is over $\mathcal{B}$ instead of $\mathcal{K}$. By definition, coverage probability in closed access is less than that of open access. Using this definition, the proof proceeds exactly same as that of Theorem 3, and hence is not provided.

Theorem 4 (Closed Access)**.** *The downlink coverage probability of a typical mobile in a K-tier closed access network where a mobile is allowed to connect to $\mathcal{B} \subseteq \mathcal{K}$ tiers assuming $\beta_i > 1,\ \forall\ i$, is*

$$\mathtt{P_c} = \frac{\pi}{C(\alpha)} \frac{\sum\limits_{i \in \mathcal{B}} p_i \lambda_i P_i^{2/\alpha} \beta_i^{-2/\alpha}}{\sum_{i=1}^{K} p_i \lambda_i P_i^{2/\alpha}} - \sum_{m=1}^{\infty} g_c(m), \tag{3.42}$$

where $g_c(m)$ and the corresponding expression for A are given by (3.7) *and* (3.8)*, respectively, with the only difference that the summations defined over set $\mathcal{K}$ are now over set $\mathcal{B}$.*

We conclude this discussion with a note that the proof technique introduced in this section is quite general and can be used to study variants of the load model introduced in the last section. For example, if the network is modeled such that it has a predefined set of BSs that are active and a typical mobile is allowed to connect only to the inactive set, it is easy to observe that the coverage probability under open access assumption is given by $\mathtt{P_c} = 1 - \mathbb{E}\left[\prod_{i=1}^{K} \mathbf{1}\left(\frac{M(\Delta_i)}{I} < \beta_i\right)\right]$. From the proof of Theorem 3, this corresponds to $1 - \mathbb{E}[\exp(-AI^{-2/\alpha})]$ and can easily be evaluated following the

proof technique of Theorem 3. The same argument can be extended to the closed access case as well.

3.4.2 Special Cases of Interest

We now use the results derived in this section to study some special cases and compare the system performance with already known results for fully loaded system. First, we note that for a fully loaded system, the value of $A = 0$ and hence $g(m) = g_c(m) = 0,\ \forall\ m$. Therefore, the coverage probability in this case can be expressed as the following Corollary of Theorems 3 and 4.

Corollary 6 (Fully Loaded)**.** *For a fully loaded system, i.e., $p_i = 1\ \forall\ i$, the coverage probability in open access is given by*

$$\mathtt{P_c} = \frac{\pi}{C(\alpha)} \frac{\sum\limits_{i \in \mathcal{K}} \lambda_i P_i^{2/\alpha} \beta_i^{-2/\alpha}}{\sum_{i=1}^{K} \lambda_i P_i^{2/\alpha}}, \tag{3.43}$$

which is the same as Corollary 1 of Chapter 2. The coverage probability in closed access is also given by (3.43) *with the only difference that the summation over the set $\mathcal{K}$ is now over set $\mathcal{B}$.*

For a single tier open access network, the coverage probability derived in Theorem 3 can be simplified and is expressed as the following Corollary.

Corollary 7 (Single Tier)**.** *The coverage probability for the single tier open access network with BS activity factor p is*

$$\mathtt{P_c} = \frac{\pi \beta^{-2/\alpha}}{C(\alpha)} - \sum_{m=1}^{\infty} g(m), \tag{3.44}$$

where the terms $\frac{A}{\eta}$ *and* $\frac{B}{\eta}$ *appearing in the expression of* $g(m)$ *given by* (3.7),

$$\frac{A}{\eta} = \frac{\pi\Gamma(1+\frac{2}{\alpha})(1-p)}{C(\alpha)p\beta^{\frac{2}{\alpha}}} \tag{3.45}$$

$$\frac{B}{\eta} = \frac{{}_2F_1(1, \frac{2m}{\alpha}, 1+\frac{(m+1)2}{\alpha}, \frac{1}{1+\beta})}{C(\alpha)\beta^{\frac{2}{\alpha}}(1+\beta)^{\frac{2m}{\alpha}}}. \tag{3.46}$$

Remark 1 (Scale invariance of a single tier network)**.** *From Corollary 7, we note that for any BS activity factor* p*, the coverage probability in a single tier open access network is independent of the BS density* λ *and transmit power* P*. This is henceforth referred to as "scale-invariance" of cellular networks to changes in the BS density and their transmit powers.*

Remark 1 is a generalization of a similar result derived for fully loaded networks in Chapter 2, which can easily be seen from Corollary 6. In addition to single tier networks, it was also observed in Chapter 2 that the general fully loaded open access multi tier networks also exhibit scale invariance if the target `SIR`s for all the tiers are the same. This can also be easily deduced from Corollary 6. Motivated by this observation, we study the coverage probability for our proposed load model in open-access multi tier networks under the assumption that the target `SIR` is the same for all tiers in the next Corollary.

Corollary 8 (Coverage Probability: K-Tier with same β)**.** *The coverage probability for a* K*-tier open access network under the proposed load model assuming target* `SIR`*s to be the same* $(= \beta)$ *for all the tiers is given by* (3.44)*, with the difference that the term* $\frac{A}{\eta}$ *appearing in the expression of* $g(m)$ *given by*

(3.7) *is*

$$\frac{A}{\eta} = \frac{\pi\Gamma(1+\frac{2}{\alpha})}{C(\alpha)\beta^{2/\alpha}} \frac{\sum_{l=1}^{K}(1-p_l)\lambda_l P_l^{2/\alpha}}{\sum_{l=1}^{K} p_l\lambda_l P_l^{2/\alpha}}, \tag{3.47}$$

and $\frac{B}{\eta}$ *appearing in* (3.7) *is given by* (3.46).

Remark 2 (Scale invariance of K-tier HetNets with same β)**.** *From Corollary 8, we note that the coverage probability for K-tier HetNets is not scale invariant in general, even when target* SIR*s of all the tiers are the same. However, the invariance property does hold when the BS activity factors of all the tiers are the same. Interestingly, the coverage probability in this case is same as that of a single tier network given by Corollary 7.*

To understand this remark, we consider the following simple example.

Example 1 (Scale invariance in a 2-tier HetNet)**.** *Consider a two tier network with BS activity factors p_1 and p_2. If $p_1 < p_2$, increasing the density of the first tier leads to a higher increase in the intended power due to the higher likelihood of having a closer tier-1 BS as the serving BS but a relatively smaller increase in the interference power. The coverage probability in this case is expected to increase. On the other hand, if $p_1 > p_2$, increasing the density of tier-1 BSs leads to higher increase in the interference power as compared to the intended power, leading to a decrease in the coverage probability. The two effects cancel each other when the activity factors of the two tiers are the same.*

We now extend this result and derive exact condition under which the addition of $(K+1)^{th}$ tier won't affect (or will improve) the coverage of the

existing K-tier network. We again assume same target SIR for all the tiers. The result is given in the following Corollary.

Corollary 9 (Same β: Effect of adding $(K+1)^{th}$ tier)**.** *The overall coverage probability increases with the addition of the* $(K+1)^{th}$ *tier if the load on the new tier satisfies*

$$p_{K+1} < \sum_{l=1}^{K} p_l \frac{\lambda_l P_l^{2/\alpha}}{\sum_{i=1}^{K} \lambda_i P_i^{2/\alpha}}, \tag{3.48}$$

decreases if the inequality is reversed and remains the same if (3.48) *holds with equality.*

Proof. From Corollary 8 we note that the only term in the coverage probability expression that will change with the addition of a new tier is A/η. It can be expressed as

$$\frac{A}{\eta} = \frac{\pi\Gamma(1+\frac{2}{\alpha})}{C(\alpha)\beta^{2/\alpha}} \left(\left[\sum_{l=1}^{K} p_l \frac{\lambda_l P_l^{2/\alpha}}{\sum_{i=1}^{K} \lambda_i P_i^{2/\alpha}} \right]^{-1} - 1 \right). \tag{3.49}$$

Defining effective load on a K-tier network as

$$p_{\text{eff}}^{(K)} = \sum_{l=1}^{K} p_l \frac{\lambda_l P_l^{2/\alpha}}{\sum_{i=1}^{K} \lambda_i P_i^{2/\alpha}}, \tag{3.50}$$

A/η can be expressed as

$$\frac{A}{\eta} = \frac{\pi\Gamma(1+\frac{2}{\alpha})}{C(\alpha)\beta^{2/\alpha}} \left(\frac{1 - p_{\text{eff}}^{(K)}}{p_{\text{eff}}^{(K)}} \right), \tag{3.51}$$

which is the same as (3.45) for the single tier coverage result derived in Corollary 7. From this equivalence, it follows that the coverage probability is a

decreasing function of p_{eff}. Therefore, if the addition of the new tier leads to lower effective load on the network, the coverage will increase. This can be shown to be the case when (3.48) holds as follows:

$$p_{\text{eff}}^{(K+1)} = \sum_{l=1}^{K+1} p_l \frac{\lambda_l P_l^{2/\alpha}}{\sum_{i=1}^{K+1} \lambda_i P_i^{2/\alpha}} \tag{3.52}$$

$$\leq \frac{\sum_{l=1}^{K} p_l \lambda_l P_l^{\frac{2}{\alpha}}}{\sum_{i=1}^{K+1} \lambda_i P_i^{\frac{2}{\alpha}}} + \frac{\lambda_{K+1} P_{K+1}^{\frac{2}{\alpha}}}{\sum_{i=1}^{K+1} \lambda_i P_i^{\frac{2}{\alpha}}} \frac{\sum_{l=1}^{K} p_l \lambda_l P_l^{\frac{2}{\alpha}}}{\sum_{i=1}^{K} \lambda_i P_i^{\frac{2}{\alpha}}} \tag{3.53}$$

$$= p_{\text{eff}}^{(K)}. \tag{3.54}$$

The other two results follow using the same argument. □

3.4.3 Bounds on the Coverage Probability

Evaluation of the exact expression of the coverage probability requires an infinite summation. Although we have argued that the summation can be tightly approximated by considering only a first few terms, we haven't yet provided a formal method to determine the exact number of terms required such that the approximation error is within predefined limit, say ϵ. Interestingly, this can be achieved as a by-product of the set of bounds we derive in this section that can be made arbitrarily tight. The idea is to use the following identity of $\exp(-x)$.

Lemma 5. *For $x \geq 0$ and $m > 0$,*

$$\sum_{i=0}^{2m-1} \frac{(-x)^i}{i!} \leq \exp(-x) \leq \sum_{i=0}^{2m} \frac{(-x)^i}{i!}. \tag{3.55}$$

Proof. The proof follows from induction. Since $\exp(-0) = 1$ and $\sum_{i=0}^{2m-1} \frac{(-0)^i}{i!} = 1$, it suffices to prove that $\frac{d}{dx} \sum_{i=0}^{2m-1} \frac{(-x)^i}{i!} - \exp(-x) < 0$, which follows from the upper bound when $m = m - 1$. □

Using this identity in the proof of Theorem 3 results in the following bounds.

Lemma 6 (Bounds on Coverage Probability)**.** *For $m > 0$, the coverage probability for the proposed load model can be bounded as*

$$-\sum_{i=1}^{2m} g(i) \leq \mathtt{P_c} - \frac{\pi}{C(\alpha)} \frac{\sum_{i=1}^{K} p_i \lambda_i P_i^{2/\alpha} \beta_i^{-2/\alpha}}{\sum_{i=1}^{K} p_i \lambda_i P_i^{2/\alpha}} \leq -\sum_{i=1}^{2m-1} g(i) \tag{3.56}$$

Clearly, these bounds can be made arbitrarily tight by increasing the value of m. Interestingly, these bounds are closely related to the exact expression of coverage probability derived in Theorem 3. In particular, the upper and lower bounds are derived by truncating the infinite sum over $g(m)$ at odd and even number of terms, respectively. Therefore, these bounds provide a direct way to find the number of terms of $g(m)$ required to ensure an approximation error within a predefined limit ϵ, which is equal to M_ϵ, where $M_\epsilon = \min_m |g(m)| < \epsilon$. We will use this observation in the study of the convergence of infinite sum over $g(m)$ in the Numerical Results Section.

We conclude this section by noting that some terms of the sequence $g(m)$ can be expressed in closed form, leading to closed form bounds for the special case when $\alpha = 4$ and $m = 2$. The bounds in this case depend only on

the first two terms of $g(m)$ that can be expressed as

$$g(1) = \frac{-A}{\eta}\left\{\frac{2}{\sqrt{\pi}} - \frac{4\sqrt{\pi}}{\eta}\sum_{i=1}^{K}\frac{\lambda_i p_i P_i^{1/2}\beta_i^{-1/2}}{1+\sqrt{1+\beta_i}}\right\} \tag{3.57}$$

$$g(2) = \left(\frac{A}{\eta}\right)^2 \left\{1 - \frac{2\pi}{\eta}\sum_{i=1}^{K}\lambda_i p_i P_i^{\frac{1}{2}}(\beta_i^{-\frac{1}{2}} - \csc^{-1}(\sqrt{1+\beta_i}))\right\}. \tag{3.58}$$

3.5 Numerical Results

Since most of the analytical results derived in this chapter are fairly self-explanatory and do not require separate numerical treatment, we will provide only those results which help in validating key modeling assumptions or help better visualize certain important trends.

3.5.1 Convergence of Infinite Sum

We study the convergence of the infinite sum appearing in the coverage probability expression in Figures 3.2 and 3.3. Figure 3.2 plots the truncated series $\sum_{i=1}^{m} g(i)$ as the function of m for a single tier network and hence gives insights about the number of terms required until the series converges. To understand the trends, recall that the ratio A/η decreases monotonically with the activity factor p. Therefore, the number of terms required for the series to converge are higher when the BS activity factor is lower. Moreover, for the case when $A/\eta > 1$, i.e., $p = .25$, the series first increases until a certain point and then decreases and finally converges to its limiting value. This trend has

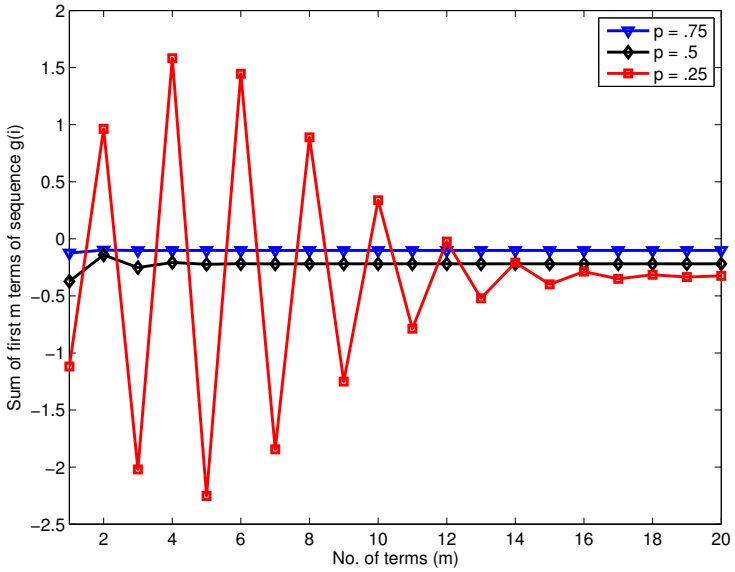

Figure 3.2: Plot showing the convergence of the series $\sum_i g(i)$ for various BS activity factors in a single tier network with $\beta = 1$.

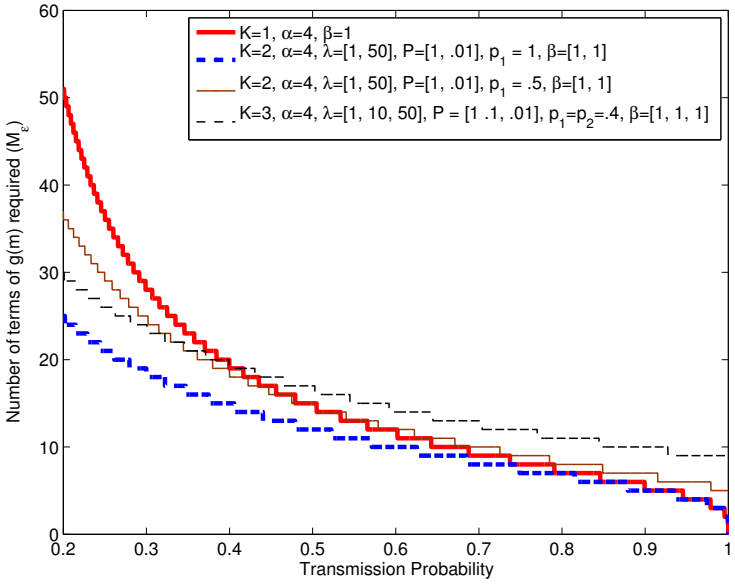

Figure 3.3: Number of terms of the sequence $g(m)$ required as the function of the transmission probability of the lowest tier for $\epsilon = 10^{-8}$.

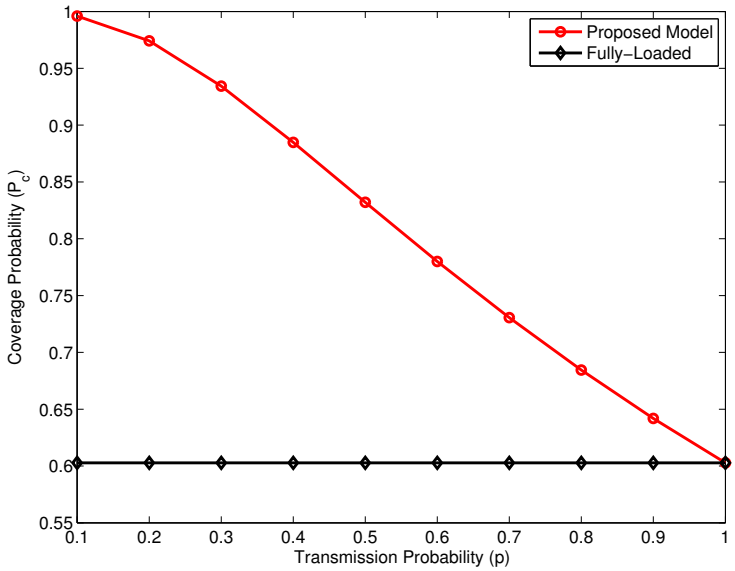

Figure 3.4: Coverage probability as a function of transmission probability is a single tier network ($\beta = 1$ and $\alpha = 3.8$).

been discussed in detail earlier in the chapter when we proved the convergence of the infinite sum. To provide an idea of the number of terms required such that the approximation is within ϵ of the exact value, we plot the number of terms M_ϵ for various scenarios in Figure 3.3. We again note that the number of terms required are reasonably small unless the transmission probability of some tier is extremely small.

3.5.2 System Model Validation

Comparison with the fully loaded system. After gaining insights into the behavior of the coverage probability expression, we now use it to highlight the importance of the proposed model by comparing the coverage

results of a single tier network with those of a fully loaded system in Figure 3.4. Although a huge difference in the coverage guarantees was expected for very low BS activity factors, it is indeed interesting that the coverage estimates assuming full load are quite pessimistic even for reasonably high load scenarios, such as $p = .7 - .8$.

Comparison with an actual 4G deployment. After highlighting the importance of the proposed load model, we now validate the PPP model in the context of the proposed load model. While this model seems sensible for the small cells, especially the ones driven by unplanned user deployments, such as femtocells, it is dubious for the centrally planned tiers such as macrocells. Therefore, with a special focus on the macrocells, we consider three location models for a two tier HetNet: i) macrocell locations modeled as a realization of a PPP, ii) macrocell locations modeled as a hexagonal grid, iii) macrocell locations drawn from an actual 4G deployment over 40×40 Km^2 area [1, 5]. The second tier is modeled as a PPP in all three cases. Recall that the same dataset of actual 4G deployment was also used for the model validation in Chapter 2. The numerically evaluated coverage probability results for all these models along with the analytical results of the proposed load model and the fully-loaded PPP model are presented in Figure 3.5. We first note that the proposed PPP model is about as accurate as the grid model when compared to the actual 4G deployment, with the grid model providing an upper bound and the PPP model providing a lower bound to the actual coverage probability. This is consistent with the conclusions of [1] and Chapter 2,

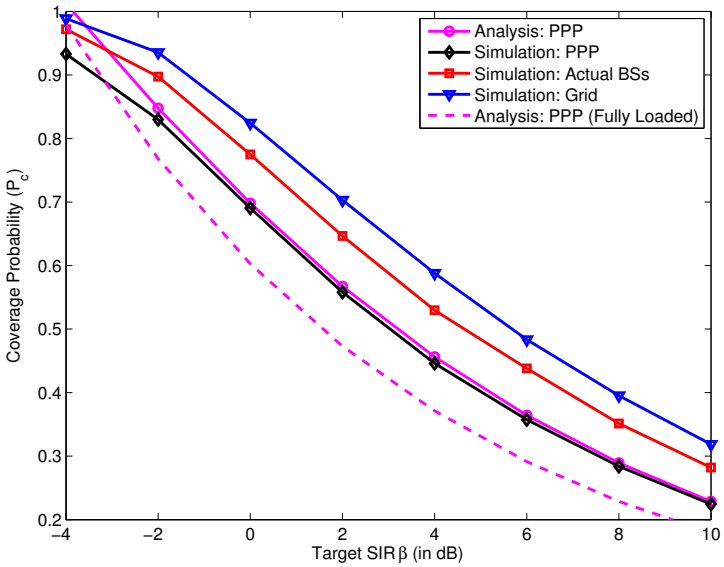

Figure 3.5: Comparison of $\mathtt{P_c}$ in PPP and grid models with the actual BS locations of macrocells. The second tier is modeled as PPP in all three cases ($K = 2$, $\lambda_2 = 2\lambda_1$, $P = [1, 0.01]$, $L = 40 \times 40$ Km^2, $\alpha = 3.8$, $p = [0.8, 0.6]$, $\beta_1 = \beta_2 = \beta$).

which focus on fully-loaded cellular models in single tier and multi tier cellular networks, respectively. Second, we note that the analytical results derived for the proposed load model are accurate down to about -2dB even though they were derived under the assumption that the target `SIR` is greater than 0dB for all the tiers. Since this covers most of the cell edge users as well, the proposed analytical results are reasonably accurate in the operational regime of the current cellular networks. Third, we note that the fully-loaded model provides a very loose lower bound to the actual coverage probability, thereby highlighting again the importance of the proposed load model.

Comparison with a detailed simulation. The following two assumptions were made to facilitate analysis: i) the activity factors are the same for all the BSs of a particular tier, and ii) the activity of each BS is independent of the other BSs. We now validate these assumptions by comparing the analytical results with a detailed system simulation. For this comparison, we consider a simulation setup consisting of a two tier HetNet, with the BSs of each tier modeled by independent PPPs. The user locations are also modeled by an independent PPP with density λ_u. As in the proposed model, each user is associated with the BS that provides the best received signal strength. From this, we calculate the actual load being served by each BS in terms of the number of users, which we denote by N_{x_i} for a BS located at x_i. Assuming the number of orthogonal resource blocks, e.g., time-frequency resource blocks in LTE [75], to be M, the activity factor of a BS in each resource block can be expressed as $p_{x_i} = N_{x_i}/M$ as discussed in Section 3.3. To keep the setup simple, we consider the regime where the probability of having $N_{x_i} > M$ for any BS is small and whenever it happens, the activity factor for that BS is assumed to be 1. For this setup, the coverage probability results are presented in Figure 3.6.

For a meaningful comparison of this simulation result with the analytical results, we first need to find analytical expressions of the activity factors p_i as a function of the user density λ_u. For this, we leverage Corollary 2 of Chapter 2, where it is shown that the fraction of users served by j^{th} tier is

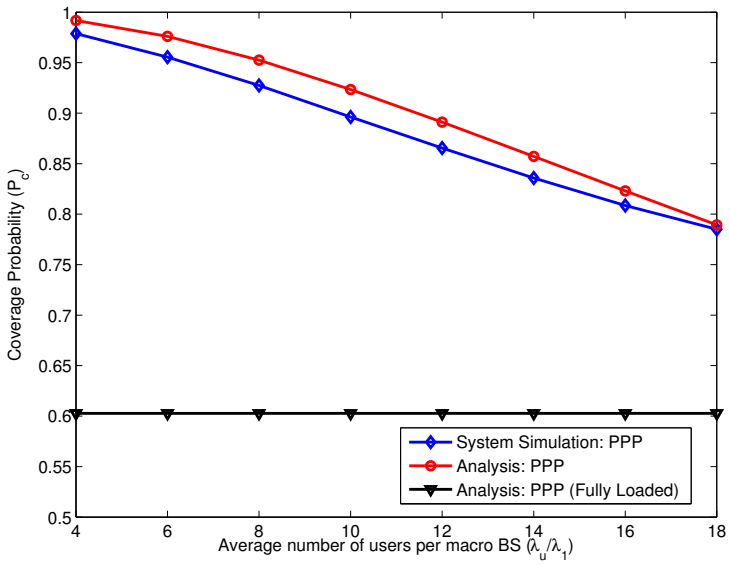

Figure 3.6: Comparison of the derived theoretical results with detailed system simulation accounting for actual load factors resulting from actual coverage regions ($K = 2$, $P = [1, 0.1]$, $\beta_1 = \beta_2 = 0$dB, $\lambda_1 = \lambda_2$, $M_{RB} = 20$, $\alpha = 3.8$).

given by

$$\bar{N}_j = \frac{\lambda_j \left(P_j/\beta_j\right)^{\frac{2}{\alpha}}}{\sum_{i=1}^{K} \lambda_i \left(P_i/\beta_i\right)^{\frac{2}{\alpha}}}. \tag{3.59}$$

Using this result, the average number of users served by a j^{th} tier BS (average load) is $\frac{\lambda_u}{\lambda_j}\bar{N}_j$. Therefore, assuming M resource blocks, the activity factor in a randomly chosen resource block is

$$p_j = \frac{1}{M}\frac{\lambda_u \bar{N}_j}{\lambda_j} = \frac{\lambda_u}{M}\frac{\left(P_j/\beta_j\right)^{\frac{2}{\alpha}}}{\sum_{i=1}^{K} \lambda_i \left(P_i/\beta_i\right)^{\frac{2}{\alpha}}}. \tag{3.60}$$

We use this analytical result for the the load factors in the coverage probability results derived in the chapter to plot the analytical results as a function of the user density in Figure 3.6. Comparing this result with the numerical result

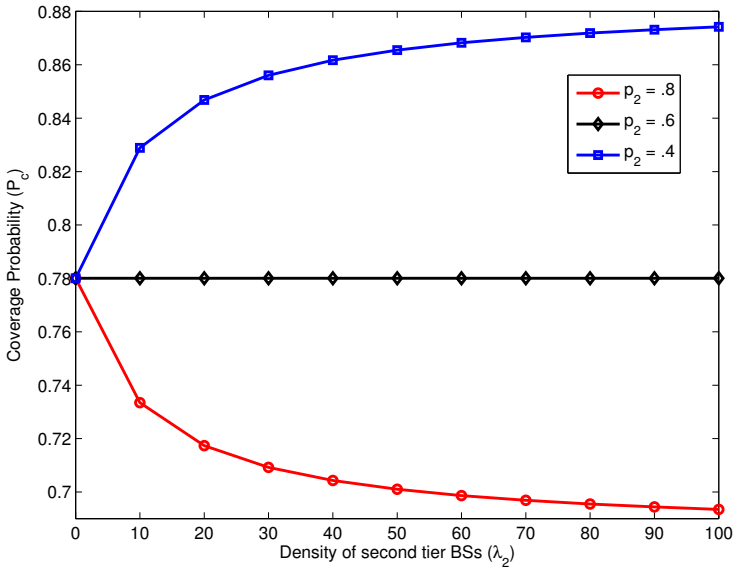

Figure 3.7: Coverage probability in a two tier network as a function of λ_2 ($\beta = [1, 1]$, $P = [1, .01]$, $\lambda_1 = 1$, $p_1 = .6$ and $\alpha = 3.8$).

obtained form a detailed simulation, we note that the two are reasonably close, especially relative to the previously known results for the fully-loaded system. This validates the two assumptions mentioned in the starting of this discussion.

3.5.3 Scale Invariance and Effect of Adding Small Cells

We now consider a two tier system and plot the coverage probability as a function of the density of second tier for various BS activity factors in Figure 3.7. The target `SIR` is fixed to be the same for both the tiers. We first note that the network is invariant to the changes in density when $p_1 = p_2$ as discussed in the last section. More importantly, we note that the coverage probability increases with λ_2 when the second tier BSs are less active than the

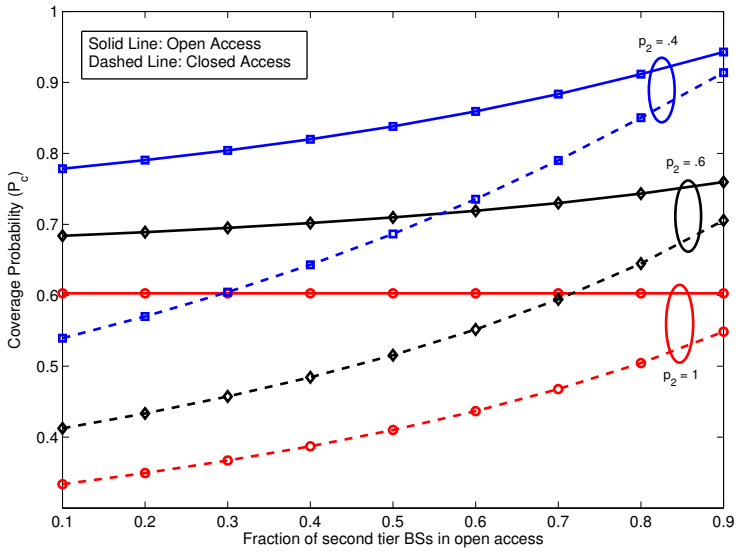

Figure 3.8: Coverage probability in a two tier network as a function of the fraction of the second tier BSs in open access ($\beta = [1, 1]$, $P = [1, .01]$, $\lambda_2^{(c)} = 10\lambda_1$, $p_1 = 1$ and $\alpha = 3.8$). The density of second tier BSs in open access $\lambda_2^{(o)} = \frac{f}{1-f}\lambda_2^{(c)}$, where f is the fraction of BSs in open access.

first tier. This is an important result from the perspective of small cells, which are generally less active than macrocell BSs. Therefore, the coverage probability of the network should increase with the addition of small cells in this regime. This is a strong rebuttal to the viewpoint that unplanned infrastructure might bring down a cellular network due to increased interference. On the other hand, if a tier of BSs is added which is more active than the macrocells, the coverage would decrease, although this case seems pretty unlikely given the high load handled by the macrocells.

3.5.4 Open vs Closed Access

So far in this section we have only studied open access networks, where a mobile user can access any BS in the network. We now study the effect of closed access on the coverage probability, with a focus on a particular scenario of interest where a certain fraction of BSs of a particular tier are in closed access while the others are in open access. This scenario is especially important in the current HetNets, where the access permissions of a particular small cell might be different for different set of users. It is easy to argue that this scenario can be visualized as a special case of the general model developed in this chapter. To understand this, assume that a fraction f of BSs of a certain tier are in open access – we assume that a BS is in open or closed access independent of the other BSs. Therefore, the density of BSs in open access $\lambda_i^{(o)}$ and closed access $\lambda_i^{(c)}$ can be evaluated from the following two equations

$$f = \frac{\lambda_i^{(o)}}{\lambda_i^{(o)} + \lambda_i^{(c)}} \tag{3.61}$$

$$\lambda_i = \lambda_i^{(o)} + \lambda_i^{(c)}. \tag{3.62}$$

Now this tier can be divided into two tiers, one with density $\lambda_i^{(o)}$, which is in open access, and other with density $\lambda_i^{(c)}$, which is in closed access – both form independent PPPs.

To study this scenario in detail, we consider a two tier HetNet, where the first tier is in open access and fraction $1 - f$ of BSs of the second tier is in closed access. For this scenario, the coverage probability as a function of f is presented in Figure 3.8 for various load scenarios. The results confirm

the intuition that the gap in open and closed access results reduces when the value of f is increased. More interestingly, the gap is smaller when the second tier BSs are lightly loaded. This implies that the effect of interference due to closed access small cells on coverage probability is negligible if there are enough small cells in open access.

3.6 Summary

In this chapter, we have incorporated a flexible notion of BS load in the baseline HetNet model developed in the previous chapter by introducing a new idea of *conditionally thinning* the interference field, conditional on the connection of a typical mobile to its serving BS. We have shown that this conditional thinning is a natural way of modeling different levels of load on different types of BSs arising mainly from the differences in their coverage footprints. We observe that the fully loaded models are extremely pessimistic in terms of coverage, and the analysis shows that adding lightly loaded access points (e.g. pico or femtocells) to the macrocell network always increases coverage probability. In Apendix B, we show that the same idea of conditional thinning can also be used to study non-uniform user distributions, e.g., in the current capacity centric deployments, where the users are more likely to lie closer to the BSs.

Chapter 4

Downlink MIMO HetNets: Modeling, Ordering Results and Performance Analysis

As discussed in Chapter 1, handling current data deluge requires much higher data rates than contemporary cellular networks were designed for. Two strategies that stand out to provide such spectral efficiencies are: i) deploy low power nodes to reduce frequency reuse distance, and ii) equip base stations (BSs) with multiple antennas to enable the use of multiple antenna techniques, such as beamforming and SDMA. Multiple antenna techniques are already relatively mature, being part of multiple wireless standards such as IEEE 802.11e WiMAX and 3GPP LTE-A [12], apart from plethora of theoretical research activities in academia [13]. Similarly, the concept of deploying low power nodes (HetNet), discussed in Chapters 2 and 3, has been researched both in industry and academia for a fairly long time, see for example [36, 86] and the references therein. The standardization activities for HetNets have also started in 3GPP release 10 [14]. These activities clearly indicate that multi-antenna techniques and HetNets will coexist and complement each other in the future wireless networks and should not be studied in isolation, as has been typically done in the literature, including all the extensions of Chapter 2 and 3, see [87] for a survey. In this chapter, we address this problem and

develop a general tractable model and the corresponding analytical tools for multi-antenna HetNets using techniques from stochastic orders and stochastic geometry.

4.1 Related Work and Motivation

As discussed in Chapter 2, a more natural approach to model HetNets is by using random spatial models, where the locations of the BSs are assumed to form a realization of a two-dimensional point process, the simplest being the Poisson Point Process (PPP) [1, 5]. This model has the advantages of being scalable to multiple classes of overlaid BSs and accurate to model location randomness, especially that of the small cells. As demonstrated in Chapters 2 and 3, powerful tools from stochastic geometry can be used to derive performance results for general multi-tier networks in closed form, which was not even possible for single-tier networks using deterministic grid model [5]. While sufficient progress has been made in modeling single-antenna (SISO) HetNets [5, 49, 51, 56], the efforts to understand multi-antenna HetNets have just begun, e.g., see [88].

The main challenge in modeling multi-antenna HetNets is the number of possible multi-antenna techniques to choose from in each tier along with their tractable characterization. As a result, most prior works on multi-antenna HetNets have focused only on two-tier networks. For this chapter, the most relevant one is [89], where SU-BF was shown to achieve better coverage than multiuser linear beamforming on the downlink of femtocell-aided cellular

network assuming perfect channel state information (CSI). Random orthogonal beamforming with max-rate scheduling and coordinated beamforming for femtocell underlay networks was analyzed in [90], [91], respectively. The effect of channel uncertainty on linear beamforming in two-tier networks was investigated in [92]. In addition to the contributions in cellular networks, there has been extensive work on analyzing multi-antenna techniques in wireless ad hoc networks, which is also related to our work since several tools and techniques developed therein can be employed and extended to HetNets. Several single-user MIMO techniques, such as spatial diversity, open loop transmission and spatial multiplexing, have been studied, see for instance [93–95]. The performance of multiuser MIMO communication in a Poisson field of interferers, with perfect and quantized CSI at the transmitter was investigated in [96] and [97], respectively.

4.2 Contributions and Outcomes

Downlink model for multi-antenna HetNets. In Section 4.3, we develop a comprehensive downlink model consisting of K tiers or classes of BSs, such as macrocells, femtocells, picocells and distributed antennas. The BSs across tiers differ in terms of transmit power, deployment density, target `SIR`, number of transmit antennas, number of users served in each resource block, and the type of multi-antenna transmission. We also consider the possibility of closed subscriber group or closed access in which a typical user is granted access to only a few BSs, while the rest purely act as interferers.

Ordering results for coverage and rate. For general system models, such as the one considered in this chapter, it is not always possible to express key performance metrics such as coverage probability and per user rate in closed form. In the absence of simple analytical expressions, it is difficult to compare different transmission techniques in general HetNet settings. To facilitate this comparison, in Section 4.4 we derive *ordering results* for both the coverage probability and the rate per user in both open and closed access networks, using tools from stochastic orders. Interested readers can refer to [98–101] for applications of stochastic orders to conventional wireless networks. While circumventing the need for deriving coverage and rate expressions, this analysis leads to several system design guidelines, e.g., it concretely demonstrates the superiority of serving a single user in each resource block, either by SISO or SU-BF, as opposed to serving multiple users by SDMA, both in terms of coverage and rate, under a per user power constraint. The BS locations for this analysis may be drawn from any general stationary point process, not necessarily independent across tiers, which is a significant generalization of the baseline HetNet model presented in Chapter 2.

Area spectral efficiency comparison. While comparison of different configurations of multi-antenna HetNets in terms of coverage probability and average rate per user is conclusive from the ordering results, it does not directly capture the fact that some transmission techniques serve more users than the others and hence provide higher sum data rate. In order to capture this effect, in Section 4.5 we additionally consider ASE, which gives the

number of bits transmitted per unit area per unit time per unit bandwidth. To facilitate the comparison of transmission techniques in terms of ASE, we first derive an upper bound on the coverage probability of a typical user in both open and closed access networks assuming that the BS locations for each tier are drawn from independent PPPs and show that it can be reduced to a closed form expression for the "full" SDMA case (where the number of users served is equal to the number of antennas). The tightness of the bound is studied and it is shown that the closed form bound derived for full SDMA is tight down to very low target SIRs. Using this expression and the SISO HetNet coverage probability results derived in Chapter 2, we derive ASE results for various transmission techniques in closed form. Main consequences of this analysis are: i) for the same density of BSs, SISO HetNets have lower ASE than SDMA since they serve fewer users. Interestingly, despite serving fewer users, SU-BF outperforms SDMA in moderate and high target SIR regime, and ii) when the BS densities are adjusted such that all the transmission techniques serve the same density of users, the ASEs of SU-BF, SISO and SDMA follow the same ordering as that of coverage probability and average rate per user.

4.3 System Model

4.3.1 System Setup and BS Location Model

We consider K different classes or tiers of BSs, indexed by the set $\mathcal{K} = \{1, 2, \ldots, K\}$. The BSs across tiers differ in terms of their transmit

Table 4.1: Notation Summary

Notation	Description
Φ_k	A point process modeling the locations of k^{th} tier BSs
Φ_u	An independent PPP modeling user locations
$P_k; \lambda_k$	Downlink transmit power to each user; deployment density of the k^{th} tier BSs
M_k, Ψ_k	Number of transmit antennas; number of users served in each resource block by a k^{th} tier BS
h_{kx}	Channel power of the direct link from a k^{th} tier BS located at x to a typical user, $h_{kx} \sim \Gamma(\Delta_k, 1)$ with $\Delta_k = M_k - \Psi_k + 1$
g_{jy}	Channel power of the interfering link from a j^{th} tier BS located at y to a typical user, $g_{jy} \sim \Gamma(\Psi_y, 1)$
$\mathcal{K}; \{x_k\}$	$\{1, 2, \ldots, K\}; \{x_{k_1}, x_{k_1+1}, \ldots x_{k_2}\}$, where the values of k_1 and k_2 will be clear from the context
$\mathcal{B}$	$\mathcal{B} \subset \mathcal{K}$ denotes the set of open access tiers
$\mathtt{P_c}; \beta_k$	Coverage probability (in terms of SIR); target SIR for k^{th} tier
$\mathtt{R_c}; \mathcal{O}_k, T_k$	Rate coverage; fraction of resources allocated to each user served by k^{th} tier; k^{th} tier target rate
η	Area spectral efficiency
$Z_{k,m}$	$Z_{k,m} = X_1/X_2$, where $X_1 \sim \Gamma(k, 1)$ and $X_2 \sim \Gamma(m, 1)$

power P_k with which they transmit to each user, deployment density λ_k, target SIR β_k, number of antennas M_k and number of users served by each BS in a given resource block $\Psi_k \leq M_k$, $\forall k \in \mathcal{K}$. While in open access networks a mobile user can connect to any BS, in closed access networks the access is restricted to $\mathcal{B} \subset \mathcal{K}$ tiers. For the ordering part (Section 4.4), the locations of BSs of each tier are drawn from a general stationary point process Φ_k. The point processes Φ_k are not necessarily independent. Please note that this is a significant generalization of the baseline HetNet model proposed in Chapter 2, which assumed each tier to be sampled from an independent PPP. This is enabled by the fact that the ordering results are based on the ordering of the fading components of the channel power distributions for various setups and do not depend upon the spatial point process governing the locations of the BSs. However, we do require further assumptions for the ASE comparison, which involves the derivation of explicit expressions for coverage probabilities. Therefore, for the ASE analysis we will consider the more familiar independent PPP model, which was the focus of Chapters 2 and 3, where each tier of BSs is modeled by an independent homogeneous PPP of density λ_k.

Nevertheless, this is a fairly general model that captures the current deployment trends in 4G networks, e.g., it is easy to imagine hundreds of femtocells coexisting in each macrocell, transmitting at orders of magnitude lower power than macrocells, having relatively small number of antennas due to smaller form factor, serving smaller number of users due to smaller coverage footprints and providing restricted access to their own users due to a smaller

backhaul capacity or privacy concerns. A two-tier illustration of the proposed system model is shown in Figure 4.1, where a high power macro tier with four transmit antennas per BS coexists with a low power pico tier with two antennas per BS. Owing to its bigger coverage footprint, each macro BS serves higher load than its pico counterpart as discussed in Chapter 3. The coverage region of each BS in this illustration corresponds to the region where it provides the maximum average received power, thereby leading to a weighted Voronoi tessellation as discussed in detail in Chapter 2.

We model the user locations by an independent PPP Φ_u and focus on the downlink analysis performed at a single-antenna user located at the origin. This analysis at the origin is facilitated by Slivnyak's theorem, which states that the properties observed at a typical point of Φ_u are the same as those observed by the point at origin in the point process $\Phi_u \cup \{0\}$ [69]. For the interference, we consider full-buffer model where the interfering BSs are assumed to be always transmitting [1,5]. More sophisticated load models [102] along with non-uniform user distributions [103] can also be considered, e.g., using ideas from Chapter 3, but are out of the scope of this chapter.

4.3.2 Channel Model

Before going into the technical details, it is important to understand that the channel power distribution of the link from a multi-antenna BS to a typical single-antenna user depends upon the transmission technique and whether it is a serving BS or an interferer. For example, if it is a serving BS,

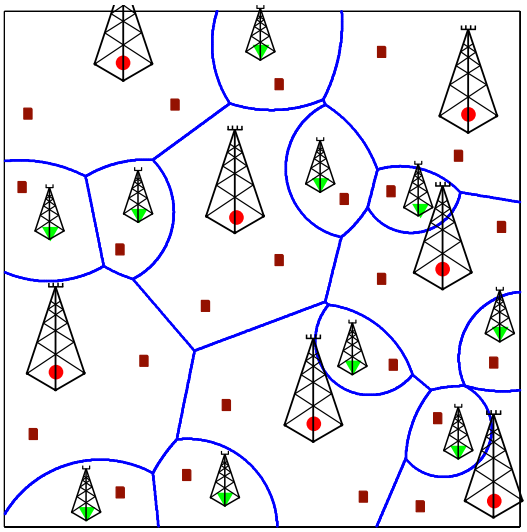

Figure 4.1: An illustration of a possible two-tier multi antenna HetNet configuration, with four antenna macro BSs serving two users and two antenna pico BSs serving one user each. The circles, triangles and rectangles represent macro BSs, pico BSs, and mobile users, respectively.

it may precode its signals for a typical user depending upon the transmission technique, which may lead to a different channel distribution from the case when it simply acts as an interferer. Therefore, to develop a general framework in which the BSs across tiers may differ in terms of the number of transmit antennas and the transmission technique, we assume that the channel power for the direct link from a k^{th} tier BS located at $x_k \in \mathbb{R}^2$ to a typical user located at origin is denoted by h_{kx_k} and for the interfering link from a j^{th} tier BS located at $y \in \mathbb{R}^2$ is denoted by g_{jy}. In this chapter, we assume perfect CSI and focus on zero-forcing precoding, under which for Rayleigh fading it can be argued that the channel power distributions of both the direct and the interfering links follow the Gamma distribution [104]. As discussed in detail in

Appendix C.1, it can therefore be shown that for zero forcing $h_{kx} \sim \Gamma(\Delta_k, 1)$ and $g_{jy} \sim \Gamma(\Psi_j, 1)$, where $\Delta_k = M_k - \Psi_k + 1$. Note that for SISO transmission there is no precoding and hence the channel gains h_{kx} and g_{kx} from a BS to a typical user are the same. Under Rayleigh fading assumption, both follow exp(1) distribution, which is the same as $\Gamma(1, 1)$ distribution.

Although for brevity we limit our discussion to Rayleigh fading channels, other fading distributions under which the channel power for both the desired and the interfering links follow Gamma distribution after precoding, e.g., Nakagami-m, can also be studied using the proposed techniques. The shape and the scale parameters for the Gamma distributions corresponding to the channel powers of the desired and interfering links can be derived using techniques well known in the literature, e.g., see [105]. For concreteness, we will focus on the following three transmission techniques in this chapter:

- **SDMA:** In this case, a k^{th} tier BS with M_k antennas serves $\Psi_k > 1$ users in each resource block. When $\Psi_k = M_k$, we term it as full SDMA, for which $\Delta_k = 1$.
- **SU-BF:** In this case, a k^{th} tier BS serves $\Psi_k = 1$ users in each resource block.
- **SISO:** Baseline single-antenna case [5], where each BS serves one user in each resource block.

For each transmission technique, the received power at a typical single-

antenna user located at origin from the BS located at $x_k \in \Phi_k$ is

$$P_r = P_k h_{kx_k} \|x_k\|^{-\alpha}, \tag{4.1}$$

where α is the path loss exponent, because we assume a per user power constraint in this formulation. The received SIR can now be expressed as

$$\texttt{SIR}(x_k) = \frac{P_k h_{kx_k} \|x_k\|^{-\alpha}}{\sum_{j \in \mathcal{K}} \sum_{y \in \Phi_j \setminus x_k} P_j g_{jy} \|y\|^{-\alpha}}. \tag{4.2}$$

For notational simplicity, we assume that the thermal noise is negligible as compared to the self interference and is hence ignored. This is justified in the current wireless networks, which are typically interference limited [83]. As will be evident from our analysis, thermal noise can be included in the proposed framework with little extra work. For cell association, we assume that the set of candidate serving BSs is the collection of the BSs that provide the strongest instantaneous received power from each tier to which a typical mobile is allowed to connect. A typical user is said to be in coverage if the received SIR from one of these candidate serving BSs is more than the respective target SIR, as discussed in detail in the next section. We conclude this section with a note that although we consider perfect CSI, it is possible to relax this assumption to study the effect of imperfect CSI on the performance of multi-antenna HetNets, as discussed below.

Remark 3 (Imperfect CSI)**.** *Using tools from [97, 106, 107], it is possible to derive the received channel power and interference statistics for both SU-BF and SDMA under quantized channel directional information (CDI). In particular, in a system where each user reports CDI using B feedback bits, the desired*

channel gain is exponentially distributed for both SU-BF and SDMA. However, in the latter case, the inter-user interference is not completely eliminated due to zero-forcing beamforming using imperfect CSI. Therefore, an additional interference term, independent of the multi-tier interference, appears in the denominator of (4.2)*, which is distributed as* $\Gamma(\Psi_k, \delta)$ *with* $\delta = 2^{-\frac{B}{M_k - 1}}$ *under quantization cell approximation [97].*

4.4 Ordering Results for Coverage and Rate

This is the first main technical section of this chapter, where we compare the performance of various transmission techniques in terms of coverage probability and rate per user. We first study coverage probability in detail and then show that the analysis can be easily extended to study rate per user. We begin by formally defining the coverage probability.

Definition 2 (Coverage probability)**.** *A typical user in an open access network is said to be in coverage if its downlink* SIR *from at least one of the BSs is higher than the corresponding target. This can be mathematically expressed as:*

$$\mathtt{P_c} = \mathbb{P}\left(\bigcup_{k \in \mathcal{K}} \max_{x_k \in \Phi_k} \mathtt{SIR}(x_k) > \beta_k\right). \tag{4.3}$$

The coverage probability can be equivalently defined as the average area in coverage or the average fraction of users in coverage. For closed access networks, the definition remains the same, except that the union is now over the set of tiers $\mathcal{B} \subset \mathcal{K}$ *to which a typical user is allowed to connect.*

Remark 4 (Open access vs. closed access coverage)**.** *The coverage probability in open access networks is always higher than in closed access networks. It follows directly by definition of coverage probability along with the fact that for* $\mathcal{B} \subset \mathcal{K}$

$$\mathbf{1}\left(\bigcup_{k\in\mathcal{B}} \max_{x_k\in\Phi_k} \mathtt{SIR}(x_k) > \beta_k\right) \leq \mathbf{1}\left(\bigcup_{k\in\mathcal{K}} \max_{x_k\in\Phi_k} \mathtt{SIR}(x_k) > \beta_k\right), \tag{4.4}$$

where the indicator function $\mathbf{1}(\mathcal{E})$ *is* 1 *when event* $\mathcal{E}$ *holds and* 0 *otherwise.*

Owing to the complexity of the system model considered in this chapter, it is not always possible to express coverage probability in simple closed form for any general system configuration, especially when the BS locations are drawn from a general point process. As evident from our analysis in the next section, this presents the first main challenge in comparing various transmission techniques. In this section, we take a slightly different view of this problem and focus on "ordering" the relative performance of different system configurations using tools from stochastic orders. Interested readers can refer to [108] for details on stochastic orders. It is important to note that stochastic orders operate on random variables, as opposed to related majorization theory, which defines partial order on deterministic vectors [109].

This powerful approach allows insights into the relative performance of different transmission techniques, while circumventing the need to evaluate complicated expressions for the performance metrics such as coverage and rate. We begin by defining first order stochastic dominance as follows.

Definition 3 (First order stochastic dominance)**.** *For any two random variables (rvs) Z_1 and Z_2, Z_1 (first order) stochastically dominates Z_2 if and only if*

$$\mathbb{P}[Z_1 > z] \geq \mathbb{P}[Z_2 > z], \ \forall z. \tag{4.5}$$

Equivalently, Z_1 is greater than Z_2 in the usual stochastic order and is denoted by $Z_1 \geq_{\text{st}} Z_2$.

Therefore, $Z_1 \geq_{\text{st}} Z_2$ if and only if the complementary cumulative distribution function (CCDF) of Z_1 dominates that of Z_2 over the whole range. It is intuitively clear and will be made precise later in this section that the proper understanding of the ordering of received `SIR` for different system configurations plays a central role in studying their coverage and rate ordering. The main technical idea behind the proposed ordering approach is to condition on the distribution of the BS locations and then order the received `SIR`s for different transmission techniques by ordering the fading components of the channel powers of both the desired and the interfering links. This idea of ordering the channel power distributions has been previously used in the literature to compare the performance of wireless links in terms of signal-to-noise-ratio (`SNR`) and related metrics such as ergodic capacity and error rates for different modulation schemes, e.g., see [98] and references therein. However, to the best of our understanding, this approach has never been used for `SIR` ordering in the context of HetNets. Now note that the received `SIR` can be alternatively

expressed as

$$\texttt{SIR}(x_k) = \frac{P_k \|x_k\|^{-\alpha}}{\sum_{j \in \mathcal{K}} \sum_{y \in \Phi_j \setminus x_k} P_j g_{jy} / h_{kx_k} \|y\|^{-\alpha}}, \tag{4.6}$$

where the randomness due to propagation channel is lumped into ratios of Gamma random variables h_{kx_k} and g_{jy}. Therefore, it turns out that it is important first to understand the ordering of the ratios of Gamma random variables, which is studied next.

4.4.1 Ordering of the Ratios of Gamma Random Variables

For concreteness, define the ratio of two random variables $X_1 \sim \Gamma(k, 1)$ and $X_2 \sim \Gamma(m, 1)$ by $Z_{k,m} = X_1/X_2$. It is easy to derive the cumulative distribution function (CDF) of $Z_{k,m}$ using basic algebraic manipulations and is given by

$$F_{Z_{k,m}}(z) = 1 - \frac{1}{\Gamma(m)} \sum_{i=0}^{k-1} \frac{\Gamma(m+i)}{\Gamma(1+i)} \frac{z^i}{(z+1)^{m+i}}. \tag{4.7}$$

Note that the ratios of Gamma random variables are known in much more general settings, e.g., [110] studies the distribution of the ratio of the powers of two possibly dependent random variables where both come from Gamma family, but these generalizations are not required in this chapter. The form of the distribution function (4.7) is such that for a given k_1, m_1 and k_2, m_2, it is not easy to derive conditions on these variables under which the CCDF of one ratio $Z_{k,m}$ dominates that of the other over the whole range of z. Therefore, the above result is of little help in providing direct ordering of two random variables Z_{k_1,m_1} and Z_{k_2,m_2}. We take an indirect route, which uses the following

technical result about the equivalence in distribution of the Gamma random variable and the sum of i.i.d. exponentially distributed random variables. Given this technical result, the main result can then be proved using *coupling* arguments. We first state the equivalence result, which is well-known and can be easily verified using characteristic functions. We then remark on how to use coupling arguments to establish stochastic dominance before stating the main result.

Lemma 7. *For i.i.d* $\{X_i\}$*, with* $X_i \sim \exp(1)$*, the random variable* $X = \sum_{i=1}^{k} X_i$ *is* $X \sim \Gamma(k, 1)$*.*

Remark 5 (Using coupling to establish stochastic dominance)**.** *One way to prove* $Z_1 \geq_{\text{st}} Z_2$ *is to find two random variables* Z_1^* *and* Z_2^* *with the same distributions as* Z_1 *and* Z_2*, respectively, such that it is always the case that* $Z_1^* \geq Z_2^*$*. This approach of using the same source of randomness to generate two random variables* Z_1^* *and* Z_2^* *satisfying the above relation and thereby establishing the stochastic dominance result is termed as* coupling *[111].*

We now prove the following result on the ordering of the ratios of the Gamma random variables.

Lemma 8 (Ordering of the ratios of Gamma rvs)**.** *A random variable* Z_{k_1,m_1} *defined as the ratio of two Gamma random variables (first order) stochastically dominates* Z_{k_2,m_2} *if* $k_1 \geq k_2$ *and* $m_1 \leq m_2$*.*

Proof. Using the equivalence in distribution of the Gamma random variable

and the sum of exponential random variables given by Lemma 7, we can generate a random variable $Z^*_{k_1,m_1}$ with the same distribution as Z_{k_1,m_1} as follows

$$Z^*_{k_1,m_1} = \frac{\sum_{i=1}^{k_1} Y_{1,i}}{\sum_{j=1}^{m_1} Y_{2,j}}, \tag{4.8}$$

where $\{Y_{m,n}\}$ is the set of i.i.d. random variables such that $Y_{m,n} \sim \exp(1)$. This equivalent representation will facilitate the use of standard coupling arguments, under which the goal now is to generate another random variable $Z^*_{k_2,m_2}$ with the same sources of randomness as that of $Z^*_{k_1,m_1}$, which has the same distribution as Z_{k_2,m_2}, and show that $Z^*_{k_1,m_1} \geq Z^*_{k_2,m_2}$. Under the condition $k_1 \geq k_2$, this can be achieved by expressing $Z^*_{k_1,m_1}$ as follows

$$Z^*_{k_1,m_1} = \frac{\sum_{i=1}^{k_2} Y_{1,i} + \sum_{i=k_2+1}^{k_1} Y_{1,i}}{\sum_{j=1}^{m_1} Y_{2,i}} \tag{4.9}$$

$$\geq \frac{\sum_{i=1}^{k_2} Y_{1,i}}{\sum_{j=1}^{m_1} Y_{2,i}} \overset{(a)}{\geq} \frac{\sum_{i=1}^{k_2} Y_{1,i}}{\sum_{j=1}^{m_2} Y_{2,i}} \overset{(b)}{=} Z^*_{k_2,m_2}, \tag{4.10}$$

where (a) follows from the condition $m_1 \leq m_2$, and (b) from Lemma 7. This completes the proof. □

Remark 6. *The set of conditions $k_1 \geq k_2$ and $m_1 \leq m_2$ is stronger than the single condition $k_1/m_1 \geq k_2/m_2$, which first comes to mind from the equivalence of Gamma random variables and the sum of exponential random variables stated in Lemma 7. In fact it is easy to argue that the above stochastic dominance is not always true if the only condition on the variables is $k_1/m_1 \geq k_2/m_2$. For instance, consider a case where $k_2 \gg k_1$ and $m_2 \gg m_1$ such that $k_1/m_1 \geq k_2/m_2$. The distribution of Z_{k_2,m_2} is concentrated around*

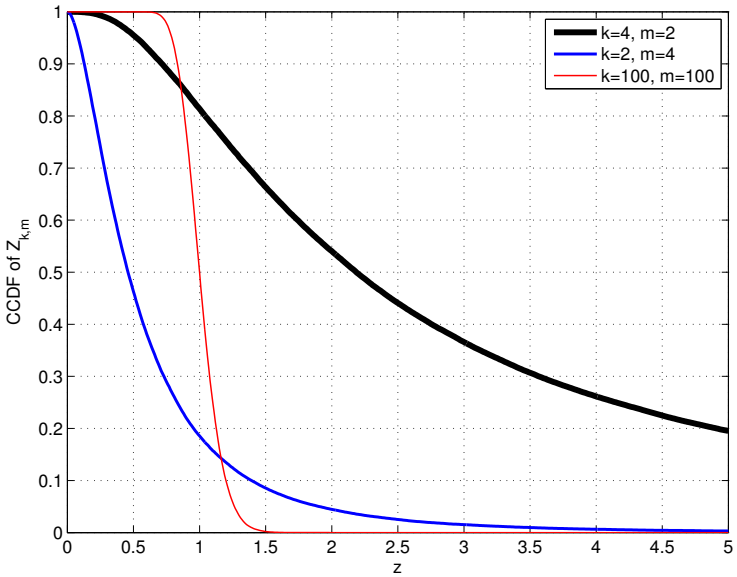

Figure 4.2: The CCDFs of the ratios of Gamma random variables for different shape parameters k and m.

its mean and cannot be dominated by the distribution of Z_{k_1,m_1} *due to significant difference in their shapes. This is illustrated in Figure 4.2, where the ratio of Gamma random variables with shape parameters* $k_1 = 4$ *and* $m_1 = 2$ *does not dominate the one with* $k_2 = 100$ *and* $m_2 = 100$ *due to concentration, although* $k_1/m_1 \geq k_2/m_2$ *holds.*

To prove the main ordering results of this section, we need to extend the stochastic dominance result of two random variables to multi-variate function of random variables. The result is given in the following Lemma and follows directly from the coupling arguments [111].

Lemma 9. *If* $X_i \geq_{\text{st}} Y_i$ *for all* $1 \leq i \leq n$*, then*

$$\mathbb{E}[g(X_1, X_2, \ldots, X_n)] \geq \mathbb{E}[g(Y_1, Y_2, \ldots, Y_n)], \tag{4.11}$$

for all multi-variate functions g that are non-decreasing in each component.

4.4.2 Coverage Probability Ordering

Using Lemma 9, we now derive the following general result on the coverage probability ordering in K-tier open access multi-antenna HetNets. As evident from the analysis and remarked later in this section, all the results and insights carry over to closed access networks as well. Recall that the goal of this analysis is to compare or "order" the performance of different systems and not to obtain the exact expressions for the performance metrics in any given system.

Theorem 5 (Coverage ordering in open access networks)**.** *The coverage probability of a K-tier open access HetNet with system parameters $\{\Delta_k\}$ and $\{\Psi_k\}$ is higher than or equal to the one with system parameters $\{\Delta'_k\}$ and $\{\Psi'_k\}$ if $\Delta_k \geq \Delta'_k$ and $\Psi_k \leq \Psi'_k$ for $k \in \mathcal{K}$.*

Proof. By definition, the coverage probability for open access networks can be expressed as

$$\mathtt{P_c} = \mathbb{E}\mathbf{1}\left(\bigcup_{k\in\mathcal{K}} \max_{x_k\in\Phi_k} \frac{P_k h_{kx_k}\|x_k\|^{-\alpha}}{\sum\limits_{j\in\mathcal{K}}\sum\limits_{y\in\Phi_j\setminus x_k} P_j g_{jy}\|y\|^{-\alpha}} > \beta_k\right) \tag{4.12}$$

$$= \mathbb{E}\mathbf{1}\left(\bigcup_{k\in\mathcal{K}} \max_{x_k\in\Phi_k} \frac{P_k \|x_k\|^{-\alpha}}{\sum\limits_{j\in\mathcal{K}}\sum\limits_{y\in\Phi_j\setminus x_k} P_j Z_{jk}\|y\|^{-\alpha}} > \beta_k\right), \tag{4.13}$$

where with slight abuse of notation (dropping the BS location from the subscript), $Z_{jk} = g_{jy}/h_{kx_k}$ is defined as the ratio of two Gamma random vari-

ables corresponding to the K-tier HetNet with system parameters $\{\Delta_k\}$ and $\{\Psi_k\}$. Denote the corresponding ratio for the other system setup by Z'_{jk}. By Lemma 8, $Z'_{jk} \geq_{\text{st}} Z_{jk}$ if $\Psi'_j \geq \Psi_k$ and $\Delta'_j \leq \Delta_k$. Now it is easy to show that the indicator function in (4.13)

$$g(\{Z_{jk}\}) = \mathbf{1}\left(\bigcup_{k\in\mathcal{K}} \max_{x_k\in\Phi_k} \frac{P_k\|x_k\|^{-\alpha}}{\sum_{j\in\mathcal{K}}\sum_{y\in\Phi_j\setminus x_k} P_j Z_{jk}\|y\|^{-\alpha}} > \beta_k\right),$$

is an element wise decreasing function of Z_{jk}. Therefore, by Lemma 9 the result follows. □

Using this result, we can make some general comments about the coverage probability in certain realistic deployments. We begin by studying the effect of the number of users served in each tier on coverage probability.

Corollary 10 (Effect of number of users)**.** *For two different K-tier open access HetNets, with the same number of antennas in each corresponding tier, the one that serves less users in each tier than the other provides higher coverage due to higher beamforming gain.*

The proof of the above corollary directly follows from the fact that under the same number of antennas for two setups, the one that serves less users in each tier has $\Delta_k \geq \Delta'_k$ and $\Psi_k \leq \Psi'_k$ for each tier, leading to higher coverage. An important extension of the above corollary is the comparison of the SDMA with SU-BF systems when the number of transmit antennas in each corresponding tier are the same. The result is stated as the following corollary.

Corollary 11 (SDMA vs. SU-BF)**.** *For two K-tier HetNets, with the same number of antennas in each corresponding tier, one performing SU-BF in each tier and the other performing SDMA, the coverage probability in the SU-BF case will always be higher.*

Another consequence of this general ordering result is the comparison of SISO with SU-BF and SDMA, with the SDMA case specialized to full SDMA. Recall that in case of full SDMA, $\Delta_k = 1$ and $\Psi_k = M_k$ for all the tiers. The result is given in the following corollary.

Corollary 12 (SU-BF vs. SISO vs. full SDMA)**.** *For three K-tier HetNet setups, one performing SU-BF in each tier, another doing SISO transmission in each tier and the last one doing full SDMA in each tier, the coverage probability in case of SU-BF is higher than that of SISO, which in turn outperforms full SDMA. The number of antennas in the corresponding tiers of SU-BF and full SDMA HetNets need not be the same.*

The proof follows from the fact that the shape parameters in case of SU-BF are $\Delta_k = M_k$ and $\Psi_k = 1$, where $M_k > 1$ is the number of antennas; in case of SISO are $\Delta'_k = \Psi'_k = 1$; and in case of full SDMA are $\Delta''_k = 1$ and $\Psi''_k = M_k$, where $M_k > 1$ is the number of transmit antennas.

For closed access networks, it can be shown that the coverage ordering result derived in Theorem 5 holds under a slightly weaker condition because a typical mobile is not allowed to connect to all the tiers. The result is given as the following Corollary of Theorem 5 and the proof is skipped. Due to the

similarity of this result with the open access case, the insights gained for the open access networks above carry over to the closed access networks as well.

Corollary 13 (Coverage ordering in closed access)**.** *For two HetNets, with* $\mathcal{B} \subset \mathcal{K}$ *open access tiers, the one with system parameters* $\{\Delta_k\}$ *and* $\{\Psi_k\}$ *has a higher or equal coverage than the one with system parameters* $\{\Delta'_k\}$ *and* $\{\Psi'_k\}$ *if* $\Delta_k \geq \Delta'_k$ *for* $k \in \mathcal{B}$ *and* $\Psi_k \leq \Psi'_k$ *for* $k \in \mathcal{K}$.

4.4.3 Ordering Result for Rate per User

Another metric of interest for the performance evaluation of HetNets is the rate achievable per user. In addition to the link quality (characterized in terms of SIR), it also depends upon the effective resources allocated to each user. For tractability, we make following two assumptions on resource allocation: i) each k^{th} tier BS serves same number of users, and ii) each BS allocates equal time-frequency resources to all its users. For SDMA, it should be noted that several users will be scheduled on the same time-frequency resource block. Interested readers can refer to [112] for more details on the motivation and validation of these assumptions. Under these assumptions, we denote the effective time-frequency resources, e.g., bandwidth, allocated to a user served by a k^{th} tier BS by $\mathcal{O}_k$. The two assumptions on resource allocation ensure that $\mathcal{O}_k$ is the same for all the users served by any k^{th} tier BS. Therefore, the downlink rate of a typical user served by a k^{th} tier BS located at $x_k \in \Phi_k$ can be expressed as

$$R(x_k) = \mathcal{O}_k \log_2(1 + \mathtt{SIR}(x_k)). \tag{4.14}$$

Due to the difficulties in modeling exact load on each BS [5], which often requires characterization of the service areas for different types of BSs, it is challenging to characterize $\mathcal{O}_k$ and hence derive exact expressions for per user rate distribution [112]. However, we now show that to compare different multi-antenna transmission techniques, this characterization is not required and the general ordering result derived above for the coverage probability can be easily extended for the rate per user as well. Before going into the technical details, it is important to note that the loading across tiers may differ significantly due to the orders of magnitude differences in their coverage footprints. Therefore, the effective resources $\mathcal{O}_k$ available in small cells for each user might be significantly higher than the macrocells. In such a case, it might be beneficial for a user to connect to a small cell even though it may not provide the best `SIR` over the network. We will capture this characteristic of HetNets in our definition of rate distribution below. Due to the interpretation of a minimum rate required by each application, e.g., video, we will study rate distribution in terms of "rate coverage", which is defined below. It is just the CCDF of rate when the target rates are the same for all the tiers.

Definition 4 (Rate coverage)**.** *A typical user in an open access network is said to be in rate coverage if its effective downlink rate from at least one of the BSs in the network is higher than the corresponding target. We denote the target rate for a k^{th} tier BS as T_k. Rate coverage can now be mathematically*

expressed as

$$\mathtt{R_c} = \mathbb{P}\left(\bigcup_{k\in\mathcal{K}} \max_{x\in\Phi_k} \mathcal{O}_k \log_2(1+\mathtt{SIR}(x_k)) > T_k\right). \tag{4.15}$$

For closed access, the expression remains the same except that the union is now over the set $\mathcal{B} \subset \mathcal{K}$.

It is easy to show that the rate coverage for open access networks is always higher than the closed access networks. This follows from the same arguments that were used in case of coverage probability earlier in this section. We now state the main ordering result for rate coverage in the following Theorem.

Theorem 6 (Ordering result for rate coverage)**.** *For two* K*-tier HetNets with the same resource allocation per user* $\mathcal{O}_k$ *for each corresponding tier, the one with system parameters* $\{\Delta_k\}$ *and* $\{\Psi_k\}$ *has equal or higher rate coverage than the one with system parameters* $\{\Delta'_k\}$ *and* $\{\Psi'_k\}$ *if* $\Psi_k \leq \Psi'_k$ *for all* $k \in \mathcal{K}$*, and* $\Delta_k \geq \Delta'_k$ *for all* $k \in \mathcal{K}$ *in open access and all* $k \in \mathcal{B}$ *in closed access.*

Proof. The rate coverage can be expressed as

$$\mathtt{R_c} = \mathbb{E}\mathbf{1}\left(\bigcup_{k\in\mathcal{K}} \max_{x\in\Phi_k} \mathcal{O}_k \log_2(1+\mathtt{SIR}(x_k)) > T_k\right), \tag{4.16}$$

where $\mathtt{SIR}(x_k)$ can be expressed as

$$\mathtt{SIR}(x_k) = \frac{P_k h_{kx_k} \|x_k\|^{-\alpha}}{\sum\limits_{j\in\mathcal{K}} \sum\limits_{y\in\Phi_j\setminus x_k} P_j g_{jy} \|y\|^{-\alpha}}, \tag{4.17}$$

$$= \frac{P_k \|x_k\|^{-\alpha}}{\sum\limits_{j \in \mathcal{K}} \sum\limits_{y \in \Phi_j \setminus x_k} P_j Z_{jk} \|y\|^{-\alpha}}, \tag{4.18}$$

where as in the proof of Theorem 5, we define $Z_{jk} = g_{jy}/h_{kx_k}$ as the ratio of the two Gamma random variables. Now note that the indicator function inside the expectation of (4.16) is an element wise decreasing function of Z_{jk}, from which the result follows on the same lines as the proof of Theorem 5. □

Remark 7 (Same ordering for coverage and rate per user)**.** *From Theorems 5 and 6, we note that the ordering conditions for rate per user are the same as that of coverage probability. Therefore, all the conclusions, including the ordering of SDMA, SU-BF and SISO transmission techniques, derived for coverage probability carry over to the rate per user case as well.*

Although it is clear from the above discussion that both SU-BF and SISO outperform SDMA, both in terms of coverage probability and average rate per user, it is important to note that we have not yet accounted for the fact that SDMA serves more users than both SISO and SU-BF, and may result in a higher sum-data rate. To address this, we compare the three transmission techniques in terms of ASE in the next section.

4.5 Coverage Probability and ASE Performance

This is the second main technical section of the chapter where we derive an upper bound on the coverage probability of a typical user in a K-tier HetNet, where the transmission techniques adopted by each tier are characterized

in terms of the shape parameters Δ_k and Ψ_k of the Gamma rvs. Recall that the coverage probability is formally defined in Definition 2. For this analysis, we assume that BS locations of each tier are drawn from an independent PPP Φ_k with density λ_k. Although this model is not as general as the one considered in the previous section, it is likely accurate for modeling the opportunistic deployment of small cells and has been validated for planned tiers, such as single-antenna macrocells by empirical observations [82] and theoretical arguments under sufficient channel randomness [113]. In this chapter, we validate it in the context of coverage probability in MIMO HetNets by comparing it with an actual 4G deployment and the popular grid model in the numerical results section.

4.5.1 Upper Bound on Coverage Probability

Before deriving the upper bound, we first derive an expression for the Laplace transform of interference. The result is given in Lemma 10. This generalizes the Laplace transform of interference derived for K-tier SISO HetNets with Rayleigh fading, i.e., exponential channel powers, in Theorem 1 of Chapter 2.

Lemma 10. *The Laplace transform of interference* $\mathcal{L}_I(s) = \mathbb{E}\left[e^{-sI}\right]$, *where* $I = \sum_{j\in\mathcal{K}} \sum_{y\in\Phi_j} P_j g_{jy} \|y\|^{-\alpha}$ *is*

$$\mathcal{L}_I(s) = \exp\left(-s^{\frac{2}{\alpha}} \sum_{j\in\mathcal{K}} \lambda_j P_j^{\frac{2}{\alpha}} C(\alpha, \Psi_j)\right), \tag{4.19}$$

where

$$C(\alpha, \Psi_j) = \frac{2\pi}{\alpha} \sum_{m=1}^{\Psi_j} \binom{\Psi_j}{m} B\left(\Psi_j - m + \frac{2}{\alpha}, m - \frac{2}{\alpha}\right), \tag{4.20}$$

and $B(x, y) = \int_0^1 t^{x-1}(1-t)^{y-1}\mathrm{d}t$ *is Euler's Beta function.*

Proof. The Laplace transform of interference $\mathcal{L}_I(s) = \mathbb{E}_{I_{x_k}}\left[e^{-sI}\right]$ can be derived as follows:

$$\mathbb{E}_I\left[e^{-sI}\right] = \mathbb{E}_I\left[e^{-s\sum_{j\in\mathcal{K}}\sum_{y\in\Phi_j} P_j g_{jy}\|y\|^{-\alpha}}\right] \tag{4.21}$$

$$\overset{(a)}{=} \prod_{j\in\mathcal{K}} \mathbb{E}\left[\prod_{y\in\Phi_j} e^{-sP_j g_{jy}\|y\|^{-\alpha}}\right] \tag{4.22}$$

$$\overset{(b)}{=} \prod_{j\in\mathcal{K}} \mathbb{E}_{\Phi_j}\left[\prod_{y\in\Phi_j} \mathcal{L}_{g_{jy}}\left(sP_j\|y\|^{-\alpha}\right)\right] \tag{4.23}$$

$$\overset{(c)}{=} \prod_{j\in\mathcal{K}} \exp\left(-\lambda_j \int_{\mathbb{R}^2} \left(1 - \mathcal{L}_{g_{jy}}\left(sP_j\|y\|^{-\alpha}\right)\right)\mathrm{d}y\right) \tag{4.24}$$

$$\overset{(d)}{=} \prod_{j\in\mathcal{K}} \exp\left(-\lambda_j \int_{\mathbb{R}^2} \left(1 - \frac{1}{(1+sP_j\|y\|^{-\alpha})^{\Psi_j}}\right)\mathrm{d}y\right) \tag{4.25}$$

$$= \prod_{j\in\mathcal{K}} \exp\left(-\lambda_j \int_{\mathbb{R}^2} \frac{(1+sP_j\|y\|^{-\alpha})^{\Psi_j} - 1}{(1+sP_j\|y\|^{-\alpha})^{\Psi_j}}\mathrm{d}y\right) \tag{4.26}$$

$$\overset{(e)}{=} \prod_{j\in\mathcal{K}} \exp\left(-\lambda_j \int_{\mathbb{R}^2} \frac{\sum_{m=1}^{\Psi_j}\binom{\Psi_j}{m}(sP_j\|y\|^{-\alpha})^m}{(1+sP_j\|y\|^{-\alpha})^{\Psi_j}}\mathrm{d}y\right) \tag{4.27}$$

$$= \prod_{j\in\mathcal{K}} \exp\left(-\lambda_j \sum_{m=1}^{\Psi_j}\binom{\Psi_j}{m} \int_{\mathbb{R}^2} \frac{(s_{x_k}P_j\|y\|^{-\alpha})^m}{(1+s_{x_k}P_j\|y\|^{-\alpha})^{\Psi_j}}\mathrm{d}y\right) \tag{4.28}$$

$$\overset{(f)}{=} \prod_{j\in\mathcal{K}} e^{-2\pi\lambda_j(s_{x_k}P_j)^{\frac{2}{\alpha}}\sum_{m=1}^{\Psi_j}\binom{\Psi_j}{m}\int_0^\infty \frac{r-\alpha m}{(1+r^{-\alpha})^{\Psi_j}} r\mathrm{d}r} \tag{4.29}$$

$$\stackrel{(g)}{=} \exp\left(-s_{x_k}^{\frac{2}{\alpha}} \sum_{j\in\mathcal{K}} \lambda_j P_j^{\frac{2}{\alpha}} C(\alpha, \Psi_j)\right), \tag{4.30}$$

where (a) follows from the independence of the tiers, (b) follows from the fact that channel powers are independent of the BS locations, (c) follows from PGFL of PPP [69], (d) follows from the Laplace transform of the $g_{jy} \sim \Gamma(\Psi_j, 1)$, (e) follows from Binomial theorem, and (f) follows from converting to Cartesian to polar coordinates, and (g) follows by substituting $(1+r^{-\alpha})^{-1} \to t$ to convert the integral into Euler's Beta function $B(x,y) = \int_0^1 t^{x-1}(1-t)^{y-1}\mathrm{d}t$. □

Using this result, we now derive an upper bound on the coverage probability and the result is given in Theorem 7.

Theorem 7. *The coverage probability of a typical user in a K-tier open access HetNet is upper bounded by*

$$\mathtt{P_c} \leq \sum_{k\in\mathcal{K}} \lambda_k \mathcal{A}_k, \tag{4.31}$$

where $s_{x_k} = \beta_k \|x_k\|^\alpha P_k^{-1}$ and

$$\mathcal{A}_k = \sum_{i=0}^{\Delta_k - 1} \frac{1}{i!} \int\limits_{x_k\in\mathbb{R}^2} (-s_{x_k})^i \frac{\delta^i}{\delta(s_{x_k})^i} \mathcal{L}_{I_{x_k}}(s_{x_k}) \mathrm{d}x_k. \tag{4.32}$$

The upper bound for closed access networks is the same except that the summation in (4.31) *is over the set $\mathcal{B}$ instead of $\mathcal{K}$.*

Proof. We prove the result for open access networks and will highlight exactly where the proof will differ for closed access networks. Starting with the

definition of the coverage probability:

$$\mathtt{P_c} = \mathbb{E}\left[1\left(\bigcup_{k\in\mathcal{K}}\bigcup_{x_k\in\Phi_k} \mathtt{SIR}(x_k) > \beta_k\right)\right] \tag{4.33}$$

$$\overset{(a)}{\leq} \mathbb{E}\left[\sum_{k\in\mathcal{K}}\sum_{x_k\in\Phi_k} 1\left(\mathtt{SIR}(x_k) > \beta_k\right)\right] \tag{4.34}$$

$$= \sum_{k\in\mathcal{K}} \mathbb{E}\left[\sum_{x_k\in\Phi_k} 1\left(P_k h_{kx_k}\|x_k\|^{-\alpha} > \beta_k I_{x_k}\right)\right], \tag{4.35}$$

where (a) follows from the union bound and I_{x_k} is the interference received by the typical user when it is connected to the k^{th} tier BS located at x_k, i.e.,

$$I_{x_k} = \sum_{j\in\mathcal{K}}\sum_{y\in\Phi_j\setminus x_k} P_j g_{jy}\|y\|^{-\alpha}. \tag{4.36}$$

Note that for closed access, the summation in (4.34) and (4.35) will be over $\mathcal{B}$ instead of $\mathcal{K}$. This is the only difference in the proofs of open and closed access cases. Continuing with the proof of open access case, since the channel power of the direct link is independent of everything else, we can take the expectation w.r.t. h_{kx_k} inside (4.35) to write the coverage probability as

$$\mathtt{P_c} \leq \sum_{k\in\mathcal{K}} \mathbb{E}\left[\sum_{x_k\in\Phi_k} \mathbb{P}\left(h_{kx_k} > \beta_k I_{x_k}\|x_k\|^{\alpha} P_k^{-1}\right)\right]. \tag{4.37}$$

Now we first evaluate the probability $\mathbb{P}(h_{kx} > z)$ as follows

$$\mathbb{P}(h_{kx} > z) \overset{(a)}{=} \frac{\Gamma(\Delta_k, z)}{\Gamma(\Delta_k)} \overset{(b)}{=} e^{-z}\sum_{i=0}^{\Delta_k-1}\frac{z^i}{i!}, \tag{4.38}$$

where (a) follows from $h_{kx} \sim \Gamma(\Delta_k, 1)$, and $\Gamma(\Delta_k, z)$ in the numerator is the upper incomplete Gamma function given by $\Gamma(\Delta_k, z) = \int_z^\infty u^{\Delta_k-1}e^{-u}\mathrm{d}u$, (b)

follows by specializing the expression of incomplete Gamma function for the case when Δ_k is an integer. Now denote $\beta_k \|x_k\|^\alpha P_k^{-1}$ by s_{x_k} and substitute (4.38) in (4.37) to get:

$$\mathtt{P_c} \leq \sum_{k\in\mathcal{K}} \mathbb{E} \sum_{x_k\in\Phi_k} e^{-s_{x_k} I_{x_k}} \sum_{i=0}^{\Delta_k-1} \frac{(s_{x_k} I_{x_k})^i}{i!} \tag{4.39}$$

$$\overset{(a)}{=} \sum_{k\in\mathcal{K}} \lambda_k \int\limits_{x_k\in\mathbb{R}^2} \mathbb{E}_{I_{x_k}} e^{-s_{x_k} I_{x_k}} \sum_{i=0}^{\Delta_k-1} \frac{(s_{x_k} I_{x_k})^i}{i!} \mathrm{d}x_k \tag{4.40}$$

$$= \sum_{k\in\mathcal{K}} \lambda_k \sum_{i=0}^{\Delta_k-1} \frac{1}{i!} \int\limits_{x_k\in\mathbb{R}^2} \mathbb{E}_{I_{x_k}} e^{-s_{x_k} I_{x_k}} (s_{x_k} I_{x_k})^i \mathrm{d}x_k, \tag{4.41}$$

where (a) follows from Campbell-Mecke Theorem [69]. Now note that if Δ_k were 1, the expectation term is just $\mathcal{L}_{I_{x_k}}(s_{x_k})$, i.e., the Laplace transform of interference evaluated at s_{x_k}. For $\Delta_k > 1$, we evaluate the expectation in terms of the derivative of the Laplace transform as follows

$$\mathbb{E}_{I_{x_k}} \left[e^{-s_{x_k} I_{x_k}} (s_{x_k} I_{x_k})^i \right] \overset{(a)}{=} s_{x_k}^i \mathcal{L}\{t^i f_{I_{x_k}}(t)\}(s_{x_k}) \tag{4.42}$$

$$\overset{(b)}{=} (-s_{x_k})^i \frac{\delta^i}{\delta(s_{x_k})^i} \mathcal{L}_{I_{x_k}}(s_{x_k}), \tag{4.43}$$

where (a) follows from the definition of the Laplace transform and (b) follows from the identity $t^n f(t) \longleftrightarrow (-1)^n \frac{\delta^n}{\delta(s)^n} \mathcal{L}\{f(t)\}(s)$. Substituting this in (4.43), we can express the upper bound on coverage probability in terms of Laplace transform of interference as follows

$$\mathtt{P_c} \leq \sum_{k\in\mathcal{K}} \lambda_k \sum_{i=0}^{\Delta_k-1} \frac{1}{i!} \int\limits_{x_k\in\mathbb{R}^2} (-s_{x_k})^i \frac{\delta^i}{\delta(s_{x_k})^i} \mathcal{L}_{I_{x_k}}(s_{x_k}) \mathrm{d}x_k, \tag{4.44}$$

which completes the proof. □

We note that the above upper bound involves a derivative of Laplace transform, which makes its numerical evaluation difficult. However, it is possible to reduce the upper bound to a simple closed form for full SDMA and easy to evaluate numerical expressions in the other cases. The simplified result is given in the following Corollary.

Corollary 14. *For $\Delta_k = 1$, $\mathcal{A}_k$ can be reduced to*

$$\mathcal{A}_k = \frac{\pi P_k^{\frac{2}{\alpha}} \beta_k^{\frac{2}{\alpha}}}{\sum_{j\in\mathcal{K}} \lambda_j P_j^{\frac{2}{\alpha}} C(\alpha, M_j)}, \tag{4.45}$$

and for $\Delta_k > 1$ to

$$\mathcal{A}_k = \sum_{i=0}^{\Delta_k - 1} \frac{1}{i!} \sum \frac{i!}{j_1! j_2! \dots j_i!} \int\limits_{x_k \in \mathbb{R}^2} (-s_{x_k})^i e^{-\mathcal{C} s_{x_k}^{\frac{2}{\alpha}}} \prod_{\ell=1}^{i} \frac{1}{(\ell!)^{jl}} \left(-\mathcal{C} s_{x_k}^{\frac{2}{\alpha}-\ell} \prod_{n=0}^{\ell-1} \left(\frac{2}{\alpha} - n \right) \right)^{j_\ell} \mathrm{d}x_k. \tag{4.46}$$

Proof. For $\Delta_k = 1$,

$$\mathcal{A}_k = \int_{x_k \in \mathbb{R}^2} \mathcal{L}_{I_{x_k}} \left(\beta_k \|x_k\|^\alpha P_k^{-1} \right) \mathrm{d}x_k \tag{4.47}$$

$$\overset{(a)}{=} \int\limits_{x_k \in \mathbb{R}^2} \exp\left(-\beta_k^{\frac{2}{\alpha}} \|x_k\|^2 P_k^{-\frac{2}{\alpha}} \mathcal{C} \right) \mathrm{d}x_k, \tag{4.48}$$

where (a) follows from the Laplace transform expression derived in Lemma 10. Recall that $\mathcal{C} = \sum_{j\in\mathcal{K}} \lambda_j P_j^{\frac{2}{\alpha}} C(\alpha, \Psi_j)$. The closed form expression now follows directly by converting the integral from Cartesian to polar coordinates.

For $\Delta_k > 1$, using the Laplace transform expression and calculating its derivative using Faà di Bruno's formula for the composite function $(f \circ g)(s_{x_k})$, with $f(s_{x_k}) = \exp(s_{x_k})$, and $g(s_{x_k}) = -\mathcal{C} s_{x_k}^{\frac{2}{\alpha}}$, the result follows. □

We note that the upper bound is in closed form if $\Delta_k = 1$ for all tiers. The result is given in the following corollary. Even for $\Delta_k > 1$, the upper bound can be numerically computed fairly easily, especially for small values of Δ_k.

Corollary 15. *The coverage probability in a K-tier open access HetNet with each k^{th} tier BS performing full SDMA to serve M_k users, i.e., $\Delta_k = 1 \; \forall \; k \in \mathcal{K}$, is given by*

$$\mathtt{P_c} \leq \pi \frac{\sum_{k \in \mathcal{K}} \lambda_k P_k^{\frac{2}{\alpha}} \beta_k^{-\frac{2}{\alpha}}}{\sum_{j=1}^{K} \lambda_j P_j^{\frac{2}{\alpha}} C(\alpha, M_j)}. \tag{4.49}$$

For the closed access case, the summation in the numerator is over $\mathcal{B}$ instead of $\mathcal{K}$.

We now comment on the tightness of the coverage probability upper bound in various regimes and for various transmission techniques.

4.5.2 Tightness of the Upper Bound

For conciseness, we will focus on the open access networks, with the understanding that all the arguments remain the same for closed access case. Since the bound is derived by using the union bound in (4.34), the tightness depends upon the number of candidate BSs that provide SIR greater than the target SIR. Denote this random variable by $X(\{\Delta_k\}, \{\Psi_k\})$, which can be expressed as

$$X(\{\Delta_k\}, \{\Psi_k\}) = \sum_{k \in \mathcal{K}} \sum_{x_k \in \Phi_k} 1\left(\mathtt{SIR}(x_k) > \beta_k\right). \tag{4.50}$$

The bound holds with equality if there is strictly one candidate serving BS for a typical user, i.e., $\mathbb{P}(X(\{\Delta_k\},\{\Psi_k\}) > 1) = 0$. This is the case in SISO HetNets for $\beta_k > 1,\ \forall k$, as shown in Chapter 2. For any other general system configuration, the tightness of the bound depends upon whether the probability $\mathbb{P}(X(\{\Delta_k\},\{\Psi_k\}) > 1)$ is close to zero or not. In general, it is hard to evaluate simple expressions for this probability. However, it is possible to make a few simple observations about the expected tightness of the bound. For instance, the bound gets tight with the increasing values of target SIRs because $X(\{\Delta_k\},\{\Psi_k\})$ is an element-wise decreasing function of β_k. For further insights, we derive the following ordering result for $X(\{\Delta_k\},\{\Psi_k\})$. The proof follows using Lemma 8 on the same lines as that of Theorem 5.

Theorem 8 (Ordering result for X)**.** *If $\Delta_k \geq \Delta'_k$ and $\Psi_k \leq \Psi'_k\ \forall\ k$, then $X(\{\Delta_k\},\{\Psi_k\})$ (first order) stochastically dominates $X(\{\Delta'_k\},\{\Psi'_k\})$, i.e.*

$$\mathbb{P}(X(\{\Delta_k\},\{\Psi_k\}) > n) \geq \mathbb{P}(X(\{\Delta'_k\},\{\Psi'_k\}) > n), \forall\ n. \tag{4.51}$$

Proof. Using the alternate expression of SIR given by (4.6), express $X(\{\Delta_k\},\{\Psi_k\})$ in terms of the channel power gains as

$$\sum_{k\in\mathcal{K}}\sum_{x_k\in\Phi_k} 1\left(\frac{P_k\|x_k\|^{-\alpha}}{\sum_{j\in\mathcal{K}}\sum_{y\in\Phi_j\setminus x_k} P_j Z_{jk}\|y\|^{-\alpha}} > \beta_k\right), \tag{4.52}$$

where $Z_{jk} = g_{jy}/h_{kx_k}$ is the ratio of the two Gamma random variables. For another system with $Z'_{jk} = g'_{jy}/h'_{kx_k}$, $Z_{jk} \leq_{\text{st}} Z'_{jk}$ if $\Delta_k \geq \Delta'_k$ and $\Psi_j \leq \Psi'_j$, which follows from Lemma 8. The result now follows on the same lines as the proof of Theorem 5 using Lemma 9 along with the fact that $X(\{\Delta_k\},\{\Psi_k\})$ is an element-wise non-increasing function of Z_{jk}. □

Remark 8 (Tight Bound in case of SDMA)**.** *One of the useful consequences of Theorem 8 is the prediction of the tightness of the upper bound for SDMA. One interpretation of the above result is that the bound gets tighter when all the BSs serve more users, i.e., Δ_k decreases and Ψ_k increases for all the tiers. A limiting case is that of full SDMA, where the number of users served by each BS is equal to the number of its transmit antennas. Beyond this point, the bound gets tighter with the addition of more transmit antennas keeping $\Delta_k = 1$. We revisit these observations in the numerical results section and show that the bound is in fact surprisingly tight even for two transmit antennas down to very low target* SIR*s.*

In the rest of this section, we will mainly focus on the full SDMA case. Recall that in this case $\Delta_k = 1$ and $\Psi_j = M_j$ and the coverage probability upper bound is given by Corollary 15. As argued in Remark 8 and validated in the numerical results section, the closed form upper bound is tight and can be used as an approximation for the coverage probability. For simplicity we will use equality instead of an approximation.

Remark 9 (Similarity with $\mathtt{P_c}$ in SISO case)**.** *The coverage probability expression derived for full SDMA case in Corollary 15 has a striking similarity with the coverage probability in the SISO case derived in Chapter 2. The only difference is that the constant $C(\alpha, M_j)$ in that case is simply $C(\alpha) = \frac{2\pi^2 \csc\left(\frac{2\pi}{\alpha}\right)}{\alpha}$.*

To facilitate direct comparison of the full SDMA and the SISO cases, we need to understand the relationship between $C(\alpha)$ and $C(\alpha, M)$. Let us

take a closer look at the expression of $C(\alpha, M)$ given by (4.20). First note that $C(\alpha, M)$ is an increasing function of M. Now let us evaluate $C(\alpha, 1)$:

$$C(\alpha, 1) = \frac{2\pi}{\alpha} B\left(\frac{2}{\alpha}, 1 - \frac{2}{\alpha}\right) \tag{4.53}$$

$$= \frac{2\pi}{\alpha} \Gamma\left(\frac{2}{\alpha}\right) \Gamma\left(1 - \frac{2}{\alpha}\right) = \frac{2\pi^2 \csc\left(\frac{2\pi}{\alpha}\right)}{\alpha}, \tag{4.54}$$

where the last step follows by Euler's reflection formula. Hence $C(\alpha, 1)$ is the same as $C(\alpha)$ derived for the SISO case in Chapter 2. From the monotonicity of $C(\alpha, M)$ it follows that $C(\alpha, M) > C(\alpha)\ \forall M > 1$.

Remark 10 (Full SDMA vs. SISO coverage)**.** *Keeping all the system parameters the same, the full SDMA coverage is always lower than that of the SISO case. This is consistent with the coverage probability ordering results derived in the previous section.*

Remark 11 (Scale invariance in open access HetNets)**.** *The full SDMA coverage probability is invariant to the density of the BSs, number of tiers and the transmit powers when the target* SIR*s and the number of transmit antennas are the same for all the tiers in open access HetNets. The coverage probability in this case is given by* $\mathtt{P_c} = \frac{\pi}{C(\alpha, M)} \beta^{-\frac{2}{\alpha}}$*. This result is again similar to the SISO result where the coverage probability reduces to* $\mathtt{P_c} = \frac{\pi}{C(\alpha)} \beta^{-\frac{2}{\alpha}}$*. The scale invariance result does not hold for closed access HetNets.*

4.5.3 Area Spectral Efficiency

Although the comparison of various system configurations and transmission techniques is quite conclusive in terms of coverage probability and the

rate per user, it does not directly account for the fact that some techniques, such as SDMA, serve higher number of users than the others, such as SU-BF, and may result in higher sum data rate. To account for this fact, we consider ASE, which gives the number of bits transmitted per unit area per unit time per unit bandwidth. For a multi-tier setup, it can be formally defined as

$$\eta = \sum_{k \in \mathcal{K}} \Psi_k \lambda_k \log_2(1+\beta_k) \mathtt{P_c}^{(k)}, \tag{4.55}$$

where $\mathtt{P_c}^{(k)}$ is the per tier coverage probability, i.e., coverage probability conditional on the serving BS being in the k^{th} tier. Since the derivations of per tier coverage probabilities are out of the scope of this chapter, for analytical comparisons we limit our discussion to the cases where $\mathtt{P_c}^{(k)} = \mathtt{P_c}$ for all tiers. This is guaranteed for the SISO case when the target SIRs are the same for all tiers and for SDMA when additionally the number of antennas per BS are also the same for all tiers. Recall that the coverage probabilities under these assumptions are scale invariant, as discussed in Remark 11. The ASE under these assumptions can be expressed as

$$\eta = \mathtt{P_c} \log_2(1+\beta) \sum_{k \in \mathcal{K}} \Psi_k \lambda_k. \tag{4.56}$$

We first compare the ASE of the full SDMA and the SISO cases below. The ASE for full SDMA case is

$$\eta_M = M \frac{\pi}{C(\alpha, M)} \beta^{-\frac{2}{\alpha}} \log_2(1+\beta) \sum_{k \in K} \lambda_k, \tag{4.57}$$

and for the SISO case is

$$\eta_S = \frac{\pi}{C(\alpha)} \beta^{-\frac{2}{\alpha}} \log_2(1+\beta) \sum_{k \in K} \lambda_k. \tag{4.58}$$

The ratio of the ASEs can be expressed as

$$\frac{\eta_M}{\eta_S} = \frac{MC(\alpha)}{C(\alpha, M)}. \tag{4.59}$$

Using the fact that

$$\lim_{M\to\infty} \frac{C(\alpha, M)}{M^{\frac{2}{\alpha}}} = \pi\Gamma(1 - 2/\alpha), \tag{4.60}$$

the ratio of the ASEs can be approximated as

$$\frac{\eta_M}{\eta_S} \approx \frac{M^{1-\frac{2}{\alpha}}C(\alpha)}{\pi\Gamma(1 - 2/\alpha)} = \Gamma\left(1 + \frac{2}{\alpha}\right) M^{1-\frac{2}{\alpha}}, \tag{4.61}$$

which shows that the ratio grows with the number of antennas when $\alpha > 2$. In the next section we will validate this observation and show that the ASE in case of full SDMA is always higher than the SISO case. As shown by us in [114], the approximation is surprisingly tight even for small M.

Another relevant comparison is that of full SDMA and SISO transmissions when both the systems are serving the same density of users. To facilitate this comparison, the densities of BSs for SDMA case will be lower than the SISO case by a factor of M. This comparison will provide insights into whether it is beneficial in terms of ASE to deploy λ BSs per unit area with M antennas or $M\lambda$ single-antenna BSs per unit area. In that case, the ratio of the ASEs can be approximated as

$$\frac{\eta_M}{\acute{\eta_S}} \approx \Gamma\left(1 + \frac{2}{\alpha}\right) M^{-\frac{2}{\alpha}}, \tag{4.62}$$

which shows that the ratio decreases sublinearly with the number of antennas when $\alpha > 2$. We will validate this observation in the next section and show that the ASE in SISO case is higher than that of the full SDMA case.

So far, we have focused only on the comparison between full SDMA and SISO cases, mainly because the coverage probability expressions for these cases are known in closed form. Since the coverage probability upper bound for SU-BF cannot be reduced to closed form and moreover the tightness of the bound is questionable, we cannot perform similar comparisons with SU-BF unless we derive a simple coverage probability expression, which is out of the scope of this chapter. Having said that, it is possible to compare the three cases in the very low target SIR regime. Note that this case is of practical relevance since current wireless standards support communication down to very low SIRs, which is about -6 dB for 3GPP LTE [115]. The result is given in the following proposition.

Proposition 4 (ASE comparison for vanishingly small SIR targets)**.** *For the same infrastructure, i.e., the densities of BSs, the ASEs of SU-BF and SISO are the same and of full SDMA is higher than the both when $\beta_k \to 0$ for all k.*

Proof. The proof follows from the fact that coverage probability is an element wise decreasing function of $\{\beta_k\}$ and approaches 1 when $\beta_k \to 0$ for all k. Therefore, the ASE for this regime is

$$\eta = \sum_{k \in \mathcal{K}} \Psi_k \lambda_k \log_2(1 + \beta_k), \tag{4.63}$$

from which the result follows by the fact that $\Psi_k = M_k > 1$ for all k for full SDMA and $\Psi_k = 1$ for all k for both SU-BF and SISO cases. □

We will revisit this result along with the ASE comparison in the moderate and high target SIR regimes in the next section.

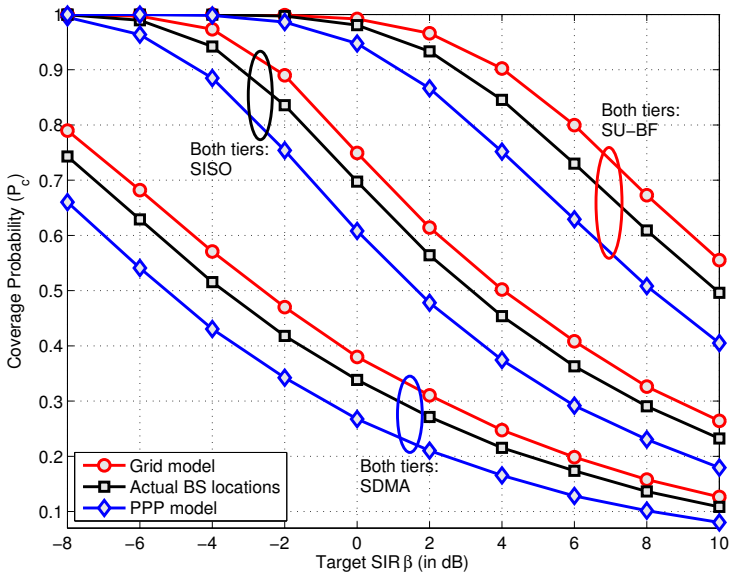

Figure 4.3: Coverage probability for three different models for macrocells. The second tier is PPP in all the cases. $(K = 2, P = [1, .01], \lambda_2 = 2\lambda_1, \alpha = 3.8)$. The number of antennas in case of multi-antenna tiers is $M = 4$.

4.6 Numerical Results

Since there is a slight difference in the simulation of the proposed multi-antenna model and the ones proposed in for the SISO HetNets in the previous chapters, we will briefly summarize the simulation procedure before explaining the results. Choose a sufficiently large window and simulate the locations of different classes of BSs as realizations of independent PPPs of given densities. Associate two independent marks h_x and g_x with each BS. Assuming the typical user lies at the origin, calculate the desired signal strength from each BS using the sequence of marks $\{h_{kx}\}$ and the interference power using the sequence $\{g_{kx}\}$. Calculate the received `SIR` from each BS. The user is now

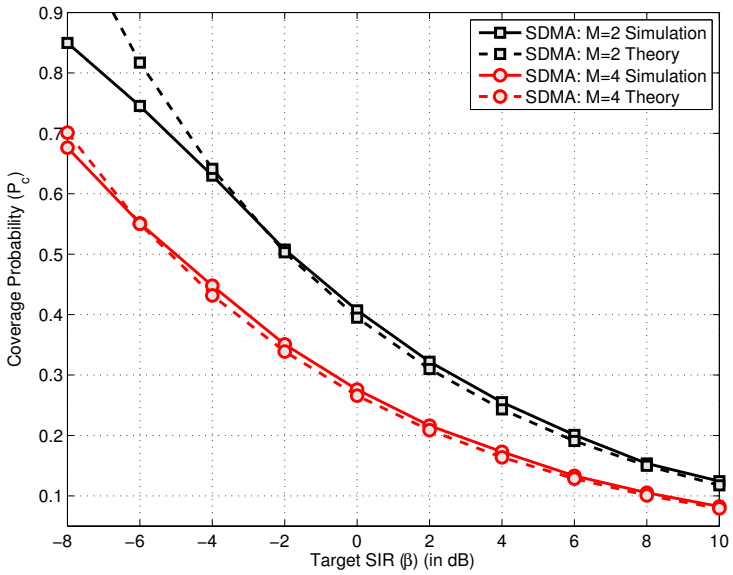

Figure 4.4: Coverage probability of a two-tier HetNet when both tiers perform full SDMA ($K = 2, P = [1, .01], M_1 = M_2 = M, \lambda_2 = 2\lambda_1, \beta_1 = \beta_2, \alpha = 3.8$).

said to be in coverage if the received SIR from at least one of the BSs belonging to the permissible tiers is more than the corresponding target. Repeating this procedure sufficient number of times, we have an estimate of the coverage probability. Using this procedure, we first validate the location model and establish the tightness of the upper bound for SDMA in the following subsection. Note that since we are focusing on the interference limited regime in this chapter, the absolute values of transmit powers and deployment densities are irrelevant. The results only depend on their respective ratios.

4.6.1 Model validation and tightness of the upper bound on $\mathtt{P_c}$

Recall that while the PPP model is sensible for small cells, especially the ones deployed without planning, such as femtocells, it is dubious for centrally planned tiers, such as macrocells. Therefore, to validate the proposed location model for MIMO HetNets, we consider following three setups for a two-tier HetNet with a special focus on macrocells: i) the macrocells are modeled by a hexagonal grid, ii) the macrocell locations are drawn from an actual 4G deployment over 40×40 km^2 area [1, 5], iii) the macrocell locations are drawn from an independent PPP, as in the proposed model. The second tier is modeled as a PPP in all three cases. Note that the actual BS locations used in this comparison can be accurately modeled as a Strauss process, as shown in [82]. Recall that the same dataset of the actual BS locations was also used in Chapters 2 and 3 for model validation. For each of these three location models, we further consider three setups: i) both tiers have 4 transmit antennas per BS and perform SU-BF, i.e. $M_k = 4, \Psi_k = 1$ for all k, ii) both tiers have a single transmit antenna per BS and perform SISO transmission, i.e. $M_k = 1, \Psi_k = 1$ for all k, and iii) both tiers have 4 transmit antennas per BS and perform full SDMA, i.e., $M_k = 4, \Psi_k = 4$ for all k. The simulation procedure remains the same as described above for the PPP model, except of course that the macrocell locations are appropriately drawn from either a PPP, grid or actual location data for each setup. From the numerical results presented in Figure 4.3, we note that in all three setups, the proposed model provides a lower bound on the coverage probability of an actual 4G deployment

and is about as accurate as the grid model, which provides an upper bound. These observations are consistent with those of Chapter 2 for SISO HetNets. In the rest of this section, we will focus solely on the proposed model, i.e., each tier is modeled as an independent PPP.

After validating the location model, we numerically evaluate the coverage probability of a two-tier HetNet in full SDMA case and compare the results with the upper bound derived in Corollary 15 in Figure 4.4. As stated in Remark 8, the bound is tight down to very low target SIRs. Even for $M = 2$, the bound is tight down to about -4 dB. A slight gap, although negligible, at moderate to high target SIRs is due to the border effects in simulation, also observed earlier in Chapter 2. In particular, the simulation is performed over a finite window whereas the analysis assumes BSs over an infinite plane. Nevertheless, this validates our assumption of considering the upper bound as an approximation of the coverage probability in case of full SDMA in the previous section.

4.6.2 Effect of adding additional tier on coverage probability

We study the effect of adding a second tier on the coverage probability of a cellular network in Figures 4.5 and 4.6, where both the first and the second tier can be one of the three possible types: i) SISO, ii) full SDMA, iii) SU-BF. In Figure 4.5, we assume that both tiers are in open access. The result shows that the case where both tiers perform SU-BF results in the highest coverage, whereas the case where both tiers perform full SDMA leads to the lowest

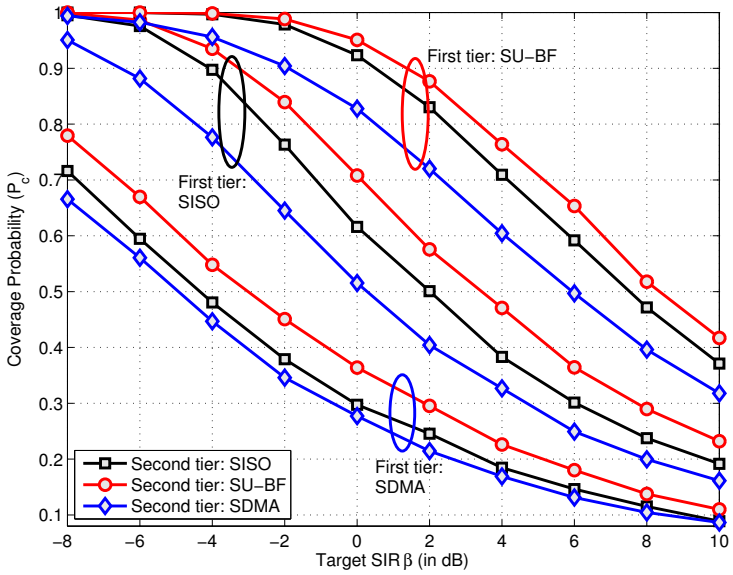

Figure 4.5: Comparison of the coverage probability in a two-tier HetNet for various combinations of multi-antenna techniques ($K = 2, P = [1, .01], \lambda_2 = 2\lambda_1, \beta_1 = \beta_2, \alpha = 3.8$). The number of antennas in case of multi-antenna tiers is $M = 4$.

coverage. This is because SU-BF case has an additional beamforming gain; in addition to the proximity gain enjoyed by the SISO case. These observations are consistent with the coverage ordering results derived in Section 4.4. In Figure 4.6, we study the effect of adding a second tier that is in closed access, i.e., a typical user cannot connect to the second tier BSs. The performance of various transmission techniques is in the same order as for the open access case studied in Figure 4.5. Interestingly, the coverage probability of a typical user is the same irrespective of whether the new closed access tier is doing SISO transmission or SU-BF. This is due to the fact that the channel power distribution of the interfering links in both the cases is $\Gamma(1, 1)$, i.e., exp(1).

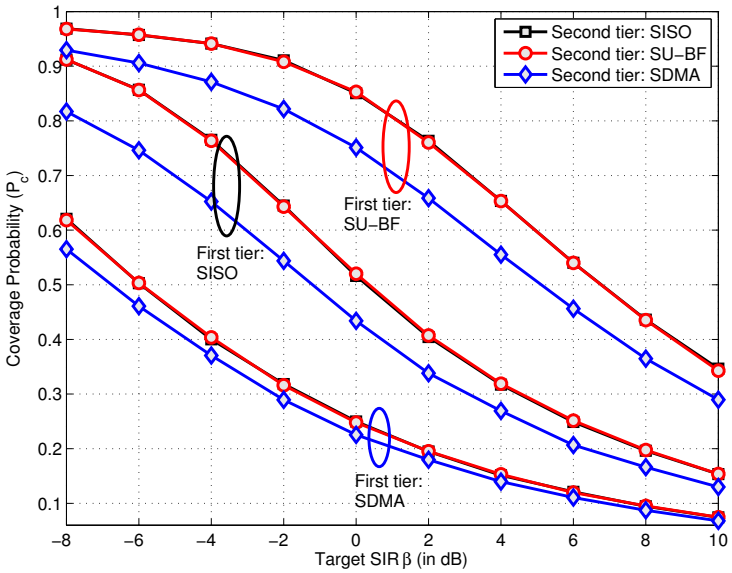

Figure 4.6: Comparison of the coverage probability in a two-tier HetNet where the second tier is in closed access ($K = 2, P = [1, .01], \lambda_2 = 2\lambda_1, \beta_1 = \beta_2, \alpha = 3.8$). The number of antennas in case of multi-antenna tiers is $M = 4$.

4.6.3 Area spectral efficiency

We compare the ASEs of SU-BF, SISO, and full SDMA transmission techniques in a 2-tier HetNet in Figure 4.7. Both tiers are assumed to follow the same transmission technique and the ASE result for SU-BF is computed numerically by computing the per tier coverage probability. For comparison, we consider two cases, one in which the density of the BSs in the three setups remain the same, and the other in which the densities are adjusted such that the density of users served in the three cases is the same. In the first case, SU-BF, which always outperforms SISO, even outperforms full SDMA in the high target SIR regime despite serving smaller number of users. The trends in the low target SIR regime are consistent with Proposition 4. In the second

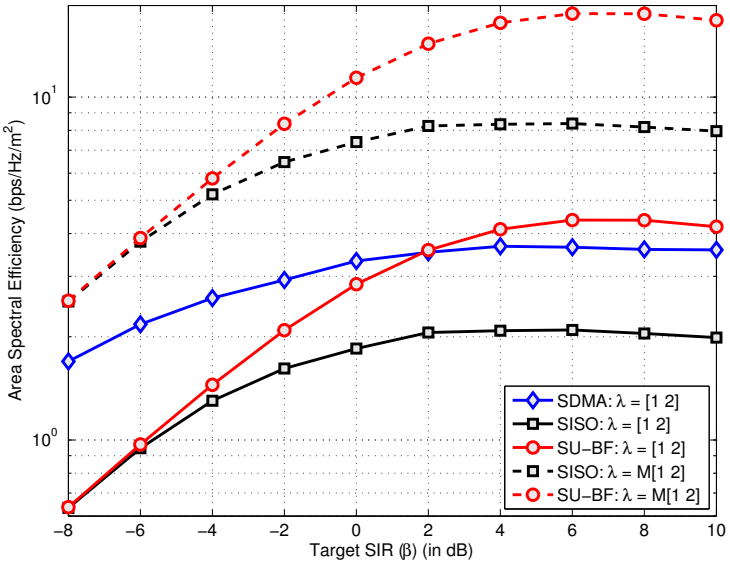

Figure 4.7: Comparison of the ASE in a two-tier HetNet ($K = 2, P = [1, .01], \lambda_2 = 2\lambda_1, \beta_1 = \beta_2, \alpha = 3.8$). The number of antennas in case of multi-antenna tiers is $M = 4$. Full SDMA corresponds to $\Psi = M$.

case, where the density of the users is the same in all the cases, the ordering of the three transmission techniques in terms of ASE is the same as that of coverage and rate per user.

4.6.4 Effect of having a fraction of BSs in closed access

Before concluding this section, it is important to recall that under PPP assumption, the proposed model is applicable even if a given fraction of BSs of a particular tier independently operates in open or closed access. In such a case, we can divide the original tier into two tiers with appropriate densities, which is enabled by the fact that independently thinning a PPP leads to two independent PPPs. For example, for a two-tier HetNet where all the BSs of the

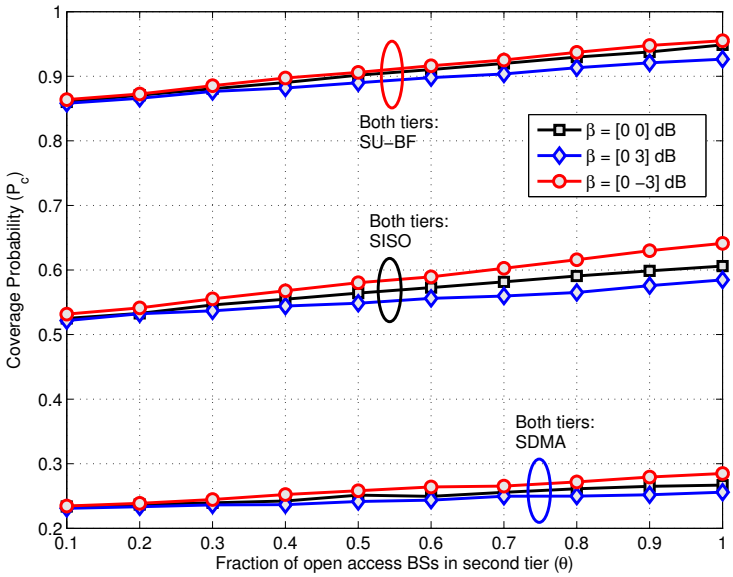

Figure 4.8: Coverage probability when a fraction $1-\theta$ of the second tier BSs are in closed access. $(K=2, P=[1,.01], \lambda_2=2\lambda_1, \alpha=3.8)$. The number of antennas in case of multi-antenna tiers is $M=4$.

first tier and the fraction $0 \leq \theta \leq 1$ of the second tier operate in open access while the rest in closed access, the second tier can be divided into two tiers modeled as independent PPPs $\Phi_{2^{(1)}}$ (open access tier) and $\Phi_{2^{(2)}}$ (closed access tier) with densities $\lambda_{2^{(1)}} = \theta\lambda_2$ and $\lambda_{2^{(2)}} = (1-\theta)\lambda_2$, respectively. Therefore, the original two-tier network can be reduced to an equivalent three tier network, where two tiers are in open access and one is in closed access. The numerical results for such a scenario are presented in Figure 4.8 for various combinations of target SIRs. Note that the coverage probability of a typical user under all considered transmission schemes increases linearly with the fraction of open access BSs θ. Secondly, the loss in coverage probability with decreasing θ is higher when the target SIR for the closed access BSs is lower

than that of the first tier open access BSs. Similarly, the loss is lower when the target SIR for the closed access BSs is higher than the first tier BSs. This is because when the target SIR for the second tier is lower than the first tier, the second tier BSs would have contributed more to the coverage probability had they been in open access than the case when their target SIR is higher than the first tier BSs.

4.7 Summary

In this chapter, we have generalized the baseline HetNet model proposed in Chapter 2 to multi-antenna HetNets. For any given BS distribution, we derived ordering results for coverage probability and per user rate to compare different transmission techniques, such as SDMA, SU-BF and baseline SISO transmission. In addition to significantly generalizing the state-of-the-art PPP based random spatial models for cellular networks, this approach circumvents the need for deriving explicit expressions for coverage and rate, which may not reduce to simple closed forms in all the cases. One interpretation of our results is that for a given total number of transmit antennas, it is preferable to spread them across many single-antenna BSs vs. fewer multi-antenna BSs, both in terms of coverage and rate per user. We also showed that SU-BF provides higher coverage and rate per user than both SISO and SDMA due to an additional beamforming gain. To account for the fact that certain transmission techniques, such as SDMA, serve more users and may provide higher sum-rate, we derived an upper bound on the coverage proba-

bility assuming an independent PPP model for BS locations and used it to compare different transmission techniques in terms of ASE.

Chapter 5

Downlink Rate Distribution in HetNets under Generalized Cell Selection

The channel randomness consists of two main effects that operate on two significantly different time scales: i) *shadowing*, which changes over a much longer time scale and may impact cell selection decisions, and ii) *fading*, which changes over a much smaller time scale and may not impact cell selection. In all the previous chapters, the channel randomness was modeled as a single random variable, which could not capture these two effects separately. In this chapter, we address this shortcoming by generalizing the channel and cell selection models to incorporate both the long-term shadowing and small-scale fading effects. For this generalized cell selection model, we characterize the downlink rate distribution at a typical user accounting for the load on the serving base station (BS).

5.1 Related Work

Despite the success of random spatial models for HetNets, there remain several shortcomings that need to be addressed for realistic performance assessment. One of them is the simplistic set of assumptions for channel and

cell selection models. With a key exception of [116], prior work including the previous chapters of this dissertation either ignores the impact of shadowing on cell selection and assumes that a UE always connects to one of the closet BSs of each tier [49, 117], or lumps all the channel randomness into a single random variable and assumes that cell selection is based on the maximum instantaneous received power [5, 118]. Due to these simplifications, neither of these models is able to capture the fact that the long-term effects such as distance-based path loss and shadowing impact cell selection, while small-scale fading does not. This generalization is the main focus of this chapter.

5.2 Contribution

Although this chapter is in the same spirit as [116], the main focus of [116] is on the downlink signal-to-interference-plus-noise ratio (SINR), whereas we focus on the downlink data rate that additionally depends upon the load on each BS class. For instance, to maximize downlink rate, it may be preferable to connect to small cells even when they offer poor SINR in some cases, because owing to their smaller load they can more than compensate by offering a large percentage of time-frequency resources to each UE. Leveraging the same general idea of *propagation (process) invariance*, as discussed in [116, 119], we show that in addition to the SINR distribution, the service area approximations resulting from multiplicatively weighted Poisson Voronoi tessellation, and hence the load on each BS class [112], can be easily extended to the general cell selection model introduced in this chapter.

Our analysis concretely demonstrates that the effect of shadowing on downlink rate and related metrics, such as rate optimal cell-selection bias, can be equivalently captured by appropriately scaling the transmit powers of each BS class and then simply selecting one of the BSs that are closest in each tier for service. This insight immediately generalizes prior art on load balancing, such as [112]. An interesting observation is that in certain regimes shadowing naturally balances load across various tiers and hence reduces the need for artificial cell selection bias.

5.3 System Model

Consider a K-tier HetNet with K classes of BSs, differing in terms of the transmit power P_k, deployment density λ_k, and cell-selection bias B_k. For notational simplicity, define $\mathcal{K} = \{1, 2, \ldots, K\}$. The locations of the k^{th} tier BSs are modeled by an independent Poisson Point Process (PPP) Φ_k of density λ_k. Define $\Phi = \cup_{k \in \mathcal{K}} \Phi_k$. For resource allocation, consider orthogonal partitioning of resources, e.g., time-frequency resource blocks in orthogonal frequency division multiple access (OFDMA), where each resource block is allocated to one UE, and hence there is no intra-cell interference. Modeling UE locations by an independent PPP Φ_u of density λ_u, the downlink analysis is performed at a typical UE assumed to be located at the origin [70]. The received power at a typical UE from a k^{th} tier BS located at $x_k \in \Phi_k$ in a given resource block is

$$P(x_k) = P_k h_{kx_k} \mathcal{X}_{kx_k} \|x_k\|^{-\alpha}, \tag{5.1}$$

where $h_{kx_k} \sim \exp(1)$ models Rayleigh fading, $\mathcal{X}_{kx_k}$ models shadowing, and $\|x_k\|^{-\alpha}$ represents standard power-law path loss with exponent α. Note that since h_{kx_k} and $\mathcal{X}_{kx_k}$ are both independent of the location of the BS, we will drop x_k from the subscript and denote the two random variables by h_k and $\mathcal{X}_k$, whenever the location of the BS is clear form the context. In the same spirit as [116,118], our analysis is capable of handling any general distribution for $\mathcal{X}_k$ as long as $\mathbb{E}\left[\mathcal{X}_k^{\frac{2}{\alpha}}\right] < \infty$. The origins of this restriction will be discussed later in this section. The most common assumption for large scale shadowing distribution is lognormal, where $\mathcal{X}_k = 10^{\frac{X_k}{10}}$ such that $X_k \sim \mathcal{N}(\mu_k, \sigma_k^2)$, where μ_k and σ_k are respectively the mean and standard deviation in dB of the shadowing channel power. Using the moment generating function (MGF) of Gaussian distribution, the fractional moment is

$$\mathbb{E}\left[\mathcal{X}_k^{\frac{2}{\alpha}}\right] = \exp\left(\frac{\ln 10}{5}\frac{m_k}{\alpha} + \frac{1}{2}\left(\frac{\ln 10}{5}\frac{\sigma_k}{\alpha}\right)^2\right), \tag{5.2}$$

which is clearly finite if both the mean and standard deviation of the normal random variable X_k are finite.

Since fading gain h_x changes over much smaller time-scale, and in a frequency selective channel (such as one using OFDM) can be averaged or mitigated in the frequency domain, we assume that it does not impact cell selection. Each UE connects to the BS that provides the highest long-term *biased received power*, as explained below. Denote the location of the candidate k^{th} tier serving BS by x_k^*, i.e.,

$$x_k^* = \arg\max_{x \in \Phi_k} P_k \mathcal{X}_x \|x\|^{-\alpha}. \tag{5.3}$$

From these K candidate serving BSs, a typical UE connects to

$$x^* = \arg \max_{x \in \{x_k^*\}} B_k P_k \mathcal{X}_x \|x\|^{-\alpha}, \tag{5.4}$$

where $B_k > 0$ is the selection bias introduced to expand the range of small cells to balance load across the network [112]. The inclusion of shadowing in cell selection is facilitated by displacement theorem [70], where the key insight is to express the received power given by (5.1) as

$$P(x_k) = P_k h_{kx_k} \|\mathcal{X}_{kx_k}^{-\frac{1}{\alpha}} x_k\|^{-\alpha}, \tag{5.5}$$

where the long-term shadowing effects can be interpreted as a random displacement of the location of the BS originally placed at $x_k \in \Phi_k$. We make this notion precise in the following Lemma. Also see [116, 118] for the application of this general idea to handle general shadowing or fading distributions in slightly different setups.

Lemma 11. *For a homogeneous PPP $\Phi_k \subset \mathbb{R}^2$ with density λ_k, if each point $x \in \Phi_k$ is transformed to $y \in \mathbb{R}^2$ such that $y = \mathcal{X}_k^{-\frac{1}{\alpha}} x$, where $\{\mathcal{X}_k\}$ are i.i.d., such that $\mathbb{E}\left[\mathcal{X}_k^{\frac{2}{\alpha}}\right] < \infty$, the new point process $\Phi_k^{(\mathrm{e})} \subset \mathbb{R}^2$ defined by the transformed points y is also a homogeneous PPP with density $\lambda_k^{(\mathrm{e})} = \lambda_k \mathbb{E}\left[\mathcal{X}_k^{\frac{2}{\alpha}}\right]$.*

Proof. Let $\mathcal{B}(\mathbb{R}^2)$ be the Borel σ-algebra on $\mathbb{R}^2$. For $A \in \mathcal{B}(\mathbb{R}^2)$, the intensity measure $\Lambda(A)$ of a homogeneous PPP Φ_k is $\Lambda_k(A) = \lambda_k |A|$, where $|A|$ denotes the Lebesgue measure of A. By displacement theorem [70, Theorem 1.3.9], the transformation of a PPP Φ_k with probability kernel $p(x, A)$ is a PPP with

intensity measure:

$$\Lambda_k^{(\mathrm{e})}(A) = \int_{\mathbb{R}^2} p(x, A)\Lambda_k(\mathrm{d}x) \tag{5.6}$$

$$\stackrel{(a)}{=} \mathbb{E}\int_{\mathbb{R}^2} \mathbf{1}(\mathcal{X}_k^{-\frac{1}{\alpha}} x \in A)\lambda_k \mathrm{d}x$$

$$= \mathbb{E}\left[\int_{\mathbb{R}^2} \mathbf{1}\left(x \in A\mathcal{X}_k^{\frac{1}{\alpha}}\right)\lambda_k \mathrm{d}x\right] \tag{5.7}$$

$$= \lambda_k |A| \mathbb{E}\left[\mathcal{X}_k^{\frac{2}{\alpha}}\right],$$

where (a) follows by using the kernel specific to this Lemma. Since $\{\mathcal{X}_k\}$ are i.i.d. and independent of the location x, setting $|A| = \mathrm{d}y$, we get

$$\Lambda_k^{(\mathrm{e})}(A)(\mathrm{d}y) = \lambda_k \mathbb{E}\left[\mathcal{X}_k^{\frac{2}{\alpha}}\right]\mathrm{d}y = \lambda_k^{(\mathrm{e})}\mathrm{d}y. \tag{5.8}$$

For a PPP, we need its intensity measure to be locally finite, which leads to the condition $\lambda_k^{(\mathrm{e})} = \lambda_k \mathbb{E}\left[\mathcal{X}_k^{\frac{2}{\alpha}}\right] < \infty$. □

An immediate consequence of this Lemma is the characterization of received power in terms of the equivalent PPP $\Phi_k^{(\mathrm{e})}$ with density $\lambda_k^{(\mathrm{e})} = \lambda_k \mathbb{E}\mathcal{X}_k^{\frac{2}{\alpha}}$. Defining $y_k = \mathcal{X}_{kx_k}^{-\frac{1}{\alpha}} x_k$, the received power can be equivalently expressed as

$$P(y_k) = P_k h_{ky_k} \|y_k\|^{-\alpha}, \tag{5.9}$$

using which the location of the candidate serving BS in k^{th} tier can be equivalently expressed as

$$y_k^* = \arg\max_{y \in \Phi_k^{(\mathrm{e})}} P_k \|y\|^{-\alpha}. \tag{5.10}$$

Note that y_k^* is simply the closest point to the origin of the equivalent point process $\Phi_k^{(\mathrm{e})}$. The location of the serving BS in the equivalent PPP $\Phi^{(\mathrm{e})} = \cup_{k\in\mathcal{K}}\Phi_k^{(\mathrm{e})}$ can be similarly expressed as

$$y^* = \arg\max_{y\in\{y_k^*\}} B_k P_k \|y\|^{-\alpha}. \tag{5.11}$$

For notational simplicity define $\mathbf{s} \in \mathbb{R}^K$, such that $\mathbf{s}(k) \in \{0,1\}$, $\sum_{k\in\mathcal{K}} \mathbf{s}(k) = 1$, and $\mathbf{s}(k) = \mathbf{1}(x^* = x_k^*) = \mathbf{1}(x^* \in \Phi_k)$, which implies that the k^{th} element of $\mathbf{s}$ takes value 1 if the serving BS belongs to k^{th} tier. We ignore thermal noise, i.e., network is interference-limited, and assume a full-buffer model for the interfering BSs [5], i.e., all the interferers are always active. The signal-to-interference ratio (SIR) at the typical UE when $\mathbf{s}(k) = 1$ is

$$\begin{aligned}\mathtt{SIR}(x^*) &= \frac{P_k h_{kx^*} \mathcal{X}_{kx^*} \|x^*\|^{-\alpha}}{\sum_{j\in\mathcal{K}} \sum_{z\in\Phi_j\setminus\{x^*\}} P_j h_{jz} \mathcal{X}_{jz} \|z\|^{-\alpha}} \\ &\overset{d}{=} \frac{P_k h_{ky^*} \|y^*\|^{-\alpha}}{\sum_{j\in\mathcal{K}} \sum_{z\in\Phi_j^{(\mathrm{e})}\setminus\{y^*\}} P_j h_{jz} \|z\|^{-\alpha}} = \mathtt{SIR}(y^*),\end{aligned} \tag{5.12}$$

where d denotes equivalence in distribution, which follows from Lemma 11. Due to this equivalence, the results based solely on SIR or SINR distributions, such as coverage probability, derived under the assumption that a typical UE always connects to one of the BSs that are closest in each tier, e.g., [49], can be easily extended to the general selection model by considering equivalent BS densities $\{\lambda_k^{(\mathrm{e})}\}$. This has also been independently shown for coverage probability in [116]. In the next section, we establish a similar equivalence for downlink rate distribution, that additionally depends upon the BS load.

5.4 Downlink Rate Distribution

In this section, we generalize the main premise of [112], and characterize the downlink rate coverage under generalized cell-selection model introduced in the previous section.

Definition 1 (Rate coverage)**.** *Rate coverage* $\mathtt{R_c}$ *is the probability that the downlink rate* $\mathcal{R}$ *achievable at a typical UE is higher than a predefined lowest rate* T *required by a given application, i.e.,* $\mathtt{R_c} = \mathbb{P}(\mathcal{R} > T)$*. Being the complementary cumulative distribution function (CCDF),* $\mathtt{R_c}$ *completely characterizes the rate distribution.*

We term the serving BS $x^* \in \Phi$ of a typical UE as a "tagged" BS. Denote the number of UEs served by the tagged BS by Ψ_k, where subscript k is for the tier to which this BS belongs. Clearly, Ψ_k is a random variable with the following two sources of randomness: i) the area of the region that the tagged BS serves, in short service area, and ii) conditioned on the area of the service region, the number of UEs served by the tagged BS is a Poisson random variable. For tractability, we assume that each BS allocates equal time-frequency resources to its UEs, i.e., each UE gets rate proportional to the spectral efficiency of its downlink channel from the serving BS. For total effective bandwidth W Hz, the downlink rate in bits/sec of a typical UE when it connects to a k^{th} tier BS is

$$\mathcal{R}_k = \frac{W}{\Psi_k} \log_2 \left(1 + \mathtt{SIR}(x_k^*)\right). \tag{5.13}$$

Note that $\mathtt{SIR}(x_k^*)$ and Ψ_k are in general correlated, e.g., when $\|x_k^*\|$ is large, the serving BS is far from the typical UE. This information skews the distribution of the service area of the tagged BS, and hence of Ψ_k, towards larger values. However, characterizing the joint distribution of Ψ_k and $\mathtt{SIR}(x_k^*)$ is out of the scope of this chapter. For tractability, we assume the two random variables to be independent, which does not compromise the accuracy of our analysis [112]. Under this assumption, the rate coverage $\mathtt{R_c}$ is

$$\mathtt{R_c} = \mathbb{P}[\mathcal{R} > T] \tag{5.14}$$

$$\overset{(a)}{=} \sum_{k\in\mathcal{K}} \mathbb{P}[\mathcal{R} > T|\mathbf{s}(k)=1]\mathbb{P}[\mathbf{s}(k)=1] \tag{5.15}$$

$$= \sum_{k\in\mathcal{K}} \mathbb{E}_{\Psi_k}\mathbb{P}\left(\mathcal{R}_k > T\right)\mathbb{P}[\mathbf{s}(k)=1] \tag{5.16}$$

$$= \sum_{k\in\mathcal{K}} \mathbb{E}_{\Psi_k}\mathbb{P}\left(\mathtt{SIR}(x_k^*) > 2^{\frac{T}{W}\Psi_k} - 1\right)\mathbb{P}[\mathbf{s}(k)=1] \tag{5.17}$$

$$\overset{(b)}{=} \sum_{k\in\mathcal{K}}\sum_{n=1}^{\infty} \underbrace{\mathbb{P}\left(\mathtt{SIR}(x_k^*) > \beta_n\right)}_{\text{Conditional } \mathtt{SIR} \text{ distribution}} \underbrace{\mathbb{P}(\Psi_k = n)}_{\text{Load}} \underbrace{\mathbb{P}[\mathbf{s}(k)=1]}_{\text{Selection probability}}, \tag{5.18}$$

where (a) follows from the total probability theorem, and (b) follows by defining $\beta_n = 2^{\frac{T}{W}n} - 1$ for notational simplicity. We now compute the three probability terms starting with the selection probability, which we denote by $\mathcal{P}_k$.

Lemma 12 (Selection probability)**.** *The probability that a typical UE connects to a k^{th} tier BS is given by*

$$\mathcal{P}_k = \mathbb{P}(\mathbf{s}(k)=1) = \frac{\lambda_k \mathbb{E}\left[\mathcal{X}_k^{\frac{2}{\alpha}}\right] B_k^{\frac{2}{\alpha}} P_k^{\frac{2}{\alpha}}}{\sum_{j\in\mathcal{K}} \lambda_j \mathbb{E}\left[\mathcal{X}_j^{\frac{2}{\alpha}}\right] B_j^{\frac{2}{\alpha}} P_j^{\frac{2}{\alpha}}}. \tag{5.19}$$

Proof. The selection probability is

$$\mathcal{P}_k = \mathbb{P}(\mathbf{s}(k) = 1) \overset{(a)}{=} \mathbb{P}(x^* = x_k^*) \overset{(b)}{=} \mathbb{P}(y^* = y_k^*), \tag{5.20}$$

where $\{x_k^*\}$ in (a) is the set of candidate serving BSs in Φ, $\{y_k^*\}$ in (b) is the set of candidate serving BSs in $\Phi^{(\mathrm{e})}$, and (b) additionally follows from Lemma 11. Recall that the candidate serving BS y_k^* is the closest point of the PPP $\Phi_k^{(\mathrm{e})}$ to the origin, which reduces to the same setup as [49]. The rest of the proof follows from the Lemma 1 of [49] using the fact that the density of $\Phi_k^{(\mathrm{e})}$ is $\lambda_k^{(\mathrm{e})} = \lambda_k \mathbb{E}\left[\mathcal{X}_k^{\frac{2}{\alpha}}\right]$. □

We now derive the conditional `SIR` distribution, i.e., `SIR` distribution conditioned on $\mathbf{s}(k) = 1$. The proof follows directly from Theorem 1 of [49] after invoking displacement theorem as was done for Lemma 12, and is hence skipped.

Lemma 13 (Conditional `SIR` distribution)**.** *The conditional* `SIR` *distribution is*

$$\mathbb{P}(\mathtt{SIR}(x_k^*) > \beta) = \frac{\sum_{j\in\mathcal{K}} \lambda_j \mathbb{E}\left[\mathcal{X}_j^{\frac{2}{\alpha}}\right] B_j^{\frac{2}{\alpha}} P_j^{\frac{2}{\alpha}}}{\sum_{j\in\mathcal{K}} \lambda_j \mathbb{E}\left[\mathcal{X}_j^{\frac{2}{\alpha}}\right] P_j^{\frac{2}{\alpha}} \left[B_j^{\frac{2}{\alpha}} + B_k^{\frac{2}{\alpha}} \mathcal{F}\left(\beta, \alpha, \frac{B_j}{B_k}\right)\right]} \tag{5.21}$$

where

$$\mathcal{F}(\beta, \alpha, z) = \left(\frac{2\beta z^{\frac{2}{\alpha}-1}}{\alpha - 2}\right) {}_2F_1\left[1, 1 - \frac{2}{\alpha}, 2 - \frac{2}{\alpha}, -\frac{\beta}{z}\right],$$

and ${}_2F_1[a, b, c, z] = \frac{\Gamma(c)}{\Gamma(b)\Gamma(c-b)} \int_0^1 \frac{t^{b-1}(1-t)^{c-b-1}}{(1-tz)^a} \mathrm{d}t$ *denotes the Gauss hypergeometric function.*

For the distribution of load Ψ_k, we use the approximation proposed in Lemma 3 of [112]. The main idea is to approximate the service area of a typical k^{th} tier BS by the area of a typical Poisson Voronoi with the same mean $\frac{\mathcal{P}_k}{\lambda_k}$. Now since a typical UE has a higher chance of selecting a BS with bigger service area, the area of the tagged BS is biased towards being larger than a typical BS of the same tier. This is similar to the waiting bus paradox associated with Point processes in $\mathbb{R}$. Accounting for this bias, the load distribution is given below. The proof is the same as Lemma 3 of [112] with the understanding that the effect of shadowing on cell selection is captured by $\mathcal{P}_k$.

Lemma 14 (Load on tagged BS)**.** *The distribution of the load served by x_k^* is* $\mathbb{P}(\Psi_k = n+1) =$

$$\frac{3.5^{3.5}}{n!}\frac{\Gamma(n+4.5)}{\Gamma(3.5)}\left(\frac{\lambda_u \mathcal{P}_k}{\lambda_k}\right)^n \left(3.5+\frac{\lambda_u \mathcal{P}_k}{\lambda_k}\right)^{-(n+4.5)}.$$

The mean load is $\mathbb{E}[\Psi_k] = 1 + 1.28\frac{\lambda_u \mathcal{P}_k}{\lambda_k}$.

Substituting Lemmas 12, 13, and 14 in (5.18), we get a fairly simple expression for rate coverage.

Theorem 9 (Rate coverage)**.** *The rate coverage is* $\mathtt{R_c} =$

$$\sum_{k=1}^{K}\sum_{n\geq 0}\frac{\lambda_k \mathbb{E}\left[\mathcal{X}_k^{\frac{2}{\alpha}}\right] B_k^{\frac{2}{\alpha}} P_k^{\frac{2}{\alpha}} \mathbb{P}(\Psi_k = n+1)}{\sum_{j\in\mathcal{K}} \lambda_j \mathbb{E}\left[\mathcal{X}_j^{\frac{2}{\alpha}}\right] P_j^{\frac{2}{\alpha}} \left[B_j^{\frac{2}{\alpha}} + B_k^{\frac{2}{\alpha}} \mathcal{F}\left(\beta_{n+1}, \alpha, \frac{B_j}{B_k}\right)\right]}$$

where $\mathcal{P}_k$ is given by Lemma 12, $\mathbb{P}(\Psi_k = n+1)$ by Lemma 14, and recall that $\beta_{n+1} = 2^{\frac{T}{W}(n+1)} - 1$.

We will validate the load approximation and study the effect of shadowing on load balancing in the next section. This section is concluded with the following remarks.

Remark 12 (Invariance)**.** *If the shadowing distribution is such that* $\mathbb{E}\left[\mathcal{X}_k^{\frac{2}{\alpha}}\right] = c$*, for all* $k \in \mathcal{K}$*, the downlink rate distribution is invariant to the shadowing distributions of all the tiers.*

Remark 13 (Equivalent HetNet model)**.** *A HetNet model with* k^{th} *tier transmit power* $\left(\mathbb{E}\left[\mathcal{X}_k^{\frac{2}{\alpha}}\right]\right)^{\frac{\alpha}{2}} P_k$*, no shadowing, and cell selection based on average biased receive power with selection bias* $\{B_k\}$*, leads to the same expression for rate coverage as given by Theorem 9 for the generalized cell selection model. Due to this equivalence, the key results derived under no shadowing, e.g., in [49, 112], can be easily extended to the generalized cell selection model by appropriately scaling the transmit powers.*

5.5 Numerical Results

For numerical results, we consider a two tier HetNet, e.g., coexisting macro and pico cells, and assume that the shadowing distribution for each tier is log-normal with mean μ_k dB and standard deviation σ_k dB. Throughout this section, we assume $\alpha = 4$, $P_2 = P_1 - 23$ dB, $W = 10$ MHz, and $\mu = [0\ 0]$ dB. We first validate the load distribution given by Lemma 14 in Figure 5.1. In addition to the actual load under the generalized cell selection model, we also plot the load offered to the tagged BS under an equivalent model suggested in

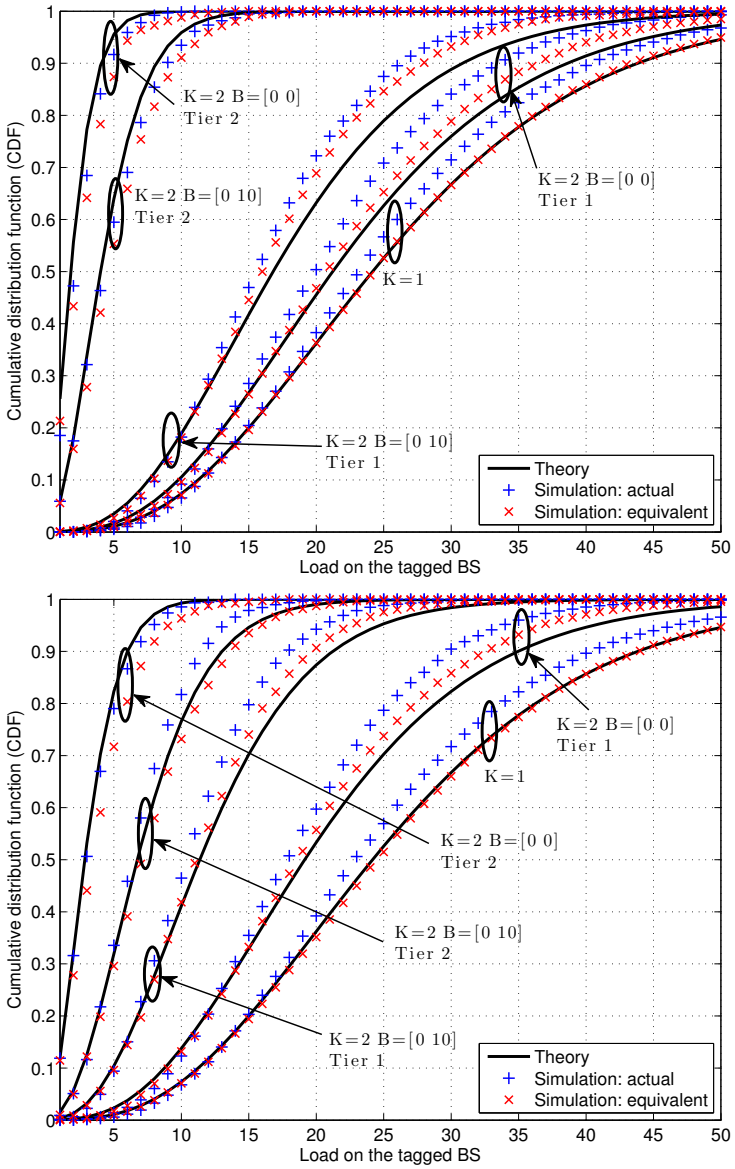

Figure 5.1: CDF of load Ψ_k with $\lambda_u = 20\lambda_1$, $\lambda_2 = 2\lambda_1$ for $K = 2$, $\lambda_2 = 0$ for $K = 1$, $\sigma = [4\ 4]$ dB *(first)* and $[4\ 8]$ dB *(second)*. B is in dB.

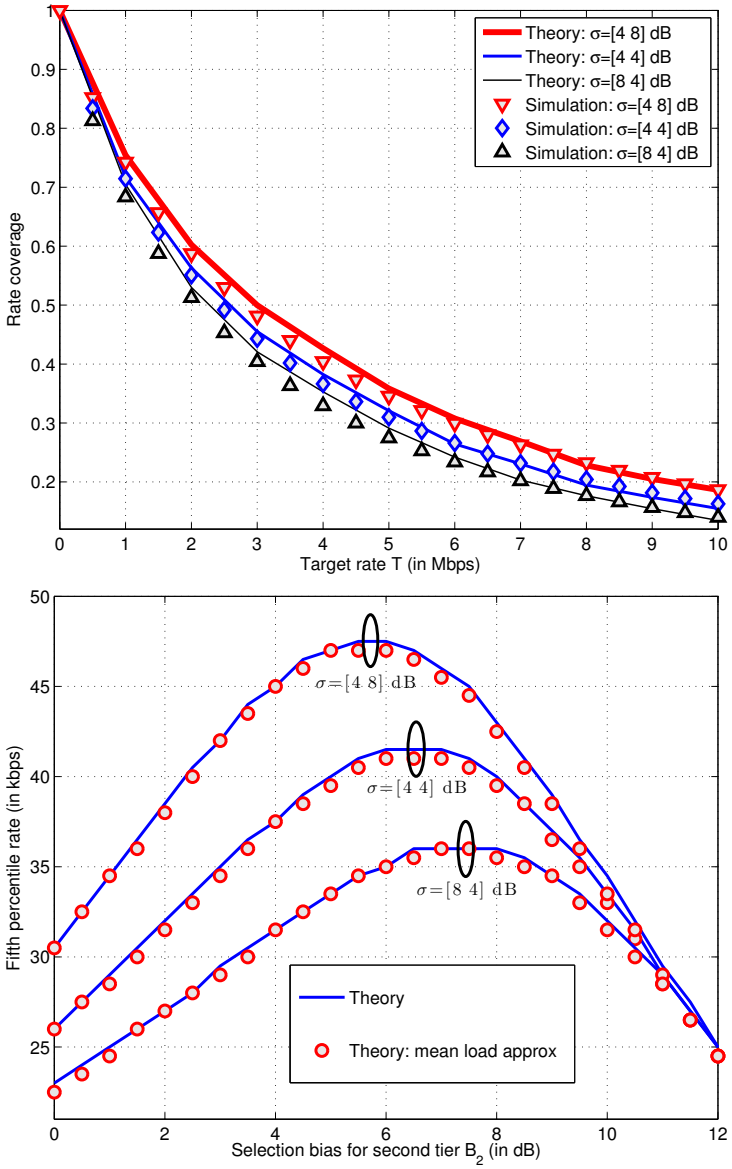

Figure 5.2: *(first)* Rate coverage for $\lambda_2 = 5\lambda_1$, $\lambda_u = 10\lambda_1$, $B = [0\ 5]$ dB. *(second)* Fifth percentile rate for $\lambda_2 = 5\lambda_1, \lambda_u = 40\lambda_1$, $B_1 = 0$ dB.

Remark 13. We first note that the analytic approximation given by Lemma 14 is fairly accurate, which along with the fact that the other components of rate expression, i.e., conditional SIR distribution and selection probability, are exact, leads to a very tight approximation for rate distribution, as validated in Figure 5.2. Comparing the rate distributions for two sub-figures of Figure 5.1, we note that there is a natural balancing of load across tiers when $\mathbb{E}\left[\mathcal{X}_2^{\frac{2}{\alpha}}\right] > \mathbb{E}\left[\mathcal{X}_1^{\frac{2}{\alpha}}\right]$ compared to the baseline case of no shadowing, which by Remark 13 is equivalent to the case when $\mathbb{E}\left[\mathcal{X}_2^{\frac{2}{\alpha}}\right] = \mathbb{E}\left[\mathcal{X}_1^{\frac{2}{\alpha}}\right]$, as in the first sub-figure. This load balancing can be understood in terms of the equivalent model proposed in Remark 13, i.e., in this case shadowing increases the effective transmit power of small cells relative to the baseline and hence expands their coverage areas. In Figure 5.2, we plot the rate coverage and the fifth percentile rate, i.e., the rate value such that 95% of the UEs achieve higher rate than this value. Both these results are consistent with the load balancing observations made in Figure 5.1, e.g., the optimal selection bias that maximizes fifth percentile rate is smaller when $\mathbb{E}\left[\mathcal{X}_2^{\frac{2}{\alpha}}\right] > \mathbb{E}\left[\mathcal{X}_1^{\frac{2}{\alpha}}\right]$. Due to a smaller artificial bias, this case also achieves the highest rate. In Figure 5.2, we also validate the rate expression by comparing it with the simulations and a special case in which the load on a tagged BS is assumed to be deterministic and equal to its mean $\mathbb{E}[\Psi_k]$, given by Lemma 14.

5.6 Summary

In this chapter, we have derived the downlink rate distribution under a generalized cell-selection model, which explicitly differentiates between long-term channel effects such as shadowing and path-loss, and small-scale effects such as fading. This generalizes the channel and cell selection models of all the previous chapters, where the channel randomness was captured using a single random variable and cell selection was based on the maximum instantaneous received signal strength. As an application of these results, we studied the effect of shadowing on load balancing, and showed that in certain regimes shadowing naturally balances load across various tiers and hence reduces the need for artificial cell selection bias.

Chapter 6

Fundamentals of HetNets with Energy Harvesting

The possibility of having a self-powered base station (BS) is becoming realistic due to several parallel trends. First, as discussed in Chapter 1, BSs are being deployed ever-more densely and opportunistically to meet the increasing capacity demand [30]. These new types of BSs (small cells) cover much smaller areas and hence require significantly smaller transmit powers compared to the conventional macrocells. Second, due to the increasingly bursty nature of traffic, the loads on the BSs will experience massive variation in space and time, as discussed in Chapter 3 [102]. In dense deployments, this means that many BSs can, in principle, be turned OFF most of the time and only be requested to wake up intermittently based on the traffic demand. Third, energy harvesting techniques, such as solar power, are becoming cost-effective compared to the conventional sources [120]. This is partly due to the technological improvements and partly due to the market forces, such as increasing taxes on conventional power sources, and subsidies and regulatory pressure for greener techniques. Fourth, high-speed wireless backhaul is rapidly becoming a reality for small cells, which eliminates the need for other wired connections [31]. Therefore, being able to avoid the constraint of requiring a wired power con-

nection is even more attractive, since it would open up entire new categories of low-cost "drop and play" deployments, especially of small cells.

6.1 Related Work and Motivation

The randomness in the energy availability at a transmitter demands significant rethinking of conventional wireless communication systems. There are three main directions taken in the literature to address this challenge, which we order below in terms of complexity and realism. The first considers a relatively simple setup consisting of single full-buffer isolated link, and study optimal transmission strategies under a given energy arrival process [121–123]. The effect of data arrivals can be additionally incorporated by considering two consecutive queues at the transmitter, one for the data and the other for the energy arrivals [124, 125].

Second, a natural extension of an isolated link, considers a broadcast channel, where a single isolated transmitter serves multiple users. Again one can assume full-buffer at the transmitter so that the transmission strategies need to be adapted only to the energy arrival process, e.g., in [126]. More realistically, one can relax the full-buffer assumption to explicitly consider data arrivals as discussed above for the isolated link, and optimize various metrics, e.g., minimize packet transmission delay [127], or maximize system throughput [128].

The third and least investigated direction is to consider multiple self-powered transmitters, which significantly generalizes the above two directions.

Generally speaking, the main goal is to adapt transmission schemes based on the energy and load variations across both time and space. While some progress has been recently made in advancing the understanding of mobile ad-hoc networks (MANETs) with self-powered nodes, see [129, 130] and references therein, our understanding of cellular networks in a similar setting is severely limited. This is partly due to the fact that conventional cellular networks consisted of big macro BSs that required fairly high power, and it made little sense to study them in the context of energy harvesting. As discussed earlier, this is not the case with a HetNet, which may support "drop and play" deployments, especially of small cells, in the future. Comprehensive modeling and analysis of this setup is the main focus of this chapter.

To capture key characteristics of HetNets, such as heterogeneity in infrastructure, and increasing uncertainty in BS locations, we consider a general K-tier cellular network with K different classes of BSs, where the BS locations of each tier are sampled from an independent Poisson Point Process (PPP), as discussed in Chapter 2. This model was proposed for HetNets by us in [5, 77], with various extensions and generalizations in [49, 51, 56]. The model, although simple, has been validated as reasonable since then both by empirical evidence [82] and theoretical arguments [113]. Due to its realism and tractability, it has become an accepted model for HetNets, see [87] for a detailed survey.

6.2 Contributions

Tractable and general system model. We propose a general system model consisting of K classes of self-powered BSs, which may differ in terms of the transit power, deployment density, energy harvesting rate and energy storage capacity. Due to the uncertainty in the energy availability, a BS may need to be kept OFF and allowed to accumulate enough energy before it starts serving its users again. In the meanwhile, its load is transferred to the neighboring BSs that are ON. Thus, at any given time a BS can be in either of the two *operational states*: ON or OFF. In this chapter, we focus on *uncoordinated operational strategies*, where the operational state of each BS is toggled independently of the other BSs. For tractability, we assume that the network operates on two time scales: i) *long time scale*, over which the decision to turn a BS ON or OFF is taken, and ii) *short time scale*, over which the scheduling and cell selection decisions are taken. As discussed in Section 6.4, this distinction facilitates analysis in two ways: a) it allows us to assume that the operational states of the BSs are static over short time scale, and b) it allows us to consider the average effects of cell selection over long time scale.

Availability region. We show that the fraction of time a k^{th} tier BS can be kept in the ON state, termed the *availability* ρ_k, is a key metric for self-powered cellular networks. Using tools from random walk theory, fixed point analysis, and stochastic geometry, we characterize the set of K-tuples $(\rho_1, \rho_2, \ldots \rho_K)$, termed the *availability region*, that are achievable with a set of

general uncoordinated strategies. Our analysis involves modeling the temporal dynamics of the energy level at each BS as a birth-death process, deriving energy utilization rate for each class of BSs using stochastic geometry, and using hitting/stopping time analysis for a Markov process to prove that there exists a fundamental limit on the availabilities $\{\rho_k\}$, which cannot be surpassed by any uncoordinated strategy. We also construct an achievable scheme that achieves this upper limit on availability for each class of BSs.

Notion of "optimality" for self-powered HetNets. The characterization of exact availability region lends a natural notion of optimality to self-powered HetNets under the assumptions of the proposed model. Our analysis concretely demonstrates that if the K-tuple $(\hat{\rho}_1, \hat{\rho}_2, \ldots, \hat{\rho}_K)$ corresponding to the optimal performance of the network, e.g., in terms of downlink rate, lies in the availability region, the performance of the HetNet with energy harvesting is the same as the one with reliable energy sources. Using recent results for downlink rate distribution in HetNets [112, 131], we also show that it is not always optimal from downlink data rate perspective to operate the network in the regime corresponding to the maximum availabilities, i.e., it may be preferable to keep a certain fraction of BSs OFF despite having enough energy.

Table 6.1: Notation Summary

Notation	Description
$\mathcal{K}$	Set of indices for BS tiers, i.e., $\mathcal{K} = \{1, 2, \ldots, K\}$
Φ_k, λ_k; Φ	Independent PPP modeling locations of k^{th} tier BSs, its density; set of all BSs, i.e., $\Phi = \cup_{k\in\mathcal{K}}\Phi_k$
$\Phi_u; \lambda_u$	An independent PPP modeling user locations, density of users
μ_k; ν_k; N_k	Energy harvesting rate, utilization rate, and energy storage capacity of a k^{th} tier BS
$\rho_k; \mathfrak{R}$	Availability of k^{th} tier BSs; availability region
$\Phi_k^{(\mathrm{a})}, \lambda_k^{(\mathrm{a})}; \Phi^{(\mathrm{a})}$	Independent PPP modeling the k^{th} tier BSs that are available, its density $\lambda_k^{(\mathrm{a})} = \rho_k\lambda_k$; all available BSs, i.e., $\Phi^{(\mathrm{a})} = \cup_{k\in\mathcal{K}}\Phi_k^{(\mathrm{a})}$
P_k	Downlink transmit power of a k^{th} tier BS to each user in each resource block
$h_k; \mathcal{X}_k; \alpha$	Small scale fading gain $h_k \sim \exp(1)$; large scale shadowing gain (general distribution) from a k^{th} tier BS; path loss exponent
$x_k^{*(z)}, x^{*(z)}$	Candidate serving BS in $\Phi_k^{(\mathrm{a})}$ for user at $z \in \Phi_u$, serving BS for $z \in \Phi_u$
$\mathtt{P_c}; \beta$	Coverage probability; target $\mathtt{SIR}$
$\mathtt{R_c}; \mathcal{T}$	Rate coverage; target rate

6.3 System Model

6.3.1 System Setup and Key Assumptions

We consider a K-tier cellular network consisting of K different classes of BSs. For notational simplicity, define $\mathcal{K} = \{1, 2, \ldots, K\}$. As in Chapters 2 and 3, the locations of the BSs of the k^{th} tier are modeled by an independent PPP Φ_k of density λ_k. Each BS has an energy harvesting module and an energy storage module, which is its sole source of energy. The BSs across tiers may differ both in terms of how fast they harvest energy, i.e., the *energy harvesting rate* μ_k joules/sec, and how much energy they can store, i.e., the energy storage capacity (or battery capacity) N_k joules. We assume that the normalization of μ_k and N_k is such that each user requires 1 joule of energy per sec. This assumption can be easily relaxed to incorporate users requiring more energy under sufficient randomization, but this case is not in the scope of this chapter. For resource allocation, we assume an orthogonal partitioning of resources, e.g., time-frequency resource blocks in orthogonal frequency division multiple access (OFDMA), where each resource block is allocated to a single user. Due to orthogonal resource allocation, there is no intra-cell interference. Note that a user can be allocated multiple resource blocks as discussed in detail in the sequel. We further assume that a k^{th} tier BS transmits to each user with a fixed power P_k in each resource block, which may depend upon the energy harvesting parameters, although we do not study this dependence in this chapter. The target `SIR` β is the same for all the tiers.

The energy arrival process at a k^{th} tier BS is modeled as a Poisson

process with mean μ_k. Since most energy harvesting modules contain smaller sub-modules, each harvesting energy independently, e.g., small solar cells in a solar panel, the net energy harvested can be modeled as a Binomial process, which approaches the Poisson process when the number of sub-modules grow large. Interestingly, this model has been validated using empirical measurements for a variety of energy harvesting modules [132]. Since the energy arrivals are random and the energy storage capacities are finite, there is some uncertainty associated with whether the BS has enough energy to serve users at a particular time. Under such a constraint, it is required that some of the BSs be kept OFF and allowed to recharge while their load is handled by the neighboring BSs that are ON. Besides, as discussed in the sequel, it may also be preferable to keep a BS OFF despite having enough energy. Therefore, a BS can be in either of the two *operational states*: ON or OFF. The decision to toggle the operational state from one to another is taken by the operational strategies that can be broadly categorized into two classes.

Uncoordinated: In this class of strategies, the decision to toggle the operational state, i.e., turn a BS ON or OFF, is taken by the BS independently of the operational states of the other BSs. For example, a BS may decide to turn OFF if its current energy level reaches below a certain predefined level and turn back ON after harvesting enough energy. The BS may additionally consider the time for which it is in the current state while making the decision. For instance, a BS may start a timer whenever the state is toggled and may decide to toggle it back when the timer expires or the energy level reaches a

certain minimum value, whichever occurs first. This class will be the main focus of this chapter.

Coordinated: In this class of strategies, the decision to toggle the state of a particular BS is dependent upon the states of the other BSs. For example, the BSs may be partitioned into small clusters where only a few BSs in each cluster are turned ON. The decision may be taken by some central entity based on the current load offered to the network. This is useful in the cases where the load varies by orders of magnitude across time, e.g., due to diurnal variation. A small fraction of BSs is enough to handle smaller load, with the provision of turning more ON as the load gradually increases. In addition to the load, other factors such as network topology and interference among BSs may also affect the decision.

For tractability, we define the following two time scales over which the network is assumed to operate.

Definition 2 (Time scales)**.** *The scheduling and cell association decisions are assumed to be taken over a time scale that is of the order of the scheduling block duration. We term this time scale as a short time scale. On the other hand, the operational policies that toggle the operational state of a BS are assumed to be defined on a much longer time scale. We will henceforth term this time scale as a long time scale.*

As discussed in the sequel, this distinction is the key to tractability because of two reasons: i) it allows us to assume the energy states of the

BSs to be static over short time scales, and ii) it allows us to consider the average effects of cell selection while determining the energy utilization rates over long time scales. Due to uncertainty in the energy availability or due to the optimality of a given performance metric, e.g., downlink rate, all the BSs in the network may not always be available to serve users. This is made precise by defining availability of a BS as follows.

Definition 3 (Availability)**.** *A BS is said to be available if it is in the ON state as a part of the operational policy and has enough energy to serve at least one user, i.e., has at least one unit of energy. The probability that a BS of tier k is available is denoted by ρ_k, which may be different for each tier of BSs due to the differences in the capabilities of the energy harvesting modules and the load served. For notational simplicity, we denote the set of availabilities for the K tiers by $\{\rho_k\}$.*

For uncoordinated strategies, it is reasonable to assume that the current operational state (ON or OFF) of a BS is independent of the other BSs, especially since the energy harvesting processes are assumed to be independent across the BSs. The coupling in the transmission of various BSs that arises due to interference and mobility is ignored. Under this independence assumption, the set of ON BSs of the k^{th} tier form a PPP $\Phi_k^{(\mathrm{a})}$ with density $\lambda_k^{(\mathrm{a})} = \lambda_k \rho_k$. This results from the fact that the independent thinning of a PPP leads to a PPP with appropriately scaled density [76]. As will be evident from the availability analysis in the next section, this abstraction is the key that makes this model tractable and leads to meaningful insights.

6.3.2 Propagation and Cell Selection Models

For this discussion it is sufficient to consider only the BSs that are available, i.e., the ones that are in the ON state. For notational ease, define $\Phi^{(\mathrm{a})} = \cup_{k\in\mathcal{K}}\Phi_k^{(\mathrm{a})}$. The user locations are assumed to be drawn from an independent PPP Φ_u of density λ_u. More sophisticated non-uniform user distribution models can also be considered, e.g., using tools from Chapter 3, but are not in the scope of this chapter. The received power at a user located at $z \in \Phi_u$ from a k^{th} tier BS placed at $x_k \in \Phi_k^{(\mathrm{a})}$ in a given resource block is

$$P(z, x_k) = P_k h_{kx_k}^{(z)} \mathcal{X}_{kx_k}^{(z)} \|x_k - z\|^{-\alpha}, \tag{6.1}$$

where $h_{kx_k}^{(z)} \sim \exp(1)$ models Rayleigh fading, $\mathcal{X}_{kx_k}^{(z)}$ models large scale shadowing, and $\|x_k - z\|^{-\alpha}$ represents standard power-law path loss with exponent α, for the wireless channel from $x_k \in \Phi_k^{(\mathrm{a})}$ to $z \in \Phi_u$. Note that since $h_{kx_k}^{(z)}$ and $\mathcal{X}_{kx_k}^{(z)}$ are both independent of the locations x_k and z, we will drop x_k and z from the subscript and superscript, respectively, and denote the two random variables by h_k and $\mathcal{X}_k$, whenever the locations are clear from the context.

For cell selection, we assume that each user connects to the BS that provides the highest long term received power, i.e., small scale fading gain $h_{kx}^{(z)}$ does not affect cell selection. For a cleaner exposition, we denote the location of the candidate k^{th} tier serving BS for $z \in \Phi_u$ by $x_k^{*(z)} \in \Phi_k^{(\mathrm{a})}$, which is

$$x_k^{*(z)} = \arg\max_{x\in\Phi_k^{(\mathrm{a})}} P_k \mathcal{X}_{xk}^{(z)} \|x - z\|^{-\alpha}. \tag{6.2}$$

A user $z \in \Phi_u$ now selects one of these K candidate serving BSs based on the average received signal power, i.e., the location of the serving BS $x^{*(z)} \in \{x_k^{*(z)}\}$

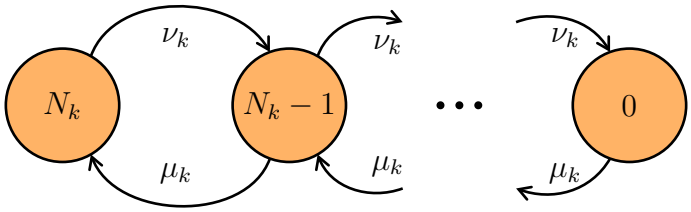

Figure 6.1: Birth-death process modeling the temporal dynamics of the energy available at a k^{th} tier BS.

is

$$x^{*(z)} = \arg \max_{x \in \{x_k^{*(z)}\}} P_k \mathcal{X}_{kx}^{(z)} \|x - z\|^{-\alpha}. \tag{6.3}$$

Owing to the displacement theorem for PPPs [70], any general distribution of $\mathcal{X}_k$ can be handled in the downlink analysis of a typical user as long as $\mathbb{E}\left[\mathcal{X}_k^{\frac{2}{\alpha}}\right] < \infty$. This is formally discussed in detail in Chapter 5. Interested readers can also refer to [116, 131] for relevant discussions. The most common assumption for large scale shadowing distribution is lognormal, where $\mathcal{X}_k = 10^{\frac{X_k}{10}}$ such that $X_k \sim \mathcal{N}(m_k, \sigma_k^2)$, where m_k and σ_k are respectively the mean and standard deviation in dB of the shadowing channel power. For lognormal distribution, $\mathbb{E}\left[\mathcal{X}_k^{\frac{2}{\alpha}}\right] = \exp\left(\frac{\ln 10}{5}\frac{m_k}{\alpha} + \frac{1}{2}\left(\frac{\ln 10}{5}\frac{\sigma_k}{\alpha}\right)^2\right)$, which can be easily derived using moment generating function (MGF) of Gaussian distribution [131]. The fractional moment is clearly finite if both the mean and standard deviation of the normal random variable X_k are finite. For this system model, we now study the availabilities of different classes of BSs.

6.4 Availability Analysis

The first challenge in studying the model introduced in the previous section lies in characterizing how the energy available at the BS changes over time. Without loss of generality, we index the energy states of a k^{th} tier BS as $0, 1, \ldots, N_k$, and model the temporal dynamics as a continuous time Markov chain (CTMC), in particular a birth-death process, as shown in Figure 6.1. When the BS is ON, the energy increases according to the energy harvesting rate and decreases at a rate that depends upon the number of users served by that BS. When the BS is OFF, it does not serve any users and hence the birth-death process reduces to a birth-only process. We now derive a closed form expression for the rate ν_k at which the energy is utilized at a typical k^{th} tier BS.

6.4.1 Modeling Energy Utilization Rate

Before modeling the energy utilization rate, there are two noteworthy points. First, if a BS is not available, the load originating from its original area of coverage is directed to the nearby BSs that are available, thus increasing their effective load. Equivalently, the coverage areas of the BSs that are available get expanded to cover for the BSs that are not available, as shown in Figure 6.2. The second one is related to the control channel coverage and given in the following remark. Recall that control channel coverage $\mathtt{P_c}$ is the probability that the received signal-to-interference-ratio (SIR) is greater than the predefined minimum SIR needed to establish a connection with the BS.

Thus the users that are not in control channel coverage cannot enter the network and hence cannot access the data channels. Therefore, these users do not account for any additional energy expenditure at the BS.

Remark 14 (Control channel coverage)**.** *The control channel coverage* $\mathtt{P_c}$ *is independent of the densities of the BSs in an interference-limited network when the target SIR is the same for all tiers [5, 49, 131]. While this result will be familiar to those exposed to recent coverage probability analysis using stochastic geometry, it is not directly required in this section except the interpretation that the density of users effectively served by the network is independent of the effective densities of the BSs and hence independent of* $\{\rho_k\}$*. We will validate this claim in Section 6.4.5.*

Assuming fixed energy expenditure for control signaling, only the users that are in control channel coverage will result in additional energy expenditure at the BS. As remarked above, the density of such users is $\mathtt{P_c}\lambda_u$. Each user is assumed to require 1 joule of energy per sec such that the net energy utilization process at each BS can be modeled as a Poisson process with mean defined by the average number of users it serves. It should be noted that the assumption of 1 joule energy requirement is without any loss of generality and is made to simplify the notation. To find the average number of users served by a typical BS of each class, we first need to define its service region whose statistics such as its area will, in general, be different for different classes of BSs due to the differences in the transmit powers as evident from Figure 6.2. The service region can be formally defined as follows.

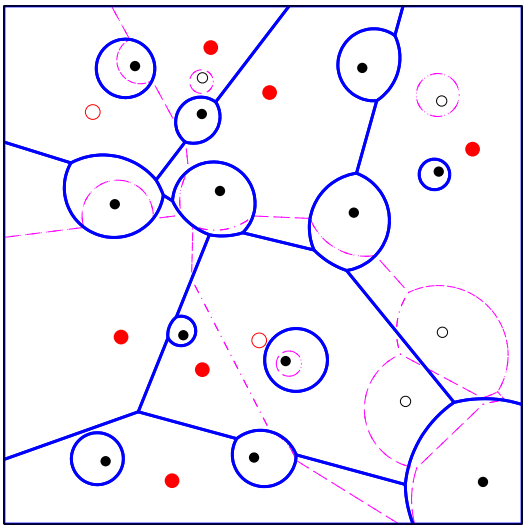

Figure 6.2: Coverage regions for a two-tier energy harvesting cellular network (averaged over shadowing). The unavailable BSs are denoted by hollow circles. The thin lines form coverage regions for the baseline case assuming all the BSs were available.

Definition 4 (Service region)**.** *The service region* $\mathcal{A}_k(x_k) \subset \mathbb{R}^2$ *of the* k^{th}*-tier BS located at* $x_k \in \Phi_k^{(\mathrm{a})}$ *is*

$$\mathcal{A}_k(x_k) = \Bigg\{ z \in \mathbb{R}^2 : x_k = \arg \max_{x \in \{x_j^{*(z)}\}} P_j \mathcal{X}_j^{(z)} \|x - z\|^{-\alpha}, \\ \text{where } \; x_j^{*(z)} = \arg \max_{x \in \Phi_j^{(\mathrm{a})}} P_j \mathcal{X}_j^{(z)} \|x - z\|^{-\alpha} \Bigg\}. \tag{6.4}$$

We now derive the average area of the service region of a typical BS of each tier in the following Lemma.

Lemma 15 (Average area of the service region)**.** *The average area of the*

service region of a k^{th} tier typical BS is given by

$$\mathbb{E}[|\mathcal{A}_k|] = \frac{\mathbb{E}\left[\mathcal{X}_k^{\frac{2}{\alpha}}\right] P_k^{\frac{2}{\alpha}}}{\sum_{j=1}^{K} \rho_j \lambda_j \mathbb{E}\left[\mathcal{X}_j^{\frac{2}{\alpha}}\right] P_j^{\frac{2}{\alpha}}}. \tag{6.5}$$

Proof. The proof follows from the definition of the service area using basic ideas from Palm calculus. Denote by $\mathbb{P}^{x_k}_{\Phi_k^{(\mathrm{a})}}(\cdot)$ and $\mathbb{E}^{x_k}_{\Phi_k^{(\mathrm{a})}}[\cdot]$, the conditional (Palm) probability and conditional expectation, conditioned on $x_k \in \Phi_k^{(\mathrm{a})}$. Please refer to [69, 70, 133] for details on Palm calculus. Before we derive the average area, note that for given realizations of the BS locations and the channel gains, the area of the service region of the k^{th} tier BS is

$$|\mathcal{A}_k(x_k)| = \int_{\mathbb{R}^2} \prod_{j\in\mathcal{K}} \prod_{x\in\Phi_j^{(\mathrm{a})}} \mathbf{1}\left(\frac{P_k \mathcal{X}_k^{(z)}}{\|x_k - z\|^{\alpha}} \geq \frac{P_j \mathcal{X}_j^{(z)}}{\|x - z\|^{\alpha}}\right) \mathrm{d}z. \tag{6.6}$$

The average service area can now be expressed as

$$\mathbb{E}[|\mathcal{A}_k(x_k)|] \overset{(a)}{=} \mathbb{E}\mathbb{E}^{x_k}_{\Phi_k^{(\mathrm{a})}}[|\mathcal{A}_k(x_k)|] \tag{6.7}$$

$$\overset{(b)}{=} \mathbb{E}\mathbb{E}^{0}_{\Phi_k^{(\mathrm{a})}}[|\mathcal{A}_k(0)|] \overset{(c)}{=} \mathbb{E}\mathbb{E}_{\Phi_k^{(\mathrm{a})}}[|\mathcal{A}_k(0)|], \tag{6.8}$$

where (a) follows by distributing the expectation over the point process $\Phi_k^{(\mathrm{a})}$ and the rest of the randomness, (b) follows from the stationarity of the homogeneous PPP, and (c) follows from Slivnyak's theorem [69]. Substituting the expression for $|\mathcal{A}_k(0)|$ in (6.8) and distributing the expectation across various random quantities, we can express the average area as $\mathbb{E}[|\mathcal{A}_k(x_k)|] =$

$$\mathbb{E}_{\mathcal{X}_k} \int_{\mathbb{R}^2} \prod_{j\in\mathcal{K}} \mathbb{E}_{\Phi_j^{(\mathrm{a})}} \prod_{x\in\Phi_j^{(\mathrm{a})}} \mathbb{E}_{\mathcal{X}_j} \mathbf{1}\left(\frac{P_k \mathcal{X}_k}{\|z\|^{\alpha}} \geq \frac{P_j \mathcal{X}_j}{\|x - z\|^{\alpha}}\right) \mathrm{d}z, \tag{6.9}$$

where the expectations over point processes $\Phi_j^{(\mathrm{a})}$ and shadowing gains $\mathcal{X}_j$ can be moved inside respective product terms due to independence, and superscript on $\mathcal{X}_k^{(z)}$ and $\mathcal{X}_j^{(z)}$ are removed for notational simplicity. The expectation over point process $\Phi_j^{(\mathrm{a})}$ can be evaluated using the probability generating functional (PGFL) [69], which simplifies the average area expression to

$$\mathbb{E}_{\mathcal{X}_k} \int_{\mathbb{R}^2} \prod_{j\in\mathcal{K}} e^{-\rho_j \lambda_j \mathbb{E}_{\mathcal{X}_j} \int_{\mathbb{R}^2} \mathbf{1}\left(\frac{P_k \mathcal{X}_k}{\|z\|^\alpha} < \frac{P_j \mathcal{X}_j}{\|x-z\|^\alpha}\right) \mathrm{d}x} \mathrm{d}z. \tag{6.10}$$

Solving the integral in the exponential, we get

$$\mathbb{E}_{\mathcal{X}_k} \int_{\mathbb{R}^2} \prod_{j\in\mathcal{K}} \exp\left(-\rho_j \lambda_j \pi \|z\|^2 \frac{P_j \mathbb{E}\left[\mathcal{X}_j^{\frac{2}{\alpha}}\right]}{P_k \mathcal{X}_k^{\frac{2}{\alpha}}}\right) \mathrm{d}z, \tag{6.11}$$

which can be equivalently expressed as

$$\mathbb{E}_{\mathcal{X}_k} \int_{\mathbb{R}^2} \exp\left(-\rho_j \lambda_j \pi \|z\|^2 \frac{\sum_{j\in\mathcal{K}} P_j \mathbb{E}\left[\mathcal{X}_j^{\frac{2}{\alpha}}\right]}{P_k \mathcal{X}_k^{\frac{2}{\alpha}}}\right) \mathrm{d}z, \tag{6.12}$$

from which the result follows by solving the integral and taking expectation with respect to $\mathcal{X}_k$. □

Using the expression for average area, the average number of users served by a typical BS of k^{th} tier, equivalently the energy utilization rate, is now given by the following corollary.

Corollary 16 (Energy utilization rate)**.** *The energy utilization rate, i.e., the number of units of energy required per second, at a typical BS of k^{th} tier is given by*

$$\nu_k = \mathtt{P_c} \lambda_u \mathbb{E}[|\mathcal{A}_k|] = \frac{\mathtt{P_c} \lambda_u \mathbb{E}\left[\mathcal{X}_k^{\frac{2}{\alpha}}\right] P_k^{\frac{2}{\alpha}}}{\sum_{j=1}^{K} \rho_j \lambda_j \mathbb{E}\left[\mathcal{X}_j^{\frac{2}{\alpha}}\right] P_j^{\frac{2}{\alpha}}}, \tag{6.13}$$

where recall that $\mathtt{P_c}$ *denotes the coverage probability, which is independent of the availabilities and will be calculated later in this section and is given by* (6.50)*.*

Remark 15 (Invariance to shadowing distribution)**.** *From* (6.13)*, note that the energy utilization rate* ν_k *is invariant to the shadowing distribution of all the tiers if* $\mathbb{E}\left[\mathcal{X}_j^{\frac{2}{\alpha}}\right] = \mathbb{E}\left[\mathcal{X}_k^{\frac{2}{\alpha}}\right]$*, for all* $j, k \in \mathcal{K}$*. For lognormal shadowing, this corresponds to the case when* $m_j = m_k$ *and* $\sigma_j = \sigma_k$*, for all* $j, k \in \mathcal{K}$*.*

It should be noted that the availabilities of various tiers are still unknown and even if all the system parameters are given, it is still not possible to determine the energy utilization rate from the above expression. This will lead to fixed point expressions in terms of availabilities, which is the main focus of the rest of this section. It is also worth mentioning that the energy utilization rate derived above is just for the service of the active users. There are some other components of energy usage, e.g., control channel signaling and backhaul that are not modeled. While we can incorporate their effect in the current model by assuming fixed energy expenditure and deducting it directly from the energy arrival rate, a more formal treatment of these components is left for future work.

6.4.2 Availabilities for a Simple Operational Strategy

After deriving the energy utilization rate in Corollary 16 and recalling that the energy harvesting rate is μ_k, we can, in principle, derive BS availabilities for a variety of uncoordinated operational strategies. We begin by looking

at a very simple strategy in which a BS is said to be available when it is not in energy state 0, i.e., it has at least one unit of energy. As shown later in this section, this strategy is of fundamental importance in characterizing the *availability region* for the set of general uncoordinated strategies. The availability of a k^{th} tier BS under this strategy can be derived directly from the stationary distribution of the birth-death process as

$$\rho_k = 1 - \left(\frac{1 - \frac{\mu_k}{\nu_k}}{1 - \left(\frac{\mu_k}{\nu_k}\right)^{N_k+1}} \right) = 1 - \left(\frac{1 - \frac{\mu_k \sum_{j=1}^{K} \rho_j \lambda_j \mathbb{E}\left[\chi_j^{\frac{2}{\alpha}}\right] P_j^{\frac{2}{\alpha}}}{\mathtt{P_c} \lambda_u \mathbb{E}\left[\chi_k^{\frac{2}{\alpha}}\right] P_k^{\frac{2}{\alpha}}}}{1 - \left(\frac{\mu_k \sum_{j=1}^{K} \rho_j \lambda_j \mathbb{E}\left[\chi_j^{\frac{2}{\alpha}}\right] P_j^{\frac{2}{\alpha}}}{\mathtt{P_c} \lambda_u \mathbb{E}\left[\chi_k^{\frac{2}{\alpha}}\right] P_k^{\frac{2}{\alpha}}} \right)^{N_k+1}} \right). \tag{6.14}$$

Interestingly we get a set of K fixed point equations in terms of availabilities, one for each tier. Clearly $\rho_k \equiv 0$, $\forall\ k \in \mathcal{K}$, is a trivial solution for this set of fixed point equations. However, this means that none of the BSs is available for service, which physically means that the users are in "outage" if there is no other, in particular positive, solution for the set of fixed point equations. We will formalize this notion of outage, resulting from energy unavailability, later in this section. Due to the form of these equations, it is not possible to derive closed form expressions for the positive solution(s) of $\{\rho_k\}$. However, it is possible to establish a necessary and sufficient condition for the existence and uniqueness of a non-trivial positive solution. Before establishing this result, we show that the function of $\{\rho_k\}$ on the right hand side of (6.14) satisfies certain key properties. For notational simplicity, we call this function

corresponding to k^{th} tier as $g_k : \mathbb{R}^K \to \mathbb{R}$, using which the set of fixed point equations given by (6.14) can be expressed in vector form as

$$\begin{bmatrix} \rho_1 \\ \rho_2 \\ \vdots \\ \rho_K \end{bmatrix} = \begin{bmatrix} g_1(\rho_1, \rho_2, \ldots, \rho_K) \\ g_2(\rho_1, \rho_2, \ldots, \rho_K) \\ \vdots \\ g_K(\rho_1, \rho_2, \ldots, \rho_K) \end{bmatrix} = \Xi(\rho_1, \rho_2, \ldots, \rho_K), \tag{6.15}$$

where we further define function $\Xi : \mathbb{R}^K \to \mathbb{R}^K$ for simplicity of notation. Our first goal is to study the properties of function $g_k : \mathbb{R}^K \to \mathbb{R}$, which can be rewritten as

$$g_k(\mathbf{x}) = 1 - \left(\frac{1 - \sum_{j=1}^{K} a_j x_j}{1 - \left(\sum_{j=1}^{K} a_j x_j \right)^N} \right), \tag{6.16}$$

where $\mathbf{x} \in \mathbb{R}^K$, $N > 1$, and $a_k \in \mathbb{R}_+$ for all $k \in \mathcal{K}$. The relevant properties are summarized in the following Lemma.

Lemma 16 (Properties)**.** *The function $g_k(\mathbf{x}) : \mathbb{R}^K \to \mathbb{R}$ defined by* (6.16) *satisfies following properties for all $a_k > 0$, $k \in \mathcal{K}$:*

1. *$g_k(\mathbf{x})$ is an element-wise increasing function of $\mathbf{x}$.*

2. *$g_k(\mathbf{x})$ is concave, i.e., it is a concave function of $x_k \in \mathbb{R}$ for all $k \in \mathcal{K}$.*

Proof. Since both the properties (monotonicity and concavity) are element-wise properties, it is enough to consider the given function as a function of single variable $x \in \mathbb{R}$. After dropping the subscript k and with slight over-loading of notation, we denote this function as $g : \mathbb{R} \to \mathbb{R}$, which is

$$g(x) = 1 - \left(\frac{1 - b - ax}{1 - (b + ax)^N} \right), \tag{6.17}$$

where $b \in \mathbb{R}_+$ is a constant when we study element-wise properties. We now do the following substitution $x + \frac{b}{a} \to x$, which just shifts the function along x-axis and hence neither impacts the monotonicity nor concavity of $g(x)$. The simplified expression is

$$g(x) = 1 - \left(\frac{1 - ax}{1 - (ax)^N} \right). \tag{6.18}$$

Note that although both the numerator and denominator of the second term in the above expression go to 0 as $x \to \frac{1}{a}$, it is easy to show that the function is continuous at this point and the limit is

$$\lim_{x \to \frac{1}{a}} g(x) = \frac{N-1}{N}. \tag{6.19}$$

To prove that the function is monotonically increasing, it is enough to show that the partial derivative with respect to x is positive. The partial derivative can be expressed as

$$g'(x) = \frac{a}{(1 - (ax)^N)^2} \left((N-1)(ax)^N + 1 - N(ax)^{N-1} \right), \tag{6.20}$$

It is easy to show that the term inside the bracket is positive except at $x = \frac{1}{a}$, where it has a minima and takes value 0. Further, using L'Hôpital's rule it is straightforward to show

$$\lim_{x \to \frac{1}{a}} g'(x) = a \frac{N-1}{2N} > 0, \tag{6.21}$$

which completes the proof for the monotonicity property. To show that the function is concave, we need to show that the double derivative with respect to x is negative, which is

$$g''(x) = -a^2 N (ax)^{N-2} \frac{1 - ax}{(1 - (ax)^N)^3} \times$$

$$\left(\frac{(N-1)(1-(ax)^{N+1})}{1-ax} - \frac{ax(N+1)(1-(ax)^{N-1})}{1-ax}\right), \tag{6.22}$$

where the term inside the bracket is positive except at $x = \frac{1}{a}$, where it has a minima and takes value 0. As in the case of the first derivative, it is easy to show using L'Hôpital's rule that the limit at this point is

$$\lim_{x \to \frac{1}{a}} g''(x) = -a^2 \frac{N^2 - 1}{6N} < 0, \tag{6.23}$$

which shows that the function is strictly concave for all $x \in \mathbb{R}$. This completes the proof. □

Lemma 16 can be easily extended to the function $\Xi : \mathbb{R}^K \to \mathbb{R}^K$ to show that it is also a monotonically increasing and concave function. The conditions for existence and uniqueness of the fixed point for such functions can be characterized by specializing Tarski's theorem [134] for concave functions. The result is stated below. To the best of the knowledge of the authors, it first appeared in [135, Theorem 3]. Since the proof is given in [135], it is skipped here.

Theorem 10 (Fixed point for increasing concave functions)**.** *Suppose* $\Xi : \mathbb{R}^n \to \mathbb{R}^n$ *is an increasing and strictly concave function satisfying the following two properties:*

1. $\Xi(0) \geq 0$, $\Xi(a) > a$ *for some* $a \in \mathbb{R}^n_+$,

2. $\Xi(b) < b$ *for some* $b > a$.

Then Ξ has a unique positive fixed point.

Before deriving the main result about the existence and uniqueness of positive solution for the set of fixed point equations (6.14), for cleaner exposition we state the following intermediate result that establishes equivalence between an energy conservation principle and a key set of conditions.

Lemma 17 (Equivalence)**.** *For $\rho_k > 0, \forall k$, the following sets of conditions are equivalent, i.e.,* (6.24) $\Leftrightarrow$ (6.25)

$$\frac{\mu_k \sum_{j=1}^{K} \rho_j \lambda_j \mathbb{E}\left[\mathcal{X}_j^{\frac{2}{\alpha}}\right] P_j^{\frac{2}{\alpha}}}{\rho_k \mathtt{P_c} \lambda_u \mathbb{E}\left[\mathcal{X}_k^{\frac{2}{\alpha}}\right] P_k^{\frac{2}{\alpha}}} > 1, \forall k \in \mathcal{K} \tag{6.24}$$

$$\sum_{k=1}^{K} \lambda_k \mu_k > \lambda_u \mathtt{P_c}, \tag{6.25}$$

where (6.25) *is simply the energy conservation principle, i.e., the net energy harvested by all the tiers should be greater than the effective energy required by all the users.*

Proof. For the proof of (6.24) $\Rightarrow$ (6.25), take the denominator of (6.24) to the right hand side of inequality and multiply both sides by λ_k to get

$$\lambda_k \mu_k \sum_{j=1}^{K} \rho_j \lambda_j \mathbb{E}\left[\mathcal{X}_j^{\frac{2}{\alpha}}\right] P_j^{\frac{2}{\alpha}} > \rho_k \lambda_k \mathtt{P_c} \lambda_u \mathbb{E}\left[\mathcal{X}_k^{\frac{2}{\alpha}}\right] P_k^{\frac{2}{\alpha}}, \forall k \in \mathcal{K}.$$

Now add all the K inequalities, i.e., sum both sides from $k = 1$ to K, which leads to (6.25) and hence completes half of the proof. For the proof of (6.24) $\Leftarrow$ (6.25), multiply both sides of (6.25) by $\sum_{j=1}^{K} \rho_j \lambda_j \mathbb{E}\left[\mathcal{X}_j^{\frac{2}{\alpha}}\right] P_j^{\frac{2}{\alpha}}$ to get

$$\sum_{k=1}^{K} \lambda_k \mu_k \sum_{j=1}^{K} \rho_j \lambda_j \mathbb{E}\left[\mathcal{X}_j^{\frac{2}{\alpha}}\right] P_j^{\frac{2}{\alpha}} > \sum_{k=1}^{K} \mathtt{P_c} \lambda_u \rho_k \lambda_k \mathbb{E}\left[\mathcal{X}_k^{\frac{2}{\alpha}}\right] P_j^{\frac{2}{\alpha}}. \tag{6.26}$$

Rearranging the terms we get

$$\sum_{k=1}^{K} \lambda_k \left(\frac{\mu_k \sum_{j=1}^{K} \rho_j \lambda_j \mathbb{E}\left[\mathcal{X}_j^{\frac{2}{\alpha}}\right] P_j^{\frac{2}{\alpha}}}{\mathtt{P_c} \lambda_u \rho_k \mathbb{E}\left[\mathcal{X}_k^{\frac{2}{\alpha}}\right] P_j^{\frac{2}{\alpha}}} - 1 \right) > 0. \tag{6.27}$$

Since λ_k is arbitrary, for the above condition to always hold, we need the term inside the bracket to be positive for all $k \in \mathcal{K}$. This set of conditions is the same as (6.24) and hence completes the proof. □

Using Theorem 10 and Lemma 17, we now derive the main result of this subsection.

Theorem 11. *The necessary and sufficient condition for the existence of a positive solution $\rho_k > 0$, $\forall\ k \in \mathcal{K}$ for the system of fixed point equations given by* (6.14) *is*

$$\sum_{k=1}^{K} \lambda_k \mu_k > \lambda_u \mathtt{P_c}. \tag{6.28}$$

Proof. For sufficiency, it is enough to show that the given condition is sufficient for the function $\Xi : \mathbb{R}^K \to \mathbb{R}^K$ defined by (6.15) to satisfy both the properties listed in Theorem 10. Further, it is enough to show this for each element

function $g_k : \mathbb{R}^K \to \mathbb{R}$ of Ξ. For $\rho_k \neq 0$, the function g_k, as a function of ρ_k can be expressed as

$$g_k(\rho_k) = 1 - \left(\frac{1 - \kappa_k \rho_k}{1 - (\kappa_k \rho_k)^{N_k+1}} \right), \tag{6.29}$$

where

$$\kappa_k = \frac{\mu_k \sum_{j=1}^{K} \rho_j \lambda_j \mathbb{E}\left[\mathcal{X}_j^{\frac{2}{\alpha}}\right] P_j^{\frac{2}{\alpha}}}{\rho_k \mathtt{P_c} \lambda_u \mathbb{E}\left[\mathcal{X}_k^{\frac{2}{\alpha}}\right] P_k^{\frac{2}{\alpha}}}. \tag{6.30}$$

Note that the function $g_k(\rho_k) < 1$ for finite N_k. Now setting b, as defined in Theorem 10, equal to 1, it is enough to find conditions under which $\exists\ a < b$ such that $g_k(a) > a$. Since $g_k(\rho_k) = 0$ for $\rho_k \to 0$, for the existence of a such that $g_k(a) > a$ it is enough to show that $g'(\rho_k) > 1$ for $\rho_k \to 0$. Furthermore, it is easy to show that $g'(\rho_k) = \kappa_k$ for $\rho_k \to 0$, which leads to the condition $\kappa_k > 1$ for the existence of a as defined above. This leads to the following set of inequalities for $1 \leq k \leq K$:

$$\frac{\mu_k \sum_{j=1}^{K} \rho_j \lambda_j \mathbb{E}\left[\mathcal{X}_j^{\frac{2}{\alpha}}\right] P_j^{\frac{2}{\alpha}}}{\rho_k \mathtt{P_c} \lambda_u \mathbb{E}\left[\mathcal{X}_k^{\frac{2}{\alpha}}\right] P_k^{\frac{2}{\alpha}}} > 1. \tag{6.31}$$

From Lemma 17, this set of conditions is the same as (6.28) and hence proves that (6.28) is a sufficient condition for the existence and uniqueness of the positive solution for $\{\rho_k\}$.

To show that the given condition is also necessary, we construct a simple counter example. Let $K = 1$ and drop all the subscripts denoting the indices of tiers for notational simplicity. The fixed point equation for this simple setup

is

$$\rho = 1 - \left(\frac{1 - \frac{\mu\rho\lambda}{\mathtt{P_c}\lambda_u}}{1 - \left(\frac{\mu\rho\lambda}{\mathtt{P_c}\lambda_u}\right)^N} \right) = g(\rho), \tag{6.32}$$

It is easy to show that $g(\rho)$ does not have a positive fixed point when $\mu\lambda < \mathtt{P_c}\lambda_u$, which proves that the given condition (6.28) is also necessary. □

The existence and uniqueness of the positive solution for the BS availabilities $\{\rho_k\}$ will play a crucial role in establishing the availability region later in this section. The unique positive solution for $\{\rho_k\}$ can be computed easily using fixed-point iteration. Before concluding this section, it is important to formalize some key ideas.

Remark 16 (Energy outage)**.** *From Theorem 11, it is clear that the total energy harvested by the HetNet must be greater than the total energy demand to guarantee a positive solution for the availabilities* $\{\rho_k\}$*. However, if this condition is not met, the system may drop a certain fraction of users to ensure that the resulting density of users* λ_u' *is such that* $\sum_{k=1}^{K} \lambda_k\mu_k > \lambda_u'\mathtt{P_c}$*. The rest of the users are said to be in outage due to energy unavailability, or in short "energy outage". The probability of a user being in energy outage is*

$$\mathcal{O}_e = 1 - \frac{\lambda_u'}{\lambda_u} \geq 1 - \frac{\sum_{k=1}^{K} \lambda_k\mu_k}{\lambda_u\mathtt{P_c}}, \tag{6.33}$$

where the lower bound is strictly positive if $\sum_{k=1}^{K} \lambda_k\mu_k < \lambda_u\mathtt{P_c}$*, i.e., when condition* (6.28) *is not met. However, if the condition* (6.28) *is met, it is in principle possible to make* $\mathcal{O}_e = 0$*. The exact characterization of energy outage*

will depend upon the protocol design and is out of the scope of this chapter. In the rest of the chapter, we will assume that the condition (6.28) *is met and hence* $\mathcal{O}_e = 0$.

Remark 17 (Effect of battery capacity on availability)**.** *Note that the function* g_k *is an increasing function of* N_k *from which it directly follows that the availability of a particular class of BSs increases with the increase in the battery capacity.*

Remark 18 (Effect of availabilities of other tiers on ρ_k)**.** *From Lemma 16, it follows that* g_k *is an increasing function of not only* ρ_k *but also of* ρ_j, $j \neq k$. *This implies that the availability of* k^{th} *tier increases if the availability of one or more of the other tiers is increased. This is consistent with the intuition that if the availability of any tier is increased, the effective load on other tiers decreases hence increasing their availabilities.*

Definition 5 (Over-provisioning factor)**.** *As mentioned above, we will henceforth assume that the system is over provisioned in terms of energy harvesting, i.e.,* $\sum_{k=1}^{K} \lambda_k \mu_k > \lambda_u \mathtt{P_c}$. *For cleaner exposition, it is useful to define an over-provisioning factor* γ *as the ratio of total energy harvested in the network and the effective energy demand, i.e.,*

$$\gamma = \frac{\sum_{k=1}^{K} \lambda_k \mu_k}{\lambda_u \mathtt{P_c}} > 1. \tag{6.34}$$

So far we focused on a particular strategy, where a BS is said to be available if it is not in the 0 energy state, i.e., it has at least one unit of energy. In

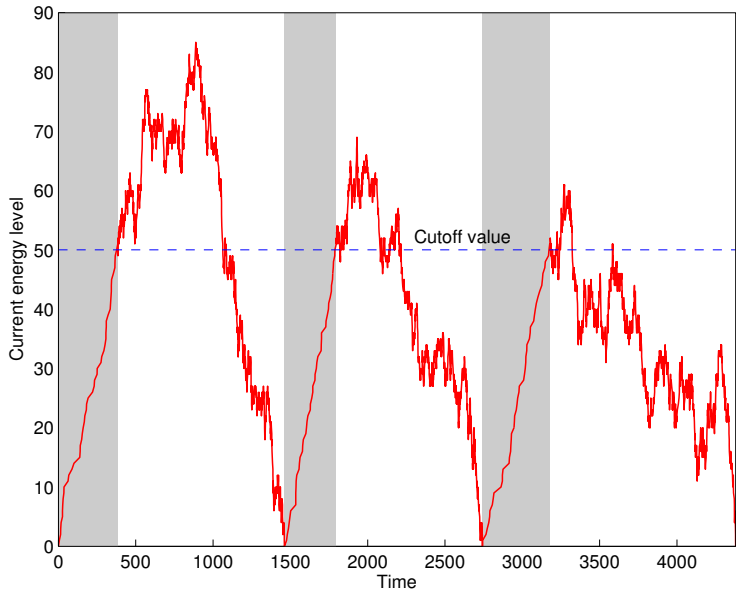

Figure 6.3: Illustration of how the energy level changes over time. The time for which BS is in OFF state is shaded. The unit of time is irrelevant.

the next subsection, we develop tools to study availabilities for any general uncoordinated strategy using stopping/hitting time analysis. Our analysis will concretely demonstrate that the simple strategy discussed above maximizes the BS availabilities over the space of general uncoordinated strategies. Extending these results further, we will characterize the availability region that is achievable by the set of general uncoordinated strategies.

6.4.3 Availabilities for any General Uncoordinated Strategy

We first focus on a general set of strategies $\{\mathcal{S}_k(N_{k\min}, N_{kc})\}$ in which a BS toggles its state based solely on its current energy level, i.e., a k^{th} tier BS toggles to OFF state when its energy level reaches some level $N_{k\min}$ and toggles

back to ON state when the energy level reaches some predefined cutoff value $N_{kc} > N_{k\min}$ as shown in Figure 6.3. Although not required for this analysis, it should be noted that the cutoff value N_{kc} can be changed by the network if necessary on an even larger time scale than the time scale over which the BSs are turned ON/OFF. Now note that for the proposed model, the strategies $\{\mathcal{S}_k(N_{k\min}, N_{kc})\}$ with energy storage capacity N_k and $\{\mathcal{S}_k(0, N_{kc} - N_{k\min})\}$ with energy storage capacity $N_k - N_{k\min}$, are equivalent because when the BS is turned OFF at a non-zero energy level $N_{k\min}$ in the first set of strategies, it effectively reduces the energy storage capacity to $N_k - N_{k\min}$. Therefore, without any loss of generality we fix $N_{k\min} = 0$ (for all tiers) and denote this strategy by $\mathcal{S}_k(N_{kc})$ for notational simplicity. For this strategy, we denote the time for which a k^{th} tier BS is in the ON state after it toggles from the OFF state by $J_{k_1}(N_{kc})$ and the time for which it remains in the OFF state after toggling from the ON state by $J_{k_2}(N_{kc})$. The cutoff value in the arguments will be dropped for notational simplicity wherever appropriate. The cycles of ON and OFF times go on as shown in Figure 6.3. It is worth highlighting that both J_{k_1} and J_{k_2} are in general random variables due to the randomness involved in both the energy availability and its utilization, e.g., J_{k_1} can be formally expressed as $J_{k_1}(N_{kc}) = \inf\{t : \mathcal{E}_k(t) = 0 | \mathcal{E}_k(0) = N_{kc}\}$, where $\mathcal{E}_k(t)$ denotes the energy level of a k^{th} tier BS at time t. For this setup, the availabilities depend only on the means of J_{k_1} and J_{k_2} as shown in the following Lemma.

Lemma 18 (Availability)**.** *The availability of a k^{th} tier BS for any operational*

strategy can be expressed as

$$\rho_k = \frac{\mathbb{E}[J_{k_1}]}{\mathbb{E}[J_{k_1}] + \mathbb{E}[J_{k_2}]} = \frac{1}{1 + \frac{\mathbb{E}[J_{k_2}]}{\mathbb{E}[J_{k_1}]}}, \tag{6.35}$$

where $\mathbb{E}[J_{k_1}]$ *is the mean time a BS spends in the ON state and* $\mathbb{E}[J_{k_2}]$ *is the mean time it spends in the OFF state.*

Proof. For a particular realization, let $\{J_{k_1}^{(i)}\}$ and $\{J_{k_2}^{(i)}\}$ be the sequences of ON and OFF times, respectively, with i being the index of the ON-OFF cycle. The availability can now be expressed as the fraction of time a BS spends in the ON state, which leads to

$$\rho_k = \lim_{n\to\infty} \frac{\sum_{i=1}^{n} J_{k_1}^{(i)}}{\sum_{i=1}^{n} J_{k_1}^{(i)} + \sum_{i=1}^{n} J_{k_2}^{(i)}}. \tag{6.36}$$

The proof follows by dividing both the numerator and the denominator by n and invoking the law of large numbers. □

To set up a fixed point equation similar to (6.14) for the strategy $\mathcal{S}_k(N_{kc})$, we need closed form expressions for the mean ON time $\mathbb{E}[J_{k_1}]$ and the mean OFF time $\mathbb{E}[J_{k_2}]$. Note that the OFF time for $\mathcal{S}_k(N_{kc})$ is simply the time required to harvest N_{kc} units of energy, which is the sum of N_{kc} exponentially distributed random variables, each with mean $1/\mu_k$. Therefore,

$$\mathbb{E}[J_{k_2}] = \frac{N_{kc}}{\mu_k} \Rightarrow \rho_k = \frac{1}{1 + \frac{N_{kc}}{\mu_k \mathbb{E}[J_{k_1}]}}. \tag{6.37}$$

To derive $\mathbb{E}[J_{k_1}]$, we first define the generator matrix for the birth-death process corresponding to a k^{th} tier BS as $A_k =$

$$\begin{bmatrix} -\mu_k & \mu_k & 0 & \cdots & 0 & 0 \\ \nu_k & -\mu_k - \nu_k & \mu_k & \cdots & 0 & 0 \\ 0 & \nu_k & -\mu_k - \nu_k & \cdots & 0 & 0 \\ \vdots & \vdots & & \ddots & & \\ 0 & 0 & 0 & \cdots & \nu_k & -\nu_k \end{bmatrix}, \tag{6.38}$$

where the states are ordered in the ascending order of the energy levels, i.e., the first column corresponds to the energy level 0. To complete the derivation, we need the following technical result. Please refer to Proposition 5.7.2 of [136] for a more general version of this result and its proof.

Lemma 19 (Mean hitting time)**.** *If the embedded discrete Markov chain of the CTMC is irreducible then the mean time to hit energy level* 0 *(state* 1*) starting from energy level* i *(state* $i+1$*) is*

$$\mathbb{E}[J_{k_1}(i)] = \left((-B_k)^{-1}\,\mathbb{1}\right)(i), \tag{6.39}$$

where $\mathbb{1}$ *is a column vector of all* 1*s, and* B_k *is a* $(N_k-1)\times(N_k-1)$ *sub-matrix of* A_k *obtained by deleting first row and column of* A_k*.*

For A_k given by (6.38), we can derive a closed form expression for each element of $(-B_k)^{-1}$ after some algebraic manipulations. The $(i,j)^{th}$ element can be expressed as

$$(-B_k)^{-1}(i,j) = \frac{1}{\nu_k^j} \sum_{n=1}^{\min(i,j)} \mu_k^{j-n} \nu_k^{n-1}. \tag{6.40}$$

Now substituting (6.40) back in (6.39) gives us the mean ON time for any strategy $\mathcal{S}_k(N_{kc})$, which when substituted in (6.37) gives a fixed point equation in $\{\rho_k\}$ similar to (6.14), as illustrated below for the two policies of interest.

6.4.3.1 Policy 1 ($\mathcal{S}_k(1)$)

In this policy, each BS serves users until it depletes all its energy after which it toggles to OFF state. It toggles back to ON state after it has harvested one unit of energy. Using (6.39) and (6.40), the mean ON time $\mathbb{E}[J_{k1}]$ for this policy can be expressed as

$$\mathbb{E}[J_{k_1}] = \frac{1}{\nu_k} \frac{1 - \left(\frac{\mu_k}{\nu_k}\right)^{N_k}}{1 - \left(\frac{\mu_k}{\nu_k}\right)}, \tag{6.41}$$

which when substituted into (6.37) leads to

$$\rho_k = 1 - \frac{1 - \frac{\mu_k}{\nu_k}}{1 - \left(\frac{\mu_k}{\nu_k}\right)^{N_k+1}}, \tag{6.42}$$

which is the same fixed point equation as (6.14). This establishes an equivalence between this policy and the one studied in the previous subsection. In particular, this policy is an achievable strategy to achieve the same availabilities as the ones possible with the strategy studied in the previous subsection.

6.4.3.2 Policy 2 ($\mathcal{S}_k(N_k)$)

As in the above policy, each BS serves users until it depletes all its energy after which it toggles to OFF state. Under this policy, the BS waits in the OFF state until it harvests N_k units of energy, i.e., its energy storage

module is completely charged. Using (6.39) and (6.40), $\mathbb{E}[J_{k_1}]$ can be expressed as

$$\mathbb{E}[J_{k_1}] = \frac{1}{\mu_k - \nu_k} \frac{\mu_k}{\nu_k} \frac{1 - \left(\frac{\mu_k}{\nu_k}\right)^{N_k}}{1 - \left(\frac{\mu_k}{\nu_k}\right)} - \frac{N_k}{\mu_k - \nu_k}, \tag{6.43}$$

which can be substituted in (6.37) to derive the fixed point equation for this policy.

While policy 1 will be of fundamental importance in establishing the availability region, we will also consider policy 2 at several places to highlight key points. We now prove the following theorem, which establishes a fundamental upper limit on the availabilities of various types of BSs that cannot be surpassed by any uncoordinated strategy. Please note that although we have discussed only "energy-based" uncoordinated strategies so far, the general set of uncoordinated strategies also additionally includes timer-based, and the combination of energy and timer-based strategies. This is taken into account in the proof of the following theorem.

Theorem 12. *For a given K tier network, the availabilities of all the classes of BSs are jointly maximized over the space of general uncoordinated strategies if each tier follows strategy $\mathcal{S}_k(1)$. The availabilities are strictly lower if any one or more tiers follow $\mathcal{S}_k(i)$, $i > 1$, with a non-zero probability.*

Proof. From (6.37), note that the availability for a k^{th} tier BS is maximized if $\mathbb{E}[J_{k_1}(N_{kc})]/N_{kc}$ is maximized. Using (6.39) and (6.40), it is straightforward

to show that

$$\arg \max_{1 \leq i \leq N_k} \frac{\mathbb{E}[J_{k_1}(i)]}{i} = 1. \tag{6.44}$$

The proof now follows from the fact that if any tier follows strategy $\mathcal{S}_k(i)$ ($i > 1$) with a non-zero probability, its availability will be strictly lower than that of $\mathcal{S}_k(1)$, which increases the effective load on other tiers and hence decreases their availabilities, as discussed in Remark 18. Therefore, to jointly maximize the availabilities of all the tiers, each tier has to follow $\mathcal{S}_k(1)$.

Now note that any strategy that is fully or partly based on a timer can be thought of as an arbitrary combination of $\mathcal{S}_k(i)$, where $i > 1$ with some non-zero probability. Hence the availabilities for such strategies are strictly lower than $\mathcal{S}_k(1)$. □

Using this result we now characterize the availability region for the set of general uncoordinated strategies.

6.4.4 Availability Region

We begin this subsection by formally defining the availability region as follows.

Definition 6 (Availability region)**.** *Let $\mathfrak{R}^{(\mathrm{UC})} \subset \mathbb{R}^K$ be the set of availabilities $(\rho_1, \rho_2, \ldots, \rho_K) \in \mathbb{R}^K$ that are achievable by a given uncoordinated strategy $\mathcal{S}^{(\mathrm{UC})}$. The availability region is now defined as*

$$\mathfrak{R} = \cup_{\mathcal{S}^{(\mathrm{UC})}} \mathfrak{R}^{(\mathrm{UC})}, \tag{6.45}$$

where the union is over all possible uncoordinated strategies.

From Theorem 12 we know that the availabilities of all the tiers are jointly maximized if they all follow strategy $\mathcal{S}_k(1)$. For notational ease, we define these maximum availabilities by $\rho^{\max} = (\rho_1^{\max}, \rho_2^{\max} \dots \rho_K^{\max})$. This provides a trivial upper bound on the availability region as follows

$$\mathfrak{R} \subseteq \{\rho \in \mathbb{R}^K : \rho_k \leq \rho_k^{\max}, \forall\ k \in \mathcal{K}\}, \tag{6.46}$$

which is simply an orthotope in $\mathbb{R}^K$. Our goal now is to characterize the exact availability region as a function of key system parameters. As a by product, we will show that the upper bound given by (6.46) is rather loose. For cleaner exposition, we will refer to Figure 6.4, which depicts the exact availability region for a two-tier setup along with the bound given by (6.46). Before stating the main result, denote by $\rho_k^*(\{\rho_j\} \setminus \rho_k)$ the maximum availability achievable for the k^{th} tier BSs, given the availabilities of the other $K-1$ tiers. It is clearly a function of $(\rho_1, \dots \rho_{k-1}, \rho_{k+1}, \dots, \rho_K)$. Following the notation introduced in (6.15), $\rho_k^*(\{\rho_j\} \setminus \rho_k)$ (denoted by ρ_k^* for notational simplicity) can be expressed as

$$\rho_k^* = g_k(\rho_1, \dots \rho_k^*, \dots, \rho_K), \tag{6.47}$$

where ρ_k^* is the solution to the fixed point equation given the availabilities of the other $K-1$ tiers. Recall that while defining ρ_k^* in terms of g_k, we used Theorem 12, where we proved that strategy $\mathcal{S}_k(1)$ maximizes availability for any given tier and also leads to the same set of fixed point equations as given

by (6.15). In Figure 6.4, the solid line denotes $\rho_2^*(\rho_1)$, and the dotted line denotes $\rho_1^*(\rho_2)$. We remark on the achievability of the availabilities corresponding to these lines for $\rho_k \leq \rho_k^{\max}$, $\forall k \in \mathcal{K}$ below.

Remark 19 (Achievability of $\rho_1^*(\rho_2)$ and $\rho_1^*(\rho_2)$)**.** *To show that for $\rho_1 \leq \rho_1^{\max}$, all the points on $\rho_2^*(\rho_1)$ are achievable, consider point $G = (\rho_1^G, \rho_2^G)$ in Figure 6.4. Given ρ_2^G, the maximum possible availability for first tier corresponds to point H on $\rho_1^*(\rho_2^G)$, which further corresponds to strategy $\mathcal{S}(1)$. Clearly $\rho_1^G \leq \rho_1^*(\rho_2^G)$, and hence achievable by some uncoordinated strategy. One option is to time share between $\mathcal{S}(1)$ and a fixed timer that keeps a BS OFF despite having energy to serve users. The timer can be appropriately adjusted such that the effective availability is ρ_1^G. Likewise, all the points on $\rho_1^*(\rho_2)$ are also achievable. Clearly, this construction easily extends to general K tiers.*

Using these insights, we now derive the exact availability region for the set of uncoordinated strategies in the following theorem.

Theorem 13 (Availability region)**.** *The availability region for the set of general uncoordinated strategies is*

$$\mathfrak{R} = \{\rho \in \mathbb{R}^K : \rho_k \leq \rho_k^*(\{\rho_j\} \setminus \rho_k), \forall\ k \in \mathcal{K}\}. \tag{6.48}$$

Proof. To show that $\mathfrak{R}$ defined by (6.48) is in fact the availability region, it is enough to show that $\rho \in \mathfrak{R}$ is achievable and $\rho \notin \mathfrak{R}$ is not achievable. For ease of exposition, we refer to Figure 6.4 and prove for $K = 2$, with the understanding that all the arguments trivially extend to general K. To show that $\rho \in \mathfrak{R}$

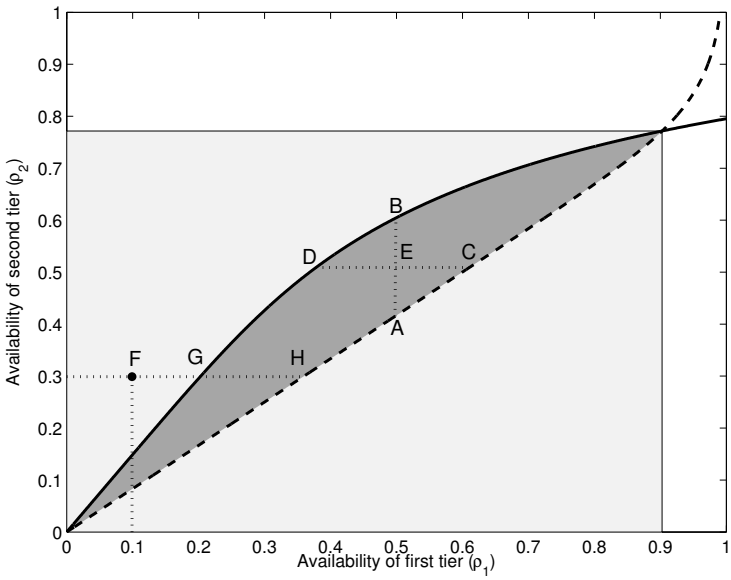

Figure 6.4: Availability region for a two-tier HetNet. The upper bound and the exact availability regions are respectively highlighted in light and dark shades. Setup: $\alpha = 4, K = 2, N_1 = 10, N_2 = 8, \gamma = 1.1, \mu_1 = 2, \mu_2 = 1, \lambda_2 = 10\lambda_1$, $m_1 = m_2$, $\sigma_1 = \sigma_2$.

is achievable, consider point E in Figure 6.4. This point is achievable by time sharing between strategies that achieve availabilities corresponding either to points A and B or C and D, which are all achievable as argued in Remark 19. This clearly shows that there are numerous different ways with which $\rho \in \mathfrak{R}$ is achievable. To show that the point $\rho \notin \mathfrak{R}$ is not achievable, consider point $F = (\rho_1^F, \rho_2^F)$ in Figure 6.4. Note that given ρ_1^F, the maximum availability possible for second tier is constrained by the corresponding value $\rho_2^*(\rho_1^F)$ on the solid curve. Since $\rho_2^F > \rho_2^*(\rho_1^F)$, it contradicts the fact that $\rho_2^*(\rho_1^F)$ is the maximum possible availability for second tier given ρ_1^F. Hence point F is not achievable. □

Remark 20 (Effect of constraining the set of strategies on $\mathfrak{R}$)**.** *Recall that* ρ_k^* *given by* (6.47) *and used in defining the availability region* $\mathfrak{R}$ *corresponds to fixed point solution for strategy* $\mathcal{S}(1)$*. In principle, it is possible to restrict one of tiers to follow a particular strategy by defining* ρ_k^* *as the fixed point solution for that strategy. For instance, we could define* ρ_k^* *as a solution to the fixed point equation corresponding to strategy* $\mathcal{S}_k(N_k)$*. Clearly, all the points* $\rho \in \mathfrak{R}$ *will not be achievable in this setup. For a two tier setup, we plot the availability region for this case in Figure 6.5, along with the availability region* $\mathfrak{R}$ *defined by Theorem 13. Note that as expected the set of points achievable under this constrained setup is strictly contained in the availability region defined by Theorem 13.*

We conclude this subsection with two remarks about the "optimality" of the availability region.

Remark 21 (Higher availability is not always better)**.** *It is not always optimal in terms of certain performance metrics to operate the network in the regime corresponding to the maximum availabilities. We will validate this in Section 6.5 in terms of the downlink rate. Interestingly, a similar idea, although applicable at a much smaller time scale, of intentionally making a macrocell "unavailable" on certain sub-frames can be used to improve downlink data rate by offloading more users to the small cells. This concept is called almost blank sub-frames (ABS) and was introduced as a part of enhanced inter-cell interference coordination (eICIC) in 3GPP LTE release 10 [137]. While this is*

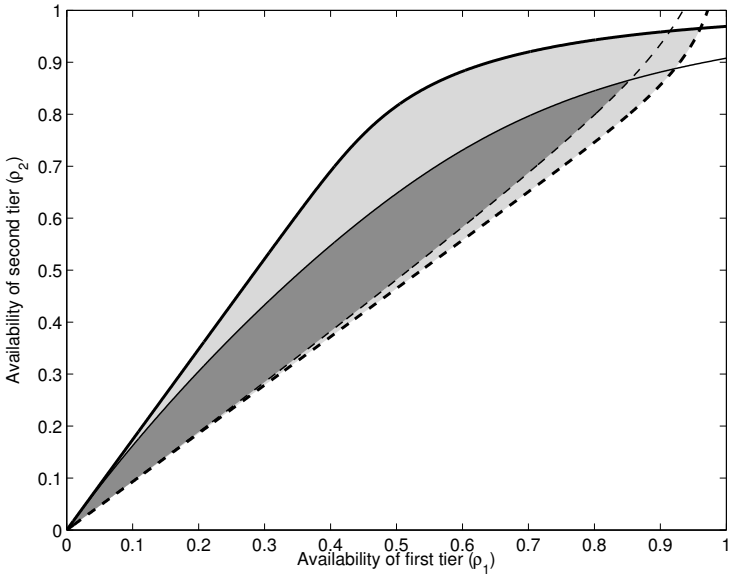

Figure 6.5: Availability region for a two-tier HetNet is denoted by lightly shaded region. The availability region when one of the tiers is constrained to use $\mathcal{S}_k(N_k)$ is denoted by the dark shade. Setup: $\alpha = 4, K = 2, N_1 = 20, N_2 = 15, \gamma = 1.1, \mu_1 = 15, \mu_2 = 5, \lambda_2 = 10\lambda_1$, $m_1 = m_2$, $\sigma_1 = \sigma_2$.

an interesting analogy, the two concepts are not exactly the same because in addition to the differences in the time scales, ABS additionally assumes coordination across BSs.

Remark 22 (Notion of optimality)**.** *The performance of a HetNet with energy harvesting is the same as the one with a reliable energy source if for the given performance metric, the optimal availabilities $\hat{\rho}$ lie in the availability region, i.e., $\hat{\rho} \in \mathfrak{R}$. For example, if $\hat{\rho}$ corresponds to point E in Figure 6.4, the HetNet despite having unreliable energy source will achieve "optimal" performance. On the other hand, if $\hat{\rho}$ is, say, point F in Figure 6.4, there will be some performance loss due to unreliability in energy availability.*

We now study the coverage probability and downlink rate in the following subsection, which will be useful in the next section to demonstrate the above ideas about optimality.

6.4.5 Coverage Probability and Downlink Rate

We now study the effect of BS availabilities $\{\rho_k\}$ on the downlink performance at small time scale. As described in Section 6.3, the availabilities change on a much longer time scale and hence the operational states of the BSs can be considered static over small time scale. Therefore, for this discussion it is enough to consider the set of available BSs $\Phi^{(\mathrm{a})}$. For downlink analysis, we focus on a typical user assumed to be located at the origin, which is made possible by Skivnyak's theorem [69]. Assuming full-buffer model for inter-cell interference [5], i.e., all the interfering BSs in $\Phi^{(\mathrm{a})}$ are always active, the $\mathtt{SIR}$ at a typical user when it connects to a BS located at $x \in \Phi_k^{(\mathrm{a})}$ is

$$\mathtt{SIR}(x) = \frac{P_k h_{kx}^{(0)} \mathcal{X}_{kx}^{(0)} \|x\|^{-\alpha}}{\sum_{j \in \mathcal{K}} \sum_{z \in \Phi_j^{(\mathrm{a})} \setminus \{x\}} P_j h_{jz}^{(0)} \mathcal{X}_{jz}^{(0)} \|z\|^{-\alpha}}. \tag{6.49}$$

Using tools developed in Chapter 5, Theorem 1 of [49] can be easily extended to derive the coverage probability under the general cell selection model of this chapter, which additionally incorporates the effect of shadowing. Since the extension is straightforward, the proof is skipped.

Theorem 14 (Coverage)**.** *The coverage probability is*

$$\mathtt{P_c} = \mathbb{P}(\mathtt{SIR}(x^{*(0)}) > \beta) = \frac{1}{1 + \mathcal{F}(\beta, \alpha)}, \tag{6.50}$$

where

$$\mathcal{F}(\beta,\alpha)=\left(\frac{2\beta}{\alpha-2}\right){}_2F_1\left[1,1-\frac{2}{\alpha},2-\frac{2}{\alpha},-\beta\right], \tag{6.51}$$

and ${}_2F_1[a,b,c,z]=\frac{\Gamma(c)}{\Gamma(b)\Gamma(c-b)}\int_0^1\frac{t^{b-1}(1-t)^{c-b-1}}{(1-tz)^a}\mathrm{d}t$ *denotes Gauss hypergeometric function.*

Clearly, the coverage probability for interference-limited HetNets is independent of the densities of the available BSs, and hence of the availabilities $\{\rho_k\}$. This validates Remark 14. However, it is not necessarily so in the case of downlink rate distribution, which we discuss next. Assuming equal resource allocation across all the users served by a BS, the complimentary cumulative distribution function (CCDF) of rate $\mathcal{R}$ (in bps/Hz) achieved by a typical user, termed *rate coverage* $\mathtt{R_c}$, is calculated in Theorem 9 of Chapter 5 for the same cell selection model as this chapter. Assuming the typical user connects to a k^{th} tier BS, $\mathcal{R}$ can be expressed as $\mathcal{R}=\frac{1}{\Psi_k}\log(1+\mathtt{SIR}(x^{*(0)})$, where Ψ_k is the number of users served by the k^{th} tier BS to which the typical user is connected. The approach of Chapter 5 includes approximating the distribution of Ψ_k and assuming it to be independent of $\mathtt{SIR}(x^{*(0)})$ to derive an accurate approximation of $\mathcal{R}$. With two minor modifications, i.e., the density of k^{th} tier active BSs is $\rho_k\lambda_k$, and the effective density of active users is $\mathtt{P_c}\lambda_u$, Theorem 9 of Chapter 5 can be easily extended to the current setup. The generalized result is given in the following theorem. For proof and other related details, please refer to Chapter 5. This result will be useful in demonstrating the

fact that the optimal downlink performance may not always correspond to the regime of maximum availabilities.

Theorem 15 (Rate CCDF)**.** *The CCDF of downlink rate* $\mathcal{R}$ *(in bps/Hz) or rate coverage* $\mathtt{R_c}$ *is*

$$\mathbb{P}(\mathcal{R} > \mathcal{T}) = \sum_{n\geq 0} \frac{1}{1+\mathcal{F}\left(\beta_{n+1},\alpha\right)} \sum_{k=1}^{K} \frac{\rho_k \lambda_k \mathbb{E}\left[\mathcal{X}_k^{\frac{2}{\alpha}}\right] P_k^{\frac{2}{\alpha}}}{\sum\limits_{j\in\mathcal{K}} \rho_j \lambda_j \mathbb{E}\left[\mathcal{X}_j^{\frac{2}{\alpha}}\right] P_j^{\frac{2}{\alpha}}}$$
$$\times \frac{3.5^{3.5}}{n!} \frac{\Gamma(n+4.5)}{\Gamma(3.5)} \left(\frac{\mathtt{P_c}\lambda_u \mathcal{P}_k}{\rho_k \lambda_k}\right)^n \left(3.5 + \frac{\mathtt{P_c}\lambda_u \mathcal{P}_k}{\rho_k \lambda_k}\right)^{-(n+4.5)}$$

where $\beta_{n+1} = 2^{\mathcal{T}(n+1)} - 1$ *and*

$$\mathcal{P}_k = \frac{\rho_k \lambda_k \mathbb{E}\left[\mathcal{X}_k^{\frac{2}{\alpha}}\right] P_k^{\frac{2}{\alpha}}}{\sum_{j\in\mathcal{K}} \rho_j \lambda_j \mathbb{E}\left[\mathcal{X}_j^{\frac{2}{\alpha}}\right] P_j^{\frac{2}{\alpha}}}. \tag{6.52}$$

Remark 23 (Invariance to shadowing distribution)**.** *From Theorem 15, we note that the rate coverage is invariant to the shadowing distribution when* $\mathbb{E}\left[\mathcal{X}_j^{\frac{2}{\alpha}}\right] = \mathbb{E}\left[\mathcal{X}_k^{\frac{2}{\alpha}}\right]$*, for all* $j,k \in \mathcal{K}$*. This is similar to the observations made in Remark 15.*

6.5 Numerical Results and Discussion

Since most of the analytical results discussed in this chapter are self-explanatory, we will focus only on the most important trends and insights in this section. For conciseness, we assume lognormal shadowing for each tier with the same mean m dB and standard deviation σ dB. Recall that both the energy utilization and the rate distribution results are invariant to shadowing

under this assumption, as discussed in Remarks 15 and 23. We begin by discussing the effect of battery capacity on the availability region.

6.5.1 Effect of Battery Capacity on Availability Region

We consider a two tier HetNet and plot its availability region for various values of the capacity of the energy storage module, i.e., battery capacity, in the first subplot of Fig 6.6. For ease of exposition, we assume that the storage capacities of the BSs of the two tiers are the same. As expected, the availability region $\mathfrak{R}$ increases with the increase in battery capacity. Interestingly, it is however not possible to achieve all the points ρ in the square $[0,1] \times [0,1]$ even by increasing the battery capacity infinitely. The maximum availability region is a function of over-provisioning factor γ, which is set to 1.1 for this result. Additionally, we note that the maximum availabilities for both the tiers approach unity even at modest battery levels. We repeat the same experiment for the case when one of the tiers is constrained to use the strategy $\mathcal{S}_k(N)$ and present the results in the second subplot of Figure 6.6. Recall that this case was discussed in Remark 20. We observe that for the same battery capacity N, the achievable region is smaller in this case compared to Figure 6.6, which is consistent with the observations made in Section 6.4. The difference is especially prominent for smaller values of battery capacity N.

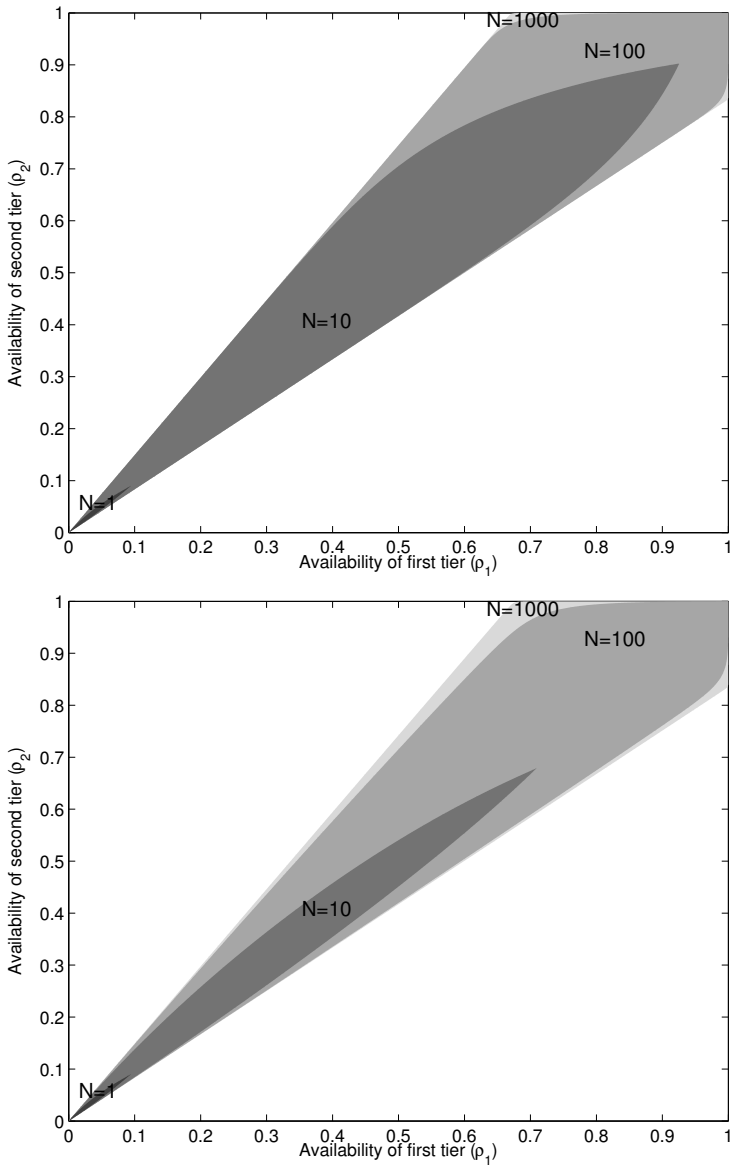

Figure 6.6: *(first)* Availabilities region for various values of energy storage capacity N, where $N_1 = N_2 = N$. *(second)* One of the tiers constrained to use strategy $\mathcal{S}_k(N)$. Setup: $\alpha = 4, K = 2, \gamma = 1.1, P = [1, 0.1], \mu_1 = 10, \mu_2 = 3, \lambda_2 = 10\lambda_1$.

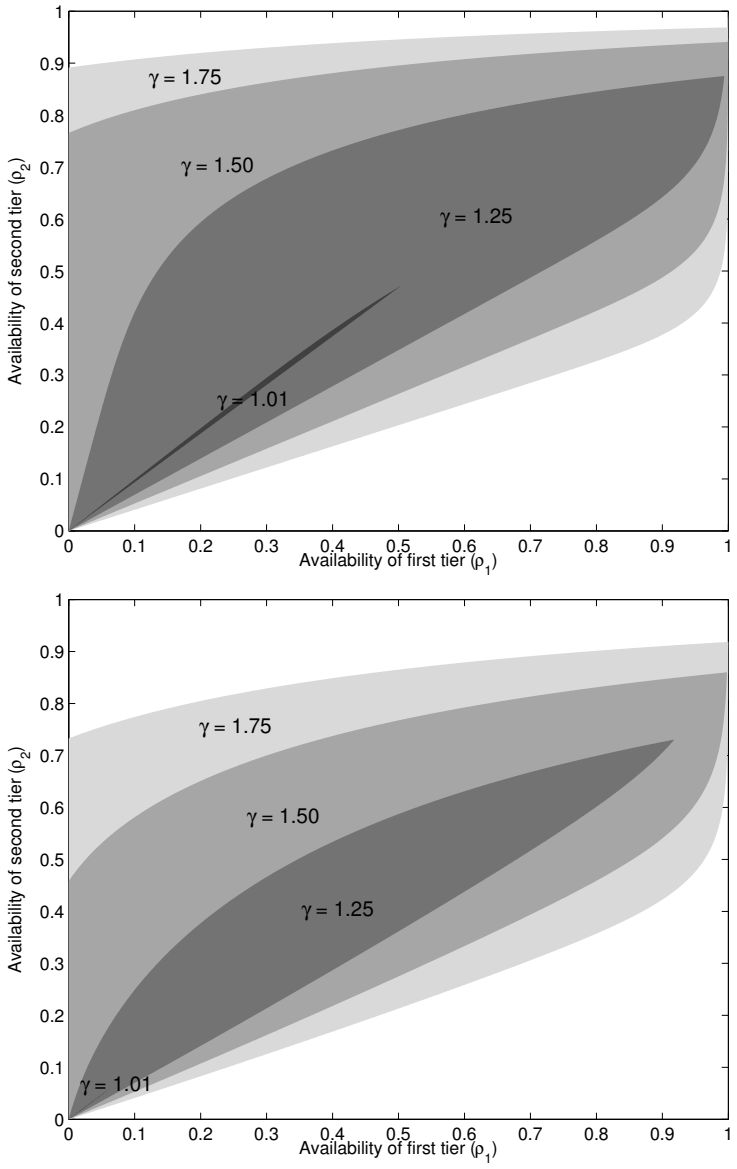

Figure 6.7: *(first)* Availabilities region for various values of γ. *(second)* One of the tiers is constrained to use strategy $\mathcal{S}_k(N)$. Setup: $\alpha = 4, K = 2, N_1 = 20, N_2 = 5, \mu_1 = 10, \mu_2 = 3, \lambda_2 = 10\lambda_1$.

6.5.2 Effect of Over-Provisioning Factor on Availability Region

We now study the effect of the over-provisioning factor on the availability region in the first subplot of Figure 6.7. Recall that the over-provisioning factor γ is the ratio of the net energy harvested per unit area per unit time and the net energy utilized per unit area per unit time. The first and foremost observation is that unlike increasing battery capacity, the availability region expands by increasing γ and will cover the complete square $[0,1] \times [0,1]$ for sufficiently large γ. Also note that the beyond a certain value of γ, the availability of a tier may be non-zero even if the availabilities of the other tiers are zero. This is the case when that tier harvests enough energy on its own to serve all the load offered to the network, i.e., $\lambda_k \mu_k > \mathtt{P_c} \lambda_u$. As in the previous subsection, we now repeat this experiment under the constraint that one of the tiers follows strategy $\mathcal{S}_k(N_k)$ and present the results in the second subplot of Figure 6.7. As expected, the availability region is considerably smaller in this case.

6.5.3 Rate coverage

Using rate coverage, given by Theorem 15, we demonstrate that it may not always be optimal to operate the network in the regime corresponding to maximum availabilities. We plot rate coverage as a function of (ρ_1, ρ_2) for two different setups in Figure 6.8. In both the cases, we note that it is strictly suboptimal to operate at the point $(\rho_1, \rho_2) = (1, 1)$. Furthermore, as the second tier density is increased, it is optimal to keep first tier BSs OFF

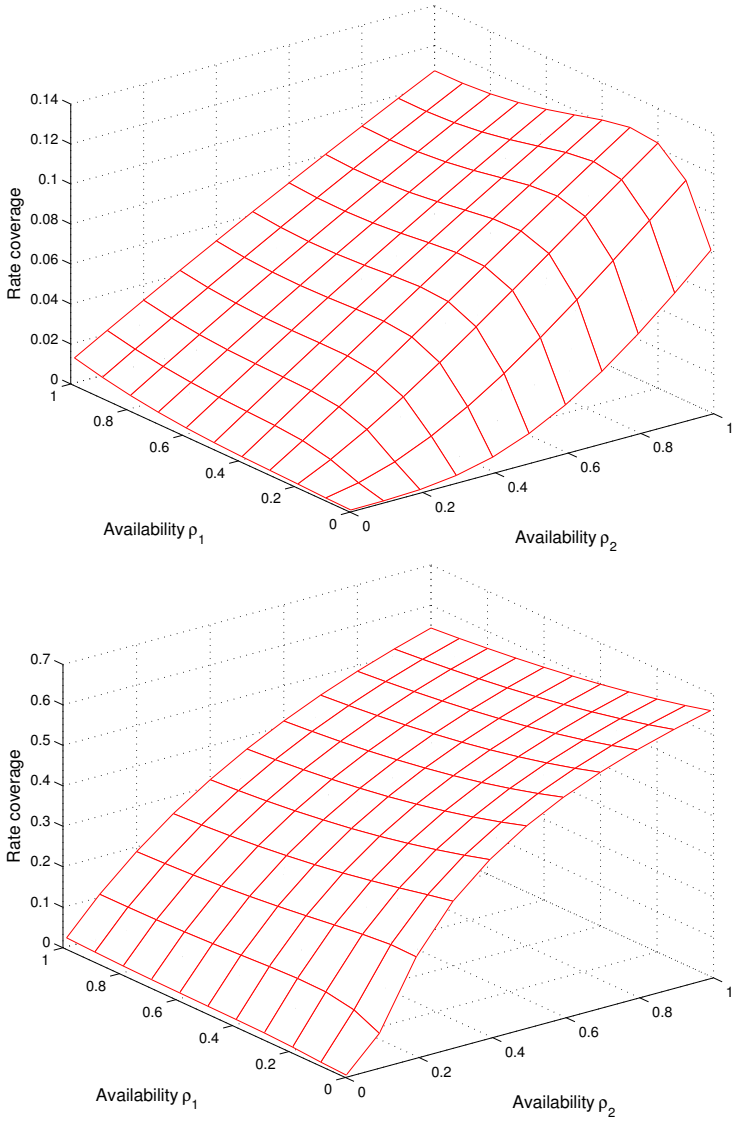

Figure 6.8: Rate coverage as a function of ρ_1 and ρ_2. Setup: $\alpha = 4, K = 2, P = [1, 0.01], \mathcal{T} = 0.1, \lambda_u = 100\lambda_1$. *(first)* $\lambda_2 = 2\lambda_1$, *(second)* $\lambda_2 = 20\lambda_1$. Note that $\rho = [1\ 1]$ is not optimal in both the cases.

more often. As expected, the rate coverage also increases with the increase of second tier density. This example additionally motivates the need for the exact characterization of $\hat{\rho}$ for various metrics of interest, which forms a concrete line of future work. Once the optimal $\hat{\rho}$ for a given metric is known, the system designers can, in principle, design the energy harvesting modules such that $\hat{\rho} \in \mathfrak{R}$. In such a case, the HetNet with energy harvesting will have the same performance as the HetNet with reliable energy sources.

6.6 Summary

In this chapter, we have developed a comprehensive framework to study self-powered HetNets, where each BS is powered solely by its energy harvesting module. Developing novel tools with foundations in random walk theory, fixed point analysis and stochastic geometry, we quantified the uncertainty in BS availability due to the finite battery capacity and inherent randomness in energy harvesting. We further characterized the availability region for a set of general uncoordinated BS operational strategies. This characterizes the regimes under which the self-powered HetNets have the same performance as the ones with reliable energy sources.

Chapter 7

Conclusion

7.1 Summary

Opportunistic capacity-driven deployment of small cells is recognized as a key solution to keep up with the increasing capacity demand from cellular networks. This has led to a paradigm shift in cellular deployments where the traditional high power tower-mounted macrocellular BSs are now joined by various low power nodes such as microcells, picocells, femtocells and distributed antennas. In addition to increasing the disparity in the BS capabilities, such as transmit power and backhaul capacity, this has also led to the increasing uncertainty in the BS locations due to the unplanned deployment of small cells. An immediate effect of the increasing heterogeneity and uncertainty on the study of cellular networks is that it has limited the applicability of classical cellular models based mainly on the regularity assumption of BS locations, such as deterministic grid-based models and Wyner model, to HetNets. In this dissertation, we proposed a new and more appealing way of modeling HetNets by using random spatial models, where the locations of the BSs are assumed to form a realization of a spatial point process. In comparison to the conventional models, this approach is especially attractive in the context of HetNets due to its: (i) realism: to capture the inherent uncertainty in deployments involving

both operator and user deployed BSs, (ii) scalability: to model ever-increasing heterogeneity in the infrastructure elements and, (iii) tractability: to gain system design insights using tools from stochastic geometry and spatial statistics. We now summarize the key contributions of this dissertation.

In Chapter 2, we proposed a baseline model for downlink HetNets consisting of K tiers of BSs, which may differ in terms of transmit power, supported data rate and deployment density. The BS locations of each tier are sampled from an independent homogeneous PPP. Using fairly general channel and cell selection models, we derived an expression for the probability of coverage (equivalently outage) over the entire network under both open and closed access, which assumes a strikingly simple closed-form when the resulting SINR is greater than 1 and the network is interference limited. We also derived simple expressions for the average rate achieved by a typical mobile and the average load on each tier of BSs. Our results demonstrate that interference-limited HetNets are scale-invariant in terms of coverage probability, i.e., adding more tiers and/or BSs neither increases nor decreases the coverage probability when all the tiers have the same target SINR.

In Chapter 3, we incorporated a flexible and accurate notion of BS load by introducing a new idea of conditionally thinning the interference field, conditional on the connection of a typical mobile to its serving BS. The resulting framework is capable of capturing different levels of load on different tiers, arising mainly from the differences in the coverage footprints. Assuming a mobile user connects to the strongest BS, we derived exact expression for

the fractional moment for interference, which was then used to derive a simple expression for downlink coverage probability. This analysis leads to following key insights: (i) fully loaded models are extremely pessimistic in terms of coverage, and (ii) adding lightly loaded small cells to the macrocellular network always increases coverage probability. In Apendix B, the same idea of conditional thinning was used to study non-uniform user distributions, especially when the users are more likely to lie closer to the BSs.

In Chapter 4, we generalized the baseline model of Chapter 2 to study multi-antenna HetNets, where BSs across tiers may additionally differ in terms of the number of transmit antennas, transmission strategy, and number of users served. Using novel tools from stochastic orders, we developed a new framework to compare different transmission techniques, such as SDMA, SU-BF and baseline SISO transmission, in terms of the downlink coverage and rate per user for any given distribution of BS locations. A direct consequence of this analysis is that for a given total number of transmit antennas, it is preferable to spread them across many single-antenna BSs vs. fewer multi-antenna BSs. While this approach is quite conclusive for coverage and rate per user, it does not account for the fact that certain transmission techniques, such as SDMA, serve more users and may provide higher sum-rate. To incorporate this fact in our analysis, we derived an upper bound on the coverage probability assuming an independent PPP model for BS locations and used it to compare different transmission techniques in terms of area spectral efficiency.

Recall that the baseline HetNet model of Chapter 2 and its extensions

in Chapters 3 and 4 do not differentiate between the long-term shadowing and small-scale fading effects. The channel randomness was captured using a single random variable and cell selection was based on the maximum instantaneous received signal strength. In Chapter 5, we addressed this shortcoming of the baseline HetNet model and derived the distribution of the downlink rate achievable at a typical user under a generalized cell-selection model, where shadowing, following any general distribution, affects cell selection while fading does not. This generalization is a simple application of displacement theorem for PPPs. We proposed an equivalent interpretation of this general cell selection model and showed that the effect of shadowing can be equivalently studied by appropriately scaling transmit powers. Using this equivalent interpretation, we studied the effect of shadowing on load balancing, and showed that in certain regimes shadowing naturally balances load across various tiers and hence reduces the need for artificial cell selection bias.

Unlike all the previous chapters, Chapter 6 deals with a slightly futuristic HetNet scenario where each BS is powered solely by its own energy harvesting module. This possibility is becoming realistic due to the increasing popularity of low power nodes, which are more likely to be powered solely by the energy harvesting modules, such as solar panels, compared to the high-power macrocells of yesterday. We extend the K-tier baseline HetNet model to additionally include differences across tiers in terms of the energy harvesting rate and energy storage capacity. Developing novel tools with foundations in random walk theory, fixed point analysis and stochastic geometry, we quanti-

fied the uncertainty in BS availability due to the finite battery capacity and inherent randomness in energy harvesting. We further characterized the availability region for a set of general uncoordinated BS operational strategies. This characterizes the regimes under which the self-powered HetNets have the same performance as the ones with reliable energy sources.

7.2 Future Directions

The models proposed in this paper have already been generalized in various forms and have found numerous applications in diverse HetNet scenarios. Please refer to [87] for a detailed survey. Here we propose two important extensions, which are relatively less investigated in the literature. First is to model the inter point interactions between the locations of various types of BSs and develop more realistic spatial models using tools from spatial statistics. Second is to develop a techno-economic model to explore possible interdependencies between network deployment cost and the HetNet performance. We now briefly discuss these future research directions below.

7.2.1 More Realistic Spatial Models for BS locations

With the exception of Chapter 4 where the spatial model was irrelevant, this dissertation assumes that each BS is deployed independently of the rest of the network. While this assumption can be justified for small cells, especially for user deployed femtocells, it is questionable for other tiers such as macrocells, where the BS locations are clearly dependent. In order to model the

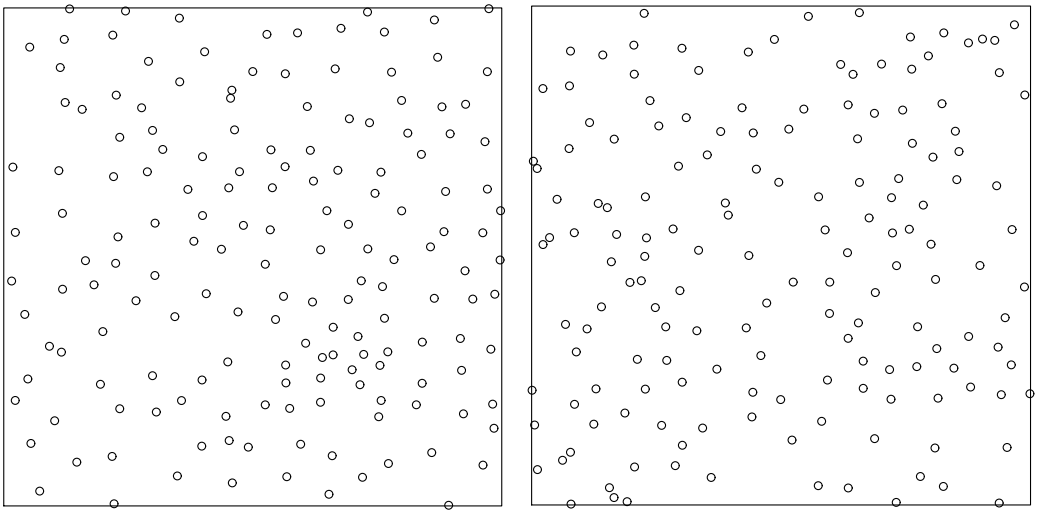

Figure 7.1: (left) Point pattern $\mathbf{x}$. (right) Realization of a *Strauss Hardcore process* fitted to $\mathbf{x}$.

performance of HetNets accurately, it is important to first characterize these inter point interactions. One possible option is to use *Gibbs models* [138], which we briefly discuss here. To fix the key ideas, we consider two point pattens $\mathbf{x}$ and $\mathbf{y}$ (shown in Figs. 7.1 and 7.2) which are subsets of the macrocellular deployments of two of the U.S.' 10 largest metropolitan areas. Point pattern $\mathbf{x}$ is from a sprawling, landlocked city, while $\mathbf{y}$ is from a coastal city.

To describe Gibbs models, we consider a point pattern $\mathbf{z}$ confined in a bounded window $\mathcal{W}$, where $\mathbf{z} = \{z_1, z_2, \ldots, z_{n(\mathbf{z})}\}$ and $n(\mathbf{z}) = |\mathbf{z}|$. Although *Gibbs models* can be used to model general inter point interaction, we focus our attention on a simple "pairwise interaction model", which is shown to be sufficient to model both $\mathbf{x}$ and $\mathbf{y}$ in [82]. For this model, the probability

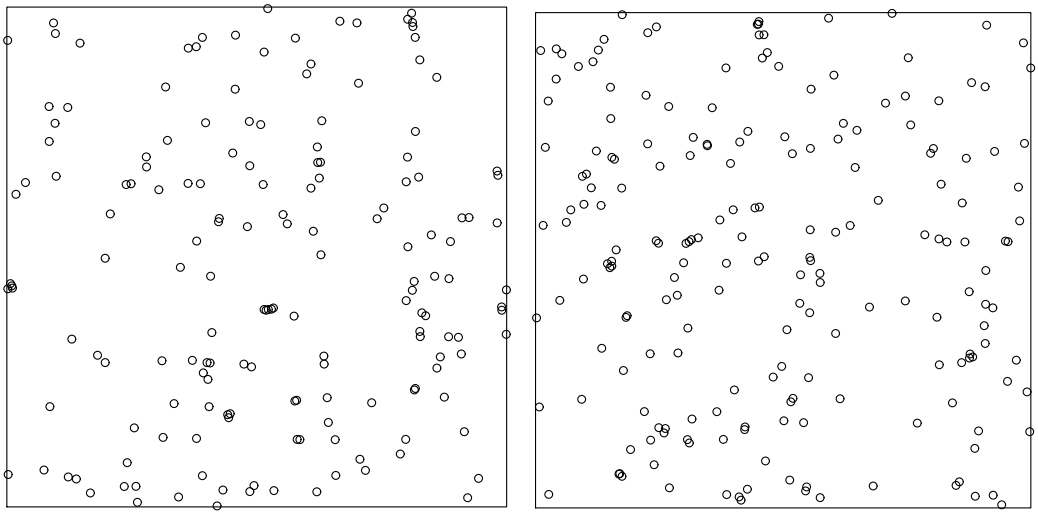

Figure 7.2: (left) Point pattern $\mathbf{y}$. (right) Realization of a *Geyer Saturation Process* fitted to $\mathbf{y}$.

density $f(\mathbf{z})$ can be expressed in the product form as follows:

$$f(\mathbf{z}) = \alpha \left[\prod_{i=1}^{n(\mathbf{z})} \phi(z_i) \right] \left[\prod_{i<j} \psi(z_i, z_j) \right], \tag{7.1}$$

where α is the normalizing factor to ensure the probability density integrates to unity, $\phi(z)$ is the function modeling the "first order trends" and $\psi(z_i, z_j)$ are the functions modeling the pairwise interaction. Two important special cases are: the *Strauss process* [139], which is useful in modeling inhibition, and its generalization the *Geyer saturation process* [140], which models both inhibition and clustering. The *Strauss process* is defined by taking $\phi(z_i) = \beta$ and defining $\psi(z_i, z_j)$ as

$$\psi(z_i, z_j) = \begin{cases} 1, & \|z_i - z_j\| > r \\ \gamma, & \|z_i - z_j\| \leq r \end{cases} . \tag{7.2}$$

The probability density function is $f(\mathbf{z}) = \alpha\beta^{n(\mathbf{z})}\gamma^{s(\mathbf{z})}$, where $s(\mathbf{z})$ is the number of distinct pairs of points less than an interaction radius r units apart. Clearly $\gamma \leq 1$ models inhibition. However, this probability density is not integrable for $\gamma > 1$ and hence cannot be used to model clustering [141]. Nevertheless, this can be overcome by including a saturation limit in the exponent of γ to obtain the following density function: $f(\mathbf{z}) = \alpha\beta^{n(\mathbf{z})}\gamma^{\min(s(\mathbf{z}),t)}$. This is termed as the *Geyer saturation process*. It reduces to a PPP for $t = 0$ and a *Strauss process* for $t \to \infty$. In [82], we have shown that the point patten $\mathbf{x}$ being inhibitive can be accurately modeled using Strauss process and $\mathbf{y}$ being clustered can be modeled using Geyer saturation process. The realizations of the fitted processes along with the original point patterns are shown in Figs. 7.1 and 7.2. Geyer saturation process was also used recently to model the spatial characteristics of an outdoor Wi-Fi deployment maintained by Google in Mountain View, CA [142].

Continuing on the similar lines, it is important to model the inter tier interaction, e.g., by using multi class Gibbs processes, and develop new metrics, such as the Voronoi cell area distribution proposed in [82] to validate the proposed models. It is also important to study the correlation of BS deployments with publicly available data, such as the population density and the road networks, to refine the models by incorporating these "covariates". The eventual goal is to identify a set of point processes that would model a variety of cities with different topologies. It would circumvent the need of knowing the actual BS locations for accurate performance analysis. Another promising

class of point processes useful for this purpose is that of *determinantal point processes*, which have an additional advantage of being tractable [143].

7.2.2 Techno-Economic Model for Cost Optimal Deployment

This dissertation and almost all its extensions so far have focused on the radio part of the HetNets and have ignored the economic factors, such as infrastructure cost, that are instrumental in driving the future deployments. A concrete future direction of work is to develop a techno-economic model that will allow us to study the interplay between the performance metrics, such as coverage probability, and the network deployment cost. While the system performance has already been modeled in this dissertation, we now propose a method to model the network deployment cost based on the prior work done in the context of wired networks [144].

To model the deployment cost, we first incorporate a notion of backbone network by including a tier of "concentrator" nodes in the K tier HetNet model. We assume these concentrator nodes form an independent PPP Φ_0 with density λ_0. For simplicity, assume that each BS is connected to its nearest concentrator node. It should be noted that in reality there would be multiple "layers" of contractor nodes that can be easily incorporated in this framework. For each BS class, we consider two components of cost required for deploying an extra BS. First component is the fixed equipment cost C_i, which models the cost of antennas, RF hardware, towers and manual labor. Second component is a function of the distance of the BS from its nearest connector point. Denoting

the distance of an i^{th} tier BS from its nearest connector point as $\|y_i\|$, we model this variable component of the cost as $a_i\|y_i\|^{b_i}$, where a_i and b_i are non-negative constants modeling the type and quality of fibers used. Using tools from Palm calculus [133], especially Neveu's exchange formula, we can derive the average cost of deploying all the BSs that are connected to a typical concentrator point as

$$\bar{X} = \sum_{i=1}^{K} \frac{\lambda_i}{\lambda_0} \left[C_i + a_i \frac{\Gamma(\frac{b_i}{2}+1)}{(\pi\lambda_0)^{b_i/2}} \right]. \tag{7.3}$$

Interestingly, this deployment cost is a linear function of the densities of various classes of BSs and together with the closed form expression of coverage probability derived in Chapter 2 provides a simple framework to pose tractable and meaningful optimization problems.

Building upon these ideas, a future direction of work is to develop a complete optimization framework to find conditions that will lead to coverage and/or cost optimal deployments given certain practical constraints on the availability of network resources, such as available spectrum.

Appendices

Appendix A

Appendix to Chapter 2: Generalization to $\beta_i \geq 0$

In Chapter 2, all the results were derived under the assumption that the SINR target $\beta_i > 1$ for all the tiers. While these results were numerically shown to be accurate down to much lower target-SINRs despite this assumption, for completeness we relax this assumption and derive expressions for both the coverage probability and the ergodic rate as a function of general β_i. Since these generalized expressions involve complex integrals, for the ease of exposition they are treated separately from the main body of the chapter.

A.1 Coverage Probability

We first provide the generalized expression for the coverage probability of a typical user which will directly lead to the ergodic rate expression in the next section.

Theorem 16. *The coverage probability of a typical mobile user is*

$$\mathtt{P_c}(\{\lambda_i\},\{\beta_i\},\{P_i\}) = \frac{2\pi\Gamma(1+\frac{2}{\alpha})}{\alpha}\sum_{m=1}^{K}\lambda_m(P_m\delta_m)^{1+\frac{2}{\alpha}}$$
$$\cdot\int_{-\infty}^{\infty}\int_{0}^{\infty}\frac{\mathcal{L}_I^y(j2\pi\omega)}{y^{1+2/\alpha}}\frac{e^{j2\pi\omega y(1-\delta_m^{-1})}-e^{j2\pi\omega y(\kappa^{-1}-\delta_m^{-1})}}{j2\pi\omega}\mathrm{d}y\mathrm{d}\omega.$$

In the above expression $\delta_i = \frac{1+\beta_i}{\beta_i}$, $\kappa = \max \delta_i$ *and*

$$\mathcal{L}_I^u(s) = e^{-\pi \sum_{m=1}^K \lambda_m (sP_m)^{\frac{2}{\alpha}} \Gamma(1+\frac{2}{\alpha})[\Gamma(1-\frac{2}{\alpha})+2/\alpha\Gamma(-\frac{2}{\alpha},\frac{su}{\delta_m})]}. \tag{A.1}$$

Proof. Since the BSs are distributed as a stationary process, we can consider a typical mobile at the origin. The coverage probability of a typical mobile user at the origin is

$$1 - \mathbb{E}\left[\prod_{i=1}^K 1 - \mathbf{1}\left(\frac{M_i}{I - M_i} > \beta_i\right)\right],$$

where

$$M_i = P_i \max_{x \in \Phi_i} \{h_x \|x\|^{-\alpha}\},$$

and I is the total aggregate interference at the origin given by

$$I = \sum_{i=1}^K \sum_{x \in \Phi_i} P_i h_x \|x\|^{-\alpha}.$$

By basic algebra, the coverage probability equals

$$\mathtt{P_c}(\{\lambda_i\}, \{\beta_i\}, \{P_i\}) = \mathbb{P}(\max_i(\delta_i M_i) > I). \tag{A.2}$$

Let

$$\mathcal{L}_I^u(s) = \mathbb{E}[e^{-sI}\mathbf{1}(\max_i(\delta_i M_i) < u)].$$

It can be reduced to (A.1) using [145, Theorem 1]. Differentiating $\mathcal{L}_I^u(s)$, we obtain

$$\frac{\partial \mathcal{L}_I^y(s)}{\partial y}\Big|_u = \frac{\mathcal{L}_I^u(s) 2\pi\Gamma(1+\frac{2}{\alpha})}{\alpha u^{1+2/\alpha}} \sum_{m=1}^K \lambda_m (P_m \delta_m)^{1+\frac{2}{\alpha}} e^{-\frac{su}{\delta_m}}.$$

Let $f(x,y)$ denote the joint probability density of I and $\max(\delta_i M_i)$. The coverage probability equals

$$\mathtt{P_c} = \int_0^\infty \int_0^\infty f(x,y)\mathbf{1}\left(y > x > \frac{y}{\max(\delta_i)}\right) \mathrm{d}x\mathrm{d}y.$$

Let $\kappa = \max(\delta_i)$. Using Parsevals theorem[1], we obtain

$$\mathtt{P_c} = \int_0^\infty \int_{-\infty}^\infty \hat{f}(\omega,y)\frac{e^{j2\pi\omega y} - e^{j2\pi\omega y/\kappa}}{j2\pi\omega}\mathrm{d}\omega\mathrm{d}y, \tag{A.3}$$

where $\hat{f}(\omega,y)$ denotes the Fourier transform of $f(x,y)$ with respect to the x variable. We also have

$$\frac{\partial \mathcal{L}_I^u(s)}{\partial u} = \int_{x=0}^\infty f(x,y)e^{-j2\pi\omega x}\mathrm{d}x = \hat{f}(\omega,y).$$

Interchanging the integrals in (A.3) and using the above equation, we obtain the result. □

A.2 Ergodic Rate

In this section, we focus on the study of the average communication rate achievable by a typical mobile user in the K-tier HCN. We assume that the capacity achieving codes are used and hence the Shannon's capacity formula, $R = \log\left(1 + \max_{x \in \cup_i \Phi_i} \mathtt{SIR}(x)\right)$ bps/Hz, is applicable. It is worth noting here that the coverage probability expression derived in Theorem 16 completely characterizes the complementary cumulative distribution function (CCDF) of

[1]This requires verifying that the integrand is integrable, which we do not provide here. The technique for verifying the integrability is common and can be found in [73].

$\max_{x \in \cup_i \Phi_i} \texttt{SIR}(x)$ and hence holds a key to the derivation of the ergodic rate. Recall that the coverage probability result derived in Chapter 2 does not completely characterize the SIR distribution and is hence not sufficient to derive the ergodic rate. Using coverage probability result derived in Theorem 16, we now derive the Ergodic rate $\mathbb{E}[R]$.

Theorem 17. *The ergodic rate achievable by a typical mobile in a K-tier HCN is given by:*

$$\mathbb{E}[R] = \int_0^\infty \mathtt{P_c}\{\{\lambda_i\}, 2^y - 1, \{P_i\}\} \mathrm{d}y. \tag{A.4}$$

$\mathtt{P_c}\{\{\lambda_i\}, 2^y - 1, \{P_i\}\}$ *is the complex integral expression for coverage probability derived in Theorem 16 by fixing $\beta_i = 2^y - 1 \ \forall \ i$.*

Proof. Let X be the random variable denoting $\max_{x \in \cup_i \Phi_i} \texttt{SIR}(x)$ and R be the random variable denoting instantaneous rate $\log(1 + X)$ in bps/Hz. Since R is a positive random variable, its expected value can be evaluated as:

$$\begin{aligned} E[R] &= \int_0^\infty \mathbb{P}[R \geq y] \mathrm{d}y = \int_0^\infty \mathbb{P}[X \geq 2^y - 1] \mathrm{d}y \\ &= \int_0^\infty \mathtt{P_c}\{\{\lambda_i\}, 2^y - 1, \{P_i\}\} \mathrm{d}y, \end{aligned} \tag{A.5}$$

which completes the proof. □

Appendix B

Appendix to Chapter 3: Modeling Non-Uniform User Distribution

In this appendix, we propose a new tractable method of sampling users by *conditionally thinning* the BS point process and show that the resulting framework can be used as a tractable generative model to study current capacity-centric deployments, where the users are more likely to lie closer to the BSs. Since the overall technical idea of conditional thinning is the same as Chapter 3, we do not include this contribution as a separate chapter in the main body of the dissertation.

B.1 Related Work and Motivation

As discussed in Chapter 2, a promising new way to model cellular networks is by using random spatial models, where the BS locations are assumed to form a realization of some spatial point process, typically the Poisson Point Process (PPP). Modeling the user locations as an independent PPP, the downlink analysis is performed at a typical user assumed to be located at the origin. Owing to its tractability, this model leads to simple closed form expressions for key metrics such as coverage and average rate over the entire network [1,5,51].

Although it provides a way to study average statistics for the uniform user distribution, it does not provide any handle on studying deployment scenarios involving non-uniform user distribution, especially when the user and BS locations are dependent. Naturally, such flexibility is desirable to study the current capacity-centric deployments where BSs are specifically deployed to be close to the areas of high user density [146]. The most popular and perhaps the only available option to handle such scenarios is through detailed system level simulations, which are both time consuming and have to be focused on a limited range of system parameters [147, 148].

B.2 Contribution

As a first step towards a tractable model with non-uniform UE distributions, we propose a slight modification in the way users are sampled by using the same idea of *conditional thinning*, which we proposed in Chapter 3 to model load on different classes of BSs. For simplicity of exposition we demonstrate the new user sampling method for a single tier cellular network, and leave the extension to HetNets as a future work. Starting with a higher density of BSs, we first assume that a typical user is located at the origin. After selecting the serving BS, we condition on this active link and independently thin the rest of the BS point process so that the resulting density matches the desired density of the actual BSs. The thinning operation pushes the typical user in the cell interior relative to the new cell edge defined by the resulting point process. The bias induced in the location of a typical user towards its

serving BS can be tuned by varying the thinning probability. We make this notion precise by deriving the distribution of the ratio of the distances of the user to its serving BS and the dominant interferer as a function of the thinning probability. We also show that this framework can be used as a tractable generative model to study non-uniform user distributions where the users are more likely to lie closer to the BS. The exact analysis of such non-uniform user distributions is in general hard due to the correlation present in the user and BS locations. The impact of the proposed model on the cellular performance analysis and its key differences from the existing model based on uniform user distribution are highlighted in terms of the coverage predictions.

It is worth noting that although this work is developed in the context of cellular networks, it applies to much wider class of point process problems involving dependence in the location of the observation point and the point process.

B.3 Proposed Method of Sampling users

We consider a homogeneous PPP Φ of density λ, a thinned version of which will eventually model the BS locations. Recall that we consider a single tier cellular network in this discussion. The downlink analysis is performed at a typical user assumed to be at the origin [69]. The received power at a typical user from the BS located at $x \in \Phi$ is

$$P_x = Ph_x\|x\|^{-\alpha}, \tag{B.1}$$

where P is the transmit power, $h_x \sim \exp(1)$ models channel power distribution under Rayleigh fading and $\|x\|^{-\alpha}$ models standard distance based path loss with $\alpha > 2$ being the path loss exponent. More general fading distributions can be studied using tools developed in [73, 131, 149] and in Chapter 5. For simplicity of exposition, we will ignore thermal noise in this discussion.

The proposed method of sampling the interior users can be understood in two simple steps shown in Fig. B.1. The first step is to identify the serving BS in Φ for a typical user depending upon the cell association technique being considered. While the proposed method is general, for brevity we consider nearest-neighbor cell association model discussed in [1], where each user connects to its nearest BS. It is also the same as maximum average power connectivity model, where each user connects to the BS that provides maximum long-term average received power. In Fig. B.1 (first), the typical user connects to its nearest BS, which is the one that corresponds to the Voronoi cell in which it lies. Denote the location of this serving BS by $x_s \in \Phi$. The second step is to independently thin the point process $\Phi \setminus x_s$ where each point is independently retained with probability p as shown in Fig. B.1 (second). Since the thinning is conditional on the serving BS, we call it *conditional thinning*. The thinned process Φ_b models the BS locations. Due to conditional thinning, the point process Φ_b is no longer a PPP. After tessellating the space based on Φ_b and keeping the position of the user fixed, we note that the user is pushed towards the cell interior compared to the new cell edge as shown in Fig. B.1 (third). As discussed in the next section, a typical user can be pushed arbitrarily close

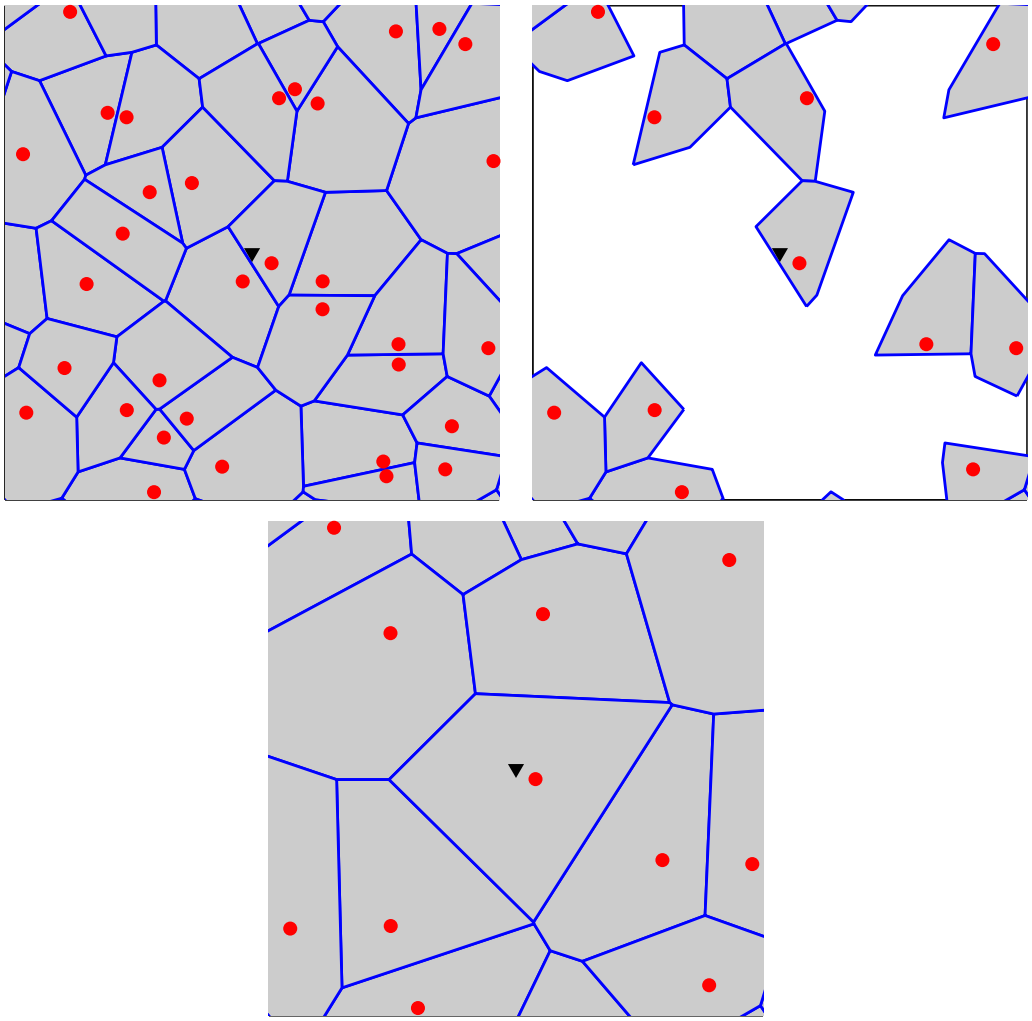

Figure B.1: *(first)* The Voronoi tessellation of the point process Φ. Dark triangle denotes a typical user. *(second)* The point process thinned by $p = .3$. The remaining points form BS point process Φ_b. *(third)* The Voronoi tessellation of Φ_b. Observe that the typical point is now in the cell interior.

to its serving BS by choosing an arbitrarily small value of p but remains edge biased for high values of p.

B.4 Impact on Cellular Networks

After providing an overview of the new user sampling model, we now formalize the effect of conditional thinning perceived by a typical user. Denoting R_1 and R_2 to be the distances of the closest and the next closest point of Φ_b to the origin, we define our first metric to be $R = R_2/R_1$. It corresponds to the ratio of the distances of a typical user to its serving BS and the dominant interferer, and provides some insights into the expected performance of a typical user. For instance, if the value of R is close to 1, it means that the user is near the cell edge, i.e., the dominant interferer is approximately at the same distance as the serving BS and hence the received signal-to-interference-ratio (`SIR`) is expected to be low. It is important to note that $R \geq 1$ by construction, since the serving BS is always the closest one in our cell association model. We now derive the distribution of R after deriving the joint distribution of R_1 and R_2 as a function of thinning probability p in the following Lemma. Interested readers can refer to [150] for the marginal distribution of R_n.

Lemma 20. *The cumulative distribution function (CDF) of R is*

$$F_R(r) = 1 - \frac{1}{1 + p(r^2 - 1)}, \ r \geq 1. \tag{B.2}$$

Proof. For notational simplicity, we first define the following disjoint sets:

$$\mathcal{E}_1 = \{x \in \mathbb{R}^2 : \|x\| \leq r_1\}$$

$$\mathcal{E}_2 = \{x \in \mathbb{R}^2 : r_1 < \|x\| \leq r_1 + \mathrm{d}r_1\}$$
$$\mathcal{E}_3 = \{x \in \mathbb{R}^2 : r_1 + \mathrm{d}r_1 < \|x\| \leq r_2\}$$
$$\mathcal{E}_4 = \{x \in \mathbb{R}^2 : r_2 < \|x\| \leq r_2 + \mathrm{d}r_2\},$$

where $\mathcal{E}_1$ denotes a circle centered at origin and the rest denote annular regions defined by concentric circles centered at the origin. Further let $N(\mathcal{E})$ be a random counting measure of a Borel set $\mathcal{E}$, i.e., $N(\mathcal{E}) = \#$ of points in $\mathcal{E}$. Now to derive the CDF of R, we first derive the joint probability density function (PDF) of R_1 and R_2, which by definition can be expressed as

$$f_{R_1,R_2}(r_1, r_2) = \lim_{\substack{\mathrm{d}r_1 \to 0 \\ \mathrm{d}r_2 \to 0}} \frac{\mathbb{P}\left(R_1 \in \mathcal{E}_2, R_2 \in \mathcal{E}_4\right)}{\mathrm{d}r_1 \mathrm{d}r_2}. \tag{B.3}$$

The numerator of the above expression can be expressed as:

$$\begin{aligned} &\mathbb{P}\left(R_1 \in \mathcal{E}_2, R_2 \in \mathcal{E}_4\right) = \\ &\mathbb{P}\left(N(\mathcal{E}_1) = 0, N(\mathcal{E}_2) = 1, N(\mathcal{E}_3) = 0, N(\mathcal{E}_4) = 1\right) = \\ &\mathbb{P}\left(N(\mathcal{E}_1) = 0\right) \mathbb{P}\left(N(\mathcal{E}_2) = 1\right) \mathbb{P}\left(N(\mathcal{E}_3) = 0\right) \mathbb{P}\left(N(\mathcal{E}_4) = 1\right), \end{aligned} \tag{B.4}$$

where the simplification follows from the fact that the sets $\mathcal{E}_i$ are disjoint. Now recall that the point process Φ is independently thinned by probability p outside the circle of radius $r_1 + \mathrm{d}r_1$. Therefore, the above expression can be written as:

$$\begin{aligned} &\mathbb{P}\left(R_1 \in \mathcal{E}_2, R_2 \in \mathcal{E}_4\right) = e^{-\lambda\pi r_1^2} \\ &\lambda\pi\left[(r_1 + \mathrm{d}r_1)^2 - r_1^2\right] e^{-\lambda\pi\left[(r_1+\mathrm{d}r_1)^2 - r_1^2\right]} e^{-p\lambda\pi\left[r_2^2 - (r_1+\mathrm{d}r_1)^2\right]} \\ &p\lambda\pi\left[(r_2 + \mathrm{d}r_2)^2 - r_2^2\right] e^{-p\lambda\pi\left[(r_2+\mathrm{d}r_2)^2 - r_2^2\right]}, \end{aligned} \tag{B.5}$$

which for vanishingly small $\mathrm{d}r_1$ and $\mathrm{d}r_2$ can be simplified to:

$$p(2\pi\lambda)^2 r_1 r_2 \exp\left(-\lambda\pi r_1^2(1-p)\right)\exp\left(-p\lambda\pi r_2^2\right)\mathrm{d}r_1\mathrm{d}r_2, \tag{B.6}$$

from which the joint PDF of R_1 and R_2 can be expressed as:

$$f_{R_1,R_2}(r_1,r_2) = p(2\pi\lambda)^2 r_1 r_2 e^{-\lambda\pi r_1^2(1-p)} e^{-p\lambda\pi r_2^2}, \tag{B.7}$$

for $r_2 \geq r_1 \geq 0$. Using this joint density, the CCDF of R can now be expressed as:

$$\mathbb{P}[R > r] = \mathbb{P}\left[\frac{R_2}{R_1} > r\right] \tag{B.8}$$

$$= \int_{r_2=0}^{\infty}\int_{r_1=0}^{\frac{r_2}{r}} f_{R_1,R_2}(r_1,r_2)\mathrm{d}r_1\mathrm{d}r_2 = \frac{1}{1+p(r^2-1)}, \tag{B.9}$$

which completes the proof. □

Recall that for $p = 1$ the proposed model reduces to the uniform distribution of users, leading to the following corollary.

Corollary 17. *The CDF of R for the typical observation point that is defined to be uniformly distributed in $\mathbb{R}^2$ independent of the BS locations ($p = 1$ in the proposed model) is*

$$F_R(r) = 1 - \frac{1}{r^2},\ r \geq 1. \tag{B.10}$$

Corollary 18. *The mean value of R as a function of p is*

$$\mathbb{E}[R] = 1 + \frac{1}{\sqrt{p(1-p)}}\left(\frac{\pi}{2} - \tan^{-1}\left(\frac{\sqrt{p}}{\sqrt{1-p}}\right)\right), \tag{B.11}$$

which for $p = 1$ is $\mathbb{E}[R] = 2$.

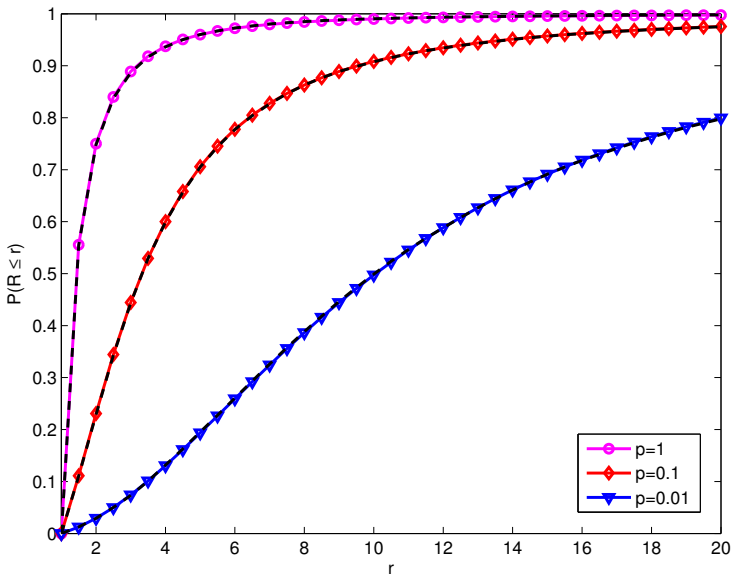

Figure B.2: The CDF of R for various values of conditional thinning probability p. The theoretical results are overlaid with dotted plots of the simulation results showing perfect match.

Remark 24 (Dependence in user and BS point processes)**.** *The level of dependence induced in the locations of the users and the BSs is inversely proportional to the thinning probability p, i.e., the probability of finding a typical user in the cell interior close to its serving BS is higher for smaller values of p. This is evident from the mean of R given by Corollary 18 and from the plot of the CDFs of R for various values of p in Fig. B.2.*

We now derive the coverage probability of a typical user sampled under the new proposed method. The coverage probability $\mathtt{P_c}$ denotes the average fraction of users in coverage and can be formally defined as the CCDF of $\mathtt{SIR}$

as follows:

$$\mathtt{P_c} = \mathbb{P}\left(\mathtt{SIR} > \beta\right) = \mathbb{P}\left(\frac{h_{x_s}\|x_s\|^{-\alpha}}{\sum_{y\in\Phi_b\setminus x_s} h_y\|y\|^{-\alpha}} > \beta\right), \tag{B.12}$$

where the serving BS is assumed to be located at x_s. Using tools developed in [1], a simple expression can be derived for the coverage probability of a typical user under the proposed sampling method. The main result is given in the following Lemma along with a brief proof sketch.

Lemma 21. *The coverage probability of a typical user when it connects to its nearest BS under the proposed user sampling method with thinning probability p is*

$$\mathtt{P_c}(\alpha,\beta,p) = \left[1 + p\beta^{\frac{2}{\alpha}}\int_{\beta^{-\frac{2}{\alpha}}}^{\infty}\frac{1}{1+u^{\frac{\alpha}{2}}}\mathrm{d}u\right]^{-1}, \tag{B.13}$$

which for $\alpha = 4$ simplifies to

$$\mathtt{P_c}(4,\beta,p) = \left[1 + p\beta^{\frac{1}{2}}\left(\pi/2 - \arctan(\beta^{-\frac{1}{2}})\right)\right]^{-1}. \tag{B.14}$$

This result directly follows from Theorem 2 of [1] with a slight modification to incorporate conditional thinning of the point process Φ. The coverage probability is first conditioned on the distance of a typical user to its serving BS, which can be computed by the null probability of a PPP with density λ. Conditioned on this distance, say u, the interference field defined over $\mathbb{R}^2 \cap B(0,u)^c$ is a PPP with density $p\lambda$, where $B(0,u)$ is a ball with radius u centered at 0 and p appears due to conditional thinning. This is the step where

the proof of the current Lemma differs from that of Theorem 2 of [1]. The remaining proof, which mainly involves the derivation of the Laplace transform of interference, remains the same.

Remark 25 (Scale invariance and effect of p on $\mathtt{P_c}$)**.** *For any given value of thinning probability p, the coverage probability is independent of the density of the BSs in an interference limited cellular network. This scale invariance result is a generalization of a similar observation reported in [1] for the uniform distribution of the users, which is a special case of the proposed model and corresponds to $p = 1$. As expected, the coverage probability is a monotonically decreasing function of p. This is consistent with the observations reported in [102], where a similar parametrization was used to model load on various classes of BSs in a heterogeneous cellular network.*

B.5 Non-Uniform user Distribution

In this section, we show that the framework developed in the previous section can be used as an accurate analytical generative model for the non-uniform user distributions where the users are clustered around their serving BSs. We first explain the simulation setup for this non-uniform user distribution model and then describe a subtle difference in this model and the user sampling framework developed in the previous section.

To simulate the non-uniform user distribution model, start with a realization of a PPP Φ with density λ and form the Voronoi tessellation. Recall

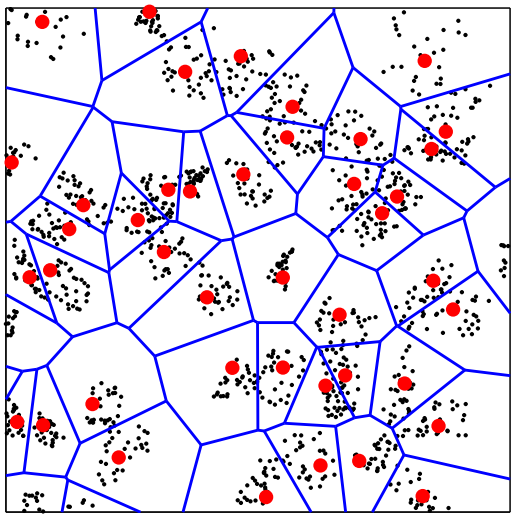

Figure B.3: A realization of the proposed non-uniform user distribution model. The big circles denote BSs and the small circles denote users.

that in case of a cellular network, the Voronoi cell of each point denotes its coverage region in the nearest neighbor connectivity model. Distribute N_u users uniformly in each Voronoi cell. For concreteness, we assume that N_u is the same for all the BSs and equal to the number of time-frequency resource blocks, which models a full-buffer system. This assumption can be relaxed under certain conditions as discussed in Chapter 3. Until this point, the user distribution is fairly uniform although there is a subtle difference in this model and the way typical user is usually defined to be uniformly distributed over $\mathbb{R}^2$. We will remark on this difference later in this section. To induce dependence in the BS and user point processes, we again use the the thinning idea and retain points of the realization of Φ independently with probability p and remove the rest. The users corresponding to the points that are removed are also

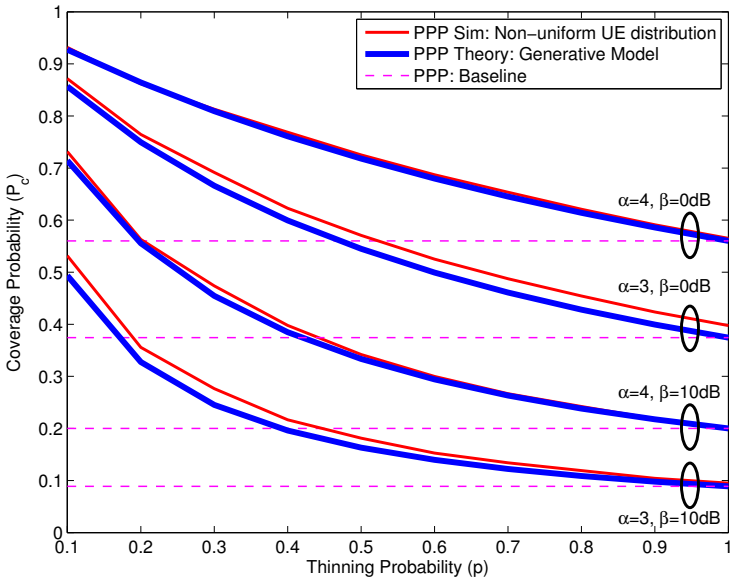

Figure B.4: Comparison of the coverage probability of the proposed non-uniform user distribution model with the analytical expression derived in Lemma 21 and the baseline model assuming uniform user distribution.

removed. The thinned version of the point process Φ with density λp models the BS locations. For the new coverage areas defined by the thinned point process, the remaining users are biased towards the cell interior as shown in Fig. B.3. A favorable characteristic of this model is the probabilistic attraction introduced in the user and BS point processes without inducing any geometric constraints. The coverage probability can now be numerically evaluated by averaging over these user locations. Recall that we assume interference-limited scenario where thermal noise is negligible. For this setup, it is easy to argue that the coverage probability is invariant to the changes in P, λ and N_u. Note that the result of Lemma 21 is not exact for this simulation model, as remarked below.

Remark 26 (User uniformly distributed in $\mathbb{R}^2$ vs. in randomly chosen Voronoi Cell)**.** *There is a subtle difference in performing downlink analysis at a typical user uniformly distributed in* $\mathbb{R}^2$ *and uniformly distributed in a randomly chosen Voronoi cell. The former corresponds to the analytical model discussed in the previous section for* $p = 1$ *and the latter corresponds to the simulation model discussed in this section. The difference is induced by the structure of Poisson Voronoi tessellation and can be understood by a simple fact that a point uniformly distributed in* $\mathbb{R}^2$ *is more likely to fall in a bigger Voronoi cell, whereas there is no such bias towards bigger cells when the Voronoi cell itself is chosen randomly.*

We now compare the coverage probability of this non-uniform user distribution model with the analytical expression derived in Lemma 21 in Fig. B.4. We first note that the plots are surprisingly close and the difference highlighted in Remark 26 does not have a significant impact on the coverage probability. Thus, the analytical model based on conditional thinning can be used as an accurate generative model to study coverage probability for this non-uniform user distribution model described in this section. Further, we compare the coverage probability with the baseline model, where the users are distributed uniformly over $\mathbb{R}^2$ independent of the BS point process. We note that the difference in coverage predictions is significant even for high values of p. This clearly highlights the importance of accurate user distribution models in the performance analysis of cellular networks.

B.6 Summary

In this appendix, we addressed the problem of incorporating non-uniform user distributions in the random spatial models for cellular networks. Based on the idea of conditional thinning, we first proposed a model to bias the location of a typical user towards cell interior and then used it as a generative model to study deployment scenarios where the users are more likely to lie close to their serving BSs. The extension of this idea to HetNets is left as a promising future work.

Appendix C

Appendix to Chapter 4

C.1 Signaling Preliminaries

The received signal y_k from k^{th} tier BS at a typical user located at the origin is given by

$$y_k = \sqrt{P_k}\|x_k\|^{-\frac{\alpha}{2}}\mathbf{v}_{kx_k}^*\mathbf{z}_k + \sum_{k\in\mathcal{K}}\sum_{y\in\Phi_j\setminus x_k}\sqrt{P_j}\|y\|^{-\frac{\alpha}{2}}\mathbf{u}_{jy}^*\mathbf{z}_j, \tag{C.1}$$

where P_k is the per user transmit power of k^{th} tier BS, and $\mathbf{z}_k \in \mathbb{C}^{M_k\times 1}$ is the normalized transmit signal vector. The channel vector from k^{th} tier BS to a typical user located at origin is denoted by $\mathbf{v}_{kx} \in \mathbb{C}^{M_k\times 1}$ and for the interfering link from a j^{th} tier BS located at $y \in \mathbb{R}^2$ is denoted by $\mathbf{u}_{jy} \in \mathbb{C}^{M_j\times 1}$. The vectors $\mathbf{v}, \mathbf{u}$ are assumed to have i.i.d. $\mathcal{CN}(0,1)$ entries, independent across BSs and of the user distances.

This chapter assumes linear precoding, in which the k^{th} tier BS multiplies the data symbol $s_{k,i}$ destined for the i^{th} user, for $1 \le i \le \Psi_k$, by $\mathbf{w}_{k,i}$ so that the transmitted signal is a linear function, i.e. $\mathbf{z}_k = \sum_{i=1}^{\Psi_k}\mathbf{w}_{k,i}s_{k,i}$. When zero-forcing beamforming with perfect CSI is employed to serve Ψ_k, Ψ_j users in tier k, j respectively, the columns of the precoding matrix $\mathbf{W}_k = [\mathbf{w}_{k,i}]_{1\le i\le\Psi_k} \in \mathbb{C}^{M_k\times\Psi_k}$ equal the normalized columns of $\tilde{\mathbf{V}}_k^*(\tilde{\mathbf{V}}_k\tilde{\mathbf{V}}_k^*)^{-1} \in \mathbb{C}^{M_k\times\Psi_k}$, for $\tilde{\mathbf{V}} =$

$[\tilde{\mathbf{v}}_1, \ \ldots, \tilde{\mathbf{v}}_k \ \ldots \ \tilde{\mathbf{v}}_{\Psi_k}]^* \in \mathbb{C}^{\Psi_k \times M_k}$ being the concatenated matrix of channel directions, where the direction of each vector channel is represented as $\tilde{\mathbf{v}}_k \triangleq \frac{\mathbf{v}_k}{\|\mathbf{v}_k\|}$. The desired channel power is given by $h_{kx} = |\mathbf{v}_{kx}^* \mathbf{w}_{k,k}|^2 = |\tilde{\mathbf{v}}_{kx}^* \mathbf{w}_{k,k}|^2 \cdot \|\mathbf{v}_{kx}\|^2$ which equals the product of two independent rv's which are distributed as Beta$(M_k - \Psi_k + 1, \Psi_k - 1)$ and $\Gamma(M_k, 1)$, respectively. Therefore, the channel power is $h_{kx} \sim \Gamma(\Delta_k, 1)$ with $\Delta_k = M_k - \Psi_k + 1$. For the distribution of the interfering marks, we assume that the precoding matrices have unit-norm orthogonal columns and that $\mathbf{W}_j$ is calculated independently of $\mathbf{u}_{jy}$. Therefore, $\tilde{\mathbf{u}}_{jy}$ and $\mathbf{w}_j$ are independent isotropic unit-norm random vectors, and $\left|\tilde{\mathbf{u}}_{jy}^* \mathbf{w}_j\right|^2$ is a linear combination of Ψ_j complex normal random variables, i.e. exponentially distributed. Neglecting the spatial correlation, we have that $g_{jy} \sim \Gamma(\Psi_j, 1)$, since it is the sum of Ψ_j i.i.d. exponential random variables.

The case $\Delta_k = 1$ and $\Psi_j = M_j$ is referred to as full SDMA. The case that each BS only serves one user, i.e. $\Psi_k = 1$, using the beamforming vector $\mathbf{w}_{kx} = \tilde{\mathbf{v}}_{kx}$ corresponds to SU-BF or MISO eigen-beamforming. In that case, the channel power is given by $h_{kx} \sim \Gamma(\Delta_k, 1)$ with $\Delta_k = M_k$ and the interference marks as $g_{jy} \sim \Gamma(\Psi_j, 1)$ with $\Psi_j = 1$, $\forall j \in \mathcal{K}$, since the beamforming vectors $\mathbf{w}_{jy}$ used by the j^{th} tier interfering BS are calculated based on $\mathbf{v}_j$, i.e. independently of $\mathbf{u}_{jy}$.

Bibliography

[1] J. G. Andrews, F. Baccelli, and R. K. Ganti, "A tractable approach to coverage and rate in cellular networks," *IEEE Trans. on Communications*, vol. 59, no. 11, pp. 3122–3134, Nov. 2011.

[2] T. X. Brown, "Cellular performance bounds via shotgun cellular systems," *IEEE Journal on Sel. Areas in Communications*, vol. 18, no. 11, pp. 2443 – 2455, Nov. 2000.

[3] F. Baccelli, M. Klein, M. Lebourges, and S. Zuyev, "Stochastic geometry and architecture of communication networks," *J. Telecommunication Systems*, vol. 7, no. 1, pp. 209 – 227, 1997.

[4] F. Baccelli and S. Zuyev, "Stochastic geometry models of mobile communication networks," in *Frontiers in queueing*. Boca Raton, FL: CRC Press, 1997, pp. 227 – 243.

[5] H. S. Dhillon, R. K. Ganti, F. Baccelli, and J. G. Andrews, "Modeling and analysis of K-tier downlink heterogeneous cellular networks," *IEEE Journal on Sel. Areas in Communications*, vol. 30, no. 3, pp. 550 – 560, Apr. 2012.

[6] A. J. Goldsmith, *Wireless Communications*. New York: Cambridge University Press, 2005.

[7] T. S. Rappaport, *Wireless Communications: Principles and Practice*, 2nd ed. Upper Saddle River, New Jersey: Prentice-Hall, 2002.

[8] L. Chen, W. Chen, B. Wang, X. Zhang, H. Chen, and D. Yang, "System-level simulation methodology and platform for mobile cellular systems," *IEEE Communications Magazine*, vol. 49, no. 7, pp. 148 – 155, Jul. 2011.

[9] K. B. Baltzis, "Hexagonal vs circular cell shape: A comparative analysis and evaluation of the two popular modeling approximations," in *Cellular Networks - Positioning, Performance Analysis, Reliability.* InTech, 2011.

[10] Cisco, "Cisco visual networking index: Global mobile data traffic forecast update, 2011 - 2016," white paper, Feb. 2012.

[11] Nokia Siemens Networks, "LTE release 12 and beyond," white paper, Oct. 2012.

[12] Q. Li, G. Li, W. Lee, M. Lee, D. Mazzarese, B. Clerckx, and Z. Li, "MIMO techniques in WiMAX and LTE: a feature overview," *IEEE Communications Magazine*, vol. 48, no. 5, pp. 86 – 92, May 2010.

[13] H. Bölcskei, D. Gesbert, C. B. Papadias, and A.-J. van der Veen, Eds., *Space-Time Wireless Systems: From Array Processing to MIMO Communications.* Cambridge University Press, 2006.

[14] 3GPP, "Overview of 3GPP Release 10", vol. 0.1.6, Sep. 2012.

[15] M. Dohler, R. W. Heath, A. Lozano, C. B. Papadias, and R. A. Valenzuela, "Is the PHY layer dead?" *IEEE Communications Magazine*, vol. 49, no. 4, pp. 159 – 165, Apr. 2011.

[16] F. Rusek, D. Persson, B. K. Lau, E. G. Larsson, T. L. Marzetta, O. Edfors, and F. Tufvesson, "Scaling up MIMO: Opportunities and challenges with very large arrays," *IEEE Signal Processing Magazine*, vol. 30, no. 1, pp. 40–60, Jan. 2013.

[17] T. L. Marzetta, "Noncooperative cellular wireless with unlimited numbers of base station antennas," *IEEE Trans. on Wireless Communications*, vol. 9, no. 11, pp. 3590 – 3600, Nov. 2010.

[18] Z. Pi and F. Khan, "A millimeter-wave massive MIMO system for next generation mobile broadband," in *Proc., IEEE Asilomar*, Pacific Grove, CA, Nov. 2012, pp. 693 – 698.

[19] O. El Ayach, S. Rajagopal, S. Abu-Surra, Z. Pi, and R. W. Heath, Jr., "Spatially sparse precoding in millimeter wave MIMO systems," submitted to *IEEE Tran. Wireless Communications*, 2013. Available online: arxiv.org/abs/1305.2460.

[20] Federal Communications Commission, "The mobile broadband spectrum challenge: International comparisons," white paper, Feb. 2013, available online: goo.gl/ZEAcR.

[21] Plum, "Future proofing Wi-Fi - the case for more spectrum," A report for Cisco, Jan. 2013, available online: goo.gl/5aNu2.

[22] P. Cramton, "Spectrum auction design," *Review of Industrial Organization*, vol. 42, no. 2, pp. 161 – 190, Mar. 2013.

[23] Federal Communications Commission, "Connecting america: The national broadband plan," 2010, available online: goo.gl/VGhQY.

[24] Huawei, "Whitepaper on spectrum," white paper, Feb. 2013, available online: goo.gl/kQSMb.

[25] R. C. Daniels and R. W. Heath, "60 GHz wireless communications: Emerging requirements and design recommendations," *IEEE Vehicular Technology Magazine*, vol. 2, no. 3, pp. 41 – 50, Sep. 2007.

[26] C. H. Doan, S. Emami, D. A. Sobel, A. M. Niknejad, and R. W. Brodersen, "Design considerations for 60 GHz CMOS radios," *IEEE Communications Magazine*, vol. 42, no. 12, pp. 132 – 140, Dec. 2004.

[27] A. M. Niknejad, "Siliconization of 60 GHz," *IEEE Microwave Magazine*, vol. 11, no. 1, pp. 78 – 85, Feb. 2010.

[28] A. Bleicher, "The 5G phone future: Samsung's millimeter-wave transceiver technology could enable ultrafast mobile broadband by 2020," *IEEE Spectrum*, vol. 50, no. 7, pp. 15 – 16, Jul. 2013.

[29] V. Chandrasekhar, J. Andrews, and A. Gatherer, "Femtocell networks: a survey," *IEEE Communications Magazine*, vol. 46, no. 9, pp. 59 – 67, Sep. 2008.

[30] J. G. Andrews, "Seven ways that HetNets are a cellular paradigm shift," *IEEE Communications Magazine*, vol. 51, no. 3, pp. 136 – 144, Mar. 2013.

[31] S. Hur, T. Kim, D. J. Love, J. V. Krogmeier, T. A. Thomas, and A. Ghosh, "Multilevel millimeter wave beamforming for wireless backhaul," in *Proc., IEEE Globecom Workshops*, Houston, TX, 2011.

[32] A. Ghosh, J. G. Andrews, N. Mangalvedhe, R. Ratasuk, B. Mondal, M. Cudak, E. Visotsky, T. A. Thomas, P. Xia, H. S. Jo, H. S. Dhillon, and T. D. Novlan, "Heterogeneous cellular networks: From theory to practice," *IEEE Communications Magazine*, vol. 50, no. 6, pp. 54 – 64, Jun. 2012.

[33] A. Damnjanovic, J. Montojo, Y. Wei, T. Ji, T. Luo, M. Vajapeyam, T. Yoo, O. Song, and D. Malladi, "A survey on 3GPP heterogeneous networks," *IEEE Wireless Communications*, vol. 18, no. 3, pp. 10 – 21, Jun. 2011.

[34] D. P. Malladi, "Heterogeneous networks in 3G and 4G," in *IEEE Communication Theory Workshop*, Maui, Hawaii, May 2012, available online: goo.gl/WN9g8.

[35] Qualcomm, "LTE advanced: heterogeneous networks," white paper, Jan. 2011.

[36] J. G. Andrews, H. Claussen, M. Dohler, S. Rangan, and M. C. Reed, "Femtocells: Past, present, and future," *IEEE Journal on Sel. Areas in Communications*, vol. 30, no. 3, pp. 497 – 508, Apr. 2012.

[37] S. Kishore, L. Greenstein, H. Poor, and S. Schwartz, "Uplink user capacity in a CDMA macrocell with a hotspot microcell: exact and approximate analyses," *IEEE Trans. on Wireless Communications*, vol. 2, no. 2, pp. 364 – 374, Mar. 2003.

[38] X. Wu, B. Mukherjee, and D. Ghosal, "Hierarchical architectures in the third-generation cellular networks," *IEEE Wireless Communications*, vol. 11, no. 3, pp. 62 – 71, Jun. 2004.

[39] A. Saleh, A. Rustako, and R. Roman, "Distributed antennas for indoor radio communications," *IEEE Trans. on Communications*, vol. 35, no. 12, pp. 1245 – 1251, Dec. 1987.

[40] W. Roh and A. Paulraj, "Performance of the distributed antenna systems in a multi-cell environment," in *Proc., IEEE Veh. Technology Conf. (VTC)*, Jeju, Korea, Apr. 2003, pp. 587 – 591.

[41] J. Zhang and J. G. Andrews, "Distributed antenna systems with randomness," *IEEE Trans. on Wireless Communications*, vol. 7, no. 9, pp. 3636 – 3646, Sep. 2008.

[42] W. Choi and J. G. Andrews, "Downlink performance and capacity of distributed antenna systems in a multicell environment," *IEEE Trans. on Wireless Communications*, vol. 6, no. 9, pp. 69 – 73, Jan. 2007.

[43] Picochip, "The case for home base stations," white paper, Apr. 2007.

[44] V. Chandrasekhar and J. G. Andrews, "Uplink capacity and interference avoidance for two-tier femtocell networks," *IEEE Trans. on Wireless Communications*, vol. 8, no. 7, pp. 3498 – 3509, Jul. 2009.

[45] A. Wyner, "Shannon-theoretic approach to a Gaussian cellular multiple-access channel," *IEEE Trans. on Info. Theory*, vol. 40, no. 6, pp. 1713 – 1727, Nov. 1994.

[46] P. F. Ash and E. D. Bolker, "Generalized Dirichlet tessellations," *Geometriae Dedicata*, vol. 20, no. 2, pp. 209 – 243, 1986.

[47] P. J. Fleming, A. L. Stolyar, and B. Simon, "Closed-form expressions for other-cell interference in cellular CDMA," Technical Report 116, Univ. of Colorado at Boulder, Dec. 1997.

[48] H. S. Dhillon, R. K. Ganti, F. Baccelli, and J. G. Andrews, "Coverage and ergodic rate in K-tier downlink heterogeneous cellular networks," in *Proc., Allerton Conf. on Comm., Control, and Computing*, Monticello, IL, Sep. 2011.

[49] H.-S. Jo, Y. J. Sang, P. Xia, and J. G. Andrews, "Heterogeneous cellular networks with flexible cell association: A comprehensive downlink SINR

analysis," *IEEE Trans. on Wireless Communications*, vol. 11, no. 10, pp. 3484 – 3495, Oct. 2012.

[50] S. Mukherjee, "Analysis of UE outage probability and macrocellular traffic offloading for WCDMA macro network with femto overlay under closed and open access," in *Proc., IEEE Intl. Conf. on Communications (ICC)*, Kyoto, Japan, Jun. 2011.

[51] ——, "Distribution of downlink SINR in heterogeneous cellular networks," *IEEE Journal on Sel. Areas in Communications*, vol. 30, no. 3, pp. 575 – 585, Apr. 2012.

[52] T. D. Novlan, H. S. Dhillon, and J. G. Andrews, "Analytical modeling of uplink cellular networks," *IEEE Trans. on Wireless Communications*, vol. 12, no. 6, pp. 2669 – 2679, Jun. 2013.

[53] T. D. Novlan, R. K. Ganti, A. Ghosh, and J. G. Andrews, "Analytical evaluation of fractional frequency reuse for heterogeneous cellular networks," to appear, *IEEE Trans. Wireless Communications*, 2012.

[54] H. Wang and M. C. Reed, "Tractable model for heterogeneous cellular networks with directional antennas," in *Proc., Australian Communications Theory Workshop*, Wellington, Jan. 2012.

[55] R. W. Heath, Jr. and M. Kountouris, "Modeling heterogeneous network interference," in *Proc., Information Theory and its Applications (ITA)*, San Deigo, CA, Feb. 2012.

[56] P. Madhusudhanan, J. G. Restrepo, Y. Liu, T. X. Brown, and K. R. Baker, "Multi-tier network performance analysis using a shotgun cellular system," in *Proc., IEEE Globecom*, Houston, TX, Dec. 2011.

[57] S. Verdu, *Multiuser Detection*. Cambridge, UK: Cambridge, 1998.

[58] G. Caire and S. Shamai, "On the achievable throughput of a multi-antenna Gaussian broadcast channel," *IEEE Trans. on Info. Theory*, vol. 49, no. 7, pp. 1691 – 1706, Jul. 2003.

[59] G. Foschini, K. Karakayali, and R. Valenzuela, "Coordinating multiple antenna cellular networks to achieve enormous spectral efficiency," *IEE Proceedings - Communications*, vol. 153, no. 4, pp. 548 – 555, Aug. 2006.

[60] D. Gesbert, S. Hanly, H. Huang, S. Shamai, O. Simeone, and W. Yu, "Multi-cell mimo cooperative networks: A new look at interferences," *IEEE Journal on Sel. Areas in Communications*, vol. 28, no. 9, pp. 1380–1408, Dec. 2010.

[61] J. G. Andrews, "Interference cancellation for cellular systems: A contemporary overview," *IEEE Wireless Communications*, vol. 12, no. 2, pp. 19 – 29, Apr. 2005.

[62] S. Annapureddy, A. Barbieri, S. Geirhofer, S. Mallik, and A. Gorokhov, "Coordinated joint transmission in WWAN," in *IEEE Communications Theory Workshop*, Cancun, Mexico, May 2010.

[63] J. Xu, J. Zhang, and J. G. Andrews, "On the accuracy of the Wyner model in cellular networks," *IEEE Trans. on Wireless Communications*, vol. 10, no. 9, pp. 3098 – 3109, Sep. 2011.

[64] C.-B. Chae, I. Hwang, R. Heath, and V. Tarokh, "Interference aware-coordinated beamforming in a multi-cell systems," *IEEE Trans. on Wireless Communications*, vol. 11, no. 10, pp. 3692 – 3703, 2012.

[65] S. Jing, D. N. C. Tse, J. Hou, J. B. Soriaga, J. E. Smee, and R. Padovani, "Multi-cell downlink capacity with coordinated processing," in *Proc., Information Theory and its Applications (ITA)*, San Diego, CA, Jan. 2007.

[66] S. Catreux, P. Driessen, and L. Greenstein, "Simulation results for an interference-limited multiple-input multiple-output cellular system," *IEEE Communications Letters*, vol. 4, no. 11, pp. 334 – 336, Nov. 2000.

[67] A. Ganz, C. M. Krishna, D. Tang, and Z. J. Haas, "On optimal design of multitier wireless cellular systems," *IEEE Communications Magazine*, vol. 35, no. 2, pp. 88 – 93, Feb. 1997.

[68] E. Ekici and C. Ersoy, "Multi-tier cellular network dimensioning," *ACM Wireless Networks*, vol. 7, no. 4, pp. 401 – 411, Aug. 2001.

[69] D. Stoyan, W. S. Kendall, and J. Mecke, *Stochastic Geometry and Its Applications*, 2nd ed. Chichester: John Wiley and Sons, 1995.

[70] F. Baccelli and B. Blaszczyszyn, *Stochastic Geometry and Wireless Networks, Volume I – Theory*. NOW: Foundations and Trends in Networking, 2009.

[71] ——, *Stochastic Geometry and Wireless Networks, Volume II – Applications*. NOW: Foundations and Trends in Networking, 2009.

[72] M. Haenggi, J. G. Andrews, F. Baccelli, O. Dousse, and M. Franceschetti, "Stochastic geometry and random graphs for the analysis and design of wireless networks," *IEEE Journal on Sel. Areas in Communications*, vol. 27, no. 7, pp. 1029 – 1046, Sep. 2009.

[73] F. Baccelli, B. Blaszczyszyn, and P. Mühlethaler, "Stochastic analysis of spatial and opportunistic Aloha," *IEEE Journal on Sel. Areas in Communications*, vol. 27, no. 7, pp. 1105 – 1119, Sep. 2009.

[74] F. Aurenhammer, "Voronoi diagrams - A survey of a fundamental geometric data structure," *ACM Computing Surveys*, vol. 23, no. 3, pp. 345 – 405, Sep. 1991.

[75] A. Ghosh, J. Zhang, J. G. Andrews, and R. Muhamed, *Fundamentals of LTE*. Prentice-Hall, 2010.

[76] J. F. C. Kingman, *Poisson Processes*. Oxford University Press, 1993.

[77] H. S. Dhillon, R. K. Ganti, and J. G. Andrews, "A tractable framework for coverage and outage in heterogeneous cellular networks," in *Proc.,*

Information Theory and its Applications (ITA), San Diego, CA, Feb. 2011.

[78] B. Rengarajan and G. de Veciana, "Architecture and abstractions for environment and traffic-aware system-level coordination of wireless networks," *IEEE/ACM Trans. on Networking*, vol. 19, no. 3, pp. 721 – 734, Jun. 2011.

[79] S. Borst, N. Hegde, and A. Proutière, "Interacting queues with server selection and coordinated scheduling – application to cellular data networks," *Ann. Oper. Res.*, vol. 170, pp. 59 – 78, 2009.

[80] S. Borst, "User-level performance of channel-aware scheduling algorithms in wireless data networks," in *Proc., IEEE INFOCOM*, San Francisco, CA, Apr. 2003, pp. 321 – 331.

[81] T. Bonald and A. Proutière, "Wireless downlink data channels: User performance and cell dimensioning," in *Proc., ACM MobiCom*, San Diego, CA, Sep. 2003.

[82] D. B. Taylor, H. S. Dhillon, T. D. Novlan, and J. G. Andrews, "Pairwise interaction processes for modeling cellular network topology," in *Proc., IEEE Globecom*, Anaheim, CA, Dec. 2012.

[83] G. Boudreau, J. Panicker, N. Guo, R. Chang, N. Wang, and S. Vrzic, "Interference coordination and cancellation for 4G networks," *IEEE Communications Magazine*, vol. 47, no. 4, pp. 74 – 81, Apr. 2009.

[84] R. Ganti and M. Haenggi, "Spatial and temporal correlation of the interference in ALOHA ad hoc networks," *IEEE Communications Letters*, vol. 13, no. 9, pp. 631 – 633, Sep. 2009.

[85] U. Schilcher, C. Bettstetter, and G. Brandner, "Temporal correlation of interference in wireless networks with Rayleigh block fading," *IEEE Trans. Mobile Computing*, vol. 11, no. 12, pp. 2109 – 2120, Dec. 2012.

[86] R. Madan, J. Borran, A. Sampath, N. Bhushan, A. Khandekar, and T. Ji, "Cell association and interference coordination in heterogeneous LTE-A cellular networks," *IEEE Journal on Sel. Areas in Communications*, vol. 28, no. 9, pp. 1479 – 1489, Dec. 2010.

[87] H. ElSawy, E. Hossain, and M. Haenggi, "Stochastic geometry for modeling, analysis, and design of multi-tier and cognitive cellular wireless networks: A survey," *IEEE Communications Surveys and Tutorials*, to appear, 2013.

[88] R. W. Heath, Jr., M. Kountouris, and T. Bai, "Modeling heterogeneous network interference using Poisson point processes," *IEEE Trans. on Signal Processing*, vol. 61, no. 16, pp. 4114 – 4126, Aug. 2013.

[89] V. Chandrasekhar, M. Kountouris, and J. G. Andrews, "Coverage in multi-antenna two-tier networks," *IEEE Trans. on Wireless Communications*, vol. 8, no. 10, pp. 5314–5327, Oct. 2009.

[90] S. Park, W. Seo, Y. Kim, S. Lim, and D. Hong, "Beam subset selection strategy for interference reduction in two-tier femtocell networks," *IEEE Trans. on Wireless Communications*, vol. 9, no. 11, pp. 3440–3449, Nov. 2010.

[91] S. Park, W. Seo, S. Choi, and D. Hong, "A beamforming codebook restriction for cross-tier interference coordination in two-tier femtocell networks," *IEEE Trans. on Veh. Technology*, vol. 60, no. 4, pp. 1651–1663, May 2011.

[92] S. Akoum, M. Kountouris, and R. W. Heath Jr., "On imperfect CSI for the downlink of a two-tier network," in *Proc., IEEE Intl. Symposium on Information Theory*, Saint Petersburg, Russia, Jul.-Aug. 2011.

[93] A. Hunter, J. G. Andrews, and S. Weber, "Transmission capacity of ad hoc networks with spatial diversity," *IEEE Trans. on Wireless Communications*, vol. 7, no. 12, pp. 5058–5071, Dec. 2008.

[94] R. H. Y. Louie, M. R. McKay, and I. B. Collings, "Open-loop spatial multiplexing and diversity communications in ad hoc networks," *IEEE Trans. on Info. Theory*, vol. 57, no. 1, pp. 317 – 344, Jan. 2011.

[95] R. Vaze and R. W. Heath Jr., "Transmission capacity of ad-hoc networks with multiple antennas using transmit stream adaptation and interference cancellation," *IEEE Trans. on Info. Theory*, vol. 58, no. 2, pp. 780 – 792, Feb. 2012.

[96] M. Kountouris and J. G. Andrews, "Transmission capacity scaling of SDMA in wireless ad hoc networks," in *Proc., Information Theory Workshop (ITW)*, Taormina, Italy, Oct. 2009.

[97] ——, "Downlink SDMA with limited feedback in interference-limited wireless networks," *IEEE Trans. on Wireless Communications*, vol. 11, no. 8, pp. 2730 – 2741, Aug. 2012.

[98] C. Tepedelenlioglu, A. Rajan, and Y. Zhang, "Applications of stochastic ordering to wireless communications," *IEEE Trans. on Wireless Communications*, vol. 10, no. 12, pp. 4249 – 4257, Dec. 2011.

[99] B. Blaszczyszyn and D. Yogeshwaran, "Directionally convex ordering of random measures, shot noise fields and some applications to wireless communications," *J. Advances Applied Probability*, vol. 41, no. 3, pp. 623 – 646, 2009.

[100] P. Madhusudhanan, J. G. Restrepo, Y. Liu, T. X. Brown, and K. R. Baker, "Stochastic ordering based carrier-to-interference ratio analysis for the shotgun cellular systems," *IEEE Wireless Communications Letters*, vol. 1, no. 6, pp. 565 – 568, Dec. 2012.

[101] J. Lee and C. Tepedelenlioglu, "Stochastic ordering of interferences in large-scale wireless networks," submitted to *IEEE Trans. on Signal Processing*, Oct. 2012. Available online: arxiv.org/abs/1204.6341.

[102] H. S. Dhillon, R. K. Ganti, and J. G. Andrews, "Load-aware modeling and analysis of heterogeneous cellular networks," *IEEE Trans. on Wireless Communications*, vol. 12, no. 4, pp. 1666 – 1677, Apr. 2013.

[103] ——, "Modeling non-uniform UE distributions in downlink cellular networks," *IEEE Wireless Communications Letters*, vol. 2, no. 3, pp. 339 – 342, Jun. 2013.

[104] H. Huang, C. B. Papadias, and S. Venkatesan, *MIMO Communication for Cellular Networks*. Springer, 2012.

[105] F. Zheng and T. Kaiser, "On the channel capacity of multiantenna systems with Nakagami fading," *EURASIP Journal on Advances in Signal Processing*, vol. 2006, pp. 039 436–1–039 436–11, 2006.

[106] N. Jindal, "MIMO broadcast channels with finite-rate feedback," *IEEE Trans. on Info. Theory*, vol. 52, no. 11, pp. 5045–5060, Nov. 2006.

[107] J. Zhang, M. Kountouris, J. G. Andrews, and R. W. Heath, Jr., "Multimode transmission for the MIMO broadcast channel with imperfect channel state information," *IEEE Trans. on Communications*, vol. 59, no. 3, pp. 803–814, Mar. 2011.

[108] M. Shaked and J. G. Shanthikumar, *Stochastic Orders*. Springer, 2007.

[109] A. W. Marshall, I. Olkin, and B. C. Arnold, *Inequalities: Theory of Majorization and Its Applications*. Springer, 2009.

[110] S. B. Provost, "On the distribution of the ratio of powers of sums of gamma random variables," *Pakistan Journal Statistics*, vol. 5, pp. 157 – 174, 1989.

[111] S. M. Ross, *An Elementary Introduction to Mathematical Finance*. New York: Cambridge University Press, 2011.

[112] S. Singh, H. S. Dhillon, and J. G. Andrews, "Offloading in heterogeneous networks: Modeling, analysis and design insights," *IEEE Trans. on Wireless Communications*, vol. 12, no. 5, pp. 2484 – 2497, May 2013.

[113] B. Blaszczyszyn, M. K. Karray, and H.-P. Keeler, "Using Poisson processes to model lattice cellular networks," available online: arxiv.org/abs/1207.7208.

[114] H. S. Dhillon, M. Kountouris, and J. G. Andrews, "Downlink coverage probability in MIMO HetNets," in *Proc., IEEE Asilomar*, Pacific Grove, CA, Nov. 2012.

[115] *Technical Specification Group Radio Access Network; Evolved Universal Terrestrial Radio Access (E-UTRA); Radio Frequency (RF) system scenarios (Release 9)*, 3GPP TR 36.942, 2010.

[116] H.-P. Keeler, B. Blaszczyszyn, and M. K. Karray, "SINR-based k-coverage probability in cellular networks with arbitrary shadowing," in *Proc., IEEE Intl. Symposium on Information Theory*, Istanbul, Jul. 2013.

[117] M. Di Renzo, A. Guidotti, and G. Corazza, "Average rate of downlink heterogeneous cellular networks over generalized fading channels: A

stochastic geometry approach," *IEEE Trans. on Communications*, to appear, 2013. Available online: arxiv.org/abs/1303.0529.

[118] P. Madhusudhanan, J. G. Restrepo, Y. Liu, T. X. Brown, and K. Baker, "Downlink performance analysis for a generalized shotgun cellular systems," 2012, available online: arxiv.org/abs/1002.3943.

[119] B. Blaszczyszyn and H.-P. Keeler, "Equivalence and comparison of heterogeneous cellular networks," available online: arxiv.org/abs/1306.0772.

[120] Worldwatch Institute and Center for American Progress, "American Energy: The Renewable Path to Energy Security", Sep. 2006.

[121] C. K. Ho and R. Zhang, "Optimal energy allocation for wireless communications with energy harvesting constraints," *IEEE Trans. on Signal Processing*, vol. 60, no. 9, pp. 4808 – 4818, Sep. 2012.

[122] O. Ozel, K. Tutuncuoglu, J. Yang, S. Ulukus, and A. Yener, "Transmission with energy harvesting nodes in fading wireless channels: Optimal policies," *IEEE Journal on Sel. Areas in Communications*, vol. 29, no. 8, pp. 1732 – 1743, Sep. 2011.

[123] K. Tutuncuoglu and A. Yener, "Optimum transmission policies for battery limited energy harvesting nodes," *IEEE Trans. on Wireless Communications*, vol. 11, no. 3, pp. 1180 – 1189, Mar. 2012.

[124] V. Sharma, U. Mukherji, V. Joseph, and S. Gupta, "Optimal energy management policies for energy harvesting sensor nodes," *IEEE Trans. on Wireless Communications*, vol. 9, no. 4, pp. 1326 – 1336, Apr. 2010.

[125] J. Yang and S. Ulukus, "Optimal packet scheduling in an energy harvesting communication systems," *IEEE Trans. on Communications*, vol. 60, no. 1, pp. 220 – 230, Jan. 2012.

[126] J. Yang, O. Ozel, and S. Ulukus, "Broadcasting with an energy harvesting rechargeable transmitter," *IEEE Trans. on Wireless Communications*, vol. 11, no. 2, pp. 571 – 583, Feb. 2012.

[127] M. Antepli, E. Uysal-Biyikoglu, and H. Erkal, "Optimal packet scheduling on an energy harvesting broadcast link," *IEEE Journal on Sel. Areas in Communications*, vol. 29, no. 8, pp. 1721 – 1731, Aug. 2011.

[128] M. Gatzianas, L. Georgiadis, and L. Tassiulas, "Control of wireless networks with rechargeable batteries," *IEEE Trans. on Wireless Communications*, vol. 9, no. 2, pp. 581 – 593, Feb. 2010.

[129] K. Huang, "Spatial throughput of mobile ad hoc networks with energy harvesting," submitted to *IEEE Trans. on Info. Theory*. Availabile online: arxiv.org/abs/1111.5799.

[130] ——, "Throughput of wireless networks powered by energy harvesting," in *Proc., IEEE Asilomar*, Monterey, CA, Nov. 2011.

[131] H. S. Dhillon and J. G. Andrews, "Downlink rate distribution in heterogeneous cellular networks under generalized cell selection," submitted to *IEEE Wireless Communications Letters*, Jun. 2013. Available online: arxiv.org/abs/1306.6122.

[132] S. Roundy, P. K. Wright, and J. M. Rabaey, *Energy Scavenging for Wireless Sensor Networks: With Special Focus on Vibrations*. Norwell, MA: Kluwer Academic Publishers, 2004.

[133] F. Baccelli and P. Brémaud, *Elements of queueing theory: Palm martingale calculus and stochastic recurrences*. Springer-Verlag, 2003.

[134] A. Tarski, "A lattice-theoretical fixpoint theorem and its applications," *Pacific J. Math.*, vol. 5, no. 2, pp. 285 – 309, 1955.

[135] J. Kennan, "Uniqueness of positive fixed points for increasing concave functions on $\mathbb{R}^n$: An elementary result," *Review of Economic Dynamics*, vol. 4, no. 4, pp. 893 – 899, Oct. 2001.

[136] S. I. Resnick, *Adventures in Stochastic Processes*. Boston: Birkhäuser, 2005.

[137] *Evolved Universal Terrestrial Radio Access (E-UTRA) and Evolved Universal Terrestrial Radio Access Network (E-UTRAN); Overall description; Stage 2*, 3GPP TS 36.300, Jul. 2012.

[138] J. Møller and R. P. Waagepetersen, "Modern statistics for spatial point processes," *Scandinavian Journal of Statistics*, vol. 34, pp. 643–684, 2007.

[139] D. J. Strauss, "A model for clustering," *Biometrika*, vol. 63, pp. 467 – 475, 1975.

[140] A. Baddeley and R. Turner, "spatstat: An R package for analyzing spatial point patterns," *Journal of Statistical Software*, vol. 12, no. 6, pp. 1–42, 2005.

[141] F. P. Kelly and B. D. Ripley, "A note on Strauss's model for clustering," *Biometrika*, vol. 63, no. 2, pp. 357 – 360, Aug. 1976.

[142] J. Riihijärvi and P. Mähönen, "Modeling spatial structure of wireless communication networks," in *IEEE NetSciCom*, San Diego, CA, Mar. 2010.

[143] R. K. Ganti, F. Baccelli, and J. G. Andrews, "Series expansion for interference in wireless networks," *IEEE Trans. on Info. Theory*, vol. 58, no. 4, pp. 2194 – 2205, Apr. 2012.

[144] F. Baccelli and S. Zuyev, "Poisson-Voronoi spanning trees with applications to the optimization of communication networks," *Operations Research*, vol. 47, no. 4, pp. 619 – 631, 1999.

[145] V. M. Nguyen and F. Baccelli, "A stochastic geometry model for the best signal quality in a wireless networks," in *Proc., Modeling and Op-*

timization in Mobile, Ad Hoc and Wireless Networks, Avignon, France, 2010, pp. 465 – 471.

[146] *Further advancements for E-UTRA physical layer aspects*, 3GPP TR 36.814, 2010.

[147] R. Ganesh and K. Joseph, "Effect of non-uniform traffic distributions on performance of a cellular CDMA systems," in *Proc. IEEE Int. Conf. on Universal Personal Communications*, vol. 2, Oct. 1997, pp. 598 – 602.

[148] A. L. Stolyar and H. Viswanathan, "Self-organizing dynamic fractional frequency reuse for best-effort traffic through distributed inter-cell coordination," in *Proc., IEEE INFOCOM*, Rio de Janeiro, Brazil, Apr. 2009, pp. 1287 – 1295.

[149] P. Madhusudhanan, J. G. Restrepo, Y. Liu, and T. X. Brown, "Carrier to interference ratio analysis for the shotgun cellular system," in *Proc., IEEE Globecom*, Honolulu, Hawaii, Dec. 2009.

[150] M. Haenggi, "On distances in uniformly random networks," *IEEE Trans. on Info. Theory*, vol. 51, no. 10, pp. 3584 – 3586, Oct. 2005.

Vita

Harpreet S. Dhillon received the B.Tech. degree in Electronics and Communication Engineering from IIT Guwahati, India, in 2008 and the M.S. degree in Electrical Engineering from Virginia Tech in 2010. He is currently a Ph.D. candidate in Electrical Engineering at UT Austin. He has held summer internships at Alcatel-Lucent Bell Labs in Crawford Hill, NJ, Samsung Research America in Richardson, TX, Qualcomm Inc. in San Diego, CA, and Cercom, Politecnico di Torino in Italy. His research interests are broadly in communication theory, stochastic geometry, and wireless ad hoc and cellular networks. His doctoral research has focused on the modeling and analysis of heterogeneous cellular networks using tools from stochastic geometry and point process theory. He is a recipient of the IEEE ICC 2013 best paper award in Wireless Communications Symposium, WNCG leadership award 2013, Agilent Engineering and Technology Award 2008, and was also awarded the Microelectronics and Computer Development (MCD) fellowship by UT Austin.

Permanent email: dhillon@ieee.org, dhillon.ee@gmail.com

This dissertation was typeset with LaTeX[†] by the author.

[†]LaTeX is a document preparation system developed by Leslie Lamport as a special version of Donald Knuth's TeX Program.